UTS UNIVERSITY OF TECHNOLOGY SYDNEY

Multifunctional cement-based sensors with integrated piezoresistivity and hydrophobicity toward smart infrastructure

by Wenkui Dong

Thesis submitted in fulfilment of the requirements for the degree of

Doctor of Philosophy

Under the supervision of

Dr. Wengui Li (Principle supervisor)

Prof. Daichao Sheng (Co-supervisor)

Prof. Kejin Wang (Co-supervisor)

University of Technology Sydney

Faculty of Engineering and Information Technology

November 2021

CERTIFICATE OF ORIGINAL AUTHORSHIP

I, Wenkui Dong declare that this thesis is submitted in fulfillment of the requirements for the award of Doctor of Philosophy, in the Faculty of Engineering and Information Technology at the University of Technology Sydney.

This thesis is wholly my own work unless otherwise reference or acknowledged. In addition, I certify that all information sources and literature used are indicated in the thesis. This document has not been submitted for qualifications at any other academic institution. This research is supported by the Australian Government Research Training Program.

Signature:

Production Note:
Signature removed prior to publication.

Date: 16/11/2021

ACKNOWLEDGEMENTS

Upon the completion of this thesis, I am grateful to those who have offered me encouragement and support during my PhD study.

Firstly, I would like to express my sincere gratitude to my principal supervisor Dr. Wengui Li for the continuous support to my PhD study and related research, for his patience, motivation and immense knowledge. His guidance provides me with many enlightening ideas as well as helps me in writing this thesis. I am also extremely grateful to my co-supervisors Prof. Daichao Sheng and Prof. Kejin Wang, for their insightful comments and encouragement throughout my study. It is a great privilege to work and study under their supervision.

Besides supervisors, I would like to appreciate my beloved families, my father Xiguan Dong, my mother Qiufen Lin and my older brother Wenxuan Dong for their persistent understanding, support and love throughout years of my study. I also appreciate my girlfriend Mingxing Li for her care and encouragement in my daily life, which creates me a comfortable environment and allows me to focus on my study and research.

Finally, my heartiest thanks go to my fellows Yipu Guo, Fulin Qu, Zhiyu Luo, Peiran Li, Zhuo Tang, Shaoqi Li, Jie Wei, Dongle Cheng, Idris Ibrahim, and many other friends who provide me with academic inspiration and help me in different experiments actively. Most importantly, they make me happier and less stressful when I am in difficult situation. It is a great honour to meet them in my PhD life and looking forward to keeping in touch with them in our future study and life.

This is a memorable time I have had, while challenging, it is rewarding and precious. Thank you to everyone I have met along the way.

LIST OF PUBLICATIONS

Dong, W., Guo Y., Sun Z., Tao Z., Li W. (2021). Development of self-sensing cement-based sensor using recycled fine waste glass aggregates coated with carbon nanotube. Journal of Cleaner Production, 127968.

Dong, W., Li, W., & Tao, Z. (2021). A comprehensive review on performance of cementitious and geopolymeric concretes with recycled waste glass as powder, sand or cullet. Resources, Conservation and Recycling, 172, 105664.

Dong, W., Li, W., Zhu, X., Sheng, D., & Shah, S. P. (2021). Multifunctional cementitious composites with integrated self-sensing and hydrophobic capacities toward smart structural health monitoring. Cement and Concrete Composites, 118, 103962.

Dong, W., Li, W., Vessalas, K., He, X., Sun, Z., & Sheng, D. (2021). Piezoresistivity deterioration of smart graphene nanoplate/cement-based sensors subjected to sulphuric acid attack. Composites Communications, 23, 100563.

Dong, W., Li, W., Wang, K., & Shah, S. P. (2021). Physicochemical and Piezoresistive properties of smart cementitious composites with graphene nanoplates and graphite plates. Construction and Building Materials, 286, 122943.

Dong, W., Li, W., Shen, L., Zhang, S., & Vessalas, K. (2021). Integrated self-healing and self-sensing cementitious composites using microencapsulation of nano-carbon black and slaked lime. Materials Letters, 128834.

Dong, W., Li, W., Wang, K., Han, B., Sheng, D., & Shah, S. P. (2020). Investigation on physicochemical and piezoresistive properties of smart MWCNT/cementitious composite exposed to elevated temperatures. Cement and Concrete Composites, 112, 103675.

Dong, W., Li, W., Luo, Z., Guo, Y., & Wang, K. (2020). Effect of layer-distributed carbon nanotube (CNT) on mechanical and piezoresistive performance of intelligent cement-based sensor. Nanotechnology, 31(50), 505503.

Dong, W., Li, W., Wang, K., Vessalas, K., & Zhang, S. (2020). Mechanical strength and self-sensing capacity of smart cementitious composite containing conductive rubber crumbs. Journal of Intelligent Material Systems and Structures, 1045389X20916788.

Dong, W., Li, W., Guo, Y., He, X., & Sheng, D. (2020). Effects of silica fume on physicochemical properties and piezoresistivity of intelligent carbon black-cementitious composites. Construction and Building Materials, 259, 120399.

Dong, W., Li, W., Luo, Z., Long, G., Vessalas, K., & Sheng, D. (2020). Structural response monitoring of concrete beam under flexural loading using smart carbon black/cement-based sensors. Smart Materials and Structures, 29(6), 065001.

Li, W., **Dong, W.***, Shen, L., Castel, A., & Shah, S. P. (2020). Piezoresistivity of nano-carbon black (NCB) enhanced functional cement-based sensor with polypropylene fibres. Materials Letters, 127736.

Dong, W., Li, W., Vessalas, K., & Wang, K. (2020). Mechanical and conductive properties of smart cementitious composites with conductive rubber crumbs. ES Materials & Manufacturing, 7, 51-63.

Dong, W., Li, W., Shen, L., Sun, Z., & Sheng, D. (2020). Piezoresistivity of carbon nanotubes (CNT) reinforced cementitious composites under integrated cyclic compression and impact load. Composite Structures, 112106.

Dong, W., Li, W., Wang, K., Guo, Y., Sheng, D., & Shah, S. P. (2020). Piezoresistivity enhancement of functional carbon black filled cement-based sensor using polypropylene fibre. Powder Technology, 373, 184-194.

Dong, W., Li, W., Wang, K., Luo, Z., & Sheng, D. (2020). Self-sensing capabilities of cement-based sensor with layer-distributed conductive rubber fibres. Sensors and Actuators A: Physical, 301, 111763.

Dong, W., Li, W., Lu, N., Qu, F., Vessalas, K., & Sheng, D. (2019). Piezoresistive behaviours of cement-based sensor with carbon black subjected to various temperature and water content. Composites Part B: Engineering, 178, 107488.

Dong, W., Li, W., Long, G., Tao, Z., Li, J. and Wang, K. (2019). Electrical resistivity and mechanical properties of cementitious composites incorporating conductive rubber fibres. Smart Materials and Structures, 28, 085013.

Dong, W., Li, W., Shen, L. and Sheng, D. (2019). Piezoresistive behaviours of carbon black cement-based sensors with layer-distributed conductive rubber fibres. Materials & Design, 182, 108012.

Dong, W., Li, W., Tao, Z., & Wang, K. (2019). Piezoresistive properties of cement-based sensors: Review and perspective. Construction and Building Materials, 203, 146-163.

TABLE OF CONTENTS

LIST OF ACRONYMS

SHM	Structure heath monitoring
AE	Acoustic emission
CNT	Carbon nanotube
MWCNT	Multi-walled carbon nanotube
CF	Carbon fibre
SF	Silica fume
CB	Carbon black
GNP	Graphene nanoplate
GNPC	Graphene nanoplate filled cementitious composite
GP	Graphite plate
GPC	Graphite plate filled cementitious composite
SCMs	Supplementary cementing materials
DC	Direct current
AC	Alternating current
SEM	Scanning electron microscope
CRC	Conductive rubber crumb
UDCC	Uniformly-dispersed CNT composites
PCP	Plain cement paste
LDCC	Layer-distributed CNT composite
LDCC1	CNT composite with 1 layer of undispersed CNT
LDCC2	CNT composite with 2 layers of undispersed CNT
DSC	Differential scanning calorimetry
TGA	Thermal-gravity analysis
PP	Polypropylene
FCR	Fractional changes of resistivity
C-S-H	Calcium silicate hydrate
XRD	X-Ray diffraction

EDX	Electron dispersion X-ray
CH	Calcium hydroxide
CAL	constant amplitude-loading
VAL	varied amplitude-loading
CBS	Cement-based sensors
NCB	Nano-carbon black
SL	Slaked lime
CP	Cement particles
SHP	Silane hydrophobic powder
CA	Contact angle
CBCS	CB filled cement-based sensor
CBCS05	CBCS with various CB contents of 0.5%
CBCS1	CBCS with various CB contents of 1.0%

LIST OF FIGURES

LIST OF TABLES

ABSTRACT

Concrete is the most widely used construction material for buildings, pavements, harbours and bridges. The piezoresistive cement-based sensor consists of the traditional cementitious composite and conductive fillers, thus the electrical conductivity is greatly improved and easily captured. Therefore, the cement-based sensors can be applied in concrete infrastructures to self-sense and monitor the damages and cracks through the measurements of concrete electrical resistivity, due to their low cost, easy manufacturing, high sensitivity and good durability compared to traditional sensors. However, several factors ranging from types and contents of conductive fillers, additives and environmental factors can affect the piezoresistivity and restrict the practical application of cement-based sensors.

In this study, the conventional cementitious materials with different conductive fillers including conductive rubber products (rubber crumbs and fibres) and carbon nanomaterials (carbon black, carbon nanotube, graphene and graphite) were developed to produce cement-based sensors, whose sensitivity was dozens or hundreds of times higher than the commercially available strain gauge. Later, the effects of additives such as rubber fibres, polypropylene fibres and silica fume on the electrical, mechanical, microstructural and piezoresistive properties of carbon black filled cement-based sensors were investigated. It was observed the enhanced durability and sensitivity of cement-based sensors containing these additives. Given working environment can significantly affect the piezoresistive performance of cement-based sensors, the effects of temperature, humidity, freeze-thaw cycles, acid erosion and drop impact on the cement-based sensors containing nanomaterials were explored regarding to the electrical resistivity and piezoresistivity. To reduce the interference from working environment, multifunctional cement-based sensors were developed with combined self-sensing, self-healing, self-cleaning and superhydrophobicity. These functions can hinder the penetration of water and ions inside of cement-based sensors, thus reduce the influences of working

environment on the piezoresistive performance of cement-based sensors. On the other hand, it provides the cement-based sensors with more functions to clean and heal themselves automatically.

In the end, this study carried out the piezoresistivity test on the small concrete beams and slabs with embedded cement-based sensors, to evaluate the sensing performance of cement-based sensors inside of concrete structures. Despite the inherent challenges, the multifunctional cement-based sensors have great potential for smart infrastructures. Overall, this study has comprehensively investigated the performance of cement-based sensors exposure to various conditions and taken a solid step forward for their practical application.

CHAPTER 1: INTRODUCTION

1.1 Research background

Concrete is the mostly widely used construction materials for buildings, pavements, harbours and bridges. With rapid development of advanced concrete technologies, such as high and ultra-high performance concrete, more and more concrete has been used in unique structures, such as high-rise buildings and marine structures, where they are subjected to corrosive environments as well as multi-forces resulting from winds, waves, earthquake, and even unexpected sabotage. Consequently, concrete cracking, scaling/spalling, and deterioration are almost inevitable, which in turn reduces longevity of the concrete structures and sometimes causes losses of human lives. Therefore, real-time monitoring and evaluation of concrete structures using self-sensing technology is attracting more and more attentions from engineering researchers and practitioners.

Traditional sensors are often made with metals and polymers, other than cement-based materials. There are always some concerns for embedding such sensors into concrete structures due to the incompatibility of the sensor materials with concrete and the high cost of the sensors. To overcome these disadvantages, development of piezoresistive cement-based sensors in the past few decades has transformed sensing technology in applications of concrete structures. Based on the piezoresistivity, cement-based sensors can sense strain or stress changes in concrete by simply measuring the altered concrete electrical resistivity. Along with the advantages of being compatible and economical, cement-based sensors, especially those made with conductive fibres as a conductor, are often multifunctional. While monitoring concrete electrical resistivity, the conductors used for sensing could also enhance mechanical properties (such as strength and ductility) and durability (such as reduced permeability and shrinkage cracking) of the concrete.

Although significant progresses have been made, researches and applications of piezoresistive cement-based sensors are still in their infancy. As vast types of sensors are developed and reported, it becomes more confusing for researchers and engineers to select a proper one to use. As considerable factors affect sensing capacity and accuracy, it becomes challenging for researchers and engineers to comprehend and compare the measurements.

1.2 Research objective

Existing studies on piezoresistive cement-based sensors are mostly focused on different conductive fillers as conductors and their discussions are primarily on piezoresistivity; limited studies have been conducted to highlight the effects of recycled conductive wastes, working environments, and to systematically address the manufacturing process and factors that affect key performance of cement-based sensors. The purpose of this study is to fill these gaps. While providing a better understanding of the fundamentals and the relationships among loading, deformation, electrical resistance, and piezoresistive behaviour, this study try to solve the moisture that influence piezoresistivity and other properties (mechanical and durability) of cement-based sensors, including those regarding sensor materials, loading/environmental conditions, hybrid multifunctionality and structural applications. It is expected that this study will provide not only an orientation for new researchers to explore and engage associated studies but also an insight for experienced researchers to perform transformational examinations into cement-based piezoresistive sensors.

The specific objectives of this study are listed as follows:

(1) To review the current status of cement-based sensors, and their limits and challenges for practical application of SHM.

(2) To explore the effect of conductive rubber products (rubber fibres and crumbs) on the conductivity and piezoresistivity of cement-based sensors.

(3) To investigated the effect of multiple carbon materials such as carbon black (CB), carbon nanotubes (CNTs), graphene nanoplate (GNP) and graphite plate on the mechanical properties and piezoresistivity of cement-based sensors.

(4) To explore the effect of working environments such as temperature, humidity, freeze-thaw cycles, acid erosion and drop impact on piezoresistive behaviours of cement-based sensors.

(5) To develop the hybrid self-sensing, self-healing, self-cleaning, and hydrophobic cement-based sensors that broaden the application ranges of cement-based sensors.

(6) To evaluate the self-sensing performance of cement-based sensors when they are embedded in small beams and large concrete plates.

1.3 Outline of thesis

Totally nice chapters are presented in this thesis, and content of each chapter is listed below:

Chapter 1: The background of cement-based sensors, research objective of this study and outline of thesis are presented in the chapter 1.

Chapter 2: This chapter reviews current studies on the cement-based sensors including different raw materials, conductive fillers, manufacturing processes, and environmental effects, etc.

Chapter 3: This chapter investigates the potential of conductive rubber fibres and crumbs as fillers in cement-based sensors.

Chapter 4: This chapter investigates the carbon nanomaterials such as carbon black, carbon nanotube, graphene and graphite as fillers in cement-based sensors.

Chapter 5: This chapter explores the effect of additives (conductive rubber fibres, polypropylene fibres and silica fume) on the electrical and piezoresistive performance of cement-based sensors.

Chapter 6: This chapter explores the effect of environmental factors such as temperature, humidity, freeze-thaw cycle, acid erosion and drop impact on the piezoresistivity of cement-based sensors.

Chapter 7: This chapter develops the self-sensing cement-based sensors with combined self-healing, superhydrophobic and self-cleaning properties.

Chapter 8: This chapter applies cement-based sensors into concrete beams and mortar slabs to assess the piezoresistivity and simulate the practical application.

Chapter 9: This chapter highlights the main contributions of this work and the recommendations for future research.

CHAPTER 2: LITERATURE REVIEW

2.1 Introduction

2.1.1 Sensing techniques, their developments and applications for SHM

Successful adoption of a new technology for field concrete structure heath monitoring (SHM) is greatly depending upon the integration of the sensor function, accuracy, installation procedure, application conditions and even costs. Figure 2.1 lists the application timeline of different sensing techniques on SHM.

In the early age of SHM, strain gauges are often developed into concrete structures for strain and deflection measurements. The application of strain gauges in construction site was testified by Backer et al. (2003) with an adequate accuracy of stress measurements in comparison to the calculated stresses under a tensile force. Kovačič et al. (2015) studied the signal collection and data processing of strain gauges for bridge loading tests in a practical project, and they obtained comparable results to those measured in a laboratory. However, even without economic considerations, the use of strain gauges is always limited due to the complexity of assembly, low sensitivity, thermal instability, and poor durability of the gauges. In contrast, optical fibre sensors have excellent performance, in terms of sensitivity and accuracy, which can be used to monitor micro-cracks in concrete through subtle alterations of intensity, wavelength, frequency, phase and polarisation of the received light signal. Leung et al. (2000) firstly proposed a method for applying optical fibre sensor to monitor crack generation in concrete, which suggested that low content of optical fibre could monitor a great deal of emerged cracks. Furthermore, Butler et al. (2016) took the advantage of embedded optical fibre to evaluate stresses in prestressed concrete beams at the early age, through which the prestress losses could be detected accurately. Even with powerful sensitivity and accuracy, optical fibre sensors are still obstructed by their high cost and complicated installation in construction. In addition, the sensors can be easily

damaged by either sharp components in matrixes (e.g. coarse aggregate) and /or improper operations during embedding procedure.

Following optical fibre sensors is the applications of piezoelectric ceramics and shape memory alloy for the strain and stress observation of concrete structures. Song et al. (2007) embedded ten piezoelectric ceramic patches in different cross sections of the concrete bent-cap for SHM, and they have developed a damage index to evaluate the structure safety, which showed a close correlation with the observed damages. Su et al. (2018) diagnosed the damage of hydraulic concrete structures by establishing a piezoelectric ceramic module, which was found especially effective for monitoring the hidden dynamic damages of hydraulic structures. Even with the foregoing advantages, it cannot be denied that these non-intrinsic embedded sensors typically have a difficulty of cohesion with their concrete substrate, thus having detrimental effects on mechanical properties and durability of the concrete elements. Another SHM technique is the non-destructive scanning method, including acoustic emission (AE), X-ray or C-scan. While detecting only surface cracks and deteriorations, this group of methods often requires a significant post-testing data process, which is time consuming. In addition, the accuracy of crack detection largely depends upon the resolution of the scanning, which needs to be further studied, and meanwhile, their costs are often too high to be widely applied commercially viable.

In view of the above-mentioned techniques, cement-based sensors on account of the piezoresistive characteristics have been developed by some researches to automatically monitor the deformation and cracks of concrete structures. The piezoresistivity refers to the electrical resistivity of a composite material that increases or decreases with external forces and induced strain. Compared to the conventional sensors, the cement-based sensor is fully intrinsic and coupling well with the concrete components. Besides, the cement-based sensor is much easier to install and manufacture with much less fabricating costs as well as has a good

compatibility with cement matrices, better durability and sensitivity when compared with other existing SHM techniques for concrete. To summarise the above mentioned sensing techniques, Table 2.1 provides a comparison of these different sensing techniques for SHM, including sensor installation methods, primary applications, and limitations.

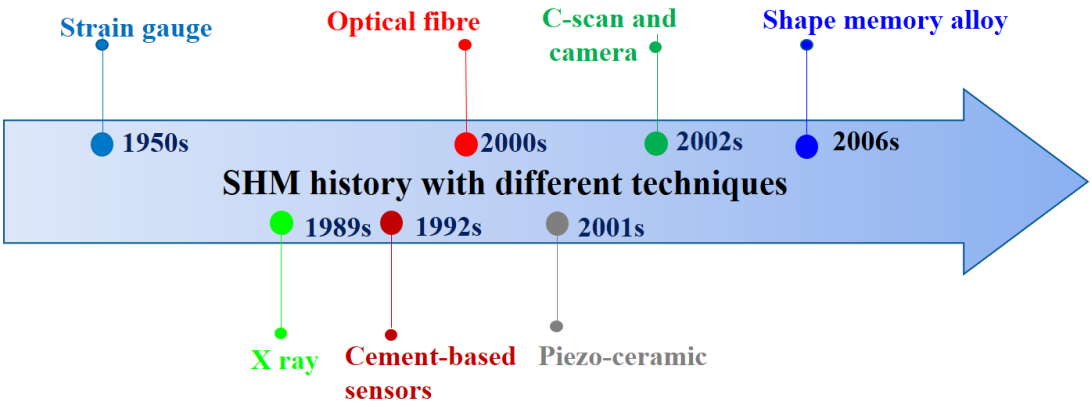

Figure 2.1. The application history of sensing techniques on SHM.

Table 2.1 Comparison of different sensing techniques used in SHM

Sensing sensor and techniques	Installation method	Features and applications	Limitations	Reference
Strain gauge	Attached on the surface	Wide application; low costs around 6.0 AUD each	Low sensitivity; worse durability; complex assembly; non-intrinsic	Backer *et al.* (Neild, Williams & McFadden 2005)
Optical fibre	Embedded	Accurate; high sensitivity; nonconductive; good durability	Dozens of AUD per meter; vulnerable; non-intrinsic	Butler *et al.* (Butler et al. 2016)
Piezoceramic	Embedded	Wide application; accurate; high sensitivity; good durability	Dozens of AUD each; non-intrinsic	Su *et al.* (Su, Zhang & Li 2018)
Shape memory alloy	Embedded	Accurate; high sensitivity; good damping property	Hundreds of AUD per meter; non-intrinsic	Mu *et al.* (Mu et al. 2018)

X-ray or C-scan	Non-contact	Wide application; non-destructive	Thousands of AUD each; extra analysis; non real-time; radiative	Suzuki *et al.* (Suzuki, Shiotani & Ohtsu 2017)
Camera	Non-contact	Convenient; easy operation;	Hundreds of AUD each; vulnerable	Aghlara and Tahir (Aghlara & Tahir 2018)
Cement-based sensor	Embedded	Sensitivity; accurate; intrinsic; costs as low as cement; good durability	Need external voltage	Chen & Chung (Chen & Chung 1996)

2.1.2 Components and principles of piezoresistive cement-based sensors

A piezoresistive cement-based sensor is a composite material, which consists of a conductive phase distributed in a matrix of a nonconductive phase. The conductive phase is often made with one material or their mixture like graphite, carbon nanotube (CNT), carbon fibre (CF), steel fibre, carbon black (CB), and other metallic alloys, while the nonconductive cementitious phase, or the matrix of the sensor, are commonly cement paste, mortar or concrete (Dong, Li, Guo, et al. 2020; Dong, Li, Shen, et al. 2019; Dong, Li, Wang, Guo, et al. 2020; Dong, Li, Wang, Han, et al. 2020; Dong, Li, Wang, Luo, et al. 2020; Shi & Chung 1999). A conductive phase is essential for providing the piezoresistive composites with a capacity for sensing stress, strain, deflection, cracks, humidity and temperature. The conductive phase (fibres and particular materials) can dope the nonconductive phase (cement-based materials) with two main mechanisms, namely percolation theory and quantum tunnelling effect theory (Banthia, Djeridane & Pigeon 1992). The percolation phenomenon can be explained by the formation of conductive passages that contributes to reduced resistivity. However, studies have indicated that the percolation theory cannot give a reasonable explanation for the piezoresistivity of sensors containing discontinuous conductive fibers/particles. Therefore, electrons' movements in the quantum tunnelling effect is often used for exploration of electrical conductivity in a quantum realm. According to the theory, low-energy electrons have possibility to overcome a

certain potential energy barrier, and thus, even with a lower external voltage and higher electrical resistivity, a minority of electrons could still move to the place with low potential energy and create a current. It is the tunnelling conductivity that enables the self-sensing ability of most commonly used piezoresistive cement-based sensors today (such as those made with discontinuous conductive fibres). The distance beyond which the tunnelling conductivity becomes invalid, or electrons are unable to pass through an insulator matrix, is called "tunnelling distance". In the consideration of tunnelling effect, the critical volume fraction of a conductive phase at which a composite can undergo a transition from insulator to conductor is called "percolation threshold". That is, percolation doesn't mean a fully physical connection.

Under a uniaxial compressive loading, the distance of the conductive particles/fibers of a cement-based composite gets closer and enables an electrical current to flow, thus decreases its resistivity. When unloading, the composite returns to its natural state and regains its initial resistivity. The ability to change the material electrical resistivity with its strain is called piezoresistivity. Piezoresistive cement-based sensors allow using electrical resistance measurement (DC or AC) to monitor the strain of the concrete that they examine. It shall be pointed out that piezoresistive cement-based sensors are highly sensitive and their measurements are easily affected by many internal and external factors, including the types and content of conductors and non-conductors, manufacture process (dispersion and curing methods), loading types (mechanical and freeze-thaw cycles), electrical resistance measurements, and environmental conditions (temperature and humidity). Figure 2.2 illustrates the major manufacturing process and applications of piezoresistive cement-based sensors, from which important factors that affect the piezoresistivity of the sensors can also be identified. These factors will be explained in more details in the following sections of the review.

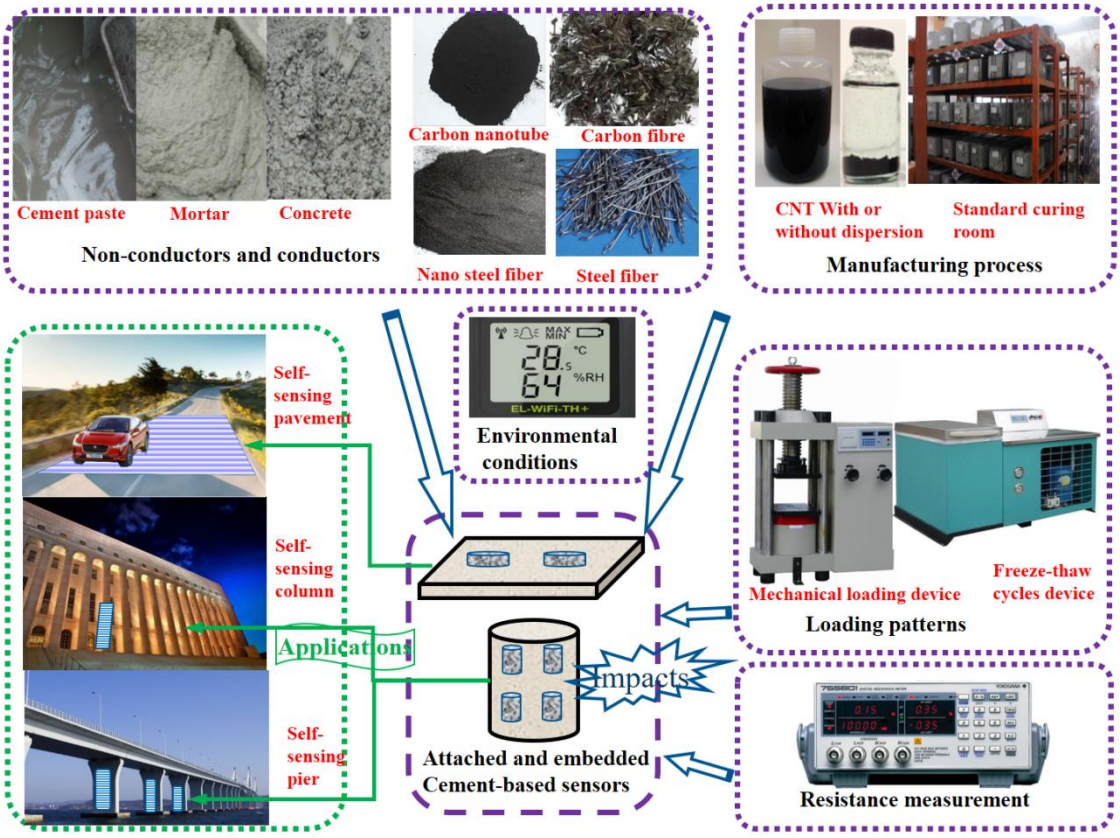

Figure 2.2. Key influential factors and applications of piezoresistive cement-based sensors.

2.2 Conductive phases

2.2.1 Commonly-used conductors

2.2.1.1 Conductive sheets and fibres

Conductive sheets, such as 2D graphene, or exfoliated graphite, have been proved with good piezoresistive output on piezoresistive-based sensors because of low cost and easy availability. However, for the cement-based sensors, conductive fibres are more commonly used as conductive phases since the invention of cement-based sensors in 1990s (Chen & Chung 1995). It has been proved that the strain sensing accuracy and sensitivity of 0.5 wt.% CNT reinforced cement-based sensor have more than 30 times higher efficiency than those of the normal strain gauge, and some investigations even produced steel fibre reinforced sensors with thousands of times higher accuracy (Teomete & Kocyigit 2013). Conductive fibres such as CF or SF have been extensively employed to improve the conductivity and piezoresistivity of cementitious

composite. The evenly distributed fibres with good conductivity in the cement mixture could bring about the composite with conductivity and sensing ability by capturing the small changes in conductivity and could detect the minimal structural alteration of composite. The mixed-use of SF and CNT could greatly improve the mechanical strength, damage control and sensing ability in the ultra-high-performance concrete. In compression, the contact between fibres, matrixes to fibres links easier than the tough between powders, matrices to powders, and the porosity is easily compressed, leading to the decrease in resistivity. It has been confirmed that the amount of CF by only 2 wt.% of cement has a similar conductivity to the composite with 10 wt.% of carbon black powders (Oberlin, Endo & Koyama 1976). It is believed that the better conductivity by using conductive fibres is due to the less possibility of conductor agglomeration and more opportunity for the contact fibres expediting conductive passages generation. Normally for small fibres (like CF or SF) in the composite, the longer the conductive fibres, the more remarkable the altered resistivity and piezoresistivity are (Dong, Guo, et al. 2021).

Although conductive fibres are excellent for improving the conductivity of cementitious composite for 2-3 orders of magnitude, many studies become conscious of the slightly irreversible resistivity of the cement-based sensors by CF or SF (Azhari & Banthia 2012). Fibres throughout the cracks possessing pull-out effect have a positive function to prohibit the growth and spread of cracks, however, owing to the structural instability of cementitious composite in the casting and curing procedure, some micro-cracks are irreversibly generated even with the addition of fibres and the functionality of pull-out effect. Besides, the phenomenon is especially significant at the initial loading stage. As mentioned before, the longer fibres express lower resistivity and better piezoresistivity, conductors' aspect ratio has relationship to its dispersion, orientation and coagulation in the composite, and the slender fibres have more advantages for conductive passages generation. For the same volume fraction,

the number of CF with a higher aspect ratio is less than that of CF with a small aspect ratio, as well as lower surface energy. Therefore, there is less probability for the agglomeration of higher aspect ratio CF in composite and thus increasing the dispersion of fibres.

As displayed in Figure 2.3, Park et al. (2010) investigated the CF with two different aspect ratios on the piezoresistivity of sensors, and found that the electrical resistivity decreased from 8×106 Ω to 6×106 Ω when the aspect ratio increased from 2 to 12, whilst the self-sensing ability also improved for the sensor with higher aspect ratio CF. Substantively consistent to the above mentioned Park's findings, Chen et al. (2004) used the CF in different lengths to study the fluctuation of percolation threshold, and proposed that the higher aspect ratio of CF had tendency to lower the percolation threshold by more potential conductive passages. Similarly, Baeza et al. (2013a) studied the effect of CF aspect ratio on the percolation threshold of cement-based composite and demonstrated that the percolation threshold was more easily reached for the CF with a higher aspect ratio. Generally, the use of conductive fibres with a lager aspect ratio benefits the conductivity of reinforced cementitious composite, while that also means the less opportunity for the contact of fibres and matrices and the induced weaker cohesion and lower mechanical properties. Constrained by the current research, the optimal aspect ratio of fibres that brings about both electrical and mechanical improvements still needs more explorations.

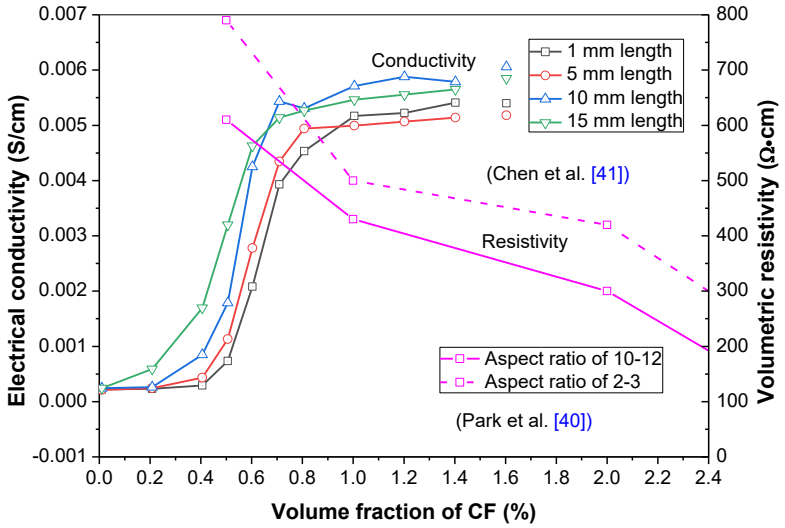

Figure 2.3. Electrical conductivity and volumetric resistivity of cement sensor to different aspect ratio of CF.

2.2.1.2 Conductive powders

Different from pull-out effect of fibres in cement-based sensor, conductive powder could not only work as conductive phase, but also play a crucial role as fillers and provide an improved mechanical property of composite by its filling effect (Dong, Li, Shen, et al. 2020; Liu et al. 2018). Various types of conductive powders have been used for piezoresistivity-based sensors, such as CB, graphite, steel powder, nickel powder, copper powder and aluminium powder etc. (Dong, Li, Vessalas, et al. 2021; Dong, Li, Wang, Vessalas, et al. 2020; Han, Han & Yu 2010; Li et al. 2020; Luheng, Tianhuai & Peng 2009), among which CB is the most frequently used in cement-based sensors for its low costs. As the powders are easily wrapped by surrounded cement paste, electrical channels are more likely blocked, leading to the fact that a low proportion of powders in the composite has limited effect enhancing the conductivity of sensors. For instance, Wen et al. (2007) investigated the effect of substitution rate of CF by CB in cement-based strain sensors, and found that the conductivity and shielding effectiveness were both reduced with increasing substitution ratio when the total conductor amount was fixed. The ability of electromagnetic shielding by conductive cement-based composite is significant and

also investigated by Fu and Wen et al. (Fu & Chung 1996a; Wen & Chung 2004), but this will not be greatly involved in the review. With increment of conductive powders, small conductive particles gather as clusters in composite, and then the conductivity path is progressively created by the linkage between clusters and particles to clusters and clusters. As for the piezoresistive mechanism, the reversible resistivity alters proportionally with the reversible strain of the sensor. Under compression, the distance of conductive particles and clusters is firstly narrowed, making the potential energy barrier reduced and promoting movements of electrons, thus enhancing the electrical conductivity of cement-based sensors. Meanwhile, the shrinkage of porosity increases the volume fraction of conductive powders, which also benefits the conductivity of composite. Furthermore, the forced denser composite decreases the contact resistance between matrices and matrices to powders, which once again contributes to the reduced electrical resistivity of sensors.

2.2.2 Percolation of conductors

As mentioned previously, percolation is defined as the generation and linkage of conductive passages and the induced sharp reduction in resistivity of composite. During percolation procedure, a gentle growth of conductor makes huge differences on the resistivity of cement-based composite, while after exceeding the upper limit of percolation threshold, the resistivity of composite is not greatly affected by the volume fraction of conductor. The percolation is fluctuated due to divergent manufacturing conditions and environments, while it is much more easily affected by the different cement matrices, conductor shapes, and proportions. According to the results presented in Table 2.2, it is believed that the percolation threshold for 2D graphene and CNT reinforced cement-based composite is close to 1% (Andrawes & Chan 2012; García-Macías et al. 2017), which slightly increases to 3% for CF and SF (Chacko, Banthia & Mufti 2007) and surges to 10% for CB. It reveals that compared to the conductive sheets and fibres, the powders have less probability to establish linkage with each other throughout the composite.

Moreover, the content of conductor influences the conductivity and percolation more directly and considerably, due to the added conductor being the only conductive phase compared to the high electrical resistivity of porosity, matrix and solidified paste. Normally, conductors at a lower proportion are individually separated by the matrix and cement paste. Thus, the resultant composite has a resistivity close to that of the plain concrete. As for the cement matrices, percolation is more likely to emerge in cement paste when compared with that in mortar and concrete, owing to the absence of aggregates. Since the percolation of cement-based sensor is different from cement matrices, conductor content, conductor type and conductor shape, the content and shape of conductive additives are very vital. The content is better controlled under the percolation threshold and the shape of fibres with a larger aspect ratio is more appropriate, for the sake of that the sensing ability meets the requirements and the mechanical property and durability could retain their original excellence.

Table 2.2 Electrical properties of cement-based sensors with sheet, fibrous, and powdery conductive fillers

Type of matrix	Type of conductor	Vol.* or wt.* ratio in cement (%)	Electrical properties $\Delta R/R_0$ (%)	Gauge factor	Resistivity ($\Omega \cdot cm$)	Reference
Mortar	Graphene	0 1.2 vol. 2.4 vol.	—	—	7.0×10^6 2.6×10^6 2.5×10^5	Le *et al.* (Le, Du & Dai Pang 2014)
Cement paste	CNT*	0.2 wt. 0.3 wt.	0.02 0.03	—	—	Andrawes *et al.* (Andrawes & Chan 2012)
Cement paste	CNT	0.6 vol. 0.7 vol. 1.2 vol.	—	1 50 2	—	Garcia-Macias *et al.* (García-Macías et al. 2017)
Cement paste	CNF*	0.5 wt. 1.0 wt. 2.0 wt.	0.9 1.0 1.8	—	—	Galao *et al.* (Galao et al. 2014)

Cement paste	CF*	0.1 wt. 0.5 wt. 1.0 wt.	13 3 2	—	—	Baeza *et al.* (Baeza et al. 2013a)
Concrete	CF	0.5 vol. 2.0 vol. 3.0 vol.	0.37 1.01 1.32	—	—	Chen *et al.* (Chen & Chung 1996)
Cement paste	CF	1.0 vol. 3.0 vol. 5.0 vol.	—	—	675 66 17	Chacko *et al.* (Chacko, Banthia & Mufti 2007)
Cement paste	CF+CNT	15vol. CF 15vol. CF+1vol. CNT	26 23	—	—	Azhari *et al.* (Azhari & Banthia 2012)
Cement paste	SF*	0.36 vol. 0.72 vol.	—	—	57 16	Wen *et al.* (Wen & Chung 2003)
Mortar	SF	0.2 vol. 0.5 vol. 0.8 vol. 1.0 vol.	—	9 100 5195 95	—	Teomete *et al.* (Teomete & Kocyigit 2013)
Mortar	CB*+SF*+CF*	15 wt. SF +0.5 wt. CB 15 wt. SF +0.5 wt. CF 15 wt. SF +1 wt. CF 15 wt. SF + 0.5 wt. CB +0.5 wt. CF	—	1.6 327 332 17	—	Wen *et al.* (Wen & Chung 2007)
Mortar	Conductive clay +CF	50 vol. clay +0.6 vol. CF 30 vol. clay +0.6 vol. CF 30 vol. clay +0.9 vol. CF	13 17 16	—	—	He *et al.* (He et al. 2014)
Cement paste	Nano-graphite	2.0 vol. 3.0 vol. 5.0 vol.	0.53 2.5 15.6	—	—	Sun *et al.* (Sun et al. 2017)

Mortar	Graphite	10 vol. 16 vol. 22 vol.	—	—	9.56×10^3 8.45×10^3 7.50×10^3	Garcia *et al.* (García et al. 2009)
Cement paste	CB	15.0 wt. 20.0 wt. 25.0 wt.	—	55.3 37.7 51.9	—	Li *et al.* (Li, Xiao & Ou 2006)
Mortar	Nano-Fe_2O_3	0.3 wt. 0.5 wt.	20 45	—	—	Li *et al.* (Li, Xiao & Ou 2004)

Note: CNT* means carbon nanotube; CNF* means carbon nanofiber; CF* means carbon fibre; SF* represents steel fibre; CB* represents carbon black; vol.* means volume fraction; wt.* represents mass fraction.

2.2.3 Treatment of conductors

Surfaces of conductors are often pre-treated by gas-treating, coatings or solvent soaking for two major purposes: (1) Pre-treatments, through a process of conductors to meliorate the mechanical, physical and electrical properties of cement composite; and (2) Pre-treatments to facilitate uniform dispersion of conductors. Fu et al. (1996b) found that ozone treated CF reinforced cement paste had better tensile strength, modulus and durability than its counterpart with non-treated CF; they experimentally testified that the improvements mainly from the elevated bond strength between the fibres and matrixes. As for the electrical property, the composite became more electrical sensitive after the treatment. Meanwhile, the fractional changes of resistivity performed uniformly to loading with good repeatability, and the irreversible resistivity in each cycle was significantly reduced and eliminated in comparison to plain CF reinforced sensors (Fu, Lu & Chung 1998). Similarly, the impacts of surface characteristics of SFs on the mechanical property of cementitious composite have been investigated by different researchers (Hughes & Fattuhi 1977); they concluded that the bond strength between SF and matrix is greatly strengthened by the coatings as well roughness and degreasing of the fibres. For the piezoresistivity of pre-treated SF reinforced cement-based sensor, a high-strength sensor with compressive strength up to 120 MPa was produced by using

brass coated SF (Sun et al. 2014). The curves of resistivity with respective to strain showed little noises with good repeatability and sensitivity, indicating the coated fibre was much more appropriate for the reinforcement of cement-based sensors.

Another function of pre-treatments relates to the dispersion of conductors. Especially for nanoparticles reinforced composite, well dispersion of the conductor is crucial to the workability of cement-based composite. Normally, the use of ozone, HNO3 solutions and other chemical compound with strong oxidizing property is predominant to maintain the surface stability of nanoparticles and benefit well dispersion. It is believed that carboxylic groups are created on the acid treated CNT, which could bring 19% and 25% increment on the compressive and flexural strength, respectively (Li, Wang & Zhao 2007). More details on dispersion will be given in the section of manufacture procedure.

2.3 Non-conductive phase

2.3.1 Types of non-conductive phases

Non-conductive phase serves as a matrix of cement-based sensors. It can be either cement paste, mortar or concrete. Cement paste is extensively used due to its relatively better conductivity (Wang et al. 2013). Cement mortar has an electrical resistivity of approximately 10^6-10^7 Ω·cm, and investigations also implied that SF reinforced mortar could achieve excellent piezoresistivity (He et al. 2014). Due to the existence of coarse aggregate, piezoresistive concrete sensors generally have high electrical resistivity (up to ~10^9 Ω·cm). Its application is limited but it still has attracted some research attempts (Wang, Dai & Wu 2008). In other words, with the existence of aggregates, the sensitivity of cement-based sensor is weakened, owing to the imperfect crack controlling capacity of conductive fibres under the interaction of aggregates. Meanwhile, aggregates tend to separate conductive passages by increasing the contact probability with the conductive phase, rather than boosting the contacts among conductors.

2.3.2 Fractional changes of resistivity

Fractional changes of resistivity are the ratio of resistivity changes to its initial resistance values. Parvaneh et al. (2019) proposed that the fractional changes of resistivity for piezoresistivity-based concrete is still satisfactory enough as a strain sensor with the amount of CNT larger than 2% to the weight of cement. Similarly, Coppola et al. (2011) conducted several experiments on CNT reinforced cement paste and mortar, and gave their fractional changes of resistivity under loadings. Chen et al. (1996) investigated CF on the electrical response of mortar and concrete, and compared their different fractional changes in resistivity. As depicted in Figure 2.4, the fractional changes of resistivity from these studies during the process of loading and unloading are presented and compared. Obviously, even mixed with different conductors and contents, the cement paste's fractional changes of resistivity are times larger than mortar and dozens of times larger than that of concrete. This was also confirmed by García-Macías et al. (2017) whose tests indicated that the resistivity changes of paste are dozens of times higher than those of mortar and concrete.

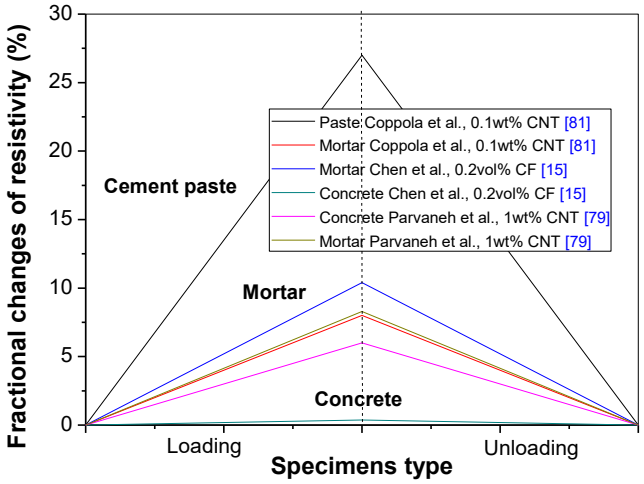

Figure 2.4. Fractional changes of resistivity in different cement matrices during loading and unloading.

2.3.3 Effect of paste proportion and composition on piezoresistivity

2.3.3.1 Water-to-cement ratio

Han et al. (2012) investigated piezoresistive sensitivity of composite with water-to-cement ratios of 0.6 and 0.5, respectively and concluded that the former is more sensitive to the electrical resistance changes under compression. Contrarily, Kim et al. (2014) believed that lower water content both benefits both fibre dispersion and piezoresistivity. As the water-to-cement ratio decreased, the piezoresistivity sensitivity of CNT reinforced cement composite was improved and the piezoresistive has a close connection with rheological property, therefore the controversy from the above studies maybe come from the difference in composite rheology. In other words, in comparison to the impacts by water-to-cement ratio, the rheology might be the root responsible for the distribution of conductors, electron movements and generation of the conductive paths in cement-based sensors.

2.3.3.2 Supplementary cementing materials (SCMs)

SCMs like silica fume, fly ash and slag greatly affect the electrical properties and piezoresistivity of cementitious composite (Wen & Chung 2001). Kyi et al. (1994) evaluated the effects of silica fume and fly ash by measuring the electrical conductivity, confirming their influences on electrical property. Chung (2005) investigated the efficiency of silica fume on the electrical resistivity of composite, and concluded that the silica fume lower the resistivity over two orders of magnitude. When studying the pore characteristics of cement-based sensors, Kim et al. (2017) observed that large pores (1.0 μm) turned into small pores (0.1 μm) with addition of silica fume, and meanwhile, the fractional changes of resistivity was also greatly improved. Figure 2.5 illustrates the electrical resistance alteration with the existence of silica fume. It is clear that for all investigations the silica fume modified composite has lower electrical resistance compared to the plain and reinforced composite. In general, as additives in cementitious composite are normally nonconductive and small-scale, their functions mainly

result from the filling effect and minimising the size of porosity to improve the piezoresistivity of sensors.

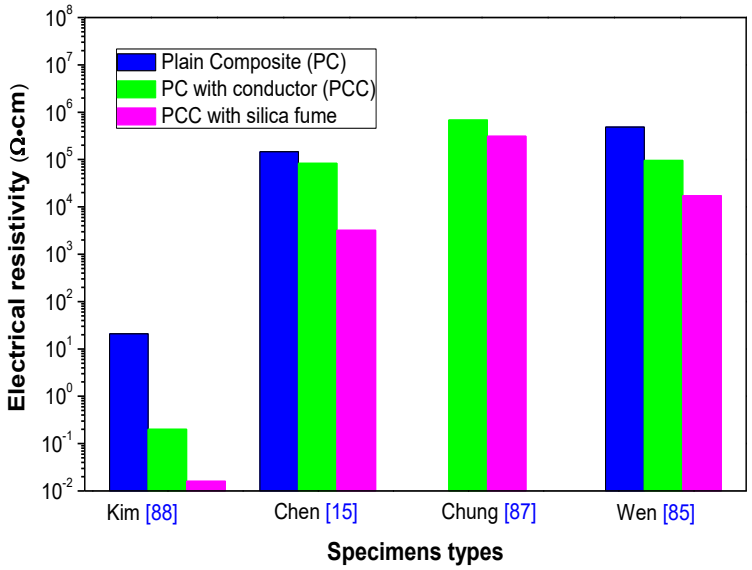

Figure 2.5. The effect of silica fume on electrical resistivity of cement-based sensors.

2.3.3.3 Chemical admixture

Even through having poor electrical conductivity, latex polymeric particles can change the electrical properties of cementitious composite. Wang et al. (2018) investigated the effects of latex on the electric permittivity of cementitious composite, and reported the increase of electric permittivity with additional latex. Chen et al. (1996) studied the latex added cement mortar, which showed lower fractional changes of resistivity than plain mortar under compressive, tensile and flexural loadings. Methylcellulose and other chemical additives of defoamer are also commonly used as dispersant in piezoresistive-based composite. Dispersion amelioration of conductive phase in composite may be critical in determining the piezoresistive expression. Chen et al. (1996) compared the effects of methylcellulose and latex on the piezoresistivity of composite. They found that higher fractional changes of resistivity for methylcellulose added composite during compression, while latex added composite was larger in fractional changes of resistivity during tensile and flexural loadings.

2.3.4 Effects of steel reinforcement on piezoresistivity

Different from cement paste and mortar which are normally unreinforced, structural concrete is normally reinforced with steel. The embedded longitudinal steel bars and stirrups with excellent conductivity will absolutely affect the conductivity of cement-based sensors. Hence for self-sensing concrete elements, the priority is to eliminate the conductivity interference from the reinforcement. Wang et al. (2008) suggested a method of coating the steel bars and stirrups by insulated epoxy resin to completely eradicate the metallic conductivity, with only four uncoated stirrups embedded into the concrete as electrodes to measure the electric resistance. There was a great repeatability of the fractional changes of resistivity at the first 5 cycles under the flexural loading, before the irreversibility was greatly increased with the loading cycles. For the epoxy resin coated steel bars reinforced concrete sensors, their workability and multi-functionality depend on the non-destructive epoxy resin coatings. When the coatings are corroded and steel is exposed in the cement substrate, the electrons will not move from the bridges between conductors and matrix, but rather moving in the conductive steel bars and leading to greatly decreased and invariable resistivity under any forces. Therefore, the long-term protection of non-conductive coatings of steel bars and stirrups is significant for the reinforced piezoresistivity-based concrete.

2.3.5 Discrepancy in Poisson' ratio

In application, cement-based sensors embedded in concrete will go through different extents of Poisson effect, which might affect the piezoresistive responses. Under compression, the axial deformations of the embedded sensor and the concrete are assumed to be identical, while the transverse deformation of these two materials may be different. Due to the difference in Poisson' ratios, the sensor and the examined concrete could generate interaction force in the interface. For SF added cement-based sensor, it has been formulated by Sun et al. (2014) and Xiao et al. (2011) that the stress σ_i in surfaces of these two materials can be expressed as Eq. (1):

$$\sigma_i = (\gamma_1 - \gamma_2)\sigma \quad (1)$$

where σ_i is the stress in the transverse direction; γ_1 means the Poisson' ratio of concrete; γ_2 means the Poisson' ratio of the embedded sensor; and σ represents the stress in the loading direction.

Gauge factor means the electrical resistance changes per unit strain of sensors. The Poisson effect under loading can cause this effect. Pioneering work has proved that for CF reinforced cement-based sensors, the gauge factor is upper to -390 in the transverse direction during compression and -59 during tensile loading (Wen & Chung 2000). However, existing experiments for investigating piezoresistivity of cement-based sensors were restricted to uniaxial compression rather than multiaxial compression coupled with confining stress. Thus, undoubtedly the piezoresistivity of one-dimensionally compressed cement-based sensor will be different from its counterpart in three-dimensionally compressive forces. According to the tests by Wu et al. (2005) on CF reinforced self-sensing mortar, the fractional changes of resistivity and gauge factor showed great differences in biaxial and uniaxial compression, with the gauge factor under biaxial compression larger than that of uniaxial compression. In other words, the piezoresistive sensitivity of cement-based sensors under biaxial compression is superior to that under uniaxial compression. Therefore, the sensing ability of cement-based sensors might be more accurate and sensitive if the calibration of cement-based sensors is conducted under the real stress condition of tri-axial compression rather under one dimensional loading.

2.4 Manufacture of sensors

2.4.1 Dispersion of conductive materials

2.4.1.1 Effects of surface treatment of conductors

To solve the dispersion difficulty of nanomaterials (especially CNT) in composite, surface functionalization of nanomaterials is becoming a research hotspot (Dong, Li, Luo, et al. 2020).

Hou et al. (2013) manufactured a piezoresistivity-based strain sensor with the conductor of alkyl-functionalized graphene, and observed the homogeneous dispersion of graphene in the composite. Also, it was found that the percolation threshold of alkyl-functionalized graphene was reduced to as low as 0.63%. Contrarily, Costa et al. (2014) draw a conclusion that the covalently functionalized CNT reinforced piezoresistivity-based sensor showed higher percolation to 8 % in weight than that of pristine CNT (around 1% in weight to cement). It indicated that the covalent functionalization might block the conductivity of the composite owing to the disturbance of conductance of the CNT.

2.4.1.2 Effects of surfactants in cement-based composite

With existence of surfactants, the surface energy of nanoparticles is reduced, so as the probability of agglomeration. According to the investigation by Coppola et al. (2011), in comparison to the treatment by ultrasonication, the surfactant treated CNT reinforced cement-based sensor showed better piezoresistivity. But an opposite conclusion was reported by Xun et al. (2009) who believed the conductive passages are more likely blocked by the surfactant, which is detrimental to piezoresistive response of the CNT reinforced composite. In the experiments by Coppola et al. (2011), the ultrasonication for surfactant treated specimens lasted 2 h, but only 10 min for the single ultrasonic treated specimens. This may be responsible for the better piezoresistivity in the surfactant assisted composite. However, if comparing surfactant-treated CNT with acid treated CNT in Xun et al. (2009), the improvement on piezoresistivity for the former is less significant.

Surfactant for the dispersion of powder materials also affects the electrical property and functionality of composite. To achieve the ability of electromagnetic wave absorption for composite, Dai et al. (2010) mixed the same amounts of surfactant and CB in water beforehand to assist powder dispersion in the cementitious composite. Similarly, Li et al. (2006) used

superplasticizer for the dispersion of CB in the composite, and the amount of 1.5 % by weight of cement could make composite with excellent piezoresistivity.

2.4.1.3 Sonication

Sonication is one of effective methods for conductive nanoparticle dispersion in composite. It is believed that the sonication time is crucial for the dispersion efficiency of nano-materials, as insufficient sonication time leads to bad piezoresistivity. However, according to the study conducted by Qiu et al. (2013), the CNT has the tendency to break into short tubes and reduce the conductivity if the sonication time lasts too long. Similarly, the electrical conductivity of nanoparticles reinforced composite was observed decreasing as the sonication time increased from 2 to 5 h. Yun et al. (2007) proposed that the bond between nanoparticles might be strengthened for the excessive sonication time.

2.4.2 Rheological properties of composite

2.4.2.1 Rheological properties

Rheological property of composites has been investigated because of its great influences on dispersion of conductors and aggregates, viscosity and bond strength (Ozyurt, Mason & Shah 2007), which in return greatly affects the piezoresistive output. Vipulanandan et al. (2015) conducted rheological and electrical tests of composite with different water-to-cement ratios, and they proposed that the rheology and viscosity decreased with increasing water-to-cement ratio and the composite with a lower viscosity showed worse piezoresistivity. Meanwhile, bond strength between matrices and conductors is vital to conductive passages' linkage, where the fractional changes of resistivity and piezoresistivity mainly directly affect the strain-sensing ability (Fu & Chung 1995).

2.4.2.2 Rheology modification

Mixing time and intensity, and even the order of ingredient addition may influence the rheological characteristics of composite (Yang & Jennings 1995). Additives, superfine mineral

admixture and water to binder ratio in particular directly affect the rheological properties. Generally a higher water binder ratio leads to lower apparent viscosity and worse rheology, whilst insufficient water could prohibit the hydration of cement and influence the final strength of composite. Therefore, plasticizer is always used to ensure the composite having both satisfactory mechanical and rheological characteristics. Papo et al. (2004) investigated the effect of superplasticizers on the rheological property of cement paste and concluded that the polyacrylate superplasticizer was the best to meliorate the rheology of composite. This is mainly due to the hydrophobic groups attached on the surfaces of cement particles and slowing down the hydration and agglomeration rate of mixture.

As for using mineral admixture for rheological modification, Ferraris et al. (2001) used the ultrafine fly ash to improve rheology of cement paste and proposed that the modified concrete rheology could maintain the mechanical properties and reduce cost, eliminating the use of more water and superplasticizer. It is believed that the mineral admixture affects the rheology of composite like the role of sand. Similarly, Chung et al. (2005) found that the composite with silica fume with an average particle size of 0.1 μm (used at 15% by mass of cement) worked very well to improve rheology.

2.4.3 Curing

2.4.3.1 Curing methods

Stream curing, moist curing and air curing are mostly used for cement composite curing. concrete steam-cured in early age can achieve high mechanical strength and durability (Liu, Xie & Li 2005). At high curing temperatures, the hydration of cement and induced drying shrinkage are accelerated. The rapidly formed hydration products at early age, however, may wrap the unhydrated cement particles and prevent water from entering them, resulting in a non-uniform microstructure of the paste that affects the conductive framework formation. Moist curing improves cement hydration and allows hydration products gradually to fill the spaces

between unhydrated cement grains, thus providing a denser microstructure and higher strength, especially long-term strength for the paste. However, non-conductive hydration products in moisture environment enhance the resistivity of cementitious composite. Besides, moisture may more easily induce the effects of capacitance and inductance than dry condition, which may cause larger electrical resistivity of cement-based sensor. As depicted in Figure 2.6, results from both Banthia and Chacko et al. (2007) showed that the moist cured conductive mortar has higher resistivity than air cured mortar. There is also a tendency for the resistivity of moist cured sensors to increase with the increasing curing ages while the value remains stable for the counterparts cured in air; such differences possibly are owing to the huge water content alteration during the moist curing process.

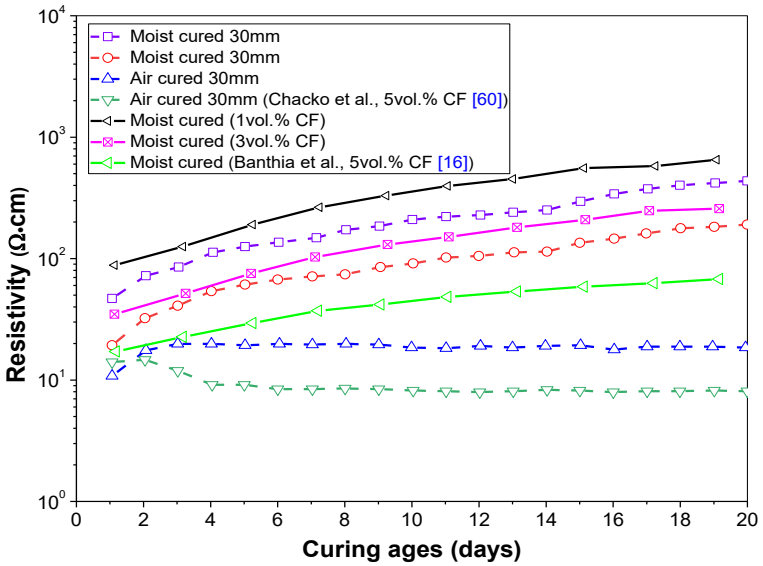

Figure 2.6. Effect of air and moist curing on the resistivity of cement mortar with curing ages.

Air curing with less moisture means a slower hydration rate at the early age. According to the research by Whiting et al. (2003), the resistivity of air-cured plain concrete is larger than that of moist cured. The discrepancy is probably due to their different conductive mechanisms. For the cement-based sensor, the conductors in composite may be enwrapped tightly by the moist stimulated hydration products, leading to the decreased conductivity. But for plain

composite, the conductivity mainly comes from the residual moisture in composite, which explain that the air-cured specimens with insufficient moisture exhibit higher electrical resistivity than the moist cured specimens.

2.4.3.2 Curing time

The piezoresistivity of cement-based sensor is affected by the curing age as the bonding forces between the conductors and matrixes are a function of the curing age. According to the research on CNT reinforced cement sensor by Galao et al. (2014), the fractional changes of resistivity to cyclic stress at an age of 28 days showed better periodicity when compared with the performance at 7 or 14 days. Because of the poorer bonding at the early curing period, the composite possesses lower resistance to external stress when subjected to loading. Furthermore, due to the swift hydration of cement mixture at the early age, the void ratio in the conductor-matrix interface increases owing to the intensive drying shrinkage, which also contributes to the resistivity growth (Fu & Chung 1997).

On the other hand, Chen et al. (2004) investigated the effect of curing time on the conductivity of cementitious composite. An unvaried percolation threshold was observed at different curing ages, even though the conductivity values at different curing times are still different. This is because the percolation threshold mainly lies on the conductors in the composite rather than the moist, although moist significantly affects the conductivity of composites. It suggests that the curing time must be sufficient to eliminate the effect of moist, or the conductivity and piezoresistivity might be greatly affected.

2.5 Loading and deformation

2.5.1 Mechanical loading style and amplitude

Loading style and amplitude affect the failure mechanism of cement-based sensors and indirectly affect their electrical properties like resistance sensitivity and repeatability. Harmonic loading is one of basic loading styles to evaluate repeatability and sensitivity of

cement-based sensors, as well as tiredness and service life. The divergence of mechanical and electrical performances of self-sensing concrete beams under the monotonic and cyclic flexural loading were investigated by Wang et al. (2008). It shows that there is reversible resistivity under cyclic loading with the amplitude below the ultimate load. Otherwise, the monotonous loading approaching to the ultimate load could cause accumulated electrical irreversibility and unneglectable errors. The amplitude of harmonic loading is normally lower than the fracture strength of composites, or the sensor will be damaged by the force that shows as a sudden increase in electrical resistivity. Table 2.3 sums up the fractional changes of resistivity for cement-based sensors under different amplitudes and cycles of harmonic loadings. Under either the compressive, tensile or flexural loading, the average fractional changes of resistivity at lower loading amplitude is less than that at higher amplitude when subjected to the same loading cycles. The increased amplitude can lead to closer conductors and smaller porosity. Meanwhile, the cement matrixes separating the nearby fibres could be damaged, increasing the possibility for adjacent fibres to touch one another to increase the fractional changes of resistivity. Similar to conclusions were drawn by Galao et al. (2014) who observed that the gauge factor of cement-based sensor increased both in the loading and unloading process with cyclic load amplitude increasing from 3 to 9 kN.

Fu and Wang et al. (1996b; 2006) reported experimental results with tensile tests, showing that their fractional changes of resistivity were negative and positive respectively. It is reasonable for the electrical resistivity in the tension zone to increase because of the large cracks, reported by Wang and Chung et al. (2006). However, in the tests by Fu and Chung et al. (1996b), the decreased electrical resistance in the tension zone mainly be explained by the higher contact possibility of conductive fibres because of the cracks in cementitious solid, and the effect of the increased contact outweighs the influence resulting from the slightly larger cracks.

Table 2.3 Effects of loading cycles and amplitudes on the fractional changes of resistivity

Loading types	Stress amplitude (MPa) or ratio to fracture stress	Number of cycles	Minimum $\Delta R/R_0$ (%)	Reference
Compression	0.30	123	-0.003	Fu and Chung *et al.* (Fu & Chung 1996b)
	0.50	217	-0.008	
	0.70	306	-0.020	
Tension	0.30	146	-0.006	
	0.50	252	-0.012	
	0.70	347	-0.020	
Compression	0.03	3	-2.90	Sun *et al.* (Sun et al. 2017)
	0.06		-6.20	
	0.12		-10.4	
	0.25		-15.6	
Compression	0.05	2	-0.050	Azhari and Banthia (Azhari & Banthia 2012)
	0.09	3	-0.170	
	0.18	5	-0.310	
	0.27	5	-0.380	
	0.55	5	-0.500	
Flexure (compression zone)	44.1	3	-0.045	Wang and Chung (Wang & Chung 2006)
	86.1		-0.077	
	129.7		-0.097	
	218.5		-0.183	

2.5.2 Loading cycles and frequency

As for the loading cycles and frequency, it seems that fatigue damage in each cycle is responsible to the irreversible electrical resistivity of sensor, illuminating the gradually increased fractional changes of resistivity under loading cycles, as can be seen from the test results reported by Fu and Chung (1996b) in Table 2.3. Normally, with increasing loading cycles, the irreversibility increases for generation of permanent cracks and deformations. But if the loading cycles are within the threshold, the fractional changes of resistivity show periodicity with loadings until the cycles exceed the limit. Meanwhile, loading frequency significantly affects the polarisation of the cement-based composite, especially when

conductive fibres are used, according to the research by Materazzi et al. (2013). This has negative impact on the piezoresistive sensitivity of cement-based sensor. However, according to the experiments on nano-graphite reinforced cement-based sensor by Sun et al. (2017), the piezoresistive response showed good sensitivity and repeatability in strain controlled compression with different loading rates from 0.8 to 40 mm/min.

As shown in Table 2.3, cement-based sensors very to bear the loading cycles and frequency because of the difference in mechanical modulus and damage resistance ability brought by the reinforcements. For sensors with good repeatability and sensitivity, the applied loading patterns must be within the limits of workability. Moreover, in the real SHM, cement-based sensors are subjected to uncertainty and various loads, such as wind and wave loads whose amplitude, rate and lasting time are randomly controlled by the weather and climate. Thus, the piezoresistive stability of sensors must be maintained for long-term safety monitoring.

2.5.3 Loading on concrete beams

As shown in Figure 2.7, for self-sensing concrete beams with coexistence of compression and tension zones, the compressive and tensile loadings on cement-based sensor lead to different fractional changes of resistivity with usually a negative value for the former and positive value for the latter. This mainly depends on the different fracture mechanisms as electrical resistance of the compression zone is decreased by closer space of matrixes, conductors and compressed pores, while contrarily the increasing resistance is from the development of micro-cracks and lager space of conductors in the tension zone. Meanwhile, it seems that the fractional changes of resistivity in the tension zone is more than one order of magnitude larger than its counterpart in the compressive zone under the same deflection of the concrete beams, as shown in Figure 2.8 (Wen & Chung 2001). This figure also shows that the irreversible resistivity is higher in the tension zone with worse repeatability, while much lower in the compression zone with both excellent sensitivity and repeatability. This might be owing to the much higher compressive

strength of concrete than its tensile strength, which means that the sensor in the tension zone can be more easily damaged to cause the larger resistivity changes.

On the other hand, the experiments by Baeza et al. (2013b) demonstrated higher gauge factor and better sensing capacity in the tension zone. The discrepancy is possibly owing to their different testing conditions where the CFs in the tests were oxidation treated before mixing. This may strengthen the bonding between the fibres and matrixes and increase the tensile strength of the cement-based sensors, making them well preserved even in the tensile zone and thus increasing their electrical sensing ability.

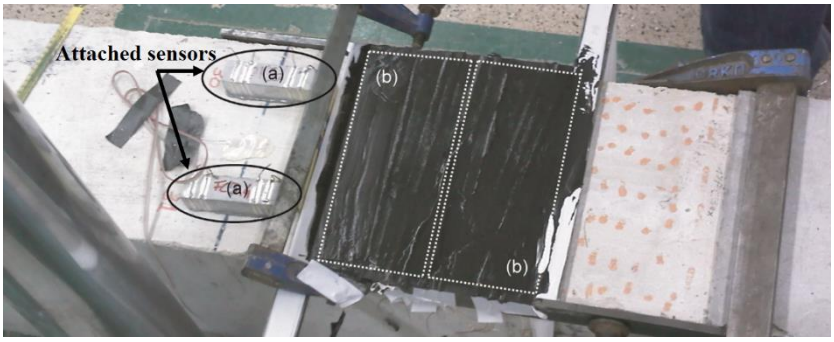

(a) Attached sensors in the concrete beam

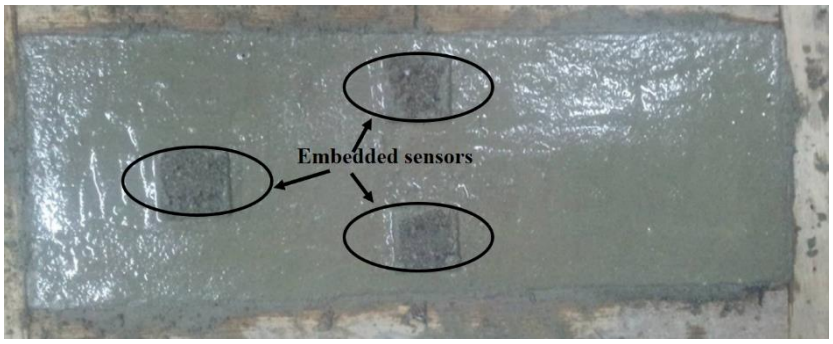

(b) Embedded sensors in the concrete beam

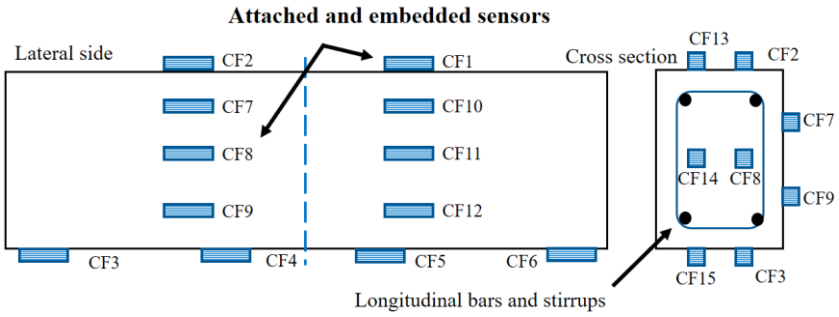

(c) Concrete beam mounted with cement-based sensors

Figure 2.7. Schematic plot of the cement-based sensors applied to the concrete beams with coexistence of tension and compression zone.

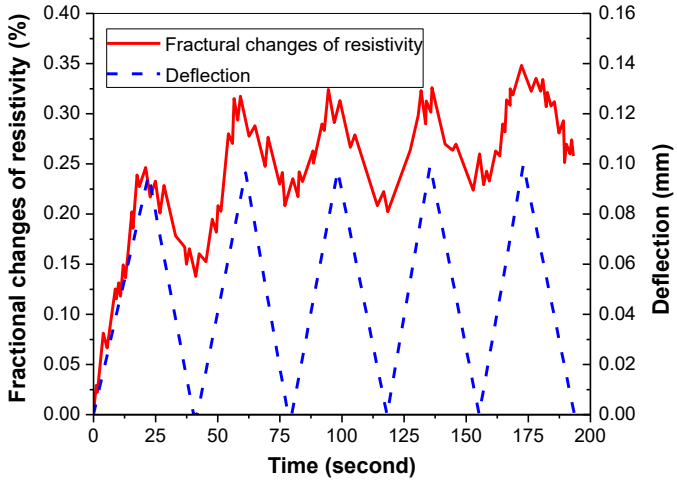

(a) Fractional changes of resistivity in tension zone

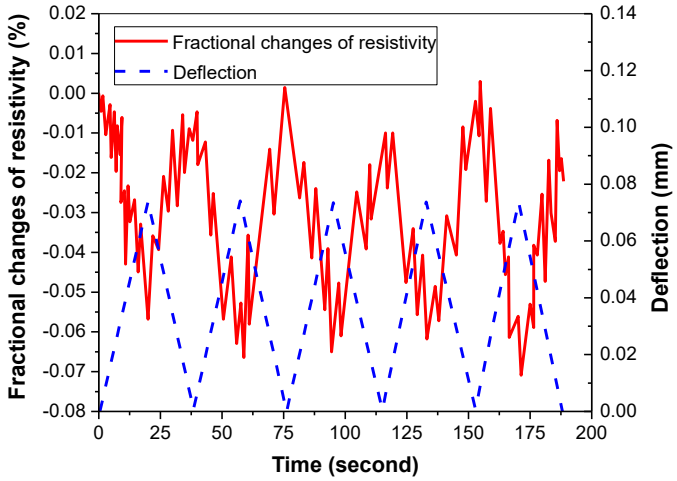

(b) Fractional changes of resistivity in compression zone

Figure 2.8. Fractional changes of resistivity of concrete beam under flexural loading with strain-sensing coating.

2.5.4 Environmental loading

Freeze-thaw cycle and drying-wetting cycle are special conditions involved with periodic alteration of both temperature and humidity. In some extreme climate regions with large temperature differences between day and night, it has been verified that the hydraulic concrete

structure is more likely to have damage caused by freeze-thaw cycles during the long-term service, owing to the expansion and shrinkage of concrete pore solution during cyclic icing and melting.

2.5.4.1 Effects of single freezing or melting on electrical property

Many investigations have evaluated the damages caused by freeze-thaw cycles through measuring the electrical conductivity or resistivity changes of composite (Cutler et al. 2010; Zhang, Cong, et al. 2017). Cai and Liu (1998) studied the electrical conductivity reduction of concrete caused by ice formation. As shown in Figure 2.9(a), the electrical conductivity of cement-based sensor with a water-to-cement ratio of 0.3 and 0.6 lost after one cycle of temperature from -20 to 0 °C and showed poor repeatability. However, Cai and Liu (1998) did not consider the process of melting. Wen and Chung (1999) studied the electrical resistance changes during heating and cooling as the temperature varied from 1 to 45 °C without the freezing procedure; they found that a relatively good reversibility on resistance. Azhari et al. (2008) conducted experiments with a temperature range from 20 to 50 °C, and the experimental results are shown in Figure 2.9(b). It is clear that the electrical resistivity increases after one cycle of temperature change, especially after experiencing the freezing procedure (Cai & Liu 1998).

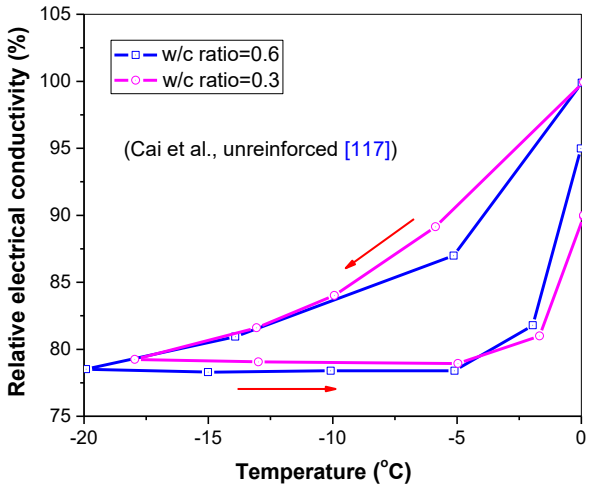

(a) Subzero temperature

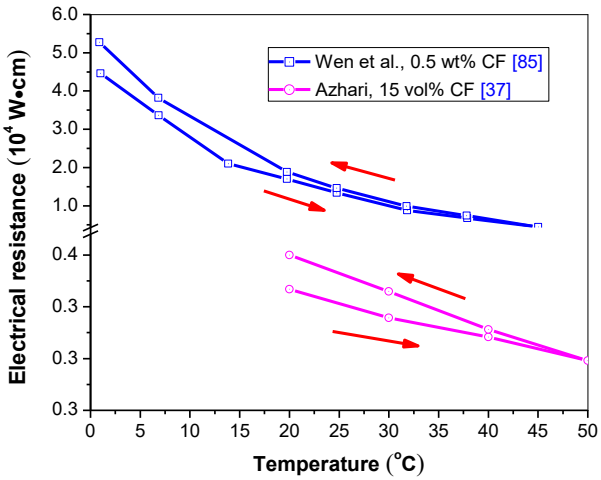

(b) Temperature above zero

Figure 2.9. Conductivity changes after one cycle of temperature change.

2.5.4.2 Effects of freeze-thaw cycles on electrical property

Cao and Chung (2002) evaluated the damage to cement-based sensors during freeze-thaw cycles. From the measured fractional changes of resistivity, they concluded that severer damages were generated in the freezing process than in the heating process. As shown in Figure 10, the fractional changes of resistivity show poor repeatability as the temperature changes from -20 to 52 °C, as shown in Figure 2.10(a), but much less irreversibility expressed when the cyclic temperature varies from 0 to 52 °C without freezing, as shown in Figure 2.10(b). It is thus evident that the ice lenses generation and melting are responsible for the permanent changes of cracks, pores and the related irreversible resistivity. Wang et al. (2013) analysed the changes of depercolation point and ice crystallizing point in the freezing process, and the repercolation point and ice melting point in the heating process. It revealed that the water redistribution during the freeze-thaw cycles is responsible for the altered percolation value. Ding et al. (2015) assessed the efficiency of carbon black, CF and SF added composite to monitor the damages of concrete under freeze-thaw cycles. According to the results, their fractional changes of impedance were increased with the number of freeze-thaw cycles from 10 to 300. Nevertheless, the nearly linear relationship between the fractional changes of

impedance and the number of freeze-thaw cycles demonstrates the suitability of cement-based sensors to monitor concrete damage for concrete in freeze-thaw environment.

To summarise, the irreversible electrical property caused by freeze-thaw cycles mainly comes from the micro-cracks during phase transformation between ice lenses and the liquid states. The ice lenses generation causes volume expansion during freezing, but contraction in the melting procedure. Therefore, the chosen matrices for cement-based sensors should have adequate thermal stability to avoid the deviation caused by physical expansion of matrices, especially in the region with higher temperature differences.

In general, piezoresistivity is individually different for sensors with different input loadings. As mentioned previously, loading style, frequency, amplitude and lasting time all contribute to the incremental changes of micro-structures and electrical resistivity. For a specific sensor, there is an optimal electrical sensitivity for loadings with certain amplitude and frequency. The lifespan of the sensor depends on the loading cycles and the lasting time until the deviation accumulates to cause errors. For the layout of cement-based sensors in concrete beams, different regions express different piezoresistive outputs, and the data reported by different investigators are not conclusive. In addition, studies on freeze-thaw cycle rely on the short term response of electrical properties rather than long-term observation; more explorations should be performed under the circumstance of freeze-thaw cycles in months or even years to serve real applications.

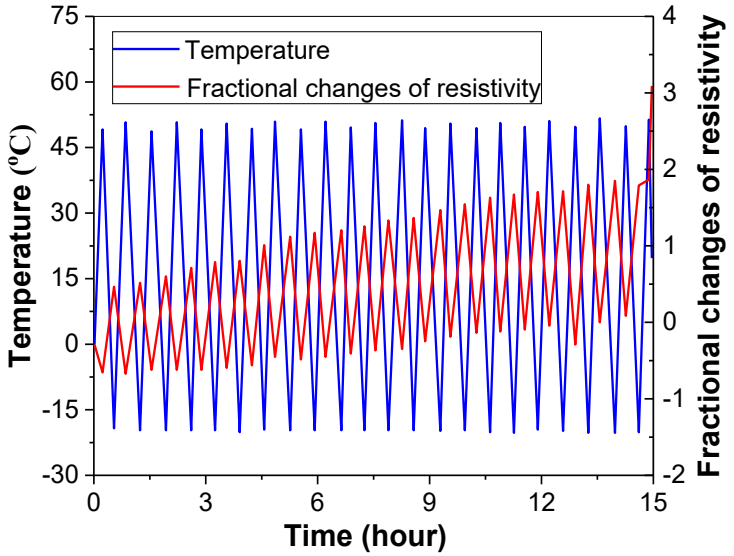

(a) Temperature from -30 to 60 °C with freezing process

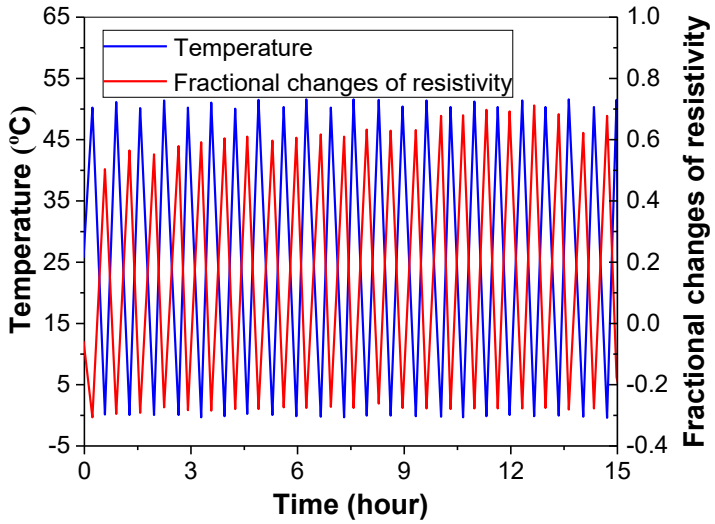

(b) Temperature from 0 to 52 °C without freezing process

Figure 2.10. Fractional changes of electrical resistivity with temperature cycles.

2.6 Electrical resistance measurement

Precision of electrical resistance measurement is vital for using piezoresistive cement-based sensors. Up to now, many improvements have been proposed in order to achieve the accurate electrical resistance of cement-based sensors. In general, the electrode configurations, applied alternating current (AC) or direct current (DC) and other factors like current/voltage intensity all affect the measured electrical resistance and may lead to different piezoresistivity.

2.6.1 Electrode configuration

2.6.1.1 Modes of electrodes

The influence of electrode configuration on the electrical resistance of CF reinforced cement paste was investigated by Reza et al. (2001). The first configuration used the parallel silver plates as electrodes on both ends of the specimens, which linked with an ammeter and voltmeter. In the second configuration, a separate voltmeter was connected to two silver paste circles mounted on the surface of the specimens, coupling with the same silver plates to access the applied current. The third one adopted the commonly-used four-probe method with four silver paste circles to measure electrical resistivity of cement sensor. It is worth mentioning that there were no embedded copper grids to substitute the conductive plates and paste as electrodes to measure the electrical resistance, so the measured resistance refers to the surface resistance rather than the volume resistance. It was found that the indicator changed sensitively with contact pressures on the interface of plate and specimens for the methods of parallel plate, while negligible alteration was observed for the four-probe method. This is mainly owing to the loose contact between the silver plates and the surface of cement substrate where the interface was not smooth enough. Similarly, Han et al. (2007) draw the conclusion that the embedded electrode is better than that on the interface of cement sensor, and the four electrodes method is even better. Consequently, compared to the two-probe and parallel plate method for electrical resistance measurement, the four-probe embedded method seems more accurate for eliminating the influential resistance from current lines, joints and interfaces.

2.6.1.2 Space between electrodes

As indicated in Figure 2.11, for both studies Chacko et al. (2007) and Banthia et al. (1992) the measured electrical resistivity decreased with increasing electrode space. Although there were only two chosen distances analysed by Chacko et al. (2007), the results by Banthia et al. (1992) did demonstrate that the electrical resistivity would become constant when the space of

electrodes reached the threshold. According to the hypothesis by Banthia et al. (1992), this phenomenon maybe lies on the weakened capacitance effect with increasing distance. In general, increasing the distance of electrodes is better than increasing the size of copper grids to minimise the effect of capacitance. Besides, for volume resistance measurement, a larger space of electrodes could also decrease the interference from surface resistance.

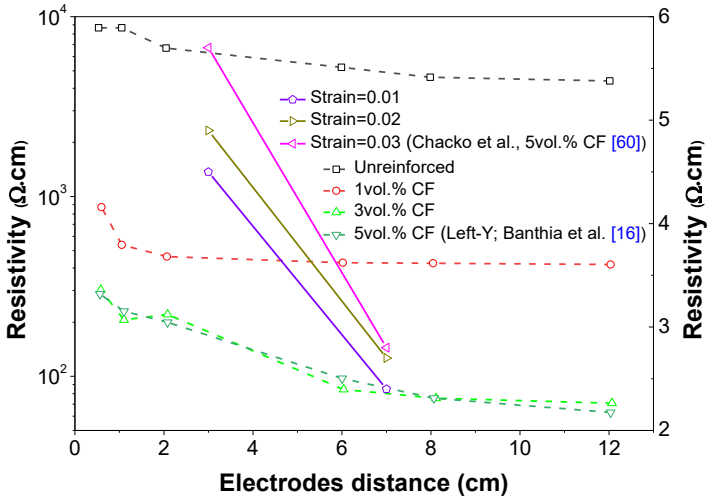

Figure 2.11. Effect of electrodes spacing on the resistivity of cement composite.

2.6.2 Applied current

2.6.2.1 Current types

Both AC and DC can be used for resistivity measurement. Researches have evidenced that DC could generate considerable polarisation in the composite, which may greatly affect the measurement of resistance (Banthia, Djeridane & Pigeon 1992; Reza et al. 2001). As shown in Figure 2.12, the residential voltage progressively decreased to zero at 30 min after the applied voltage was terminated at 20 min, indicating that the polarisation induced by DC may cause severe errors for measuring electrical resistance.

For AC supplied resistance measurement, there are capacitive effect and skin effect, causing a fluctuation in measured resistance. The capacitive effect could be reduced at higher frequency of AC, while the skin effect might come into force when the frequency reaches a threshold. As a result, proper choice of the AC frequency is of equal importance to the other factors. Normally

the frequency is chosen to ensure that the electrical resistance maintains constant with the continual increment of AC frequency.

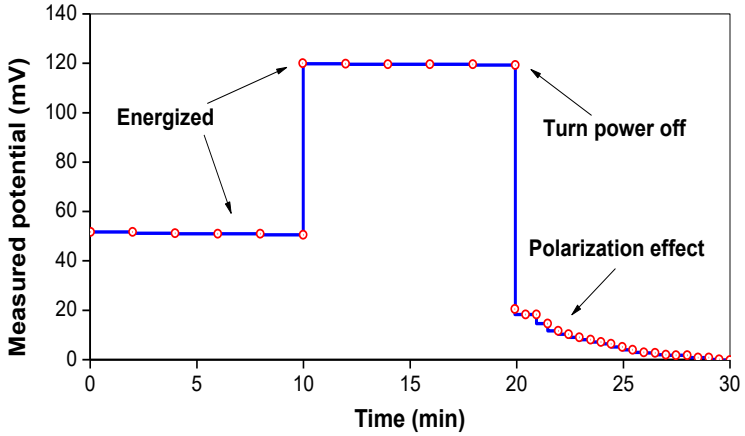

Figure 2.12. Potential drops out of polarisation after the termination of DC current.

2.6.2.2 Current intensity

As for the intensity of applied current/voltage, Galao et al. (2014) applied current of 0.1, 1.0 and 10 mA respectively to cement-based sensors to observe the altered resistivity with longitudinal strain, and the results are shown in Figure 2.13. With increasing current intensity from 0.1 to 10 mA, the repeatability of resistivity is gradually improved and the current of 10 mA shows the best consistency, demonstrating a correlation with the longitudinal strain. However, the research did not check the piezoresistive performance of cement-based sensor with current intensity higher than 10 mA. Nevertheless, it can be predicted that the resistivity of sensor might decrease, since large current intensity may be detrimental to the piezoresistivity of cement sensor. Almost at the same time, Konsta-Gdoutos and Aza (2014) applied voltages of 10, 20, and 30 V respectively to the composite to pursuit the optimum applied voltage. The voltages of 10 and 30 V led to poor electrical property with up to 12% deviation in the measured resistivity, whilst the voltage of 20 V was the best to achieve stability in resistivity. From the above investigations, it can be inferred that a proper intensity of applied current/voltage is significant to achieve the piezoresistivity of sensor with good repeatability and sensitivity.

Perhaps the input current/voltage intensity depends on the types and amount of cement matrix and the coupled conductors. Due to limited researches, no conclusive recommendations can be made in this aspect.

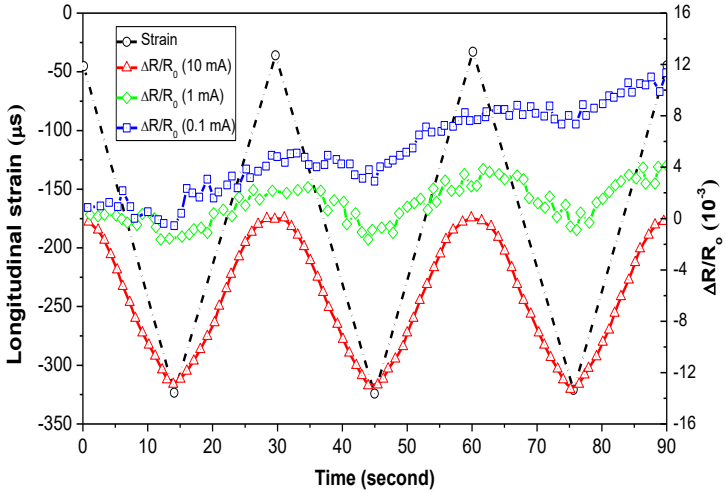

Figure 2.13. Influence of current intensity on piezoresistive responses.

2.7 Environmental conditions on the performance of cement-based sensors

Different from section 2.5.4 to demonstrate influence of freeze-thaw cycles on electrical properties, this section is to review environmental factors on the sensitivity and workability of cement-based sensors. Conductive materials whose atomic cores move more fiercely and disorderedly with increase of temperature have more possibility to overcome the potential energy barrier, causing reduction in electrical resistivity. As a consequence, the resistivity of a cement-based sensor in working circumstance will be affected by environmental temperature changes. Thus, field resistivity measurements depend upon the combined action of external forces and temperature. Humidity also affects resistivity of cement-based sensor by altering the water content inside the composite. It has been proved that the resistivity decreases with increasing relative humidity in exposure environment. However, the appropriate humidity leading to optimal piezoresistive output has not yet been established.

2.7.1 Effects of temperature on piezoresistivity

Reza et al. (2001) analysed the influence of temperature on the electrical resistance of CF reinforced cement mortar, and they found that the resistance decreased as temperature increased from 270 K to 320 K. Compared to plain mortar under the same environmental condition, the CF modified mortar had higher resistance sensitivity to temperature. However, Reza et al. (2001) did not analyse the electrical property in the cool-down process. Furthermore, Chacko et al. (2007) observed that the resistivity of CF reinforced cement-based sensor decreased with increasing temperature but returned back in the cooling process with temperature decreasing to the initial value. The phenomenon maybe relates to the viscosity of pore solution, which decreases with increasing temperature and allows more free movements of ions. However, the results were recorded and compared only in one cycle of temperature alteration between -20 to 65 °C. Meanwhile, Shen et al. (2015) argued that the effect of temperature on piezoresistivity varies in different temperature ranges. The resistivity decreases with increasing temperature lower than a threshold, but increases when the temperature above the threshold. Based on this assumption, they explained that the tunnel effect was compensated by the thermal expansion of a sensor at high temperature, leading to increased electrical resistance.

Figure 2.14 compares the electrical properties of reinforced and unreinforced cement mixtures. It is consistently observed that the resistivity drops with increasing temperature due to fiercer movements of electrons for either plain cement composites and cement-based, except the epoxy-based sensors with an increase tendency at high temperature, which are worth further investigations. It is predictable that the electrical resistivity of cement-based sensor will increase at higher ranges of temperature as a consequence of physical expansion.

To eliminate the influences of temperature on piezoresistivity of cement-based sensor, a compensation circuit is commonly attached onto the cement-based sensor to correct the

temperature drift. Song et al. (2006) and Ou and Han (2009) incorporated a temperature compensation circuit into the electrical circuit to detect and measure the resistance of cement-based sensors in loaded beam. The results showed a good ambient temperature resistance with good piezoresistive sensitivity and repeatability. However, when the temperature is high enough to induce clear thermal expansion, the positive effects of the compensation circuit may be affected and weakened.

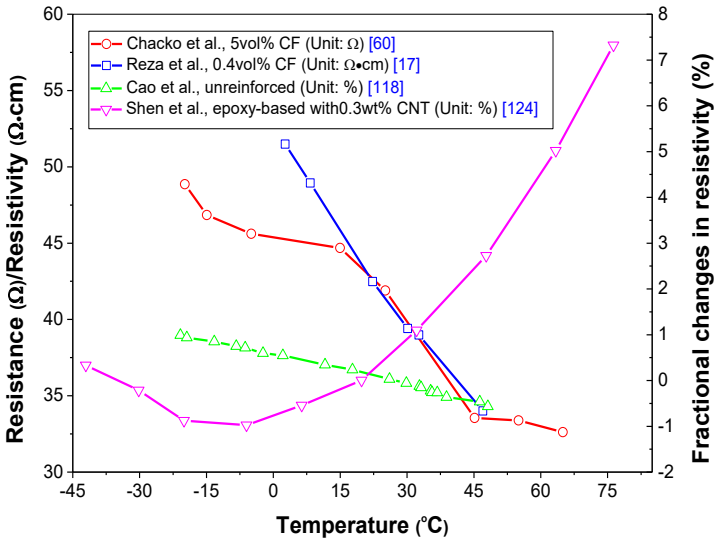

Figure 2.14. Changes of electrical resistivity as a function of temperature.

2.7.2 Effects of relatively humidity on piezoresistivity

As depicted in Figure 2.15, the resistivity of CF reinforced mortar is less sensitive to relative humidity while considerable alterations were observed for the electrical resistivity of plain mortar. The more pronounced effect of humidity on the plain mortar than on the CF reinforced mortar is owing to their conductive mechanisms. The conductivity of plain mortar mainly comes from the moisture in the mortar but the reinforced one is mainly through the conductive phases. Furthermore, by arranging a cement-based humidity sensor in moisture desorption and absorption condition, Rajabipour and Weiss (2007) proposed that the conductivity of sensor primarily depended on the pore solution in gaps, but was also affected by the thickness of absorbed moisture layer in the surface of matrices. The thicker the maintained moisture layer,

the better is the conductivity of the sensor. In order to take the scenario of hydraulic structure monitoring into consideration, Wen and Chung (2008) investigated the piezoresistivity of CF reinforced cement paste sensor in dry state and saturated state, and they found that the resistivity was much lower for wet state, but the gauge factor decreased and the output became instable after soaking. It has already been noticed that the piezoresistive response mainly comes from the pull out and filling effect through connectivity of fibres to fibres and fibres to matrices, while the pore solution with various concentration of ions complicates the piezoresistivity of cement-based sensor when subjected to external forces or any other factors. In addition, for conductors susceptible to corrosion such as steel fibres, no attentions has been paid to the corrosion effect on their piezoresistive response, which needs further study in this area.

Drying methods like air-drying or oven-drying contribute to the moisture content in cement-based sensors and have considerable impacts on the generation of electrical polarisation and capacitance. Sun et al. (2014) compared the effects of air-drying and oven-drying on the influences on piezoresistivity of cement-based sensors, and the results are displayed in Table 4. Due to the moisture loss, resistivity of the oven-dried sensor was more than two times larger than that of the air-dried sensor, but gauge factor of the former was five times larger than that of the latter. Meanwhile, the oven-dried sensor showed better repeatability because of the weakened electrical polarisation. However, even for the oven-dried cement-based sensors, their piezoresistivity also depends on the oven temperature; this temperature dependence has been discussed previously. Since water content in a cement-based sensor could cause severe polarisation and capacitance effect, the drying temperature and lasting are crucial for piezoresistivity of cement-based sensor. For practical applications, more controlled experiments should be conducted to investigate the drying condition on cement-based sensors.

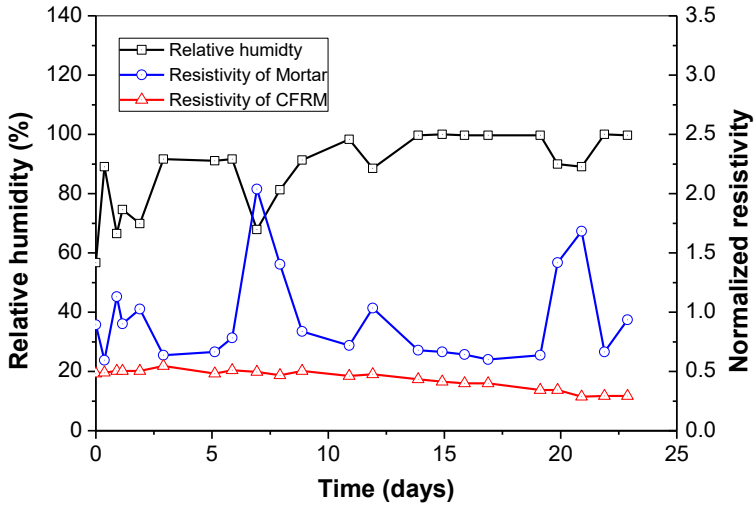

Figure 2.15. Change in resistance with relative humidity for plain mortar and CFRM specimens.

2.8 Summary

With increasing demands on automatic, non-destructive monitoring of concrete structures, intrinsic piezoresistive cement-based composite is gradually attracting more attentions. To develop sensors with high accuracy, both conductive and non-conductive phases, manufacturing procedures, mechanical and environmental loadings, electrical resistance measurements and environmental conditions are key factors for achieving effective piezoresistivity. This paper has systematically summarized these key factors affecting piezoresistivity of cement-based sensors, and main conclusions are as follows:

(1) The piezoresistivity of a cement-based self-sensing sensor is affected by various factors ranging from raw materials, manufacturing procedure, loading patterns, resistance measurement and environmental conditions. All of these factors exert an influence on the piezoresistivity to various degrees and by various mechanisms.

(2) The types of both conductive and non-conductive phases significantly influence piezoresistivtiy of sensors. There is an optimal conductor content, below which the sensor would perform more like plain concrete with high resistivity and low sensitivity, while

excessively higher than which, the dispersion of the conductive phase could become difficult, thus increasing resistivity.

(3) Manufacturing procedure significantly affects the dispersion of conductors and microstructures of cement-based sensors, which in turn influences the sensitivity and repeatability of the sensors. Cement-based sensors show excellent sensitivity and repeatability for freeze-thaw cycles monitoring.

(4) Increased temperature and humidity can enhance the piezoresistivity of sensors within certain limits but decrease the piezoresistivity when the limits are exceeded. Most importantly, accurate measurement of electrical resistance may be the highest priority among priorities.

(5) Uniform dispersion of carbon materials in cementitious composites is critical to the electrical and piezoresistive properties. Moreover, the modelling of electrical and piezoresistive properties of cementitious composites filled with carbon materials has been limitedly investigated. Future studies should be more emphasized on the above-mentioned two research gaps.

CHAPTER 3: PIEZORESISTIVITY OF CEMENTITIOUS MATERIALS WITH CONDUCTIVE RUBBER PRODUCTS

In this chapter, the conductive rubber wastes as conductive fillers were applied in the cementitious materials, to prepare the cement-based sensors. The mechanical, electrical, microstructural and piezoresistive properties of rubberized cement-based sensors were investigated.

3.1 Experimental program

3.1.1 Raw materials

Table 3.1 provides the physical, electrical and mechanical properties of conductive rubber wires, which represents an excellent electrical conductivity as low as 0.008 Ω·cm for aluminium/silver filled rubber. Also, the experimental results show that the rubber products possess poor water absorption ability and low surface activity, which will not greatly affect the hardening process of cementitious composites. The mixture of cement and silica fume was used as binder. The cement used was General Purpose cement, which was manufactured by the mixture of Portland cement clinker, gypsum and additional minerals. The silica fume was to partially replace cement, to reduce the capillary pores of cementitious composite and improve its density and strength. High range water reducer was in the form of aqueous solution of sodium naphthalene formaldehyde sulphonate. It could provide higher early strength and better workability for the composite, with very less air entrainment. Tables 3.2-3.4 list the physical and chemical properties of cement, silica fume and water reducer, respectively. Tap water from the lab was used throughout the experiment.

Table 3.1 Electrical, physical and mechanical properties of conductive rubber product

Conductive filler	Density (g/cm^3)	Volume resistivity ($\Omega \cdot cm$)	Tensile strength (MPa)	Elongation (%)	Shore hardness	Working temperature (°C)
Carbon black	2.1 ±0.25	0.1	1.5	230	70 ±5	-55-160
Aluminium/silver	2.2 ±0.25	0.008	2.5	150	75±5	-55~160

Table 3.2 Physical properties and main compositions of General purpose cement

Appearance	Fineness Index (m^2/kg)	Initial setting time (hr)	Final setting time (hr)	Chloride (%)	Portland Clinker (%)	Gypsum (%)	Mineral addition (%)
Grey	370-430	1.5	3	0.01	85-94	5-7	Up to 7.5

Table 3.3 Chemical compositions and the physical properties of silica fume

Silicon as SiO_2	Sodium as Na_2O	Potassium as K_2O	Available alkali	Chloride (Cl)	Sulphuric anhydride	Moisture content	Bulk density (kg/m^3)
89.6%	0.11%	0.23%	0.25%	0.16%	0.83%	1.5%	625

Table 3.4 Physical and chemical properties of superplasticizer

Properties	Appearance	Density under 20 °C	pH under 20 °C	Chloride content	Air entrainment
Polycarboxylate	Clear brown	~1.07 kg/L	5 ±1	No added chloride	May slightly increase air bubble

3.1.2 Treatment of conductive rubber products

Given the purchased conductive rubber were in the form of wires rather than fibres or crumbs, extra treatment on these rubber wires was conducted before coming into service. The detailed manufacturing process of rubber fibres is depicted in Figure 3.1. Firstly, the rubber wires were

cut into small bars with 30 mm in length. Then the rubber bars were sliced into another 8 rubber fibres. According to the measured diameter, the aspect ratio of the rubber fibres was increased more than threefold compared with the original rubber bars. Moreover, the conductive rubber fibres are flexible and easily bended after the cut and slice treatment.

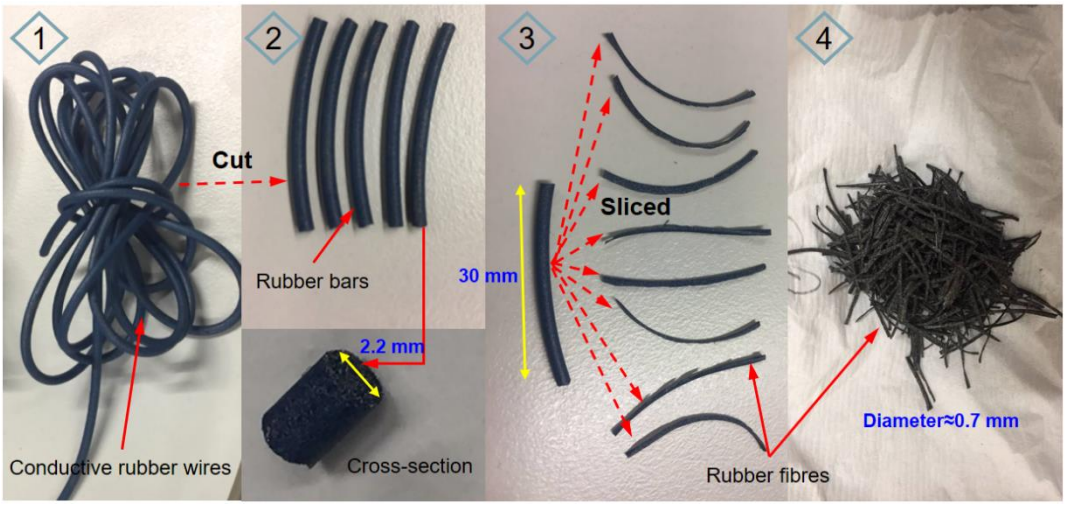

Figure 3.1. Special treatment on rubber wires to produce rubber fibres with high aspect ratio.

For the preparation of rubber crumbs, the rubber fibres were cut by a cutting machine until reaching the similar particle size to fine aggregate. The grading curves of the rubber crumbs and fine sand are plotted in Figure 3.2.

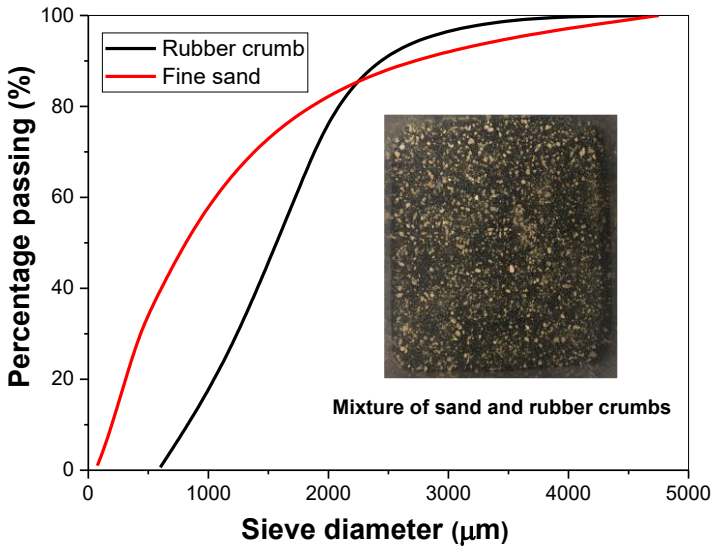

Figure 3.2. Grading curves of the conductive rubber crumb and fine sand.

3.1.3 Specimens preparation

Different contents of conductive rubber from 20 to 140 fibres (0.32-2.24 vol.%) and water to binder (w/b) ratios of 0.34, 0.38 and 0.42 were attempted to explore the conductivity interference by amount of rubber and w/b ratios, as shown in Table 3.5. Water and water reducer were firstly mixed in a Hobart mixer, before adding the mixture of cement and silica fume. The mixing procedure followed the international standard of C305-14, by first mixing at low rate of 140 ±5 r/min for 30 s and then raising the rate to 280 ±10 r/min for another 1.5 min. Afterwards, pour the mixture into the oil treated moulds at the first 20 mm height and vibrate to compaction, before directionally allocate half of the rubber fibres in the centre of composite. Then fill the mould with cement mixture to the height of 30 mm and the same distribution method for the rest of rubber fibres. Afterwards fill up the mould, and two copper meshes with width of 45 mm and length of 65 mm were symmetrically embedded into the cubic composite as electrodes, with the average space at approximately 30 mm. One day curing at standard curing chamber, the specimens were demolded and numbered, before further cured in the chamber with controlled temperature at 25 ±2 °C and humidity of 95%.

Table 3.5 Mixture ratios of cement paste containing conductive rubber fibres

Number of rubber fibres	Rubber content (vol.*)	c/s*	wr/b* (%)	w/b_1*	w/b_2	w/b_3
0	0	9	0.8	0.34	—	—
20	0.32%	9	0.8	0.34	—	—
40	0.64%	9	0.8	0.34	—	—
60	0.96%	9	0.8	0.34	—	—
80	1.28%	9	0.8	0.34	—	—
100	1.6%	9	0.8	0.34	—	—

140	2.24%	9	0.8	0.34	—	—
0	0	9	0.8	—	0.38	—
20	0.32%	9	0.8	—	0.38	—
40	0.64%	9	0.8	—	0.38	—
60	0.96%	9	0.8	—	0.38	—
80	1.28%	9	0.8	—	0.38	—
100	1.6%	9	0.8	—	0.38	—
140	2.24%	9	0.8	—	0.38	—
0	0	9	0.8	—	—	0.42
20	0.32%	9	0.8	—	—	0.42
40	0.64%	9	0.8	—	—	0.42
60	0.96%	9	0.8	—	—	0.42
80	1.28%	9	0.8	—	—	0.42
100	1.6%	9	0.8	—	—	0.42
140	2.24%	9	0.8	—	—	0.42

Noted: vol.* means the volume fraction of rubber fibres to cubic specimen; c/s* represents weight ratio of cement to silica fume; w/b_1* means water to binder (sum of cement and silica fume) ratio; wr/b* indicates the ratio of high range water reducer to binder.

The rubberized cement mortar with five concentrations of rubber crumbs ranging from 0, 10, 20, 30 and 40%, were used to replace fine aggregate. For all composites, the 10% (by mass) silica fume was used to replace cement and the superplasticizer was 0.8% to the weight of binder (cement and silica fume). The application of silica fume can diminish the porosity of composites which is beneficial to the piezoresistive expression. Three groups of rubberized cement mortars were made at water-to-binder (W/B) ratios of 0.40, 0.42 and 0.45, respectively. The selected W/B ratios were to ensure the acceptable workability and compressive strength of the composites. The mix proportion of the rubberized cement mortar is listed in Table 3.6.

Table 3.6 Mix proportion of rubberized cement mortar with various contents of rubber crumb

Index	Cement	Silica fume	Fine sand	Rubber crumb	water	Superplasticizer (%)
M0*	0.9*	0.1	2.0	0	0.40 0.42 0.45	0.8
M10*	0.9	0.1	1.8	0.2	0.40 0.42 0.45	0.8
M20	0.9	0.1	1.6	0.4	0.40 0.42 0.45	0.8
M30	0.9	0.1	1.4	0.6	0.40 0.42 0.45	0.8
M40	0.9	0.1	1.2	0.8	0.40 0.42 0.45	0.8

Note: M0 and M10 present the plain cement mortar and the rubberized cement mortar with 10% CRC, respectively; figures under the cement, silica fume, sand, CRC, water and superplasticizer represent their ratios to the weight of binder, e.g. 0.9* under cement presents the cement to binder ratio of 0.9.

3.1.4 Definition on new sensitive coefficient Fi

Working performance of cement-based sensors is normally assessed according to the fractional changes of resistivity per unit strain, which known as gauge factor, to evaluate the sensitivity of cement-based sensors. It can be expressed as follows:

$$F = \frac{FCR}{\varepsilon} \tag{2}$$

where F means the fractional changes of resistivity per unit strain (gauge factor); FCR means the fractional changes of resistivity and ε represents the compressive strain during the process. Among them the FCR can be represented as:

$$FCR = \frac{\Delta\rho}{\rho_0} \approx \frac{\Delta R}{R_0} \tag{3}$$

where $\Delta\rho$ the changes of resistivity, ρ_0 the original resistivity, ΔR the changes of resistance, and R_0 the original resistance. Considering the loading patterns applied in this paper, the formula is reliable because of the small deformation of cementitious composites.

However, the expressions used cannot achieve the connection between electrical resistivity changes and the loading force (or stress) directly, especially when the force amplitude altered, not alone in the plastic stage of composite. Moreover, for cementitious composites, there exists irreversible deformations in the initial stage, and experimental results from literatures have shown that the gauge factor of cement-based sensors was not unchangeable even in the elastic stage . Therefore in this study, different sensitivity assessment coefficient F_i from the above mentioned gauge factor F was proposed as follows:

$$F_i = \frac{FCR}{\sigma_i} \tag{4}$$

where F_i means the fractional changes of resistivity per unit stress; and σ_i is the stress level in the loading process, which can be altered in different loading amplitudes. The new sensitive coefficient F_i is promising for the evaluation of piezoresistivity in the stage where its sensitivity can be affected by stress amplitude.

3.1.5 Electrical resistivity measurement

Figure 3.3 illustrates the preparation of uniaxial compression machine AGX50, rubber/cement specimens and their connection to multimeter, strain gauge and strain collector in loading process. The compressive loading direction showed same orientation with the length of rubber fibres. In this study, DC rather than AC, was chosen for electrical resistance measurement. To eliminate the problem of polarization, longer time running of SIGLENT SDM3045X digital multimeter to measure the electrical resistance of rubber/cement composite was conducted before the compression, until generating a stable output of electrical signal. In addition, two

probes method to measure the electrical resistivity of rubber/cement composite was applied through embedded two copper meshes, and the resistivity can be calculated as follows:

$$\rho = RA / L \tag{5}$$

where R means the measured electrical resistance in ohm (Ω); A the cross sectional area of copper meshes to specimens in squire meter (m^2); L the distance between two copper meshes, unit: m.

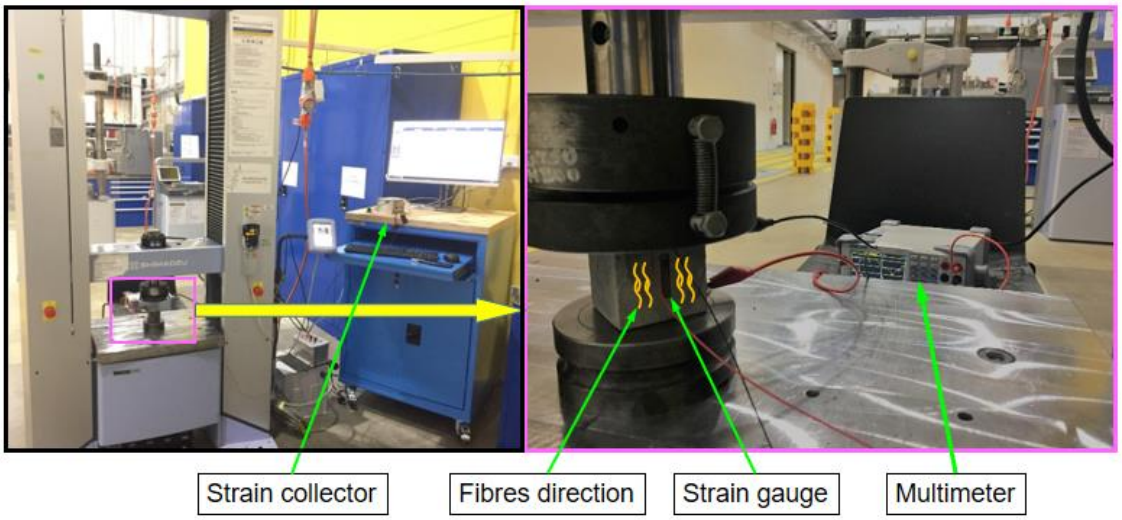

Figure 3.3. Schematic diagram of the compression machine and the multimeter to record resistance.

3.1.6 Flowability

The flowability of the mortar mixtures was evaluated through the flow table test in accordance with ASTM C1437 (Standard Test Method for Flow of Hydraulic Cement Mortar), where the spread diameters of the tested mixture at 0 and 25 drops of the flow table were measured. For each spread, diameters were in three locations and the average value was chosen as the final flowability measurement.

3.1.7 Mechanical properties

To reduce the errors from individual differences, ultimate compressive strength was achieved from the average strength of three identical specimens by the compression machine of UH500.

The loading process is applied by deformation controlled mode, with the loading rate preseted 0.2 mm/min.

3.1.8 Microstructure characterization

The Zeiss EVO LS15 scanning electron microscope (SEM) was used to examine the morphology of the surfaces of saw-cut specimens, rubber fibres, rubber crumb particles and the interfaces between rubber particles and cement matrix. The results are used to elucidate the mechanical and electrical properties of cement mortar in a microscale.

3.2 Cement paste with aligned conductive rubber fibres

3.2.1 Percolation threshold

Figure 3.4 shows the electrical resistivity of composites reinforced by different amounts of rubber fibres in three different w/b ratios ranging from 0.34, 0.38 to 0.42. The chosen of these w/b ratios is mainly due to the excellent fresh property of cement paste. Percolation means the significant electrical resistivity decrease or conductivity amelioration in conductor reinforced composite (Al-Dahawi et al. 2016). Obviously, conductivity percolation could be observed for all rubber/cement composites with increase of rubber content. It could be seen that for composites at the w/b ratio of 0.34 and 0.38, their resistivity was greatly decreased with rubber contents from 60 to 100 fibres (0.96-1.6 vol.%). However, for the composites at w/b ratio of 0.42, the resistivity decreased more gently with rubber content. This may be due to the reduced electrical resistivity by more water content, which diminished the positive effects of conductive rubber fibres on the electrical conductivity. Also, the tendency could be observed that the higher w/b ratio, the lower resistivity of the composite was, demonstrating the influences on resistivity of the water content in cementitious composite.

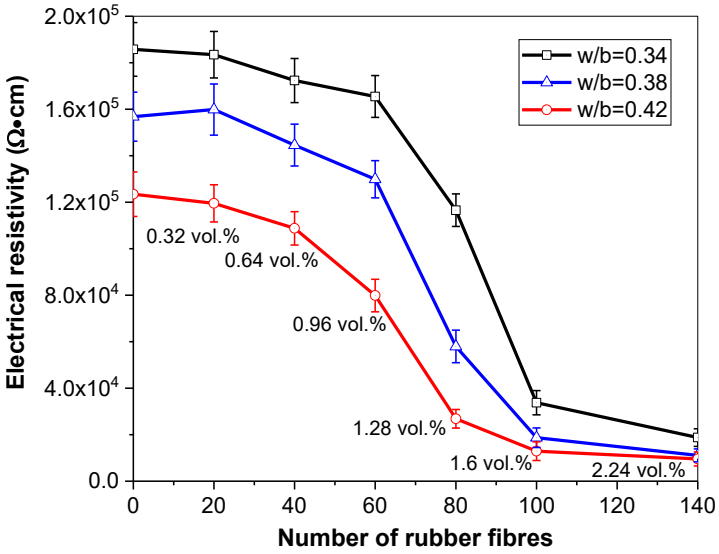

Figure 3.4. Electrical resistivity of rubber/cement composite with different contents of rubber fibres at w/b ratios of 0.34, 0.38 and 0.42.

3.2.2 Piezoresistivity

Fractional changes of resistivity of rubber/cement composite under cyclic loadings could immediately reflect sensitivity, repeatability and stability on the piezoresistivity. The content of conductor had firm relationship to the conductivity and percolation of composites, which was critical to the piezoresistive expression. The water content made contribution to the pore solutions and concentrations, as well as influencing cement hydration process, thus composites at different w/b ratios of 0.34, 0.38 and 0.42 were proposed to explore the optimal water content in the rubber/cement composite. Overall, influences by stress amplitude, rubber and water content have been investigated in the next sections on the piezoresistivity of rubber/cement composites.

3.2.2.1 Composites at w/b ratio of 0.34

Fractional changes of resistivity of rubber/cement composites at the w/b ratio of 0.34, are illustrated in Figure 6, where sub-images Figures 3.5(a) to (f) represents the composites with different rubber contents from 20 to 140 fibres. Generally, the resistivity decreased upon loading and increased upon unloading, despite it was greatly fluctuated for the composite filled

with 140 rubber fibres. Specifically, the composites embedded with less than 140 rubber fibres showed an excellent repeatability on resistivity under cyclic stress below 10 MPa, while a continual increase on resistivity was observed for the composite with 140 rubber fibres. This phenomenon could be simply explained by the formed conductive rubber networks in the composite. The percolation threshold was approximately 60 to 100 rubber fibres (0.96-1.6 vol.%), thus it could be assumed that the connected conductive passages have been established for the composite with 140 rubber fibres. Under the circumstances, small disturbance on the composite might detach the neighbouring rubber fibres and interrupt the conductive networks to cause the increased resistivity.

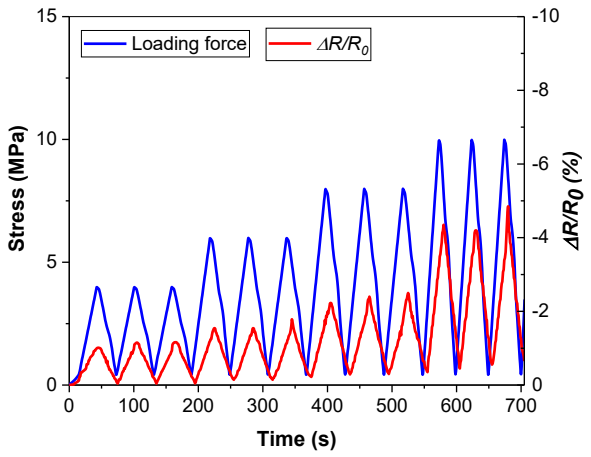

(a) Composite with 20 rubber fibres

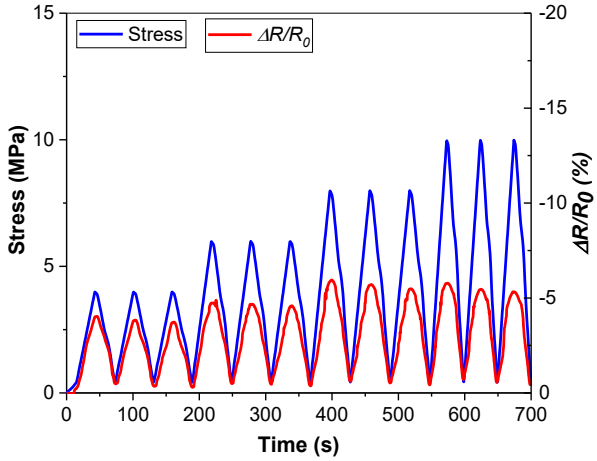

(b) Composite with 40 rubber fibres

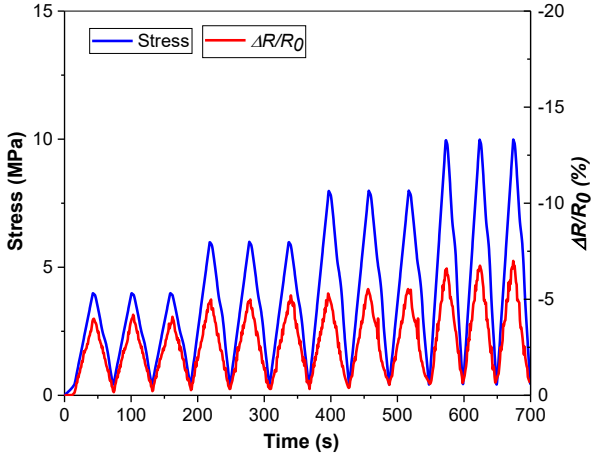

(c) Composite with 60 rubber fibres

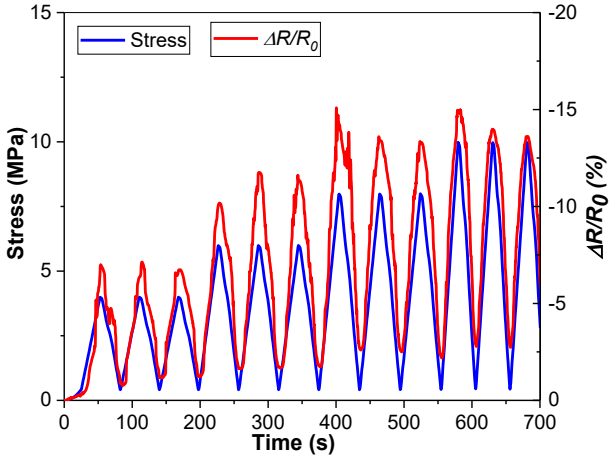

(d) Composite with 80 rubber fibres

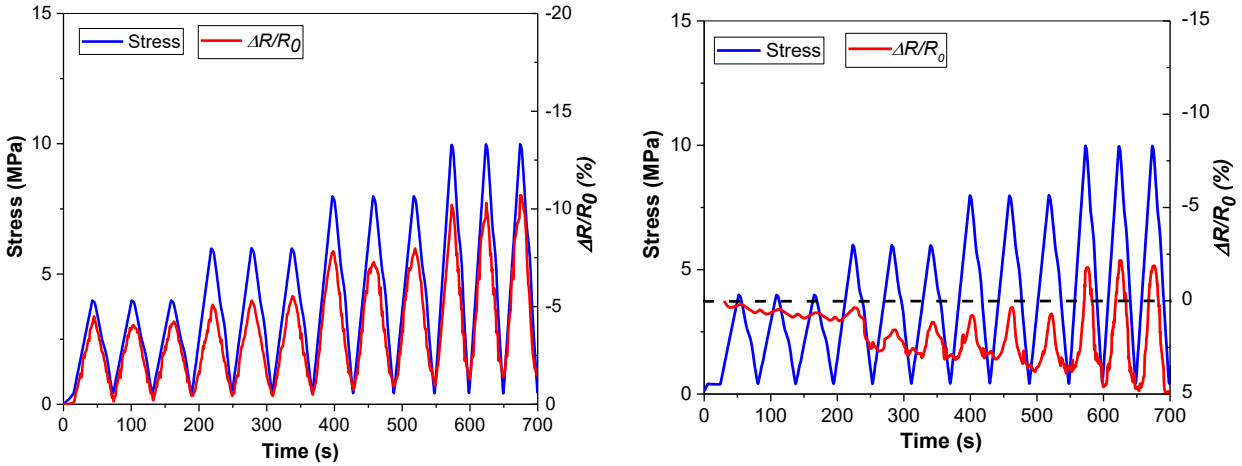

(e) Composite with 100 rubber fibres (f) Composite with 140 rubber fibres

Figure 3.5. Fractional changes of resistivity with different rubber contents and stress magnitudes for the composites at w/b ratio of 0.34.

In terms of the resistivity repeatability, the composites at the w/b ratio of 0.34 showed good performance when rubber content less than 80 fibres, with the deviation narrowed to ⩽1%. However, it seems that the irreversibility increased with rubber content, and reached approximately 2% for the composites with 80 and 100 rubber fibres. For the composite filled with 140 rubber fibres, the resistivity increased gradually with loading process and showed poor repeatability. In addition, for all composites, larger loading amplitudes made more contributions to the irreversible resistivity. However, compared to the values of fractional changes of resistivity, the changes by loading amplitudes could be neglected.

Piezoresistive sensitivity is one of most vital factors to evaluate the application potential of cement-based sensor in engineering application. Based on the rubber installation process, the rubber/cement composite was non-homogeneous and anisotropic, thus the fractional changes of resistivity was nonlinearly altered and fluctuated with loading forces. Table 3.7 lists the sensitive coefficient Fi with different rubber fibres under loading magnitudes from 4, 6, to 8 and to 10 MPa. For all composites, the average values from there cycles for each amplitude were collected, and for the 140 rubber fibres reinforced composite with significant fluctuation,

the fractional changes of resistivity were selected from the minimum and maximum in every cycle ignoring the increasing resistivity. Furthermore, the relationships between conductive rubber fibres, loading amplitudes, and the sensitive coefficient (Fi) were exhibited in Figure 3.6, which demonstrated the dependence of sensitive coefficient Fi on the rubber fibres and stress amplitudes.

It could be seen that for each stress magnitude, the sensitive coefficient Fi firstly increased then decreased with rubber content. It was the composite containing 80 rubber fibres that achieved the best sensitivity, with Fi of 1.725, 1.858, 1.750 and 1.420 at the amplitudes of 4, 6, and 8 to 10 MPa, respectively. The composites reinforced by 60 or 100 rubber fibres possessed secondary sensitivity, and the worse sensitivity was emerged for the composite with 20 or 140 rubber fibres. Therefore, it could be concluded that the rubber/cement composites in the range of percolation threshold were more likely to change its resistivity under external forces, while the composites became insensitive to forces if outside the ranges. In terms of the influences of stress amplitudes on sensitivity, it was observed that the sensitive coefficient Fi was higher when the stress amplitudes were small at 4 and 6 MPa, which gradually decreased with the magnified stress to 8 and 10 MPa. This phenomenon can be explained by the higher stress level which could cause more micro-cracks and disconnect the conductive passages. In addition, the loading forces is continually increasing from small stress magnitude to the high stress magnitude. Therefore, the previous cyclic loadings might cause micro-defects and result in the reduction on electrical sensitivity during the next compression.

Table 3.7 Sensitive coefficient for cementitious composites at w/b ratios of 0.34, 0.38 and 0.42

w/b ratios	Stress amplitudes (MPa)	Sensitive coefficient (F_i) at various rubber contents					
		20 (0.32 vol.%)	40 (0.64 vol.%)	60 (0.96 vol.%)	80 (1.28 vol.%)	100 (1.6 vol.%)	140 (2.24 vol.%)

0.34	4	0.250	0.963	1.025	1.725	1.075	0.050
	6	0.267	0.767	0.847	1.858	0.883	0.258
	8	0.300	0.706	0.685	1.75	0.963	0.331
	10	0.440	0.565	0.670	1.42	1.038	0.661
0.38	4	0.600	1.213	1.290	2.210	1.415	2.500
	6	0.547	0.958	1.075	2.308	1.350	1.300
	8	0.684	0.850	1.125	2.193	1.188	1.438
	10	0.645	0.810	1.155	2.385	1.560	1.301
0.42	4	0.825	0.783	0.533	0.738	0.525	—
	6	0.570	0.763	0.600	0.722	0.833	—
	8	0.579	0.713	0.650	0.721	0.916	—
	10	0.573	0.661	0.960	0.843	1.007	—

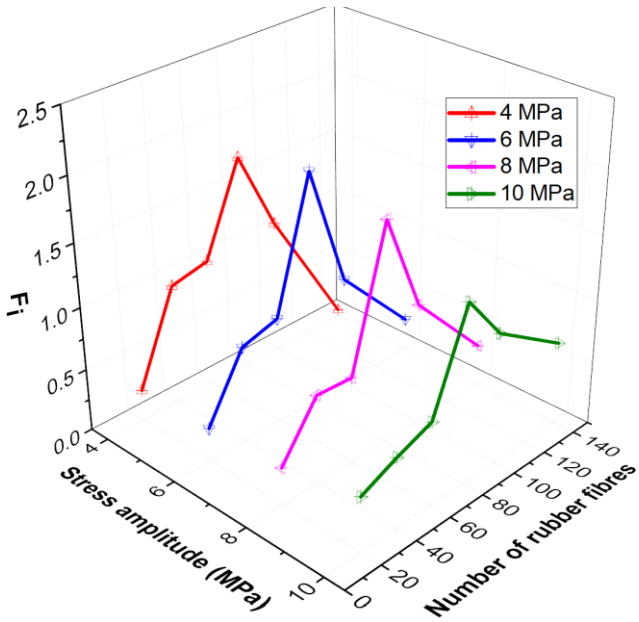

Figure 3.6. Illustration of the relationship between sensitive coefficient, stress magnitude and the rubber fibres for the composite at w/b ratio of 0.34.

3.2.2.2 Composites at w/b ratio of 0.38

The fractional changes of resistivity of rubber/cement composite at the w/b ratio of 0.38 are similar to the counterparts at the ratio of 0.34, as illustrated in Figure 3.7. Apart from the composite with 140 rubber fibres, which showed fluctuated changes of resistivity, the

resistivity changes for other composites were consistent well with the loading forces. Generally, the higher stress magnitude and rubber content of the composites led to higher instability and fluctuation on the electrical resistivity. In comparison to the composites at the w/b ratio of 0.34, much less irreversibility observed for the composites at w/b ratio of 0.38, especially the composite filled with 140 rubber fibres.

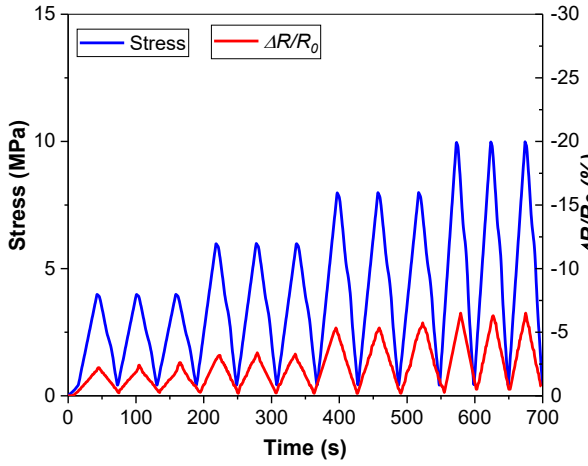

(a) Composite with 20 rubber fibres

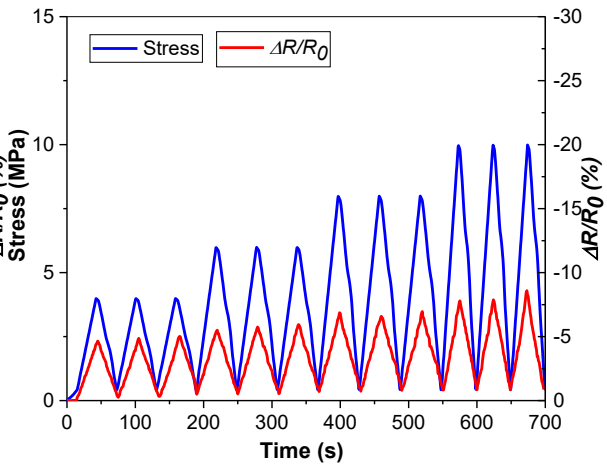

(b) Composite with 40 rubber fibres

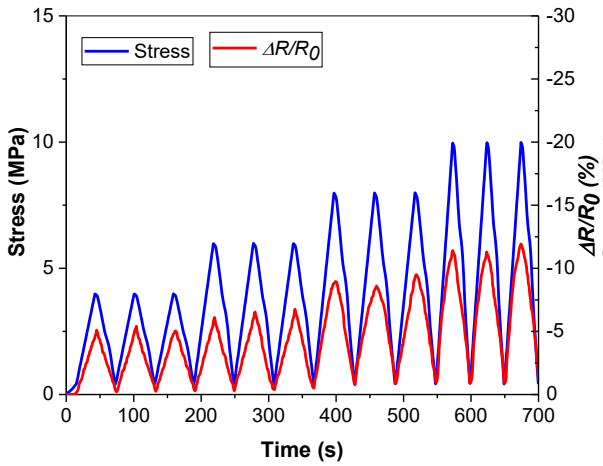

(c) Composite with 60 rubber fibres

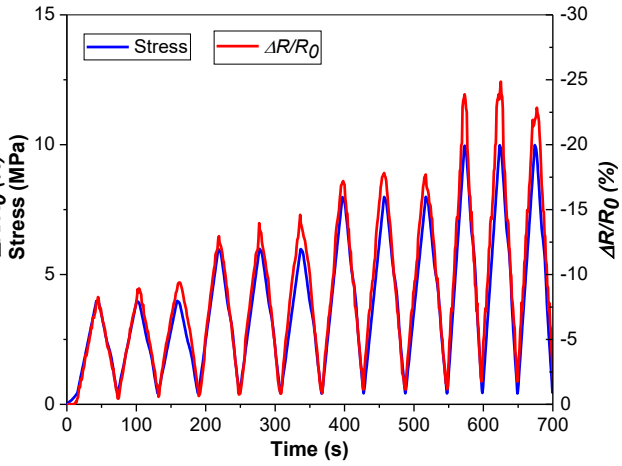

(d) Composite with 80 rubber fibres

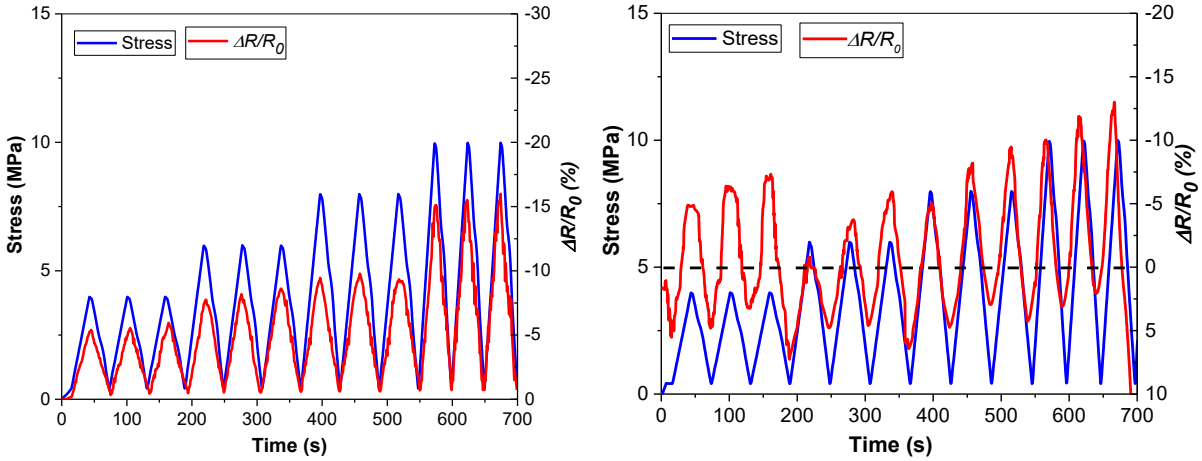

(e) Composite with 100 rubber fibres (f) Composite with 140 rubber fibres

Figure 3.7. Fractional changes of resistivity with different rubber contents and stress magnitudes for the composite at w/b ratio of 0.38.

Similarly, the sensitive coefficient Fi for composites at the w/b ratio of 0.38 were listed in Table 3.7. To more clearly represent the relationship between sensitive coefficient Fi, content of rubber fibres and stress magnitudes, three-dimensional coordinate system was assisted, as shown in Figure 3.8. Except the composites under stress magnitude of 4 MPa, it could be observed that the sensitive coefficient Fi was firstly increased with rubber content increasing to 80 fibres, then decreased when more rubber fibres added. The highest sensitive coefficients Fi of the composites reached 2.308, 2.193 and 2.385, respectively for the stress magnitude of 6, 8 and 10 MPa. Howbeit under the stress magnitude of 4 MPa, the sensitive coefficient Fi of 2.210 was observed for the composite with 80 rubber fibres, which smaller than the coefficient Fi of the counterpart with 140 rubber fibres. As it is shown in Figure 3.8(f), the fractional changes of resistivity were quite large for the stress magnitude of 4 MPa, but it decreased with increasing stress magnitude. The reason is due to the formed conductive networks by excessive conductive rubber, whose networks were more volatile to forces because of more conductive passages. Hence after the first cyclic loading at the stress magnitude of 4 MPa, the conductive

passages in the rubber/cement composite were considerably interfered, and that is why the fractional changes maintained the original value even if the stress increased.

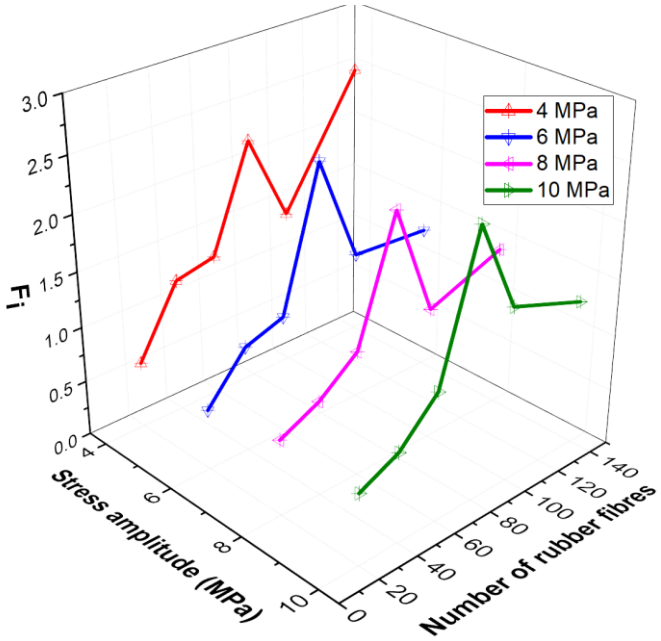

Figure 3.8. Relationship between sensitive coefficient, stress magnitude and the rubber fibres for the composite at w/b ratio of 0.38.

On the other hand, in comparison to the composites at the w/b ratio of 0.34, the discrepancy of sensitive coefficient between various stress magnitudes was reduced, by higher sensitive coefficient in the larger stress magnitude. As the variable was only water content between two composites, it could be deduced that the increased water content from the w/b ratio of 0.34 to 0.38 was beneficial to the piezoresistivity of rubber/cement composite, as well as increasing its sensitivity. Moreover, for the composites filled with 20 rubber fibres, the sensitive coefficient Fi of 0.6 and 0.3 were observed respectively for the composites at the w/b ratios of 0.38 and 0.34. It further demonstrated that the effect of water content was more significant since the less impacts by rubber fibres.

3.2.2.3 Composites at w/b ratio of 0.42

Subjected to cyclic loading from 4 to 10 MPa, the fractional changes of resistivity of rubber/cement composites at the w/b ratio of 0.42 are illustrated in Figure 3.9. It could be

observed that only the composites filled with 20 and 40 rubber fibres showed the consistency between the resistivity changes and stress. Compared with the composite with 20 rubber fibres which represented similar fractional changes of resistivity under any stress magnitudes, the composite with 40 rubber fibres exhibited increased resistivity changes with stress magnitude, although the sensitivity was at a low level. As for the composites reinforced by more than 40 rubber fibres, various degrees of fluctuation were observed. It depicted that for the composites filled with 60, 80 and 100 rubber fibres, moderately fluctuated resistivity changes still have consistency to stress, while irregular changes of resistivity were generated with loading stress for the composite with 140 rubber fibres. Different from the fractional changes of resistivity which normally decreased under load, it was found that the composite with 140 rubber fibres rapidly increased even under small stress. This is due to the great amount of rubber fibres and pore solutions established conductive networks, small disturbance on these vulnerable networks could destroy the rubber fibres' connection to increase the electrical resistivity of composite.

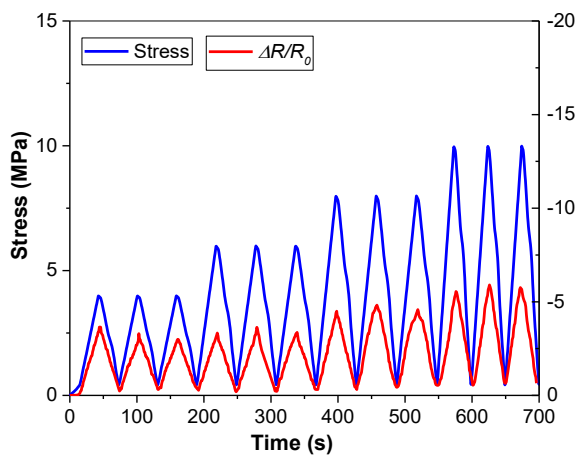

(a) Composite with 20 rubber fibres

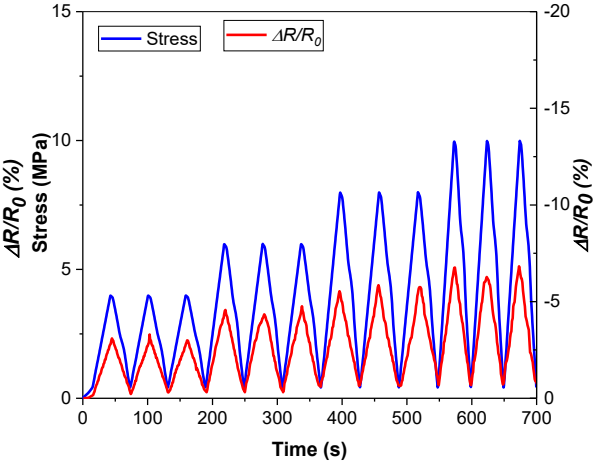

(b) Composite with 40 rubber fibres

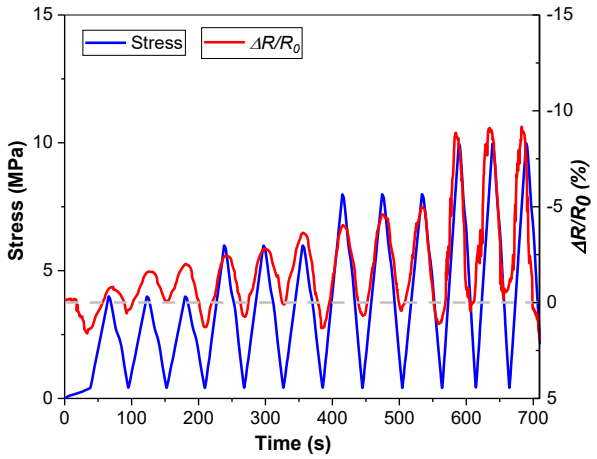

(c) Composite with 60 rubber fibres

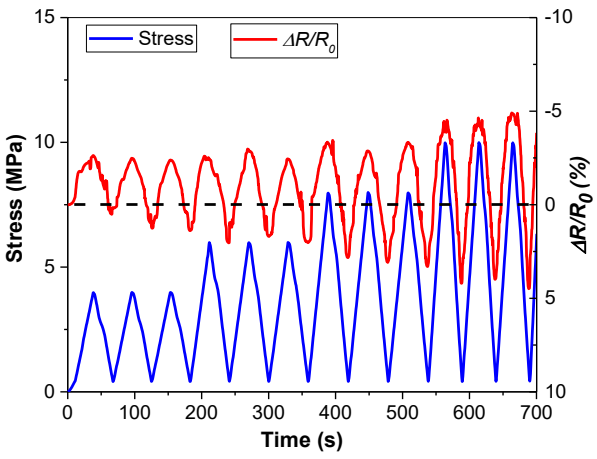

(d) Composite with 80 rubber fibres

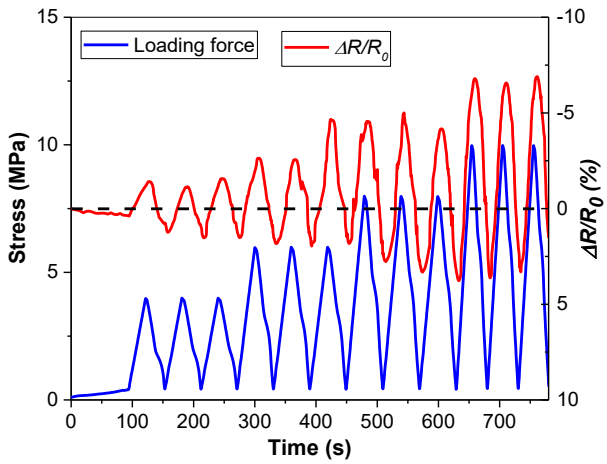

(e) Composite with 100 rubber fibres

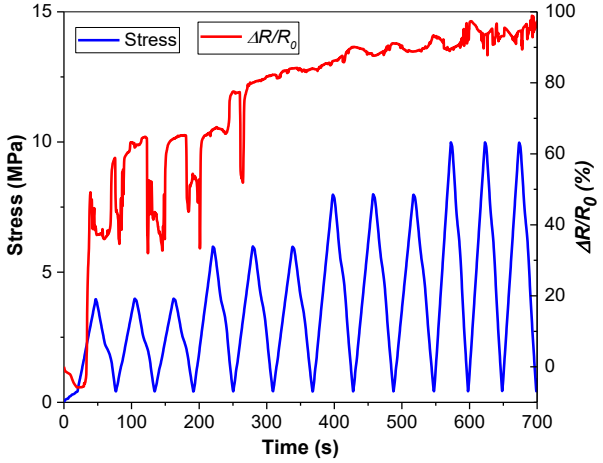

(f) Composite with 140 rubber fibres

Figure 3.9. Fractional changes of resistivity with different rubber contents and stress magnitudes for the composite at w/b ratio of 0.42.

The sensitive coefficient Fi of rubber/cement composite at each stress magnitude is listed in Table 3.7, which got rid of the composite with 140 rubber fibres because there were no clear patterns on the fraction changes of resistivity. It could be observed that the sensitivity was greatly reduced to $\leqslant 1$ at the w/b ratio of 0.42. The dependence of sensitive coefficient Fi on the stress magnitude and rubber content was depicted in Figure 3.10. In comparison to the composites with less water content, the sensitive coefficient Fi showed obscure relationship to rubber content for the composites under all stress magnitudes. Generally, when the stress magnitude was higher than 4 MPa, the tendency could be observed that the composites had

better sensitivity with higher rubber content. It seemed that the composites with 100 rubber fibres expressed the best sensitivity, with coefficient Fi reaching 0.833, 0.916 and 1,007 for the stress magnitudes of 6, 8 and 10 MPa, respectively. In comparison to the piezoresistive sensitivity of the composites at lower w/b ratios, the decreased discrepancy on the sensitivity was found for the composite with 20 and 100 rubber fibres. It could be deduced that the fractional changes of resistivity in the composite mainly came from the inside water content, rather than conductive rubber fibres. In other words, the remained pore solution will disturb the resistivity changes, and play the major role on the fractional changes of resistivity under stress. On the other hand, different from the composites at lower w/b ratios whose sensitive coefficient Fi usually decreased with increase of stress magnitude, the composites at the w/b ratio of 0.42 illustrated an increased sensitivity with increased stress magnitude, except the composites with 20 rubber fibres. It has been mentioned that the decreased sensitivity at high stress level was owing to the defects and irreversible deformations, especially for the composite at low w/b ratio. Although the composites were provided with lower sensitivity, the slightly increased sensitivity with increased stress magnitude demonstrated that the composite at the w/b ratio of 0.42 have better ductility and deformability.

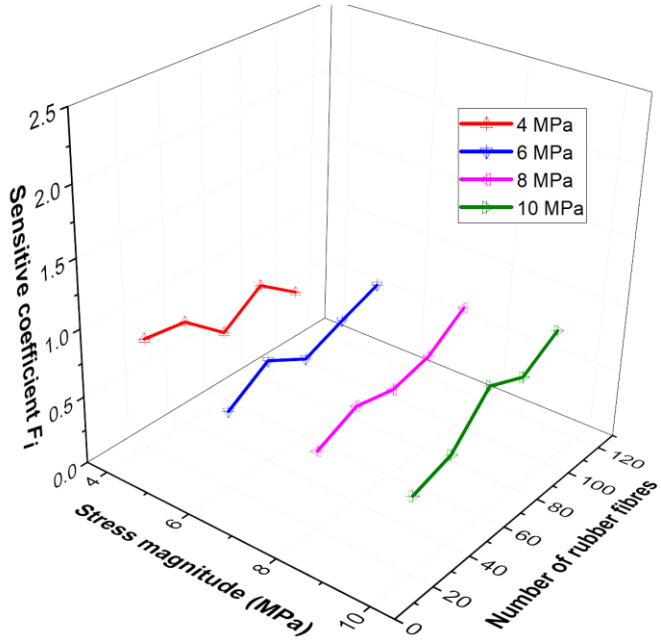

Figure 3.10. Illustration of the relationship between sensitive coefficient, stress magnitude and the rubber fibres for the composite at w/b ratio of 0.42.

3.2.3 Mechanism discussion

Figure 3.11 is a schematic plot of the rubber/cement composite, where conductive phases of pores and rubber fibres with four possible distributions in the cement matrix might create conductive passages. When the composite was connected into an external power supply, the pores, rubber fibres and their linkages will help to complete the circuit and achieve electron transition to generate current. However, on account of the profound discrepancy on the resistivity of pores, rubber fibres and their connected conductive passages, the conductivity amelioration brought by these conductive phases was in a huge difference. It caused the complicated piezoresistivity of rubber/cement composites because of the various degrees of piezoresistive expression by different conductive phases.

Pores containing solutions could improve the conductivity of cementitious composite, since the free movement of ions such as Ca^{2+}, SO_4^{2-}, OH^- and so on. There includes two conductive possibilities through pores with one by already connected pores running through the composite, and another by the neighbour pores which might be linked with each other under external forces, as shown in Figure 3.11-(1-2) . It can be concluded that the former has a direct relationship to both electrical conductivity and piezoresistivity of cementitious composite, while the latter is more related to the piezoresistivity only, until the separated pores are connected irreversibly with external forces. As illustrated in Figure 3.11(a), pore solutions can be squeezed in compression to lead higher concentration and better conductivity, and vice versa in tension. Hence, the fractional changes of resistivity alter with the solution concentrations and generate the piezoresistivity. For the pores connected passages with gaps, the conductivity amelioration and piezoresistivity might be more obvious if the gaps are eliminated under external forces. On the other hand, better conductivity and piezoresistivity could be observed for the composites

with high w/b ratios because of the more number of pores. However, the impacts of pores and pore solutions are very limited on the piezoresistivity, because of the non-conductive and compact structures of cement hydration products.

The conductivity and piezoresistivity induced by conductive rubber fibres are responsible for the conductive and piezoresistive properties of rubber/cement composite, as mentioned that the electrical resistivity could be greatly reduced with increase of rubber fibres. As depicted in Figure 3.11-3, the separated rubber fibres will overlap or connect with each other to form conductive paths under external forces, and alter electrical resistivity. Because of the excellent electrical conductivity of rubber fibres, a small scale connection of rubber fibres can produce a significant fractional change of resistivity in composite. Moreover, not only the overlapped or connected rubber fibres, the tightness degree between two rubber fibres, which is determined by initial micro structures and external forces, also affects the contact resistivity and piezoresistivity. It is considered that the closer contact of rubber fibres, the more electron transition and the lower contact resistivity, which causes larger fractional changes of resistivity and better piezoresistivity.

Another conductive mechanism comes from the contact between rubber fibres and pores solutions as shown in Figure 3.11-4. Just like the functionality of fibres in cementitious composite, rubber fibres in composite are more likely to connect the neighbour pores solutions and reduce electrical resistivity. As depicted in Figure 3.11(c), when the composite is subject to external forces, the separated two phases of rubber and pore solutions might become connected and form conductive passages. Contrarily, the unloading process might detach the rubber fibres from the pore solutions and increase the resistivity. For the composites at high w/b ratio, reasonable assumption can be concluded that higher resistivity changes come from the touch and detach between conductive fibres to pore solutions. Generally, the positive effects on the conductivity and piezoresistivity of rubber/cement composites by the incorporation of

rubber fibres and pores are better than that brought by only pores, but weaker than that induced by only rubber fibres.

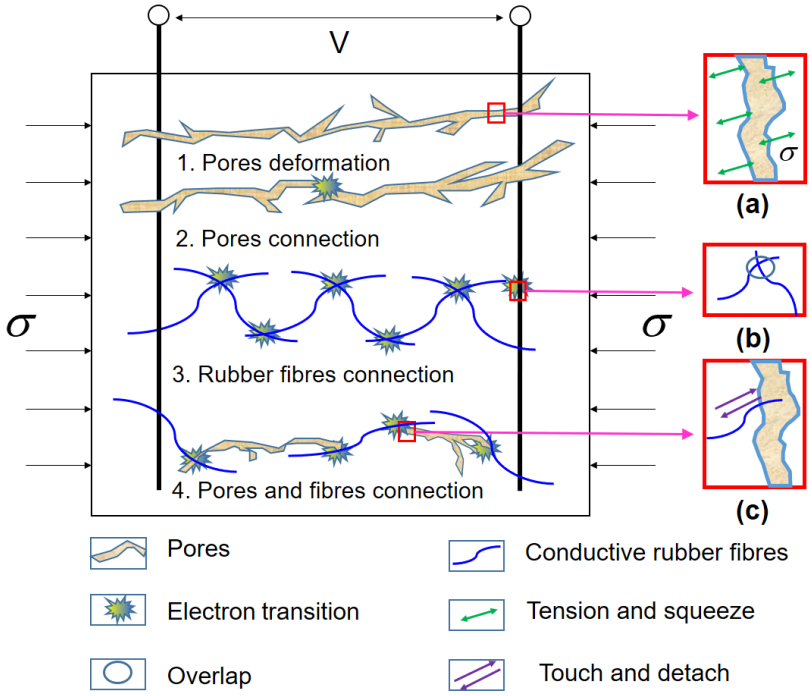

Figure 3.11. Schematic illustration for the electrical conductivity and piezoresistivity mechanism of rubber/cement composites

3.2.4 Mechanical and micro properties of composites

Compressive strengths of rubber/cement composites with various rubber contents and w/b ratios are represented in Figure 3.12. The compressive strengths of plain cement paste (without rubber) were the largest, reaching 56, 45 and 33 MPa for the w/b ratio from 0.34, 0.38 to 0.42, respectively. Overall it is found that the compressive strength was gradually decreased with increase of rubber fibres and w/b ratios. The composite with 20 rubber fibres experienced slight strength reduction and the strength was very close to that of original composites; the strength of composites embedded with 80 rubber fibres, fell to 43, 36 and 23 MPa by the decreasing rate of 23.2%, 20% and 30.3% respectively. For the composite with 140 rubber fibres, the reduction rate boomed to 46.4%, 44.4% and 51.5% and the compressive strength left as 30, 25 and 16 MPa, respectively. In addition, it could be observed that the negativities on compressive

strength were more out of higher w/b ratios, rather than rubber fibres. For example, the composite with 100 rubber fibres at the w/b ratio of 0.34, had higher compressive strength than that of plain cement paste at the w/b ratio of 0.42. The reason might be due to the heterogeneity of rubber/cement composite, in which the rubber fibres were mainly concentrated in two layers and the central part, thus the other compact cement matrix could still bear the external forces. Furthermore, to explore the strength reduction with increase of rubber content, the interfaces between conductive rubber fibres and cement matrix were studied through SEM.

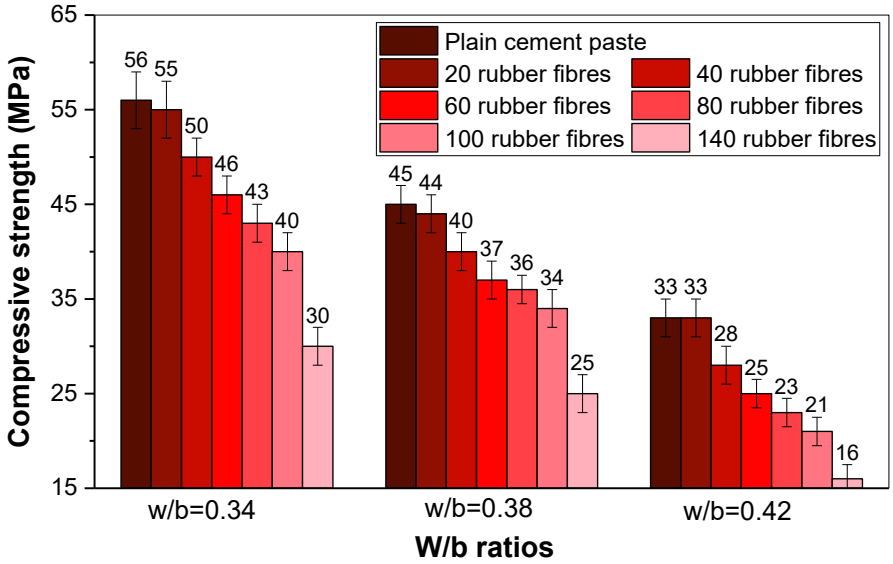

Figure 3.12. Compressive strength of rubber/cement composites with different contents of rubber fibres and w/b ratios.

The SEM images on the cross-section of rubber/cement matrix boundaries with different magnifications are shown in Figure 3.13. It must be noted that the two phases were easy to distinguish because of their huge discrepancy on electrical conductivity. Hence, a general distribution of one conductive rubber fibre in cementitious composite could be observed in Figure 3.13(a), where the light colour area means conductive rubber, and the slightly darker colour area represents cement matrix. In their boundaries, two kinds of regions could be seen, with one named smooth boundaries for its good connections between rubber and cement matrix, and another called disturbed boundaries with gaps and cracks. In addition to the lower

mechanical properties of rubber fibres, it implied that the decreased compressive strength of rubber/cement composite might also be attributed to the gaps and cracks. Moreover, a large proportion of smooth boundaries and only a small disturbed region in the interface explained that why the composite with 20 rubber fibres had nearly no influences on compressive strength. To have a better view on the disturbed boundaries, more images with higher magnification from 100-times to 500-times are displayed in Figures 3.13(b) to (d). Even the disturbed boundaries containing gaps and cracks, are relatively limited in the boundaries of one fibrous rubber and cement matrix, it can be deduced that the composites with high content of rubber fibres could possess larger disturbed boundaries and more gaps and cracks. Therefore, for the composite with 140 rubber fibres, which was halved on compressive strength, was mainly owing to the long gaps and connected cracks in their boundaries. As previously mentioned that the electrical conductivity of composite with 80 rubber fibres was in the range of percolation threshold, and the piezoresistive sensitivity coefficient Fi was higher than 2 when the composite at the w/b ratio of 0.38. Combing the behaviours from electrical and mechanical properties, it could be concluded that the composite at the w/b ratio of 0.38, and reinforced by 80 rubber fibres, were provided with both satisfactory compressive strength and piezoresistivity with excellent repeatability and stability.

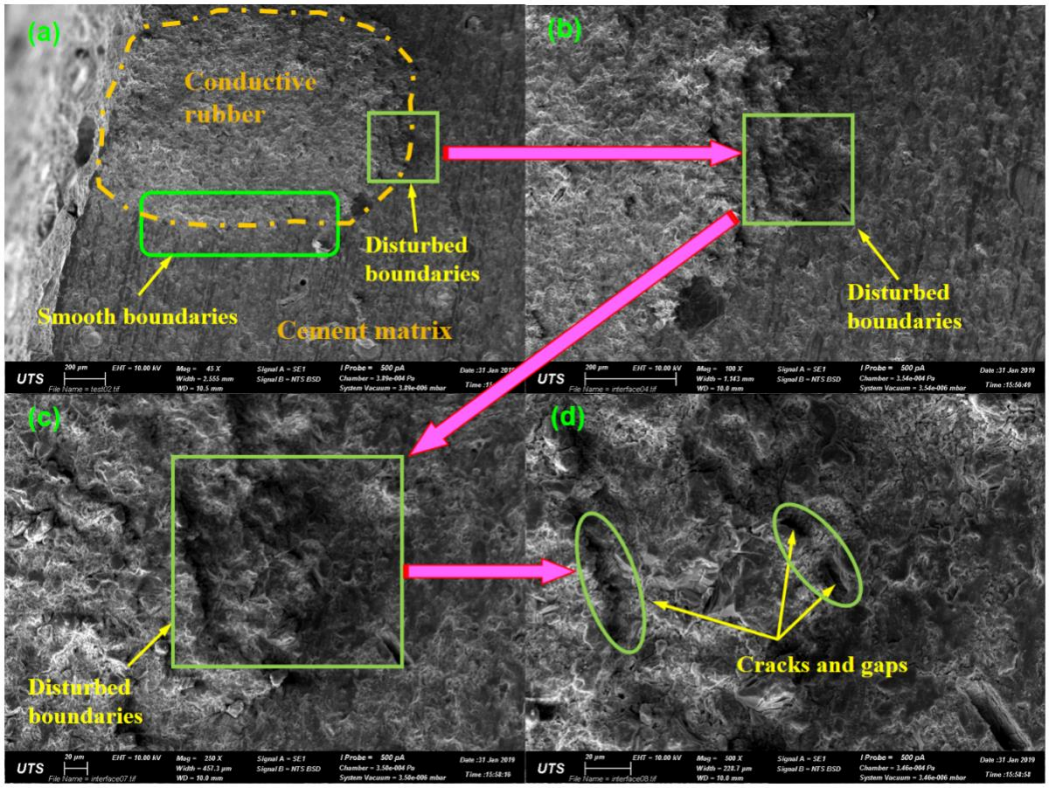

Figure 3.13. SEM images on the boundaries of rubber fibre to cement matrix.

3.3 Cement mortar with conductive rubber crumbs

3.3.1 Flowability

The flowability of rubber modified cement mortars was normalized, and it is expressed as a ratio of the measured diameter to the diameter of the cement mortar without rubber crumbs at the W/B ratio of 0.4. The flowability of plain cement mortar and rubberized cement mortar with various rubber contents and W/B ratios is shown in Figure 3.14. Generally, it was observed that the flowability of modified cement mortar increased with the increase of W/B ratio. However, it seems that the effects of rubber crumbs on the flowability were not always decrease, since the slightly increased flowability for the composites with 10% rubber replacement ratio. Afterwards, with the increase of rubber crumbs replacement ratio, gradually decreased flowability was observed for all composites at various W/B ratios.

There are several reasons for the firstly improved workability followed by the decreased flowability with the increasing rubber replacement ratio. It has been tested that the hydrophobic

rubber crumbs have poor water absorption ability compared to the fine aggregate, so that the cement particles involved in hydration have more opportunities to react with the water molecule and that is why the mixtures performed higher flowability (Su et al. 2015). Even through, based on the proposal by Güneyisi et al. (Güneyisi, Gesoğlu & Özturan 2004), the rubber crumbs added have possibility to increase the inter-particle friction between rubber crumbs and other mix components such as aggregate, which contributes to the decreased workability for the rubber crumbs modified cement mortar. In addition, the poor particle grading of rubber crumbs also contributed to the poor flowability (Raffoul et al. 2016). In this study, when the rubber content was low (10%), the superiorities of the hydrophobic rubber crumbs played the major role on the improved workability. Howbeit, the effect gradually weakened as the increased rubber crumbs induced higher inter-particle friction and led to the worse flowability.

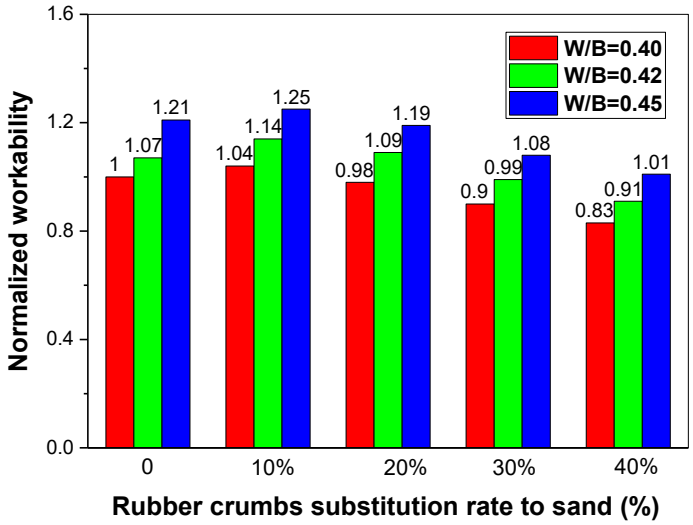

Figure 3.14. Flowability of conductive rubber crumbs modified cement mortar with different W/B ratios and rubber contents.

3.3.2 Compressive strength

The compressive strength of the CRC filled cement mortar at W/B ratios of 0.40, 0.42 and 0.45 is depicted in Figure 3.15(a). The plain cement mortar without any rubber fillers is used as

control group to study the effect of CRC on the compressive strength of cement mortar. It could be seen that the compressive strength of plain cement mortar decreased with the increase of W/B ratios. As for the CRC filled cement mortar, similar to the previous studies on the conductive rubber fibres filled cement paste (Dong, Li, Long, et al. 2019), the compressive strength of the cement mortar showed a monotone decrease with the increase of CRC content. In the case of the cement mortar filled with 40% CRC, the ultimate compressive strengths decreased to lower than 20 MPa regardless of the W/B ratios. Furthermore, when the CRC content higher than 20%, the cement mortar at the W/B ratio of 0.42 started to possess the highest compressive strength compared to that of the cement mortar at the W/B ratios of 0.40 and 0.45.

Figure 3.15(b) displays the reduction rate of compressive strength for the CRC filled cement mortar. It could be observed that the cement mortar at the W/B ratios of 0.40 and 0.45 went through slight larger compressive strength reduction than the cement mortar at the W/B ratio of 0.42. It indicated that the content of CRC in the cement mortar made less adverse effect on the cement mortar at the W/B ratio of 0.42. Even though the characteristics of poor water absorption for CRC, it has been reported that the added rubber crumbs will cause higher inter-particle friction and influence the workability of cementitious composites (Güneyisi, Gesoğlu & Özturan 2004). Therefore, the dense structures of composites might be influenced when the workability is weakened. In other words, it demonstrated that both the defects caused by the weakened workability and the added CRC was responsible for the swift compressive strength reduction for the cement mortar at the W/B ratio of 0.40. As for the cement mortar at the W/B ratio of 0.45, it was believed that the compressive strength reduction was mainly due to the combined actions by the excessive water content and the increasing CRC. Overall, it could be deduced that the cement mortar at the W/B ratio of 0.42 were more suitable to be filled with CRC, in which the compressive strength slightly higher than the counterparts at W/B ratio of

0.40 or 0.45 when the filled CRC content was larger than 10%. The reason might be due to the relative better workability than the composites at W/B ratio of 0.40.

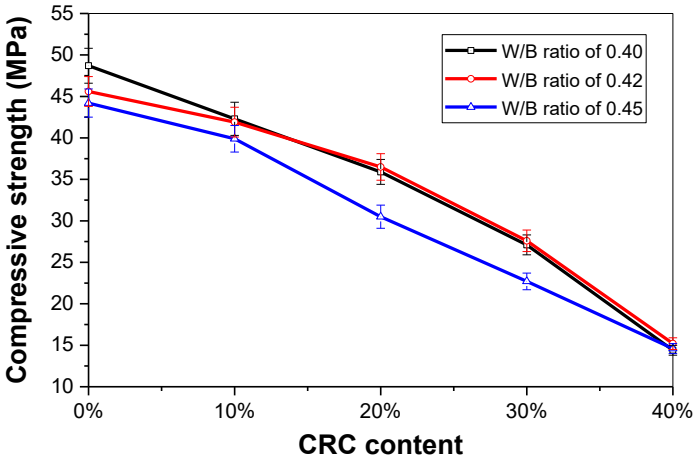

(a) Compressive strength

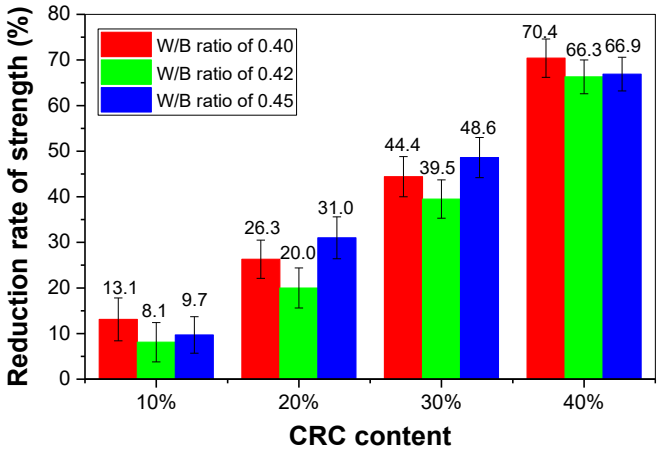

(b) Strength reduction rate

Figure 3.15. Compressive strength and the reduction rate for the CRC filled cement mortar at various W/B ratios.

To explain the reduced compressive strength, Figure 3.16 shows the cross-sectional morphology of rubberized cement mortar filled with different contents of rubber crumbs. Since rare discrepancies among composites at various W/B ratios, only the composites at the W/B ratio of 0.42 were selected to illustrate their macro morphology. Generally, it could be seen that the rubber crumbs were evenly distributed in the cement matrix for both composites with 20 and 40% CRC. In addition, more number of separated rubber crumbs could be observed in

the rubberized mortar with 20% CRC, while a larger amount of connected rubber crumbs was found in the mortar with 40% CRC. These rubber crumbs possessing low strength and elastic modulus, especially for the connected crumbs which nearly having no cohesion in the boundaries, can easily produce a deformation under the external forces. As a result, the stress concentration can be caused in the boundary of the cement matrix to rubber crumbs, which leads to the generated cracks along the rubber crumbs. Overall, the aforementioned reduced compressive strength was exactly sourced from the substitution of cement matrix and fine aggregate to the rubber crumbs. In particular, the boundaries between cement matrix to rubber crumbs, sand to rubber crumbs, and especially the interfaces among rubber crumbs (connected rubber crumbs) can generate high stress concentration and damage the mechanical properties of composites.

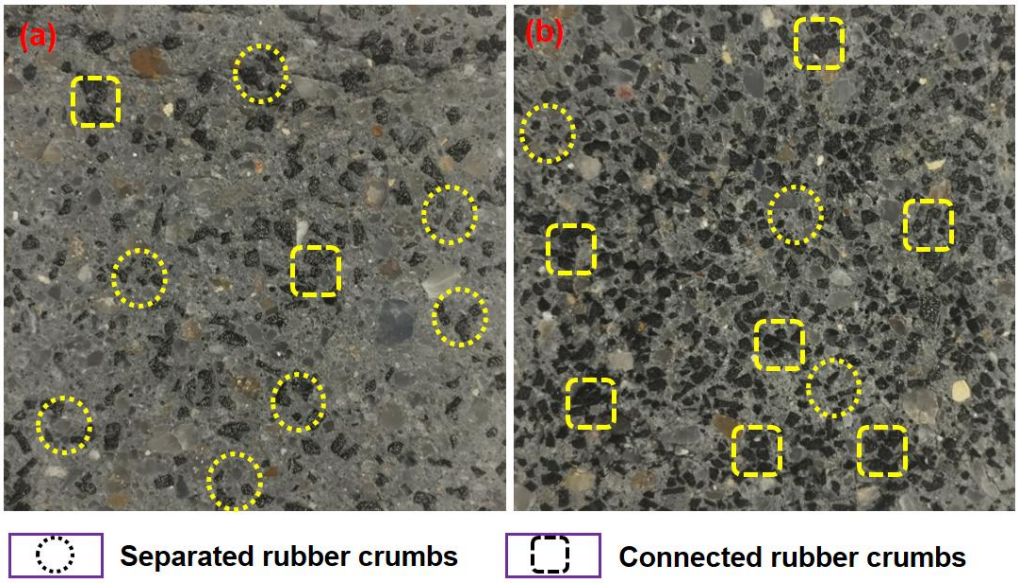

Figure 3.16. Cross-sectional morphology of rubberized cement mortar with (a) 20% CRC and (b) 40% CRC.

3.3.3 Electrical resistivity

Figure 3.17(a-b) display the electrical resistivity for the rubberized mortar filled with various contents of CRC at W/B ratios of 0.40, 0.42 and 0.45 with/without drying treatment. For the composites without drying treatment, it could be seen that the electrical resistivity of the mortar

decreased with the increase of W/B ratios. The lower resistivity for the composites at W/B ratios of 0.45 was mainly owing to the higher water content in the cement matrix. In terms of the effect of CRC, the electrical resistivity of the rubberized mortar slightly varied when the added CRC reached 10%, where the decreased resistivity for the composites at W/B ratios of 0.40 and 0.45 and the increased resistivity for the composites at W/B ratio of 0.42 could be observed. The discrepancy represented that the low replacement ratio of fine sand by CRC nearly made no differences on the electrical resistivity of the rubberized cement mortar, in which the rubber crumbs were completely separated and enclosed by cement matrix. Afterwards, with the increase of CRC content, the electrical resistivity of mortar monotonously decreased by more than one order of magnitude when the CRC replacement ratio reached 40%. In terms of the dried composites in Figure 3.17(b), all the mortar showed dramatic increases on the electrical resistivity and the discrepancy between composites at various W/B ratios greatly reduced after the drying treatment. It was clear that the resistivity reduction mainly originated from the decreased water content and pore solutions in the composites. Therefore, since the mortar with higher W/B ratio of 0.45 containing larger water content, the drying treatment could decrease the water content to the utmost, and that was why the resistivity increase reached the maximum compared to the counterparts at lower W/B ratios. Moreover, it was observed that the mortar with 30% rubber crumbs substitution rate illustrated much faster resistivity reduction than that with 20% rubber crumbs substitution rate. This was due to the fact that more rubber crumbs could bring more air bubbles and pores in the mixture, which were filled with conductive solutions before drying and exhibited better conductivity. However, the pore solutions were considerably decreased after the specimens were dried and displayed even higher resistivity than the mortar with lower rubber content. Still, it was seen that the rubberized cement mortar after drying gently decreased with the increase of rubber crumbs, especially when the substitution rate reached 40%. Different from the cementitious composites

reinforced with commonly used conductive nanomaterials, it was seen that there never existed sudden and swift electrical resistivity reduction with the rising content of CRC from 10% to 40% for the composites no matter drying or not. In other words, it means that the conductive passages penetrating the whole specimens never generated with the increase of CRC. Even though, the separated conductive passages might be elongated and partially connected by means of the contact CRC distributed in the cement matrix, thus the electrical resistivity of the rubberized mortar could be reduced. As aforementioned that the rubberized mortar filled with 40% CRC had larger number of connected rubber crumbs, it further demonstrated the fact that the connected rubber crumbs should be responsible for the decreased electrical resistivity.

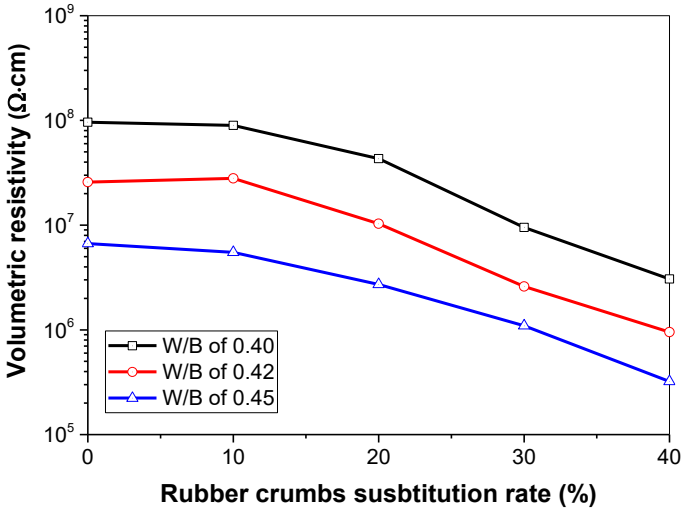

(a) Composites without drying

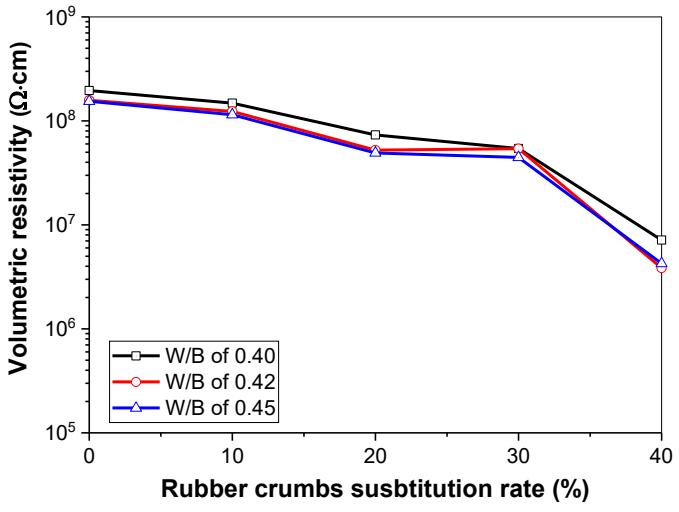

(b) Composites after drying

Figure 3.17. Electrical resistivity for the rubberized mortar with various contents of CRC at different W/B ratios.

Figure 3.18 represents the effects of conductive rubber crumbs to increase the electrical conductivity of the modified cement mortar, incorporating the above-mentioned cross-sectional morphology of rubberized cement mortar on the macro and micro scales. Different from the initially existed conductive passages filled by conductive solutions, the added conductive rubber crumbs in the mortar could work as another solid electron and ions carrier and promote the free movements of conductive ions. Moreover, the introduction of rubber crumbs in the mixing process could bring additional air bubbles and increase the porosity, which were normally filled with conductive solutions and elongate the conductive passages. Another characterization of rubberized cement mortar was due to the different thermal and physical properties between rubber crumbs and cement matrix. Hence, the micro cracks had higher possibility to appear between two rubber crumbs. It means that the pore solutions filled cracks could be easily connected in the assistance of conductive rubber crumbs, which directly leads to the electrical resistivity reduction. Generally, the more conductive rubber crumbs in the cement mortar, the more numbers of connected micro cracks and the longer conductive passages the composites possessed. In terms of the effect of water content, it could be deduced that the initial conductive passages disappeared owing to the decreased pore solutions after drying treatment. Different from the cementitious composites filled with conductive nanoparticles, whose electrical conductivity probably improved with the drying process due to the decreasing surrounded water content to reduce the contact resistance between nanoparticles (Dong, Li, Lu, et al. 2019), the lost water content and disappeared conductive passages connecting nearby rubber crumbs caused the worse conductivity for the rubberized cement mortar. It can be demonstrated that the enhanced conductivity of cementitious composites was

not simply due to the connected rubber crumbs, but also with the assistance of conductive pore solutions.

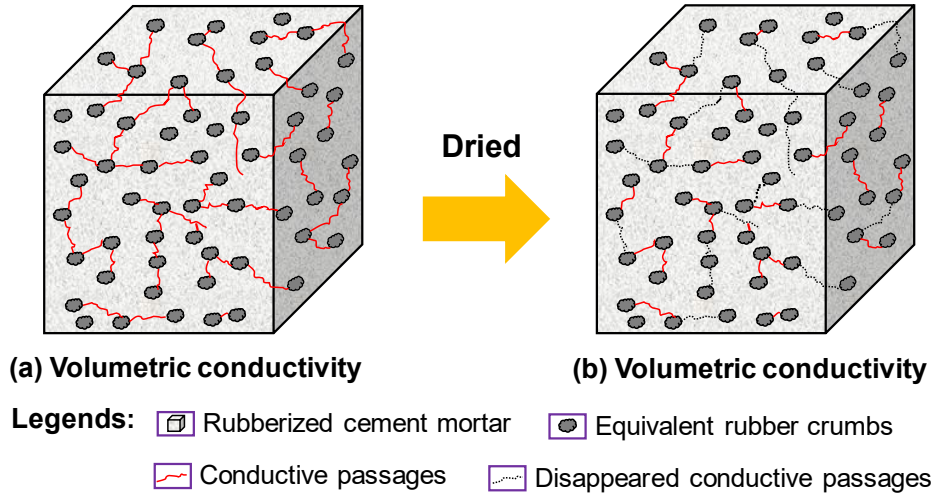

Figure 3.18. Schematic diagram of conductive passages in rubberized cement mortar before and after drying treatments.

3.3.4 Piezoresistivity

3.3.4.1 W/B ratio of 0.40

Figure 3.19 plots the electrical resistivity changes of CRC filled cement mortar at the W/B ratio of 0.40 while subjected to uniaxial cyclic compression. Generally, the fractional changes of resistivity decreased with the applied load, and increased to the initial value during the unload stage. It was observed that all the CRC filled cement mortar showed repeatable electrical resistivity after six cycles of compression, demonstrating that the rubberized cement mortar had excellent piezoresistive repeatability. In addition, the cement mortar filled with 40% CRC was provided with highest fractional changes of resistivity, by the average values reaching approximately 2.45%. However, for the counterpart filled with 10% CRC, the fractional changes of resistivity at the stress peak was only 1.48%. It can be deduced that the cement mortar filled with higher content of CRC had higher tendency to alter their electrical resistivity in the same stress environment. For the cement mortars filled with 20% and 30% CRC, whose

fractional changes of resistivity were very similar, reached approximately 2.07% and 2.14%, respectively.

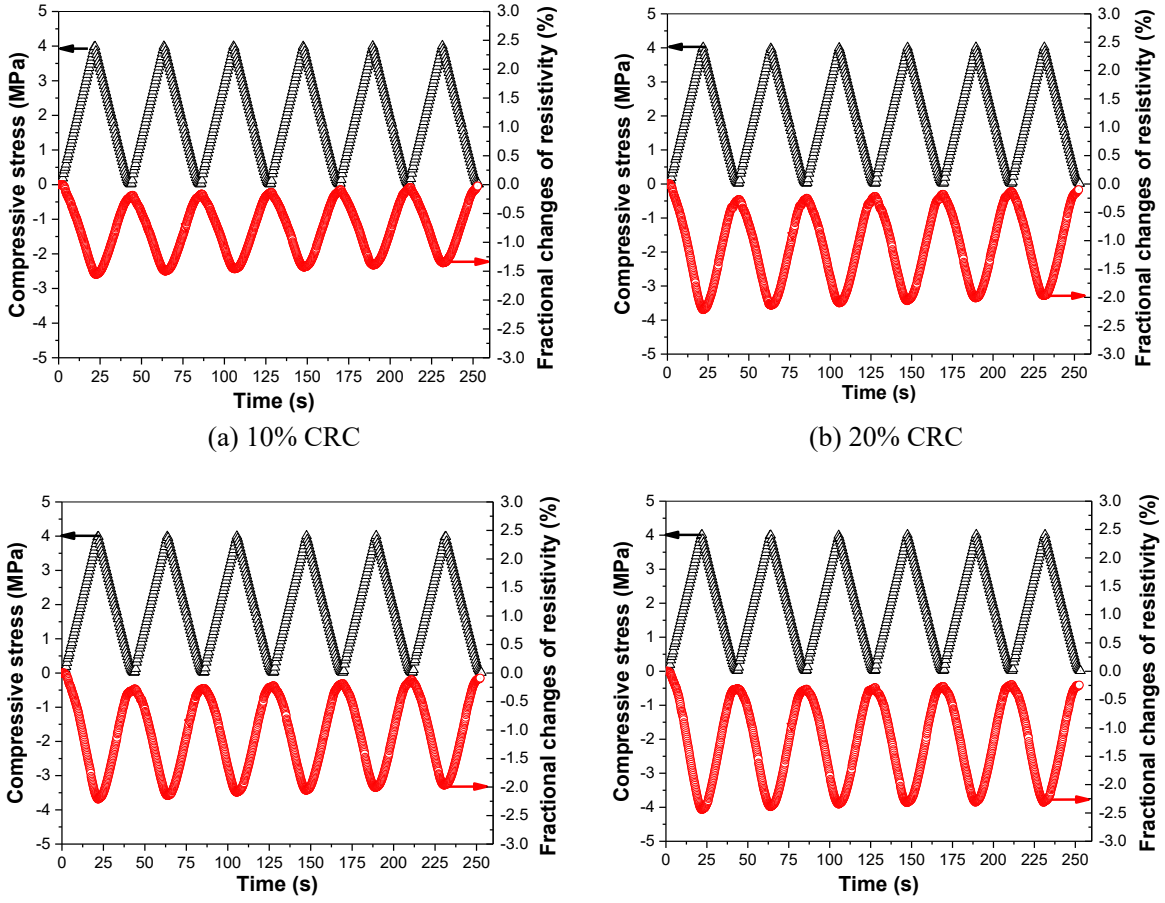

(a) 10% CRC (b) 20% CRC

(c) 30% CRC (d) 40% CRC

Figure 3.19. The fractional changes of resistivity for the rubberized cement mortar at the W/B ratio of 0.40 under cyclic compression.

Gauge factor calculated for piezoresistive sensitivity evaluation is equal to the slope of the curves of fractional changes of resistivity to compression strain. Therefore, the fractional changes of resistivity as a function to the compressive strain for the cement mortar filled with different contents of CRC are plotted, as shown in Figure 3.20. It was seen that the compressive strain of cement mortar increased with the increase of CRC, illustrating the better deformability for the cement mortar filled with more CRC. This is consistent to the previous studies on the rubberized cement mortar, due to the lower elastic modulus of rubber crumbs (Khaloo,

Dehestani & Rahmatabadi 2008; Pham, Toumi & Turatsinze 2018; Siddika et al. 2019). Moreover, the gauge factors were calculated from the fitting lines, with the values of 72.2, 77.6, 62.7 and 57.6 respectively for the cement mortar filled with 10%, 20%, 30% and 40%. It was found that the cement mortar filled with 20% CRC possessed the best piezoresistivity. In comparison to the commercial strain gauge which has the gauge factor of 2, the 20% CRC filled cement mortar are given nearly 39 times higher sensitivity to monitor the compressive deformations. In particular, the reason for the decreased sensitivity for the cement mortar filled with more than 20% CRC is mainly owing to the considerable increases of compressive strain.

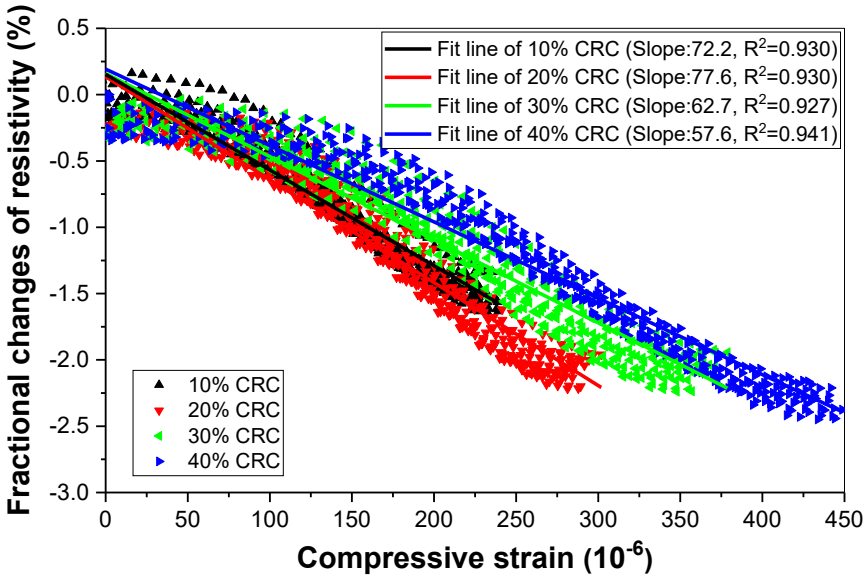

Figure 3.20. Fractional changes of resistivity as a function to compressive strain for the rubberized cement mortar at the W/B ratio of 0.40.

3.3.4.2 W/B ratio of 0.42

The electrical resistivity changes under cyclic compression for the rubberized cement mortar at the W/B ratios of 0.42 is depicted in Figure 3.21. Similar to the counterparts at the W/B ratio of 0.40, the cement mortar at the W/B ratio of 0.42 illustrated excellent repeatability on the electrical resistivity when subjected to 6 cycles of compression. Even though, there existed very small permanent reduction on the electrical resistivity for the cement mortar filled with 30% and 40% CRC. It might be originated from the permanent deformations for the cement

mortar, due to the weakened compressive strength and elastic modulus caused by rubber crumbs. As for their magnitude of resistivity variations, higher fractional changes of resistivity were observed than that of the cement mortar at the W/B ratio of 0.40. Also, the cement mortar filled with more CRC exhibited higher amplitude to change their electrical resistivity under compressive stress. It was observed that the cement mortar filled with 10% to 40% decreased their electrical resistivity under uniaxial stress of 4 MPa by approximately 1.99%, 2.37%, 2.45% and 2.58%, respectively. Since all the cement mortar are dried before the piezoresistive test, the relatively higher fractional changes of resistivity for the cement mortar at the W/B of 0.42 is more likely due to the larger deformation of the cement mortar, rather than the influences by pore solutions.

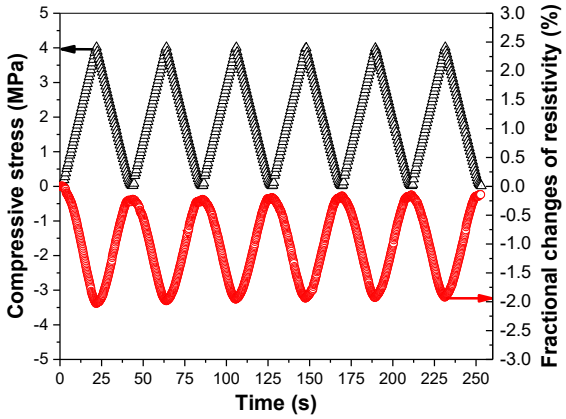

(a) 10% CRC

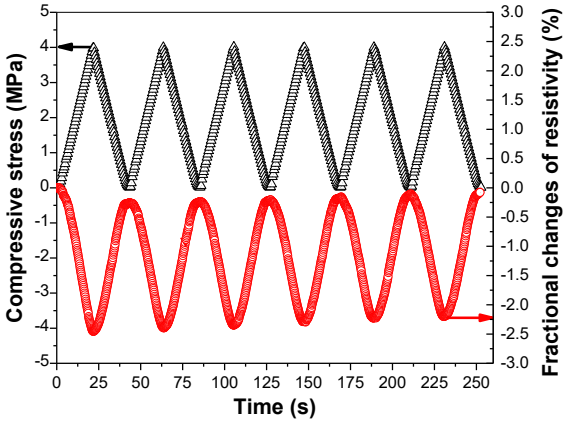

(b) 20% CRC

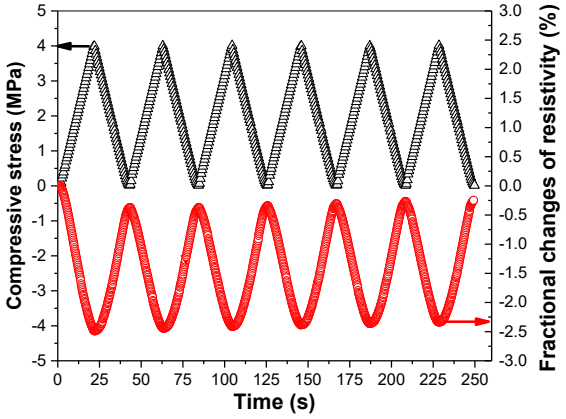

(c) 30% CRC

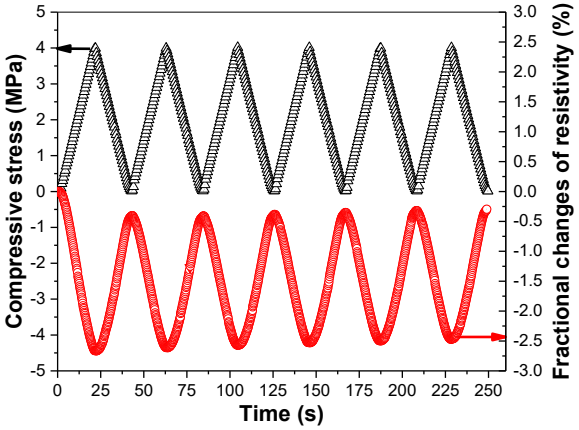

(d) 40% CRC

Figure 3.21. The fractional changes of resistivity for the rubberized cement mortar at the W/B ratio of 0.42 under cyclic compression.

Figure 3.22 illustrates the relationship between fractional changes of resistivity and compressive strain for the CRC filled cement mortar at the W/B ratio of 0.42. Not only was the compressive strain of the cement mortar increased with the increase of CRC content, but the strain of cement mortar itself become higher values than that of the cement mortar at the W/B ratio of 0.40. It demonstrated the above explanation that the permanent resistivity reduction might be due to the permeant deformation of cement mortar since they had larger compressive strain, especially for the composites filled with 30% and 40% CRC. On the other hand, the gauge factors for the rubberized cement mortar were figured out, with the values of 84.2, 87.9, 65.0 and 54.9 respectively for the 10%, 20%, 30% and 40% CRC filled cement mortar. It shows that the cement mortar filled with 20% CRC was provided with largest piezoresistive sensitivity, similar with the results of the cement mortar at the W/B of 0.40.

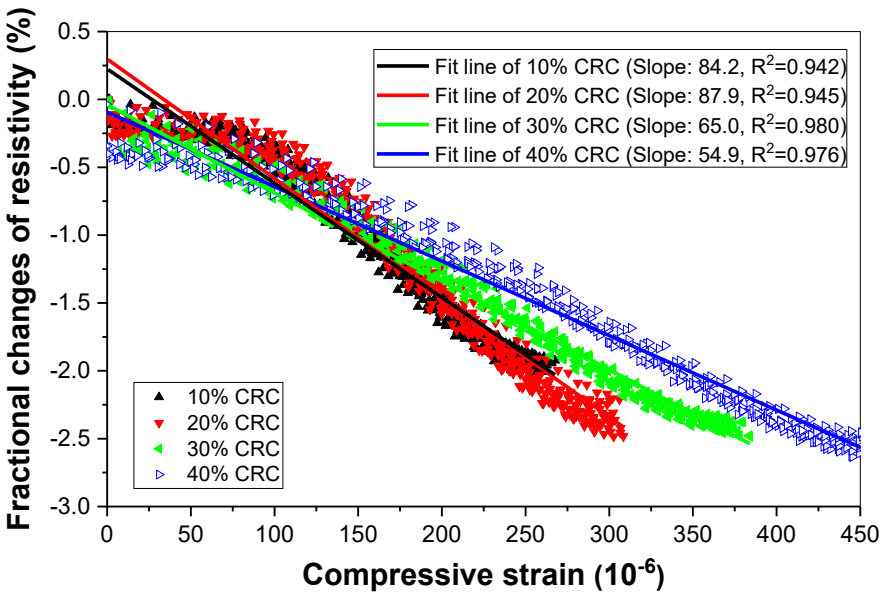

Figure 3.22. Fractional changes of resistivity as a function to compressive strain for the rubberized cement mortar at W/B ratio of 0.42.

3.3.4.3 W/B ratio of 0.45

Figure 3.23 shows the fractional changes of resistivity for the rubberized cement mortar at the W/B ratios of 0.45 under the stress magnitude of 4 MPa. Generally all the cement mortar expressed satisfactory repeatability on the electrical resistivity. However, slight resistivity increases along with the loading procedure was observed for the cement mortar filled with 10% and 20% CRC. As for the cement mortar filled with 30% and 40% CRC, it showed much better repeatability on the electrical resistivity. In terms of the capacity to alter electrical resistivity, the cement mortar at the W/B ratio of 0.45 had lower fractional changes of resistivity to compressive stress than that of the mortar at the W/B ratio of 0.42, with the average values of 1.58%, 2.09%, 2.32% and 2.38% respectively for the cement mortar filled with 10%, 20%, 30% and 40% CRC.

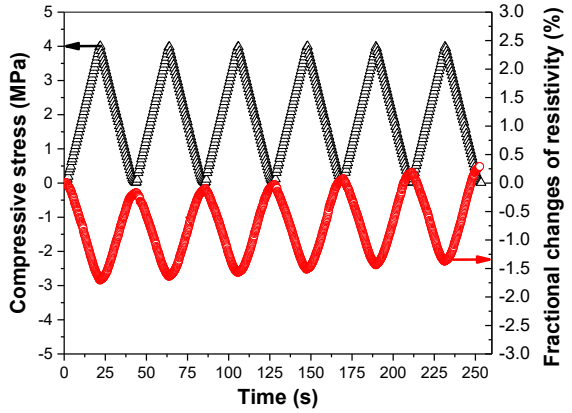

(a) 10% CRC

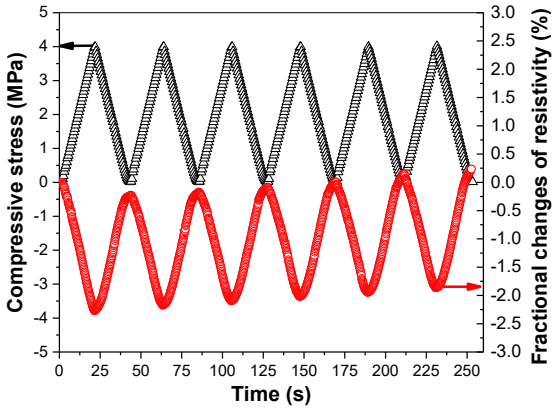

(b) 20% CRC

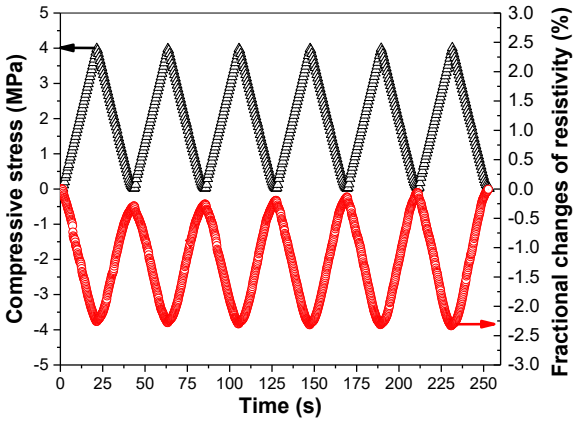

(c) 30% CRC

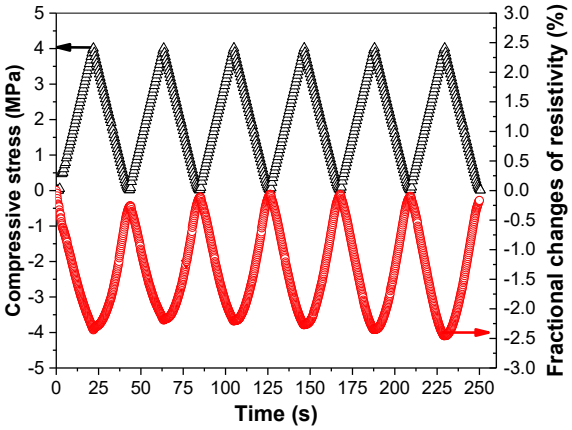

(d) 40% CRC

Figure 3.23. The fractional changes of resistivity for the rubberized cement mortar at the W/B ratio of 0.45 under cyclic compression.

The relationship between fractional changes of resistivity and the compressive strain for the composites at the W/B ratio of 0.45 is shown in Figure 3.24. In comparison to the cement mortar with lower W/B ratios, higher compressive strain was observed for the cement mortar at the W/B ratio of 0.45. In addition, since the fractional changes of resistivity was relatively lower, the gauge factors for the cement mortar filled with 10%, 20%, 30% and 40% CRC reached approximately 69.0, 72.2, 66.4 and 56.3, respectively.

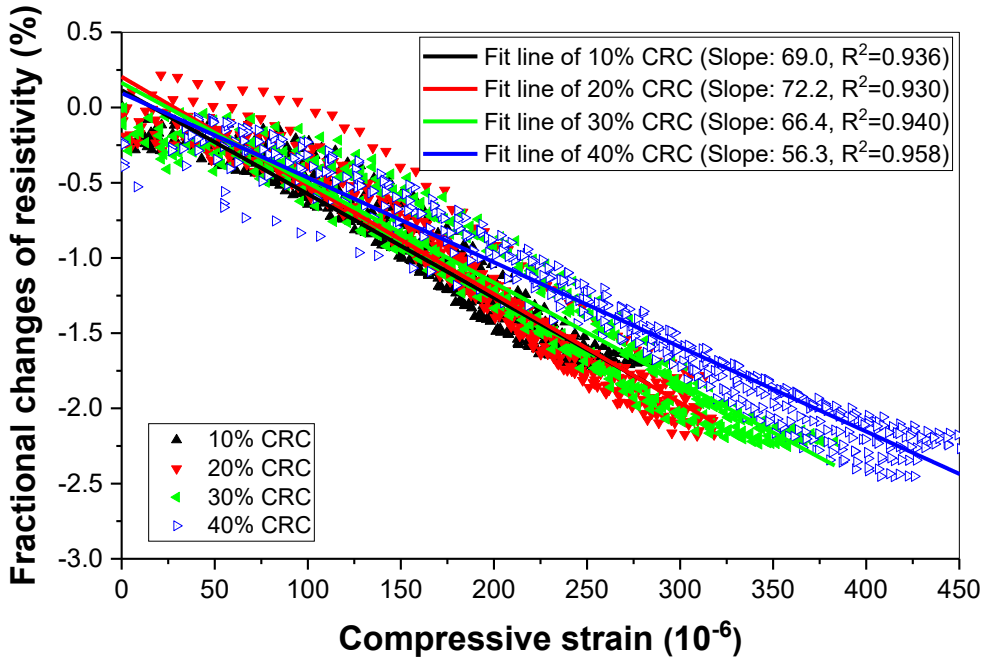

Figure 3.24. Fractional changes of resistivity as a function to compressive strain for the rubberized cement mortar at the W/B ratio of 0.45.

3.4 Summary

Conductive rubber fibres and crumbs filled cementitious composites were firstly explored on their electrical conductivity and piezoresistivity, and the potential mechanisms were also investigated. Mechanical properties were tested and analyzed through microstructural characterization, and the related conclusions can be drawn as follows:

(1) The conductive rubber content of higher than 80 fibres (1.28 vol.%), could significantly improve electrical conductivity of cementitious composite. Moreover, the rubber/cement composite at high w/b ratio could more easily reduce electrical resistivity, but instead without clear percolation.

(2) Four conductive and piezoresistive mechanisms based on experimental results were proposed for the rubber/cement composites, including the conductive passages created by penetrated pores, connected rubber fibres and pores. Among them, the conductive rubber fibres played a dominant role to influence the electrical conductivity and piezoresistivity.

(3) The compressive strength of the CRC-filled cement mortar decreased with the increase in CRC content. For the cement mortar with 40% CRC, the ultimate compressive strength was lower than 20 MPa for all cement mortar regardless of the W/B ratios. It indicates that the filled CRC content is better controlled within 30%, which possesses both satisfactory compressive strength (25 MPa) and self-sensing efficiency.

(4) Three relative positions among CRC in the cement mortar were proposed, and they were the complete isolation, neighbouring to the connection state. As for the complete isolation, the piezoresistivity mainly came from the resistivity changes in the cement matrix. The neighbouring state caused pores or loose microstructures in the ITZs of CRC, which led to easier contact between nearby CRC and decreased the electrical resistivity. The complete connection reduced the contact resistance between CRC under uniaxial compression, which led to the higher FCR of the mortar with high content of CRC.

CHAPTER 4. PIEZORESISTIVITY OF CEMENTITIOUS MATERIALS WITH CARBON NANOMATERIALS

In this chapter, the carbon nanomaterials as conductive fillers were applied in the cementitious materials, to prepare the cement-based sensors. The mechanical, electrical, microstructural and piezoresistive properties of nano-engineered cement-based sensors were investigated.

4.1 Carbon black (CB)

4.1.1 Electrical resistivity

The electrical resistivity of the CB/cement composites only filled with different contents of CB, generally decreased with the increase of CB, and the reduction tendency was significant within the percolation threshold, but became more obscure when beyond the percolation range (Ding et al. 2013; Ding et al. 2019; Gong et al. 2009; Irshidat et al. 2021; Li et al. 2019; Monteiro, Cachim & Costa 2015; Monteiro et al. 2020; Nalon et al. 2020; Pârvan, Voicu & Bădănoiu 2020; Rezania et al. 2019; Xiao, Li & Ou 2010). In this study, the percolation threshold of CB filled cement-based composite was in the ranges of 0.5 wt.% to 2.0 wt.%, and the initial percolation threshold was approximately 0.5 wt.% to 1.0 wt.% as shown in Figure 4.1. This was very close to the results of Dai et al. (2010), but with further improvements in narrowing down the percolation ranges.

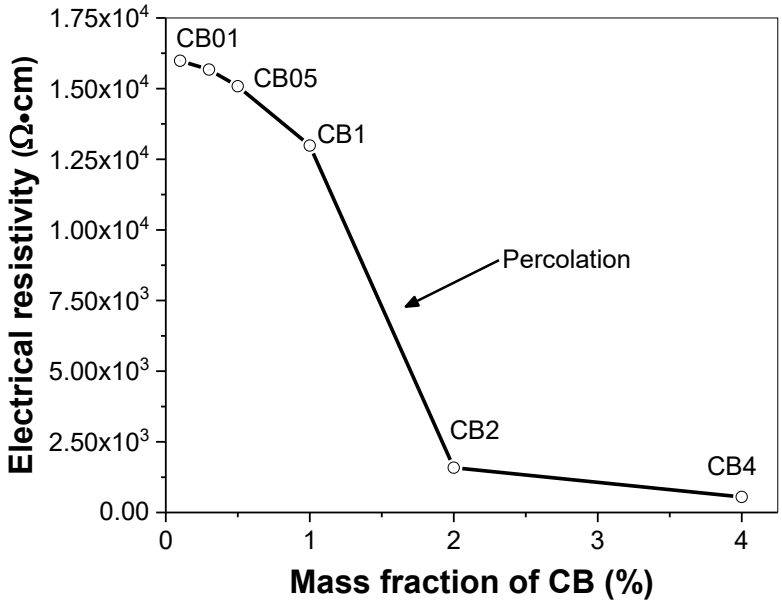

Figure 4.1. Electrical resistivity of CB/cement cementitious composites with multiple contents of CB.

4.1.2 Compressive strength

As shown in Figure 4.2, the composites filled with 0.1 wt.% and 0.5 wt.% CB were provided with excellent compressive strength of both higher than 50 MPa, and similar to the plain cement paste with 55 MPa. It can be considered that small amount of CB particles could fill up the micro pores in composite and improve the compressive strength, while negativities were also accompanied by larger w/b ratios. However, considerable strength decreases occurred when the CB content was larger than 1.0 wt.% to the weight of binder, where the reduction rate reached 32.7%, 56.4% and 72.7% respectively for the content of 1.0 wt.%, 2.0 wt.% and 4.0 wt.% CB filled composites, with only 37 MPa, 24 MPa and 15 MPa remained, respectively. The reasons for their differences mainly came from the special physical characteristics of CB, which possessed excellent water absorption ability. Therefore, the CB particles had the capacity to absorb water content or attach on the cement surface when being mixed with cement mixture, which affected the cement hydration process. Fortunately this could be partially solved by adding more water according to the amount of CB in the composite. But on the other

hand, CB particles with surface energy were extremely inclined to absorb together and form agglomerations and clusters, which showed no resistance to the loading forces compared to the harden hydration products.

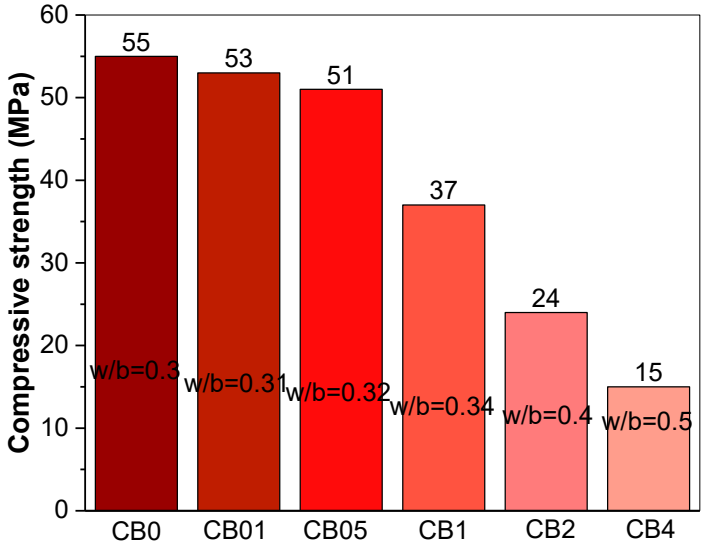

Figure 4.2. Compressive strength of CB/cement cementitious composites with multiple contents of CB.

4.1.3 Piezoresistivity

Figure 4.3(a) to (c) illustrates the fractional changes of resistivity for the composites filled with 0.5 wt.% CB, 1.0% CB and 1.0% CB, respectively. The selection of approximately 2000 με as the ultimate strain is to ensure that the composites at the elastic stages, which outputs a more stable strain to determine the fractional changes of resistivity and gauge factor. Among them, positive correlation between fractional changes of resistivity and strain could be observed. For the composites with 0.5% CB, a stable output of fractional changes of resistivity was observed, with the ultimate changes reaching 10.6%. The gentle resistivity increase at the beginning was owing to the polarization of composites, which could be negligible compared with the resistivity reduction caused by the compressive strain. Cementitious composites filled with 1.0 wt.% CB were really close to reach the percolation threshold. It could be foreseen that there existed significant fractional changes of resistivity if the phenomenon of percolation took place

simultaneously when the composite subjects to external loadings. Given the lack of description of piezoresistivity during electrical percolation, new definition on the word of "piezoresistive percolation" was proposed, to represent the sudden increase of fractional changes of resistivity or piezoresistivity and distinguish from the concept of generally used electrical percolation. The fractional changes of resistivity for the 2.0 wt.% CB filled cementitious composites showed smooth increase with the compressive strain when compared with the composites filled with 1.0 wt.% CB.

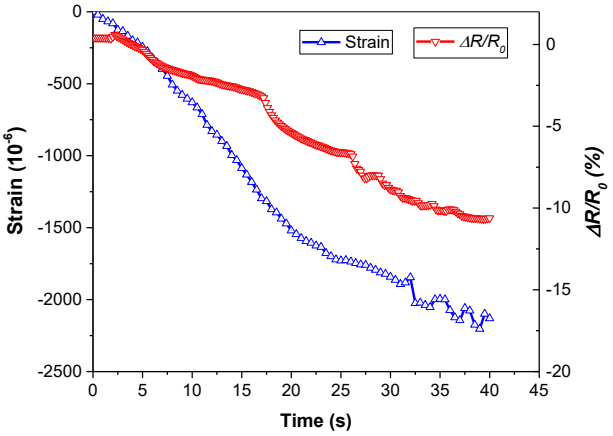

(a) With 0.5% CB

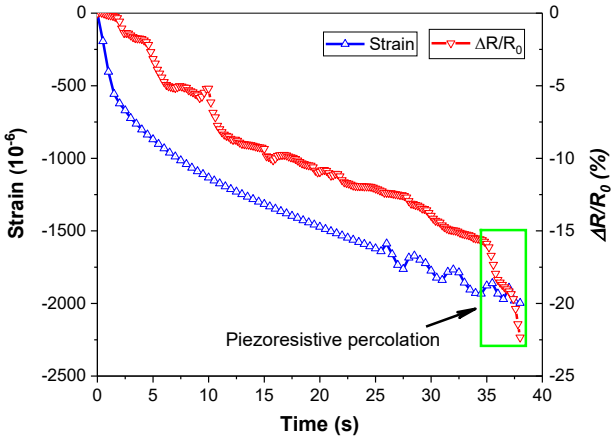

(b) With 1.0% CB

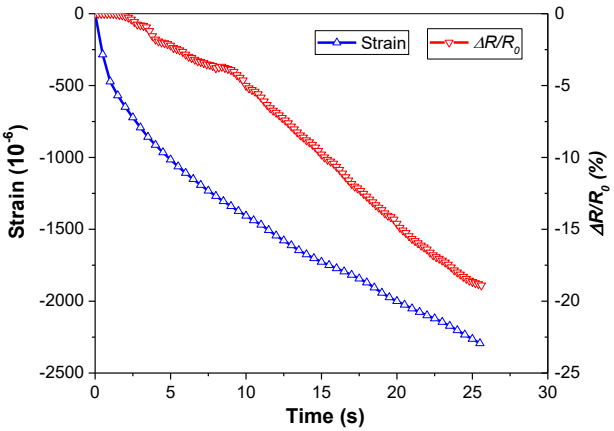

(c) With 2.0% CB

Figure 4.3. Fractional changes of resistivity of CB/cement cementitious composites with (a) 0.5% CB; (b) 1.0% CB and (c) 2.0% CB.

4.1.4 Hydration heat

Figure 4.4 shows the effect of CB nanoparticles on the cement hydration in 72 hr, including the rate of hydration heat and the accumulative heat of hydration. In this study, the hydration test involving the composite filled with 0, 0.5 wt.%, and 1.0 wt.% CB can successfully elucidate the effect of CB in the cementitious composites. It could be observed that the second peak gradually emerged with the increase of CB, which indicated the delaying effect of CB nanoparticles on the cement hydration acceleration stage. One reason is the dilution effect of CB in the composite, which reduced the concentration of compositions involved in the cement hydration procedures (Li, Li, et al. 2017). Another reason is probably due to the high surface energy of CB nanoparticles, which can absorb and enclose the water particles to hinder their contact to cement (Dai et al. 2010). In addition, the second peak of composite even higher than the first peak, representing the hydration was greatly improved at the acceleration stage as confirmed by the cumulative heat of hydration in Figure 4.4(b). Moreover, it was found that both the first and second peaks gradually shifted to left, which means the decreased duration to reach the hydration peak with the increase of CB content.

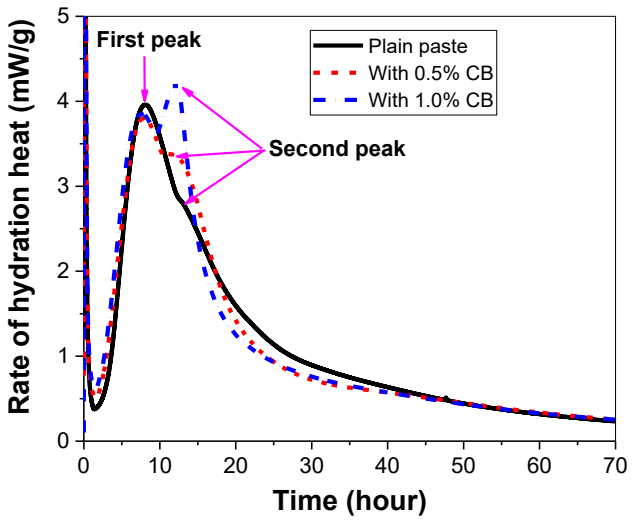

(a) Rate of hydration heat

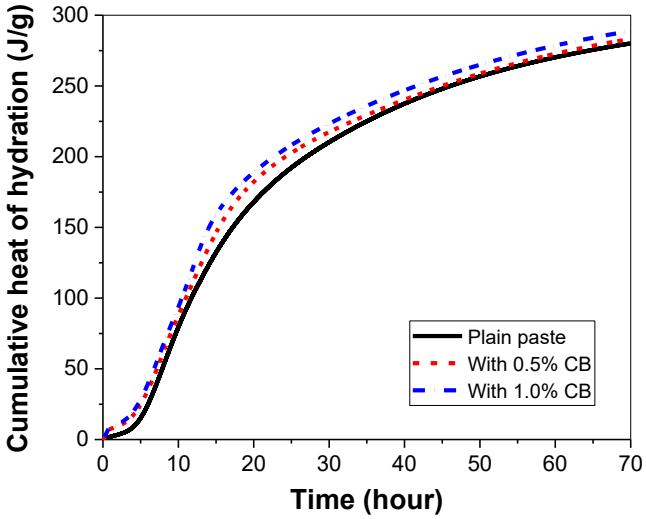

(b) Cumulative heat of hydration

Figure 4.4. Effect of carbon black powder on cement hydration heat in 72 hrs.

4.2 Carbon nanotube (CNT)

The clustered and dispersed CNT filled cement-based sensor will be compared in this section, indicating that the layer-distributed carbon nanotube can greatly reduce the amount of CNT used, so as to reduce the cost of cement-based sensors.

4.2.1 Raw materials

The lengths of CNT were thousands of times larger than their diameters and represented ultra-high aspect ratios, which was considered responsible for the significantly ameliorated electrical

and mechanical properties of the CNT blended cementitious materials (Chen et al. 2011; del Carmen Camacho et al. 2014; Garcia-Macias et al. 2017; Han et al. 2013; Han, Yu & Kwon 2009; Kim et al. 2016; Konsta-Gdoutos, Metaxa & Shah 2010a, 2010b; Singh et al. 2013; Ubertini, Materazzi, et al. 2014; Wansom et al. 2006; Zhang et al. 2018). Figure 4.5 shows the microstructural morphology of the CNT used in this study before and after the dispersion treatment. The right image implied that there still existed a small proportion of CNT agglomerations even after dispersion treatment.

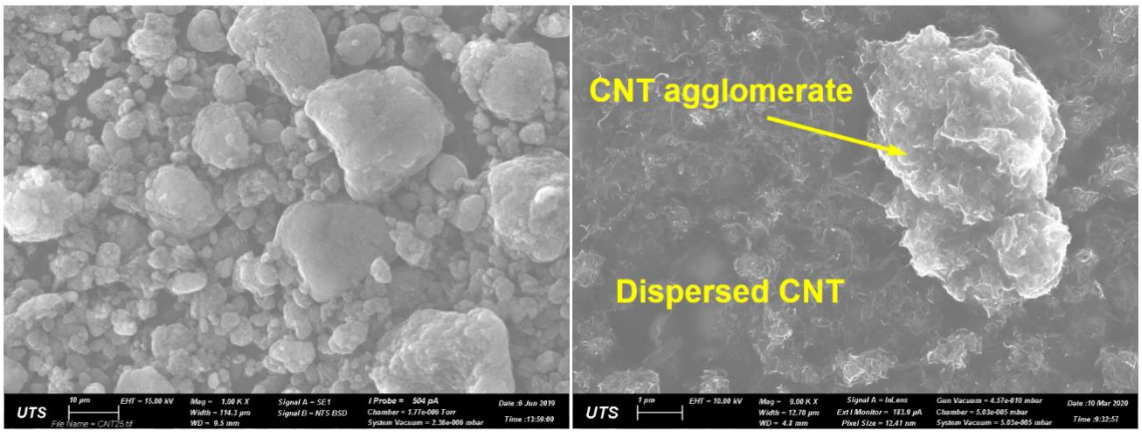

(a) CNT agglomeration (b) Dispersed CNT

Figure 4.5. Morphologies of clustered and dispersed CNT.

4.2.2 Specimen preparation

Figure 4.6 shows that there are two manufacturing processes for the CNT reinforced cementitious composite, within regime A the CNT being dispersed by ultrasonic bath then mixing with binders (mixture of cement and silica fume), and another by scattering as received CNT powder into the cement-based composite layer by layer in the regime B. For the UDCC, there are 4 steps as usually applied: (1) firstly mix the CNT with water and disperse the mixture in the ultrasonic bath for 1 hr; (2) pour the mixture into Hobart mixture for another 5mins stirring to ensure the well dispersion of CNT; (3) add the mixture of cement and silica fume in the CNT solution, and mix for 3 mins. (4) cast the CNT reinforced cementitious composites into the cleaned and oiled moulds (50 mm × 50 mm × 50mm) and cure the specimens in the

curing chamber for 1 day, which is followed by the demolding and further curing for another 27 days. The final product of the uniformly-dispersed CNT composites (UDCC) by regime A is shown in Figure 4.6(a).

In terms of regime B with layer-distributed CNT in the composite, there are three principal procedures, including manufacturing cement paste, casting cement paste, and scattering CNT layer-by-layer during the casting. For example, for the composite having two layers of CNT, its manufacturing process was: (1) mix the water and superplasticizer and stir it for 5mins; (2) add the mixture of cement and silica fume in the solution, and mix for 3mins to make the cement paste. (3) pour the cement paste into moulds to the height of approximately 16.7 mm, and followed by scattering one layer of CNT. To make the as received CNT powder evenly distributed in composites, the casting of cement paste and the scattering of CNT powder is conducted in the vibration table. (4) add another cement paste to the height of 33.6 mm and distribute another layer of CNT. (5) cast the cement paste to the top of moulds and cure the specimens in the curing chamber for 1 day. (6) demold the specimens to another 27 days curing. Similarly, for the specimens with 3 layers of CNT, the cast of cement paste is to 12.5 mm at a time, and so on, to whatever layers the composites have. The final product of layer-distributed CNT composite (LDCC) by regime B is plotted in Figure 4.6(b), from which we can observe the layered distribution of CNT and the plain cement paste in the composites.

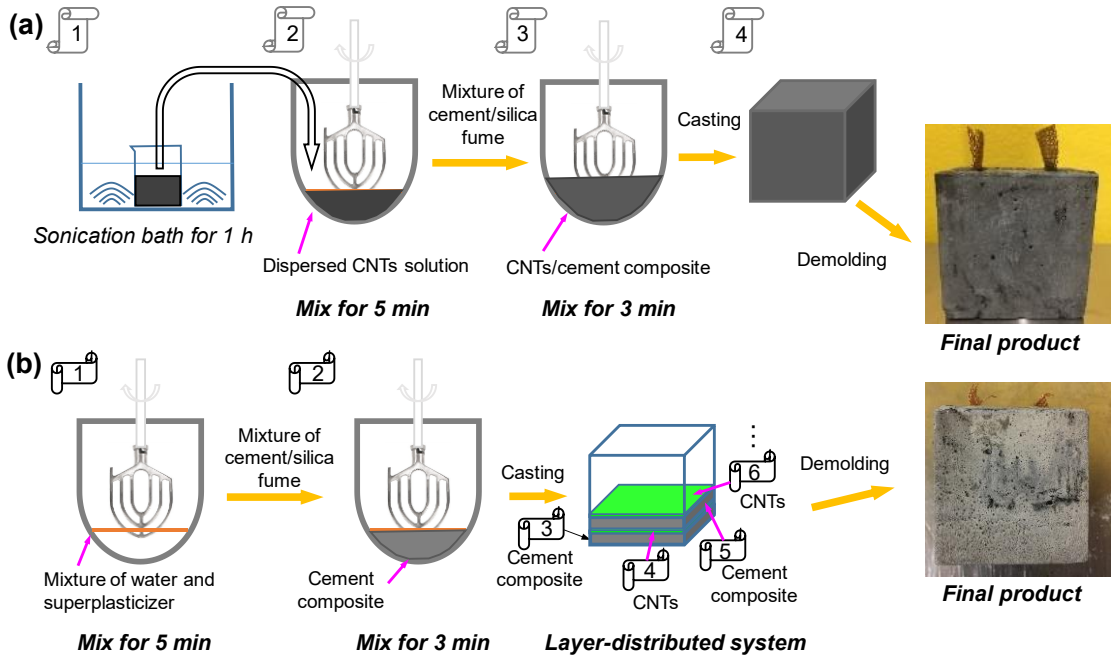

Figure 4.6. Preparation of CNT reinforced cementitious composites: (a) UDCC and (b) LDCC.

4.2.3 CNT agglomerations

To characterize agglomerations, a SEM image in Figure 4.7(a), which possessed various sizes and shapes of CNT agglomerations, was separated into several images in Figures 4.7(c) to 4.7(f), where CNT agglomerations with the same diameter (D) were grouped in the same colour. The diameter (D) was determined by the averages distance of the lines passing through the centroid of agglomerations. Five groups were developed for agglomerations in the ranges of ≥ 12 μm, 8-12 μm, 5-8 μm, 2-5 μm and ≤ 2 μm. The division based on the sizes not only facilitated the analysis, but also was more convenient to distinguish the CNT agglomerations in different sizes, especially for the smaller one which might have been attached to the larger agglomerations. The shapes of CNT agglomerations were irregular and varied with different sizes and roundness. It could be found that the number of larger sized agglomerations was lower than that of agglomerations in smaller sizes.

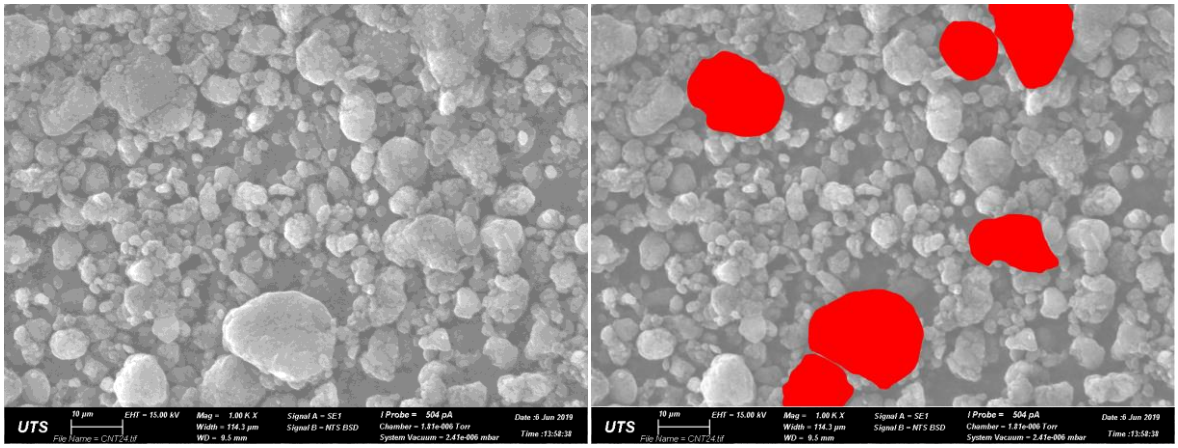

(a) Original image -different sized CNT agglomeration

(b) Agglomeration with sizes larger than 12 µm (red)

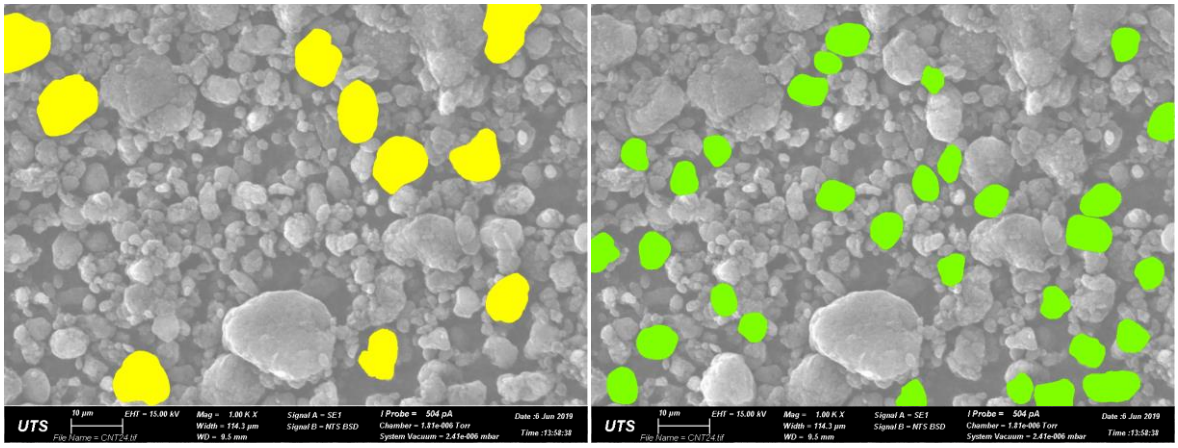

(c) Agglomeration with sizes of 8-12 µm (yellow)

(d) Agglomeration with sizes of 5-8 µm (green)

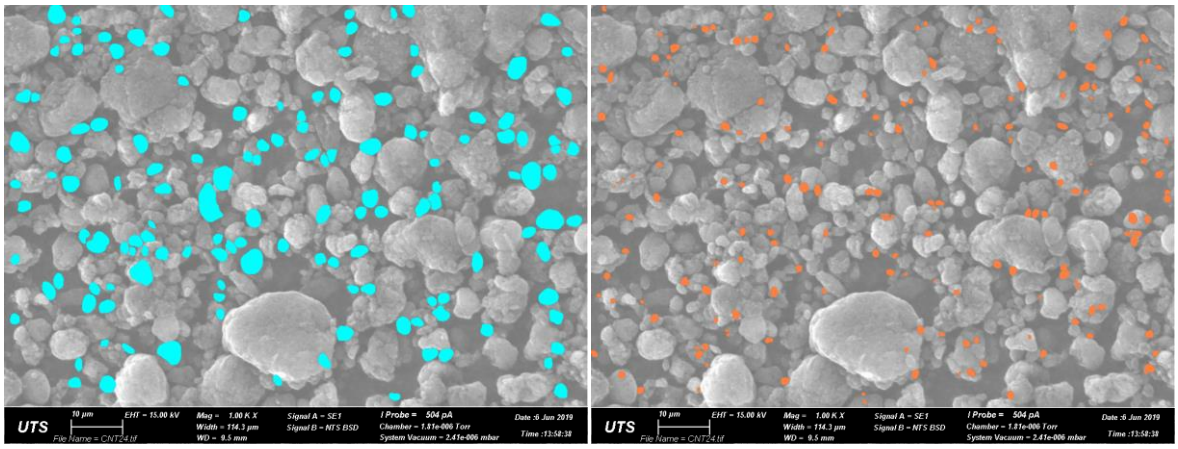

(e) Agglomeration with sizes of 2-5 µm (blue)

(f) Agglomeration with sizes less than 2 µm (brown)

Figure 4.7. Classification of CNT agglomerations based on size distribution.

Figure 4.8 illustrates the diameter distribution of CNT agglomerations and the proportion of their occupied areas. It could be found that the CNT agglomerations in the diameter ranges of ≥ 12 μm possessed the smallest quantity (1.64%), but ranked the second on the area occupied (25.25%). On the contrary, the smallest agglomerations with the diameter < 2 μm accounted for the highest proportion in the aspect of numbers (49.05%) and the lowest ratio (5.91%) in the area occupied. The results implied that although a minority of CNT agglomerations were in the larger sizes such as ≥ 12 μm, the volumetric proportion occupied by these agglomerations was in a large value. In addition, it could be observed that the majority of CNT agglomerations were in the sizes smaller than 8 μm (95.62%).

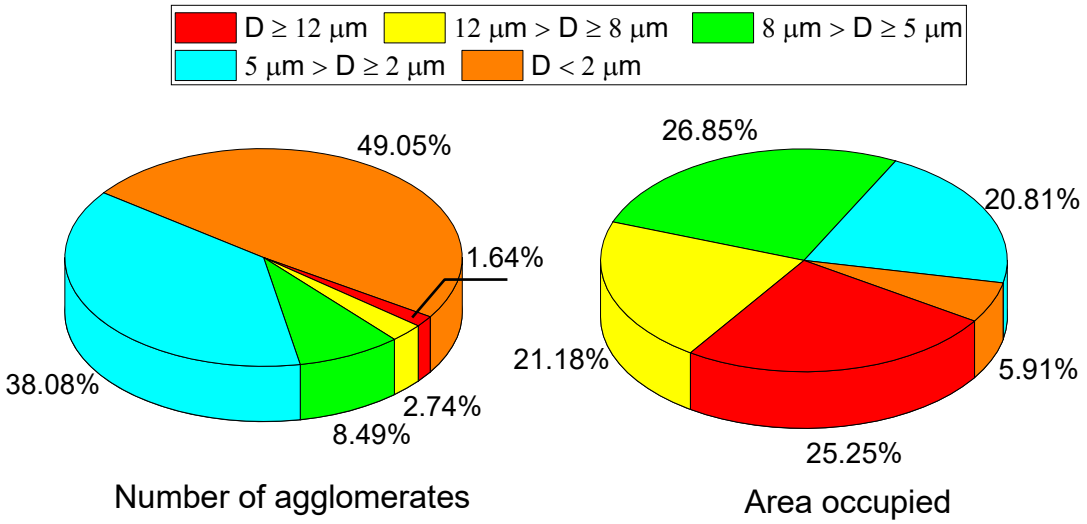

Figure 4.8. Size distribution of CNT agglomerations and the proportion of the occupied areas.

The shape of CNT agglomerations can be reflected by the parameter of roundness, which is determined by the ratio of agglomeration's largest length to the smallest width. With the coarser or more edges and corners the agglomerations, the higher values the roundness possessed. Similarly, the smaller roundness indicated the smooth and more rounded agglomerations. As previously mentioned, the CNT agglomerations having high surface energy always formed

pores in the cement matrix because the cement paste was hard to penetrate. It could be deduced that the micropores had similar shapes to CNT agglomerations, thus the shapes of inner porosity of cement matrix could be partially represented by the shapes of CNT agglomerations. The average roundness of the CNT agglomerations in various sizes is depicted in Figure 4.9(a), which showed continually increased roundness with the growth of agglomeration sizes. Particularly, the conclusion could be drawn that the roundness of the pores induced by CNT agglomerations increased with their sizes. Figure 4.9(b) schematically plots the stress concentration in the pores with a roundness of 1 and > 1. For the spherical pores, the inner stress is uniformly distributed on the surface of pores and maintained a moderate intensity. However, for the irregular pores with sharp corners or edges, the inner stress concentrates in the specific region and reaches a high stress level to damage the porosity. In summary, it could be concluded that the mechanical properties of the cementitious composites with excessive larger sized CNT agglomerations will be reduced due to the poor roundness and stress concentration, in comparison to the composites with smaller sized agglomerations. The results quantitatively demonstrated that the CNT agglomerations should be controlled as smaller as possible in cementitious composites, to ensure satisfactory mechanical strengths.

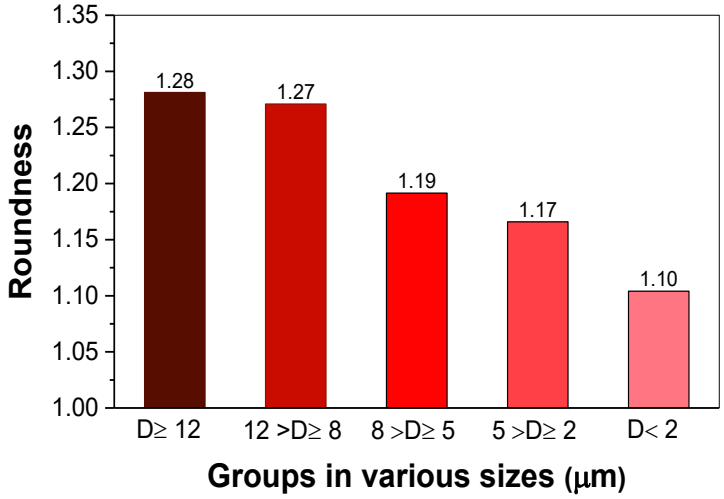

(a) Roundness distribution

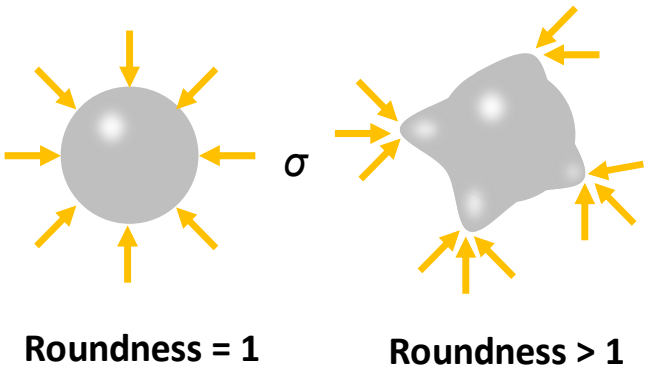

(b) Stress concentration in pores

Figure 4.9. Average roundness of CNT agglomerations in various sizes and schematic plot of stress concentration in pores.

4.2.4 Mechanical and micro properties

The compressive strengths of the plain cement paste (PCP), UDCC with 0.5% well-dispersed CNT and the LDCC with various CNT layers are displayed in Figure 4.10. Because of the anisotropic behaviour of LDCC, it should be noted that loading direction is vertical to the plane with CNT agglomerations and the same for the piezoresistive test. It shows that the uniformly distributed CNT reinforced the cementitious composites and increased the compressive strength of PCP from 44 to 51 MPa. However, for the cementitious composites with CNT without dispersion, the compressive strength of the LDCC gradually decreased with the increase of CNT layers. The compressive strength was still acceptable for the LDCC with 1 layer of undispersed CNT (LDCC1), reaching approximately 40 MPa. However, it significantly decreased when the CNT layers increased ≥ 2, and the compressive strengths of only 31 and 13 MPa were remained for the LDCC with 2 (LDCC2) and 6 layers (LDCC6) of CNT, respectively. Previous studies have drawn contradictory results on the enhanced/weakened compressive strength of CNT engineered cementitious composites . Nevertheless, both of them reach the consensus that the CNT dispersion had a firm relationship to the mechanical properties. The well-dispersed CNT possessing filling and bridging effect is beneficial for the

compressive strength, while the CNT agglomerations and the inappropriate surfactant can greatly affect the density and mechanical strengths of cementitious composites.

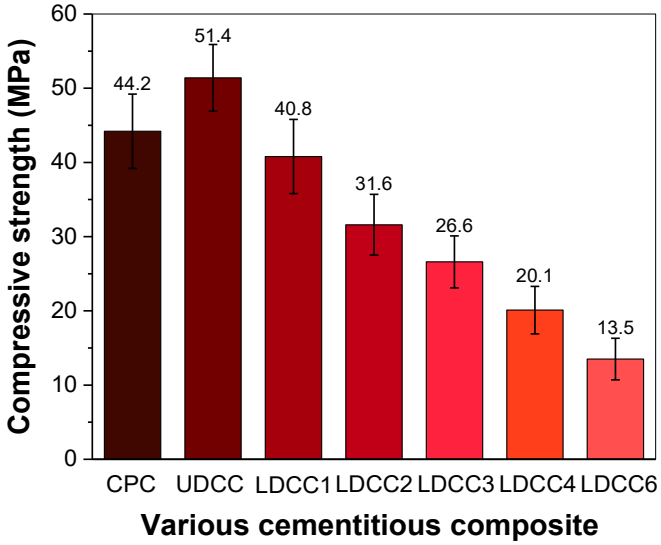

Figure 4.10. Compressive strength of plain cement paste and cementitious composites with various distributions of CNT.

The microstructures of the UDCC and LDCC are depicted in Figure 4.11, to explicate the compressive strength increase of UDCC and the strength reduction in LDCC. It could be found that the CNT in UDCC is straight and separated, while the CNT in LDCC is curved and intertwined. For the cracks in UDCC, it was observed that the well-dispersed CNT having the fibre bridging effect could prohibit the further deformation of cracks. Hence, in comparison to the PCP, the compressive strength of UDCC was greatly improved. In terms of the LDCC, in the transition zone between a CNT layer and cement matrix, a proportion of CNT bundles were found possessing bridging effect as aforementioned. However, the reinforcement effect was much weakened because of the twined CNT. Not only the CNT bundles possessed weaker cohesion to cement matrix than single CNT, but also led to more porous structures surround the agglomerations, thus reduced the density and compressive strength of composites. In addition, the above discussions have proved the stress concentration in the pores induced by larger sized CNT agglomerations. More layers of CNT presented more CNT agglomerations

in a larger size, thus severe stress concentrations and more defects generated for the LDCC with multiple layers of CNT and directly caused the worse compressive strengths.

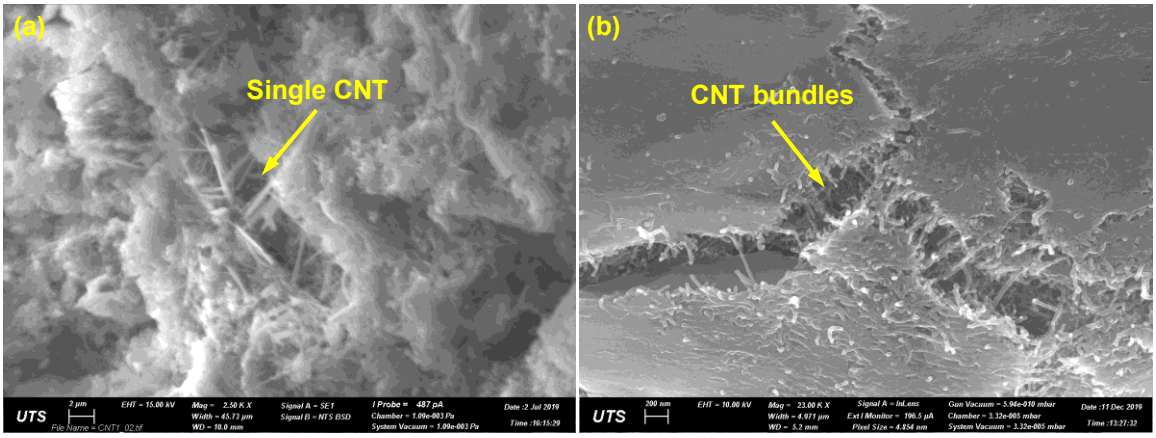

Figure 4.11. Microstructural morphology of CNT in cracks or gaps in different specimens (a) UDCC and (b) LDCC.

4.2.5 Piezoresistivity

The strain sensing efficiency or the piezoresistive sensitivity of the UDCC and LDCC, the FCR as a function to compressive strain is depicted in Figure 4.12. The smallest ultimate compressive strain could be found for UDCC, due to the better density and resistance to deformation. In addition, the strain increasing with the number of CNT layers indicated that the worse mechanical properties of LDCC, especially for those reinforced with excessive CNT layers and agglomerations. To evaluate the strain sensing efficiency of those composites, the ratio of *FCR* to strain named gauge factor *G* was assessed according to the Eq. (6):

$$G = \frac{FCR}{\varepsilon} \tag{6}$$

where *G* the gauge factor; *FCR* the fractional changes of resistivity; ε the compressive strain. It could be seen that the gauge factors of both UDCC and LDCC were changeable due to the non-linearity of FCR-strain curves. As a consequence, linear fitting formulas of these curves were proposed, whose slopes represented the gauge factor based on the Eq. (1). Furthermore,

the parameter to evaluate the unrepeatability of the fitting curves was proposed as well. The unrepeatable rate T was determined according to the Eq. (7):

$$T = \frac{\Delta FCR_m}{FCR_m} \times 100\% \tag{7}$$

where W is the irreversible rate; ΔFCR_m denotes the largest differences of FCR under the identical compressive strain. FCR_m is the average FCR values at the strain/stress peaks.

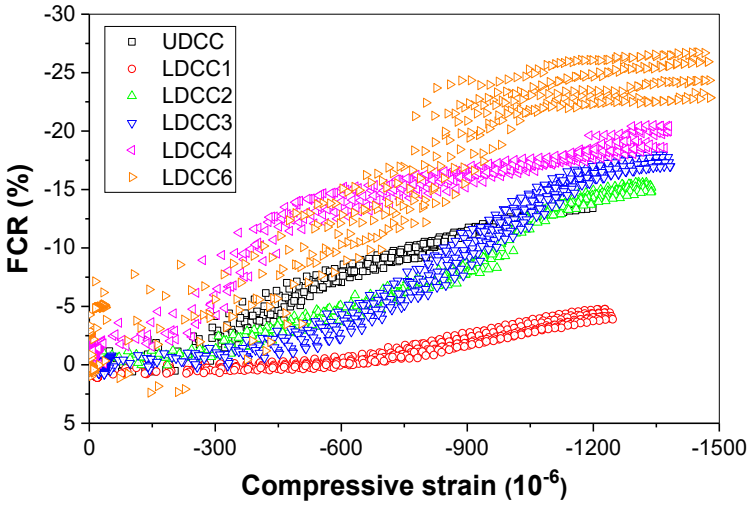

Figure 4.12. FCR as a function to compressive strain for specimens of UDCC and LDCC.

Table 4.1 lists the fitting formulas, deviations, determination coefficient R^2, gauge factor G and the unrepeatable rate T of the UDCC and LDCC. The gauge factor of UDCC reached 127.2, which was more than 60 times higher than that of commercial foil strain gauge (G=2). Unfortunately, the unrepeatable rate of UDCC reached approximately 20.8%, especially when the strain was in small values. The FCR of UDCC altered faster in the initial loading stage than that in the high stress/strain level, which increased the instability of the resistivity output and should be responsible for the high unrepeatability. In addition, only the LDCC1 and LDCC2 possessed a lower gauge factor than that of UDCC, with the values of 38.2 and 112.8, respectively. The reason for the highest unrepeatable rate T is mainly owing to the small ultimate FCR values and the gradually increased resistivity during compression. Because the

composites were subjected to 1-day drying, the continual resistivity increases might due to the polarization effect. As for the LDCC3 and LDCC4, both the gauge factors and unrepeatable rates were slightly larger than those of UDCC, with the former of 136.2 and 149.2 and the latter of 22.9% and 23.0%, respectively. It implied that the LDCC3 and LDCC4 had the potential to replace the UDCC to automatically monitor the compressive strain of cementitious composites. The largest gauge factor of 182.7 occurred for the LDCC6, the samples filled with 6 CNT layers. However, the unrepeatable rate peaked 44.5% due to the significant variations of electrical resistivity under the same strain. In summary, the LDCC2, LDCC3 and LDCC4 possessed similar sensitivity and repeatability to monitor the compressive strain of composites in comparison to the UDCC.

Table 4.1 Proposed parameters of UDCC and LDCC assessing strain sensitivity and linearity

Type	Fitting formula	Deviation of intercept	Deviation of slope	Determination (R^2)	Gauge factor (G)	Unrepeatable rate (T)
UDCC	Y=0.494%+127.2X	±0.038%	±0.6	0.987	127.2	20.8%
LDCC1	Y=1.152%+38.2X	±0.037%	±0.5	0.890	38.2	33.3%
LDCC2	Y=0.566%+112.8X	±0.077%	±1.1	0.947	112.8	23.5%
LDCC3	Y=1.672%+136.2X	±0.109%	±1.4	0.939	136.2	22.9%
LDCC4	Y=-1.796%+149.2X	±0.115%	±1.5	0.936	149.2	23.0%
LDCC6	Y=-1.401%+182.7X	±0.161%	±2.0	0.932	182.7	44.5%

4.3 Graphene (GNP) and graphite (GP)

4.3.1 Physiochemical properties

4.3.1.1 Dispersion efficiency

The absorbance of GNP and GP solutions after ultrasonic treatment and mechanical stirring is illustrated in Figure 4.13. Duration in the x-axis is the time escaped after completion of ultrasonic dispersion. Generally, the higher absorbance means the better dispersion of GNP and GP in the solutions, since the agglomerated and precipitated plates and segregated solutions

have poor performance to absorb light. It was observed that both the GNP and GP solutions at the beginning of measurement showed constant absorbance values regardless of the dispersion methods but the values varied with time because of the GNP/GP particle segregation (Chuah et al. 2014; Devi & Khan 2020; Du, Gao & Dai Pang 2016; Shamsaei et al. 2018). For the solutions with ultrasonic treatment, the absorbance of the GNP solution was maintained very well in the first 50 min. Until it reached 60 min, the absorbance of the solutions started a small reduction. However, for the GNP solution with mechanical stirring, clear absorbance reduction occurred in the first 10 min, followed by a sharper decline in the next 30 min. After that, the absorbance decreased at a much lower rate. Similarly, an identical tendency could be observed from the GP solutions, whose decreasing rate was even higher than that of GNP solutions with mechanical stirring. As mentioned previously that the GP has larger and thicker plates than GNP, the larger weights of GP are more easily to precipitate and responsible for the rapid decrease of absorbance. Overall, it indicates that the ultrasonic treatment of GNP and GP solutions is better than that only with mechanical stirring for uniform dispersion . The dispersion efficiency of GNP is better than GP in the same solutions under identical treatment and duration. Also, since the treated GNP and GP solutions are just followed by the preparation of cementitious composites within 10 min, it demonstrates that the GNP and GP are evenly dispersed in the solutions during the mixing procedure (Dimov et al. 2018).

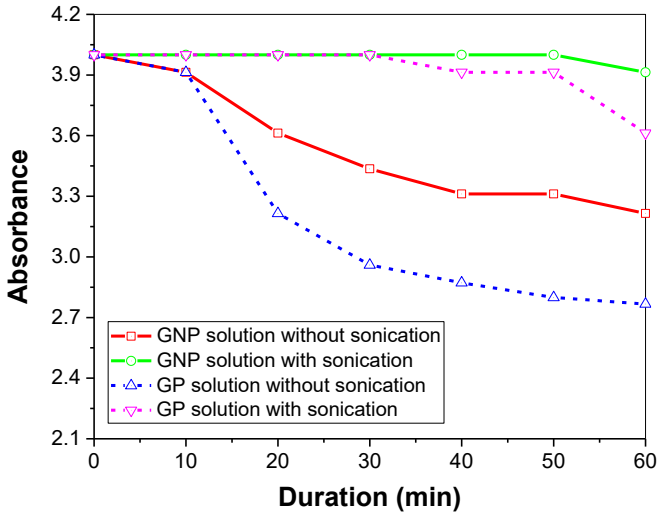

Figure 4.13. Absorbance of GNP and GP solutions after ultrasonic treatment and mechanical stirring under ultraviolet wavelength of 200 nm.

4.3.1.2 Electrical resistivity

Figure 4.14(a) shows the electrical resistivity of GNPC and GPC with different concentrations. Generally, when the content of conductors less than 1%, the electrical resistivity of GNP and GP filled cementitious composites were very similar, and both as high as 1×10^7 Ω·cm. It showed that the contents of GNP and GP from 0.5% to 1% failed to considerably reduce the electrical resistivity of the cementitious composites. Still, the electrical resistivity of GNPC was slightly lower than the counterparts filled with GP. Afterward, the electrical resistivity of GNPC experienced a moderate reduction to approximately 1×10^6 Ω·cm as the content increased to 2%, whilst the GPC only slightly decreased electrical resistivity to nearly 6×10^6 Ω·cm at the same concentration. As for the concentration of 3%, the electrical resistivity of GNPC considerably decreased to only 1×10^2 Ω·cm. It implies that the percolation occurred for GNPC as the content of GNP increased from 2 to 3%. However, the electrical resistivity of GPC did not illustrate an apparent reduction, with the values still up to 4×10^6 Ω·cm.

To explain the performance of GNP and GP for improving the electrical conductivity of cementitious composites, Figure 4.14(b) schematically displays the geometric structures of

GNP and GP in atomic size. Both the GNP and GP are carbon atomic structures combined by sp2 covalent bond. Their difference is that GNP is composed of a single layer of carbon atoms with the thickness of a single carbon atom, while the GP is the stacked carbon atomic layers because of Van der Waals force. It proves that the single-layer atomic structures provide GNP with more excellent electrical conductivity than the GP, which partially contributed to lower electrical resistivity for the GNP filled cementitious composites. Moreover, it was seen that GNP could be manufactured through special treatments on the layered GP from ultrasonication, ball milling to mechanical exfoliation. Once overcome the Van der Waals force, the number of conductive plates for GNP is much higher than that of GP under the same concentration and caused lower resistivity for the GNP reinforced cementitious composites (Dalal & Dalal 2021; Lu & Ouyang 2017; Papanikolaou, Arena & Al-Tabbaa 2019).

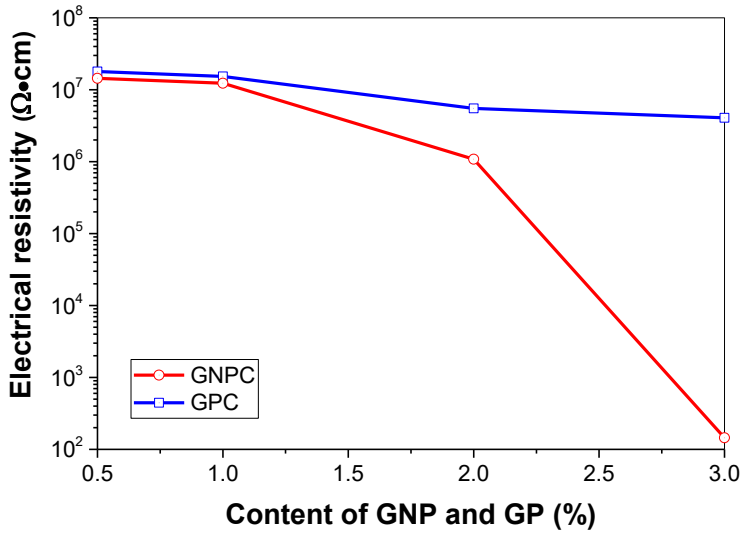

(a) Electrical resistivity of GNPC and GPC

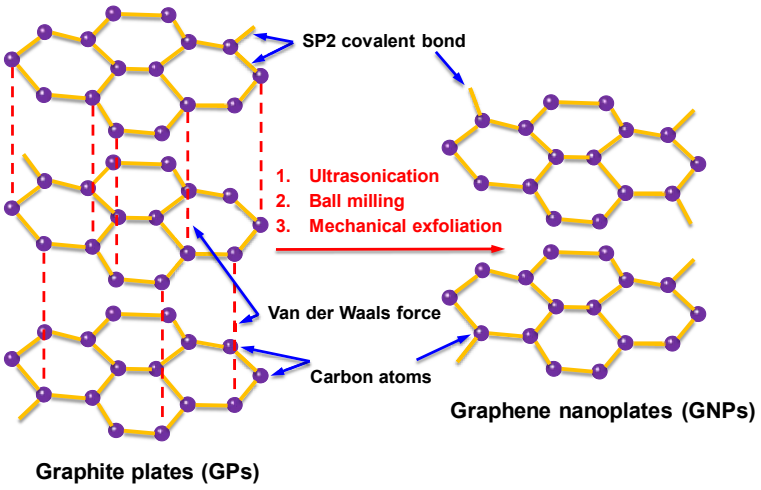

(b) Atomic structures between GNP and GP

Figure 4.14. Electrical resistivity and atomic structures of cementitious composites with different contents of GNP and GP.

4.3.1.3 TGA analysis

Figures 4.15(a) and 4.15(b) show the thermogravimetric results of PCP and the cementitious composites filled with various contents of GNP and GP, to explain the influenced pyrolysis characteristics by GNP and GP. The final mass loss reached 25.7% for GNPC3 while only 21.1% for GNPC05. In addition, the mass losses of the cementitious composites filled with 1.0% and 2.0% GNP were very close at the intermediate level of 21.5% and 22.2%, respectively. The mass changes are consistent with the results by differential scanning calorimetry (DSC), and it can be deduced that the mass losses of GNPC increased with the increase of GNP. Previous studies proposed that the GNP in cementitious composites has a nucleation effect of accelerating the cement hydration (Ghazizadeh et al. 2018; Li, Liu, et al. 2017; Lu et al. 2017; Peng et al. 2019). Moreover, it was found that GNP has the capacity to ameliorate the thermal stability of cementitious composites through the heat transfer by sheets, which also benefits the cement hydration. In this section, the increasing mass losses represented increased hydration products amount of bound water and C-S-H in cementitious composites, which indicated that the cement hydration was improved for the composites with higher GNP. In terms of the

cementitious composites filled with GP, a similar tendency was observed by the increased mass loss and DSC values with the increased contents of GP. In comparison to the cementitious composites filled with GNP, the mass losses reached approximately 18.1%, 21.2%, 22.8% and 24.8% respectively for the composites filled with 0.5%, 1.0%, 2.0% and 3.0% GP, and all lower than the counterparts with same content of GNP. As mentioned before that the loss mass could qualitatively assess the hydration degree of composites, the smaller mass losses demonstrate lower generation of C-S-H and other hydration products for the composites filled with GP.

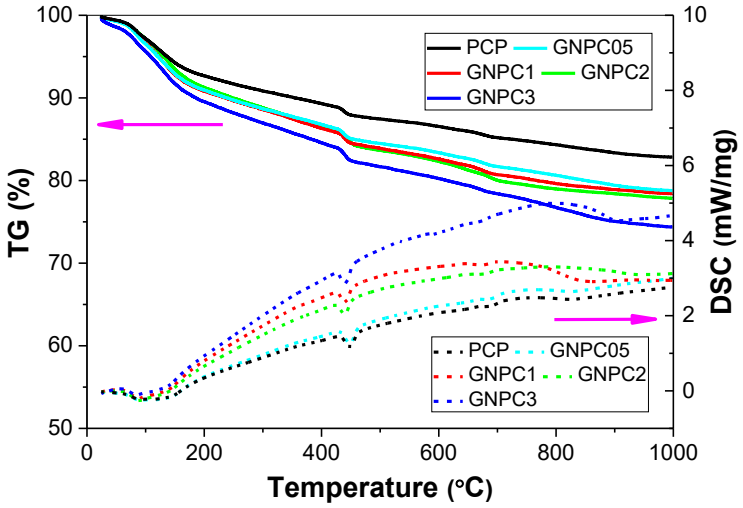

(a) Composite filled with GNP

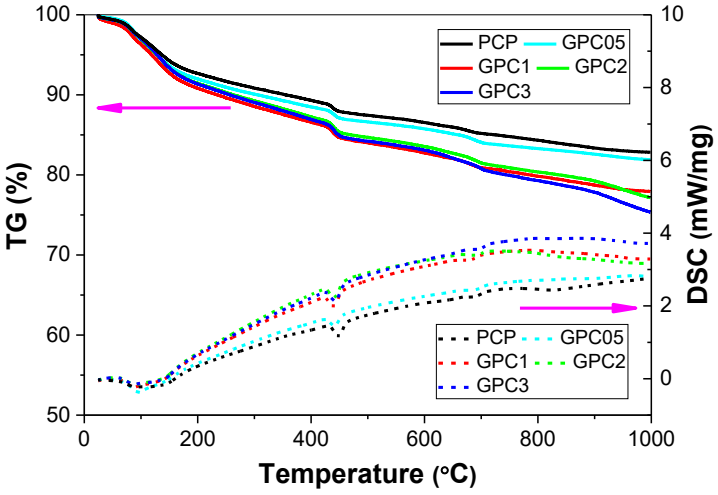

(b) Composite filled with GP

Figure 4.15. Thermogravimetric results of cementitious composites with various content of GNP or GP at 28-day age.

Figure 4.16 presents the first derivative of thermal-gravity results (DTG) to further compare the pyrolysis characteristics influences by GNP and GP. Generally, the first peak at around 100 °C means the decomposition of ettringite and C-S-H, the second peak at 440 °C represents the dehydration of portlandite and the third peak at 680 °C is the decarbonation of calcium carbonate. In particular, the area under the peaks can evaluate the amount of generated hydration products. For all the dosages, it was observed that the areas by the blue lines (GNP) are larger than those by red dotted lines (GP), indicating the more generated hydration products for the composites filled with GNP.

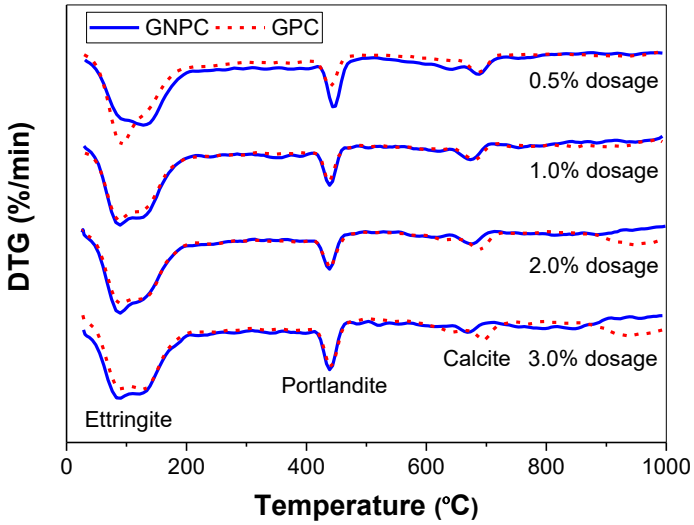

Figure 4.16. DTG curves of cementitious composites with various contents of GNP and GP.

4.3.1.4 Hydration heat analysis

Figures 4.17(a) and 4.17(b) show the effect of GNP on the hydration heat release and cumulative hydration heat of cement paste and the cementitious composites with 0.5, 1, 2, and 3% GNP. It was found that the hydration heat at the acceleration period (before the peak of the hydration rate) increased with the increase of GNP. The results are consistent with the conclusions drawn by TGA that the nucleation effect of GNP can accelerate the hydration of cement paste. Moreover, the peak of hydration rate shifting to the left indicated that the

hydration duration to reach the hydration heat peak decreased with the increase of GNP, demonstrating that the GNP had the capacity to promote the early hydration of cementitious composites. Instead, the hydration in the late stage was slightly retarded compared to that of the cement paste. In terms of the cumulative heat of hydration, both the early hydration at the first 0.5 hr and the late hydration at 70 hrs were plotted. It was detected the higher cumulative hydration heat with the increase of GNP, which were more apparent, especially in the early hydration stage. Although the late hydration rate gently decreased with the increase of GNP, the cumulative heat of hydration is still higher than that of cement paste or the composites with less GNP due to the significant hydration acceleration in the early stage.

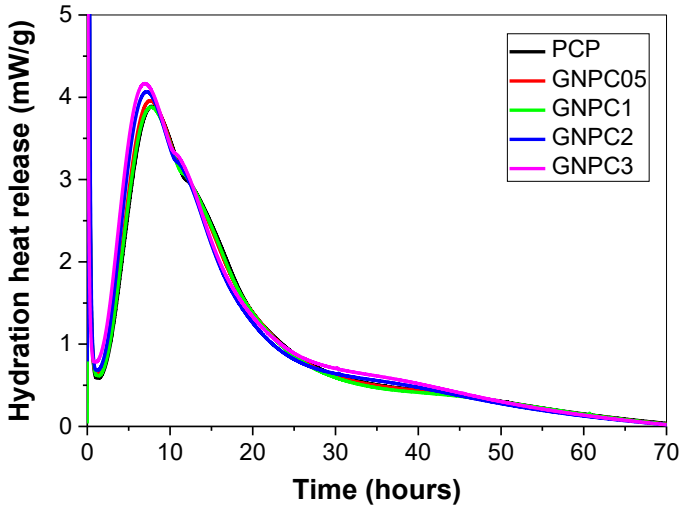

(a) Hydration heat release

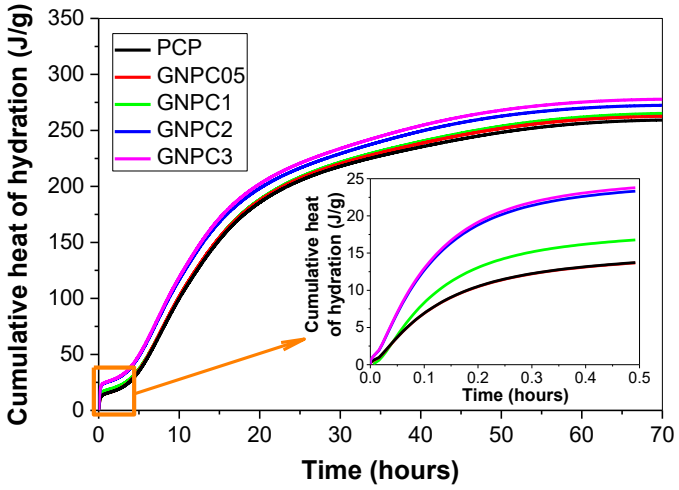

(b) Cumulative heat of hydration

Figure 4.17. Hydration heat release and accumulative heat for cementitious composites with various content of GNP.

Similarly, Figures 4.18(a) and 4.18(b) show the rate of hydration heat and cumulative hydration heat of cementitious composites filled with GP. Different from the counterparts filled with GNP whose hydration heat peaks shifted to left, it was observed that the rate of hydration heat increased with the increased GP content but without clear advance. It means that the GP still possesses the nucleation effect to improve the peak of hydration rate in cementitious composites, just like the effect of GNP on hydration acceleration. However, because of the larger thickness of GP which has lower efficiency to achieve the nucleation effect, it seems that the GP was failed to reduce the duration to obtain the hydration heat peak at an earlier date. As illustrated in Figure 8(b), even though the results were similar among composites with 0.5, 1.0 and 2.0% GP, the final hydration heat accumulation still increased with the increase of GP. In addition, it was found that the cumulative heat of hydration within the first 0.5 h ranked the highest values for the composites filled with 0.5% GP. It proposes that the sheets in cementitious composites have a dilution effect of diluting the main compounds during cement hydration . The small content of GP worked as nucleation site can promote the hydration in comparison to the cement paste, and meanwhile cause the minimal dilution effect. However, the increased GP gradually enhance the dilution effect, and cause fewer contacts between hydrated compounds. Due to the larger thickness of GP, the nucleation effect cannot be fully achieved at the beginning of hydration, and lead to the fact that the positivity brought by the nucleation effect is overwhelmed by the negativity brought by the dilution effect.

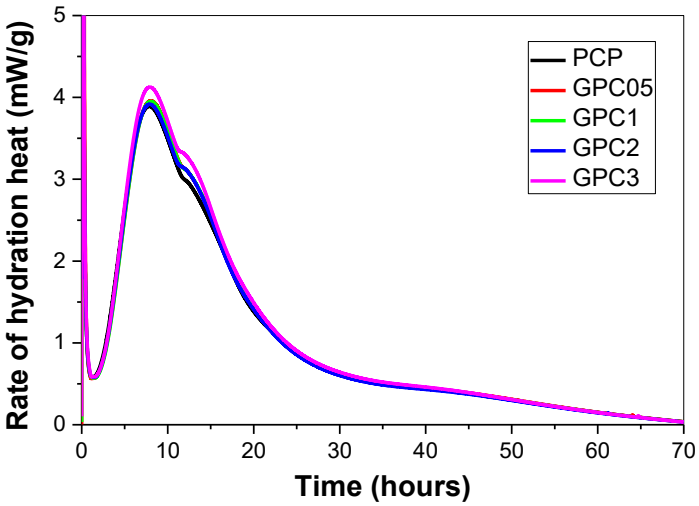

(a) Rate of hydration heat

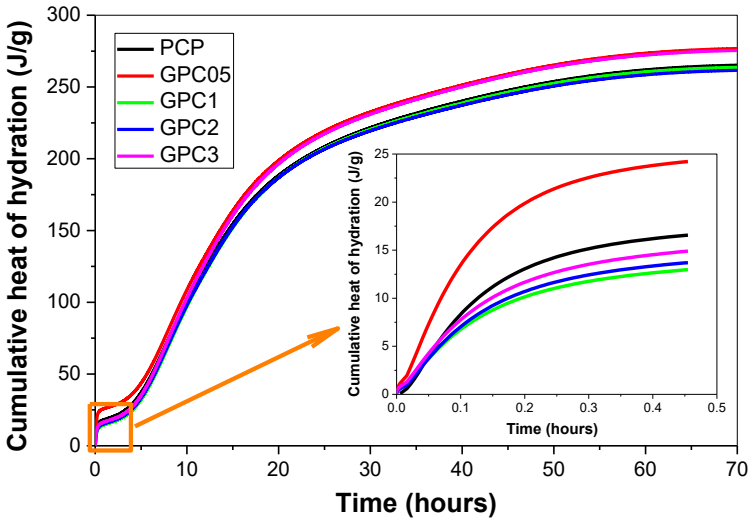

(b) Cumulative heat of hydration

Figure 4.18. Rate of hydration heat and accumulative heat for cementitious composites with various content of GP.

4.3.1.5 XRD analysis

Figures 4.19(a) and 4.19(b) illustrate the XRD results for the cement paste and the composites filled with GNP and GP, which can quantitatively represent the phase differences among various composites. For all composites, it was observed that the intensity of portlandite increased with the increase of GNP and GP, which indicated a higher degree of hydration with the increased conductors. Moreover, the hydration degree can be reflected by the X-ray

intensity of OPC clinkers. The gradually decreased OPC clinkers with the increased content of GNP and GP presented a higher hydration degree and demonstrated the positive effects of GNP and GP on the hydration of cement paste.

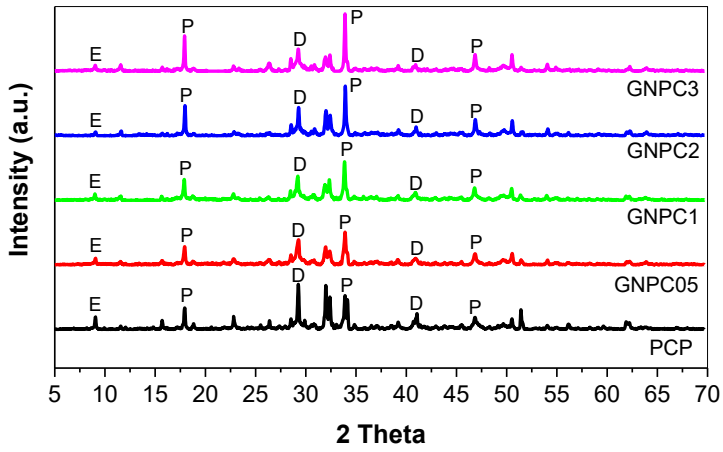

(a) Composites filled with GNP

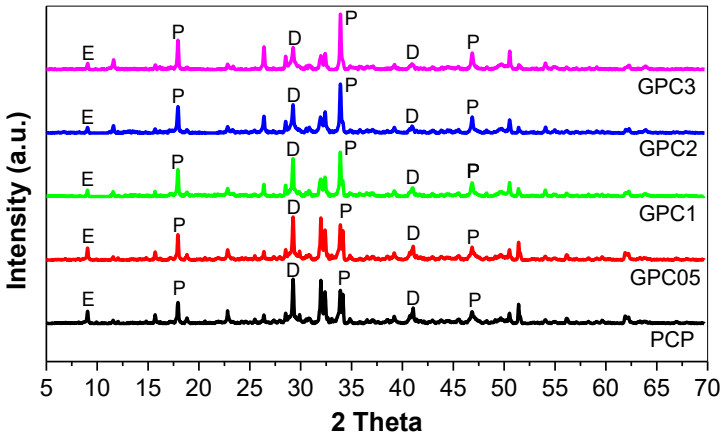

(b) Composites filled with GP

Figure 4.19. XRD analysis for the cementitious composites with: (a) GNP, and (b) GP. (E = ettringite; P = portlandite; D = OPC clinkers) at 28 days age.

4.3.2 Mechanical and micro properties

The compressive and flexural strengths of GNPC and GPC are illustrated in Figures 4.20(a) and 4.20(b). For the composites filled with GNP, both compressive and flexural strengths were firstly increased then decreased with the increase of GNP content. The optimal content of GNP reaching 1.0% could achieve the cementitious composites with the best mechanical properties,

whose compressive and flexural strengths reached 53.6 and 3.6 MPa, respectively. The strengths slightly decreased as the GNP content reached 2% but still larger than that of PCP. Until the concentration of GNP reached 3%, the negativity started to emerge with both lower compressive and flexural strengths to the plain cement paste. Different from the GNP filled cementitious composite, it seems that the GP nearly made no improvements on the mechanical properties of cementitious composites. The compressive and flexural strengths only slightly increased in the case of a small dose of GP of 0.5%, and then the strengths dramatically declined with the increase of GP. For the GPC3, the reduction rates for the compressive and flexural strength peaked at 18.9% and 17.2%, respectively.

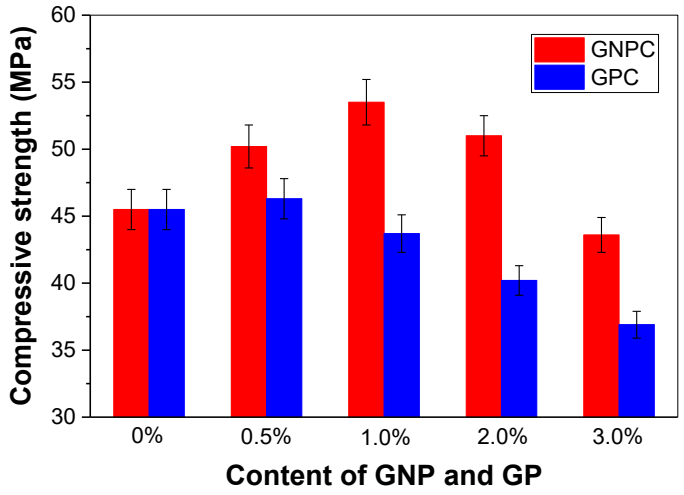

(a) Compressive strength

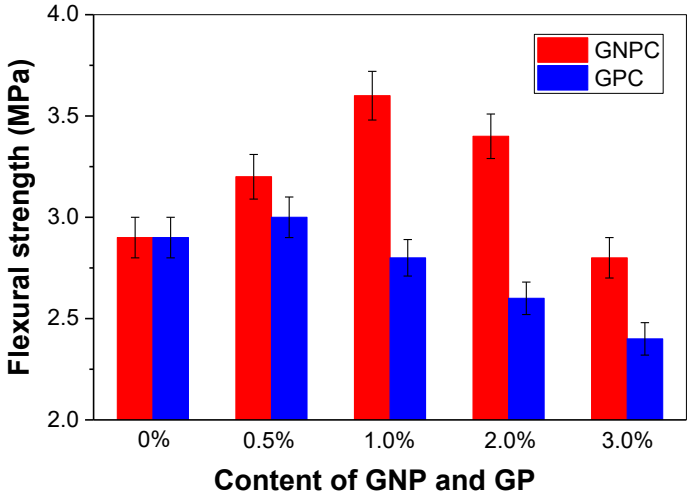

(b) Flexural strength

Figure 4.20. Compressive and flexural strength of cementitious composite with GNP or GP at 28-day age.

Figure 4.21 shows the microstructures of GNPC05 by SEM, attempting to explain the reinforcement and reduction mechanism on the mechanical properties. It was seen that the thickness of GNP is in the nanoscale, which not only has high strength and modulus, but also possesses an extremely high specific surface area. Therefore, it was clearly observed that the GNP provided a large space in the cementitious composites so the hydration products generation could adhere to the surface, just as illustrated in Figure 4.21(a). The EDX results on carbon element were applied to distinguish the GNP from the cement hydration products, as shown in Figure 4.21(b). In addition to the nucleation effect, GNP as the reinforcements in the cementitious composite also played a bridging effect to bond the cement matrix because of the structures of nano-sheets. The reinforcement effect relates to the specific concentration of conductive fillers. Combining the aforementioned TGA and TAM air results, this is consistent with the fact that the cement hydration is stimulated with the increase of GNP. As for the decreased mechanical properties for the composites with 3% GNP, the reason is mainly due to the poor distribution of GNP in the composites. Figures 4.21(c) and 4.21(d) illustrate the microstructures of GNPC3, where significant GNP agglomerations and the induced micro defects could be found. Since all the GNP solutions were prepared under identical circumstances, the higher concentration of GNP means the worse dispersion of GNP solutions and more GNP agglomerations. The GNP agglomeration without any bearing capacity is prone to lower the density of cementitious composites and make loose microstructures. Furthermore, the macro pores around the GNP agglomerations were observed.

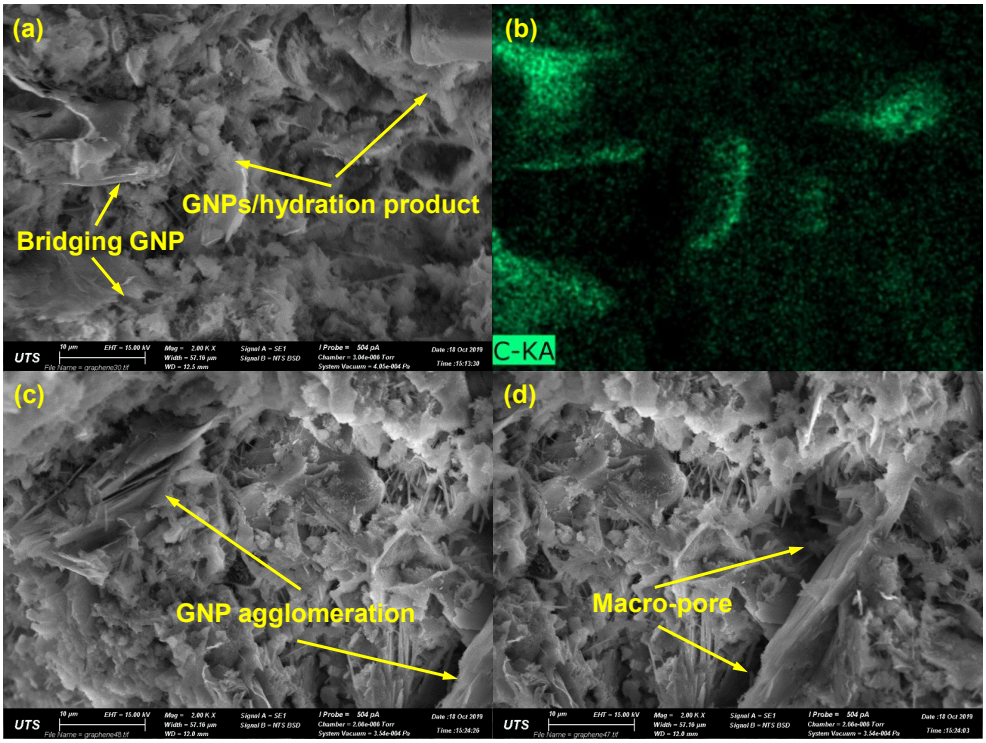

Figure 4.21. Microstructural morphology of GNP reinforced cementitious composites.

In terms of the composites with a small GP dose, it seems that both the accelerated cement hydration and the filled pores contributed to the improved mechanical properties. However, the large sheets of GP which are not involved in the hydration process have worse cohesion to cement matrix. As shown in Figures 4.22(a) and 4.22(b), it was observed that the GP in the cementitious composites tended to spall from the cement matrix. In addition to the worse cohesion between GP and cement matrix, as mentioned before that there exists Van der Waals force between sheets in GP, the small forces make the GP easily to slip between layers . When the GP filled cementitious composites under external forces, the slipped layers will greatly damage the microstructures and cause decreased mechanical properties. Furthermore, there existed similar agglomeration problems between GP when the dosage of the GP is high in the cementitious composites. Figures 4.22(c) and 4.22(d) show the micromorphology of the GPC3, where the GP agglomerations could be clearly observed. Different from the GNP which agglomerated layer by layer, it was observed that the GP clustered much randomly. This is probably due to the smaller surface activity for the GP than that of GNP. Overall, in comparison

to the microstructures of the GNPC and GPC, the excellent connection between cement matrix to GNP and poor cohesion between GP to cement matrix could be found, which should be responsible for their mechanical properties differences.

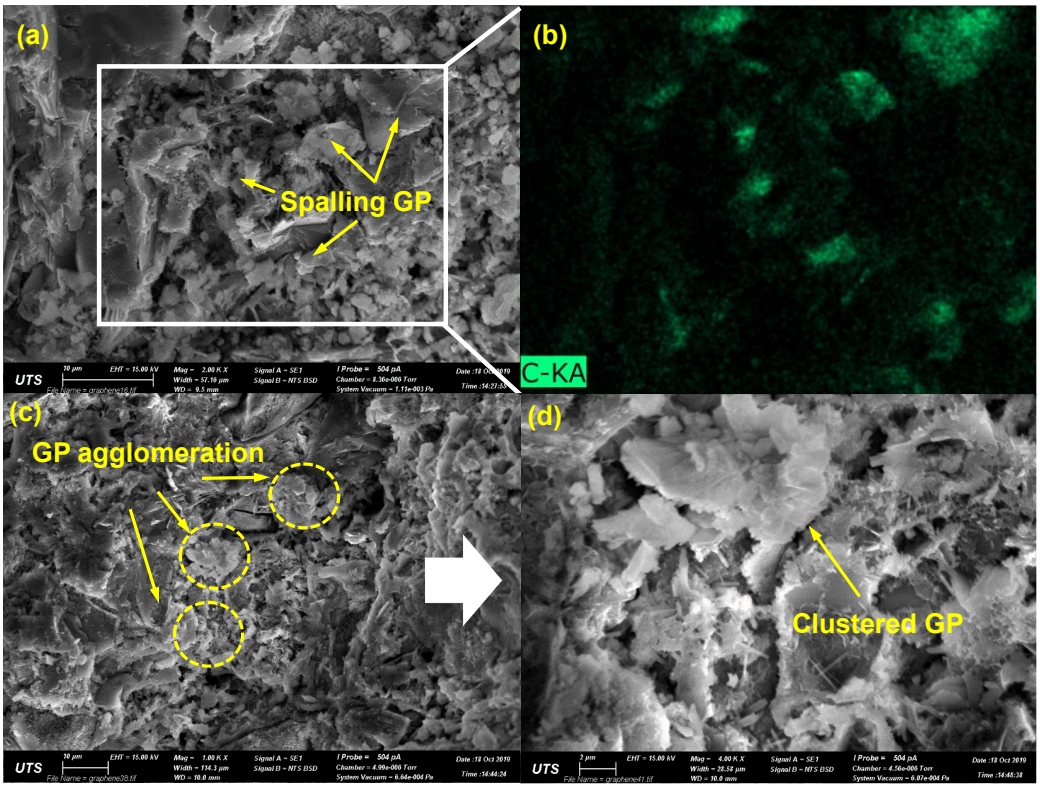

Figure 4.22. Microstructural morphology of GP reinforced cementitious composites.

4.3.3 Piezoresistive behaviours

4.3.3.1 Piezoresistive characterization

Figure 4.23 illustrates the relationship between fractional changes of electrical resistivity and the applied compression for the cementitious composites with GNP and GP, to compare their piezoresistive stability, sensitivity and repeatability. Since the composites were dried before the piezoresistive test to eliminate the polarization effect, stable resistivity output was observed without continual increasing or decreasing during resistivity measurement. Also, the stability of the composites could be assessed through the well-maintained electrical resistivity when the compressive stress was kept constant. The piezoresistive stability can lay a foundation for the cementitious composites with GNP and GP to become the stress sensor.

In addition to the acceptable stability, the sensing efficiency of the cementitious composites is important to practical applications. Generally, the GNPC and GPC presented completely different piezoresistive sensitivity. It was observed that the GNPC was provided with more significant fractional changes of resistivity than the counterparts with GP at any dosages. Moreover, for the composites with identical conductors, the fractional changes of resistivity increased with the increase of GNP or GP. Especially for the composites with a dosage of 3% conductors, the resistivity changes were as great as approximately 30% and 13%, respectively for the GNPC3 and the GPC3. Combining the results of electrical resistivity, it was found that the better electrical conductivity for the cementitious composites benefited the piezoresistive sensitivity. This can be explained by the number of conductive passages and the contact points in the composites . The high concentration of conductors and lower electrical resistivity of composites represented the more generated conductive passages and more contact points. During the piezoresistive test, the more contact points between nearby conductors tended to link or separate with each other, and caused the higher fractional changes of resistivity.

In terms of the piezoresistive repeatability, repeatable electrical resistivity could be observed for all the GNPC because of the small resistivity irreversibility after the cyclic compression. As for the GPC, satisfactory repeatability was observed in the case of the small dosages at 0.5% and 1.0%. However, considerable irreversibility immerged when the concentration increased to 2.0 and 3.0%, with the irreversible resistivity reached approximately 2.5% and 5.0%, respectively. This is consistent to the abovementioned mechanical properties and the microstructures of the cementitious composites with GNP and GP. The GNP had an excellent connection to cement matrix and made denser microstructures of GNP/cement composites with higher compressive and flexural strength. In contrast, the GP tended to cause worse cohesion with the cement matrix due to the weak Van der Waals force between sheets which might lead to slippage and the spalling of GP, and resulted in reduced mechanical properties. Therefore,

the irreversible electrical resistivity could be easily generated for the composites with a high dosage of GP, owing to the lower compressive strength and the loose microstructures.

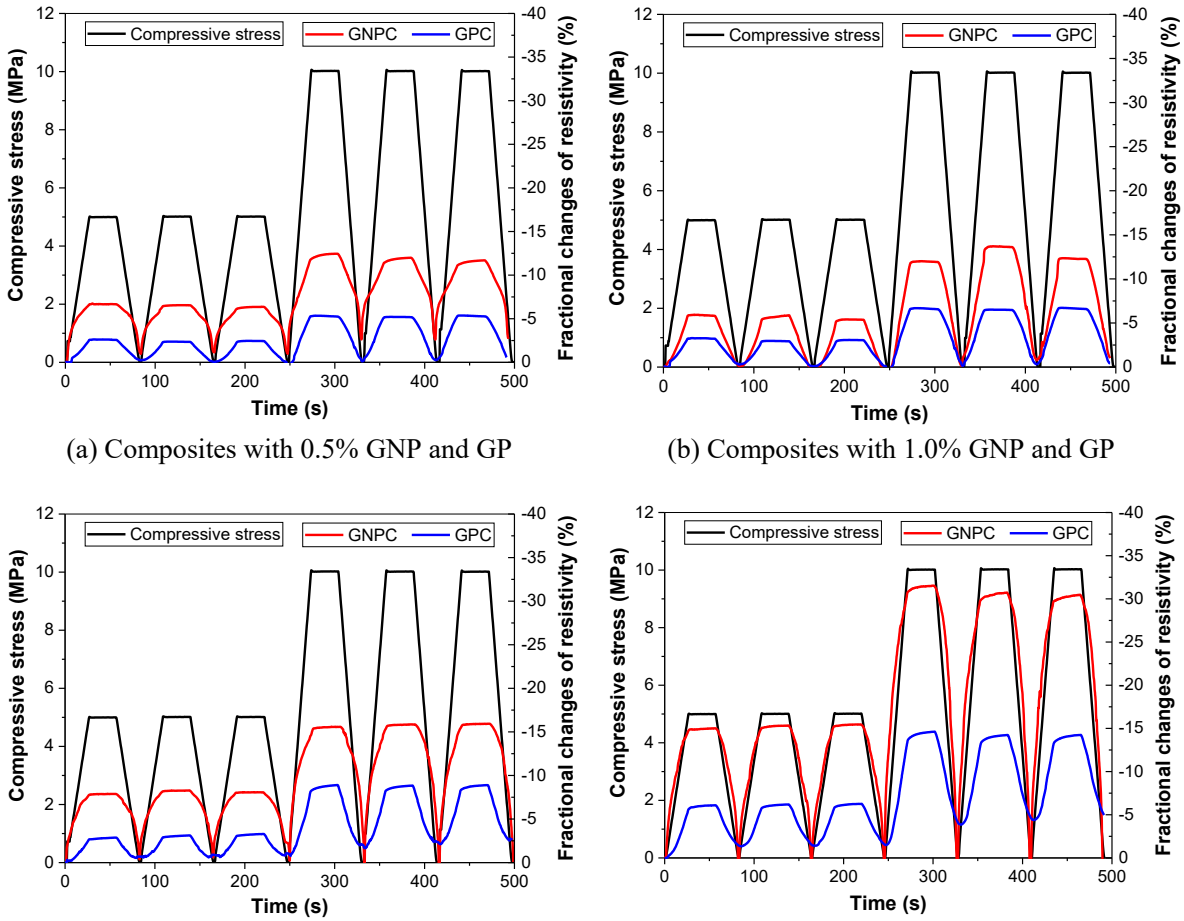

(a) Composites with 0.5% GNP and GP

(b) Composites with 1.0% GNP and GP

(c) Composites with 2.0% GNP and GP

(d) Composites with 3.0% GNP and GP

Figure 4.23. Fractional changes of resistivity for cementitious composites with GNP and GP under cyclic compression.

4.3.3.2 Mechanism discussion

The GP is in the shape of a small thick plate and GNP is a similar plate with a larger size and thinner thickness. Previous studies have demonstrated that the conductive fillers with a high aspect ratio could more efficiently improve the electrical conductivity of cementitious composites. However, none of the studies explored the effect of shape of conductive plate on the electrical conductivity and piezoresistivity of cementitious composites. Based on the piezoresistive results and the SEM images, Figure 4.24 plots the morphological

characterization of the conductive fillers of GP and GNP. For the better improved electrical conductivity of composites with GNP, it could be simply explained by the larger conductive plates that could easier form continual conductive passages. Besides, in the case of identical concentration of GP and GNP, the number of GNP is much larger than GP in the composites which are also beneficial to establish conductive passages, as plotted in Figure 4.24(a). This could explain why the percolation threshold only occurred on the composites filled with GNP rather than that with GP. In terms of the piezoresistivity, as shown in Figure 4.24(b), more potential contact points could be observed for the conductive filler of GNP in comparison to the GP. The potential contact points mean the specific locations where adjacent conductive fillers have the possibility to contact with each other under external forces. The connection of conductive fillers under compressive forces provides the passage for electrons movement and decreases the total electrical resistivity of composites. Since the GNP has a larger size and more numbers of plates than GP, the number of potential contact points in the GNP filled composites is hence more than that in the composites with GP. That is why the fractional changes of resistivity or the piezoresistivity is larger for the composites reinforced with GNP.

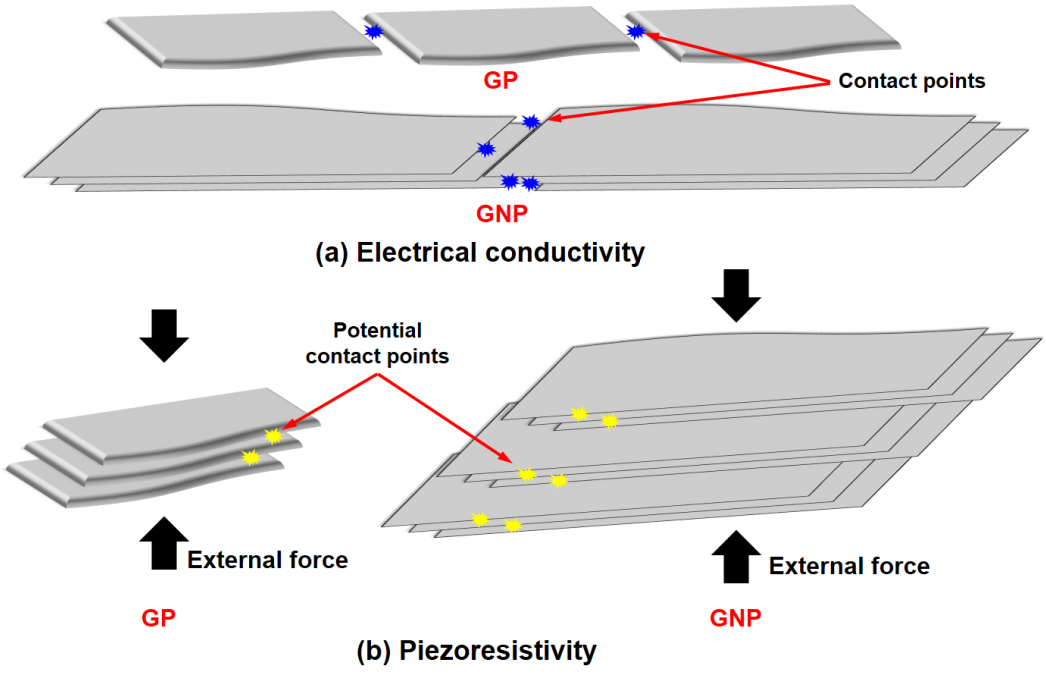

Figure 4.24. Schematic plot of contact points among GP and GNP in cementitious composites under external force.

4.4 Summary

The CB, CNT, GNP and GP filled cementitious composites with different dosages of fillers were explored, including their compressive strength, the improved electrical conductivity and piezoresistivity. The main conclusions can be drawn up as follows:

(1) For composites filled with 0.1 wt%, 0.5 wt%, 1.0 wt%, 2.0 wt% and 4.0 wt% CB, the w/b ratios of 0.31, 0.32, 0.34, 0.4 and 0.5, respectively, could provide the composites with similar and excellent workability. The composites with 1.0 and 2.0% CB seemed to possess an excellent piezoresistivity.

(2) The sizes of CNT agglomerations in the LDCC were in the ranges of several microns to dozens of microns. The smaller sized agglomerations had smoother boundaries and became more spherical. In contrast, the larger sized agglomerations possessed worse roundness and led to more similar shaped pores, which might cause stress concentration in cementitious composites and reduced mechanical properties.

(3) As for the strain-sensing performance, the LDCC1 possessed the lowest gauge factor of 38.2. The LDCC6 possessed the highest gauge factor of 182.7, but it exhibited the worst linearity and repeatability to restrict the application. The UDCC, LDCC2, LDCC3 provided with both acceptable stability and sensitivity with the gauge factor of 127.2, 112.8 and 136.2, respectively.

(4) UV results indicated that the absorbance values of the GNP and GP solutions made from ultrasonication were much higher than that of the corresponding solutions made from mechanical stirring. The absorbance values of these solutions decreased with time escaped after completion of dispersion, implying the potential GNP and GP agglomeration or segregation.

(5) Both the GNP/cementitious and GP/cement composites exhibited excellent stability on the electrical resistivity, due to the well-maintained resistivity under the invariable forces. GNP/cementitious composites provided higher fractional changes of piezoresistive resistivity than GP/cementitious composites, probably due to the more contact points between GNP.

CHAPTER 5: ENHANCED CONDUCTIVITY AND PIEZORESISTIVITY WITH ADDITIVES

In this chapter, multiple solutions have been proposed such as the addition of rubber fibres, PP fibres and silica fume to enhance the electrical conductivity and piezoresistivity of cement-based sensors.

5.1 Effect of conductive rubber fibres

5.1.1 Conductivity percolation of CB cementitious composites

This section introduces the conductive rubber fibres mixed with the CB composites, to track the trace of percolation threshold of rubber/CB filled composites under the influence of conductive rubber fibres. The only CB filled composites, and the rubber/CB filled composites with 20 (0.32 vol.%), 40 (0.64 vol.%) and 80 (1.27 vol.%) conductive rubber fibres were investigated and compared in accordance of their resistivity development, as displayed in Figure 5.1. The composites with 20 rubber fibres (0.32 vol.%) exhibited slightly lower resistivity than that without rubber fibres, and that tendency became more noticeable for the composite with 40 (0.64 vol.%) conductive rubber fibres. The end of percolation worked as demarcation point, and two sections were created with one being before/in the process of percolation and another being at the stage after the percolation. In the first section, the electrical resistivity was sensitive to the amount of rubber fibres and an obvious reduction could be observed with the increase of rubber fibres. However, this reduction was gradually decreased and significantly narrowed after the percolation. For the composites with 4.0 wt.% CB, the effect of conductive rubber fibres on electrical resistivity was nearly disappeared. Similar results were observed from the composites with 80 rubber fibres (1.27 vol.%), the influence by conductive rubber fibres was negligible when the CB content exceeded 1.0 wt.%.

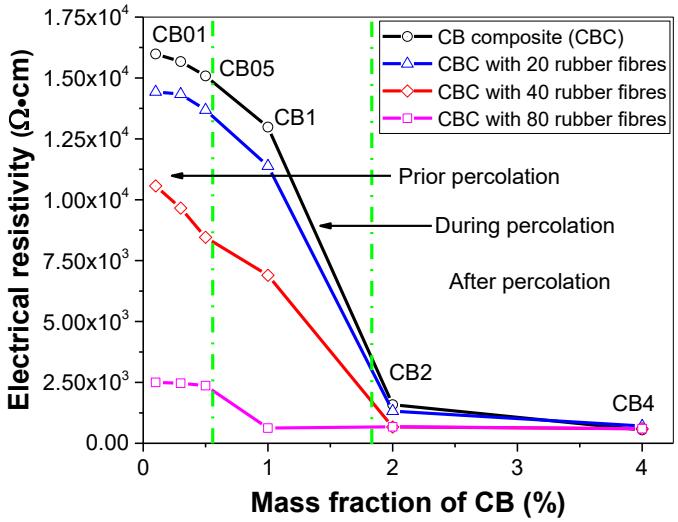

Figure 5.1. Resistivity as a function of different contents of CB composites with various amounts of conductive rubber fibres.

In terms of the percolation threshold, the composites with only CB had initial percolation threshold from 0.5 wt.% to 1.0 wt,%, which decreased with the increase of rubber fibres and dropped as low as 0.5 wt.% for the same composite embedded by 80 rubber fibres (1.27 vol.%). It indicates that the conductive rubber fibres could lower the threshold and make the composite easier to achieve percolation. This phenomenon could be explained by the schematic diagrams in Figure 5.2. The conductive passages (red lines) might exist when the CB content was low with the majority of CBs being short and separated. Thus, the resistivity of composites was relatively high. Howbeit with the assistance of conductive rubber fibres (blue lines), the separated conductive paths gradually contacted with each other and linked to form continual conductive passages, which presented resistivity decrease. The more rubber fibres, the more connected conductive passages, and the lower resistivity the composites exhibited. Nevertheless, for the composites with CB content exceeding the percolation threshold, where conductive passages already formed and connected, limited impacts could be provided by the conductive rubber fibres, and that may be the reason for the negligible influences after percolation.

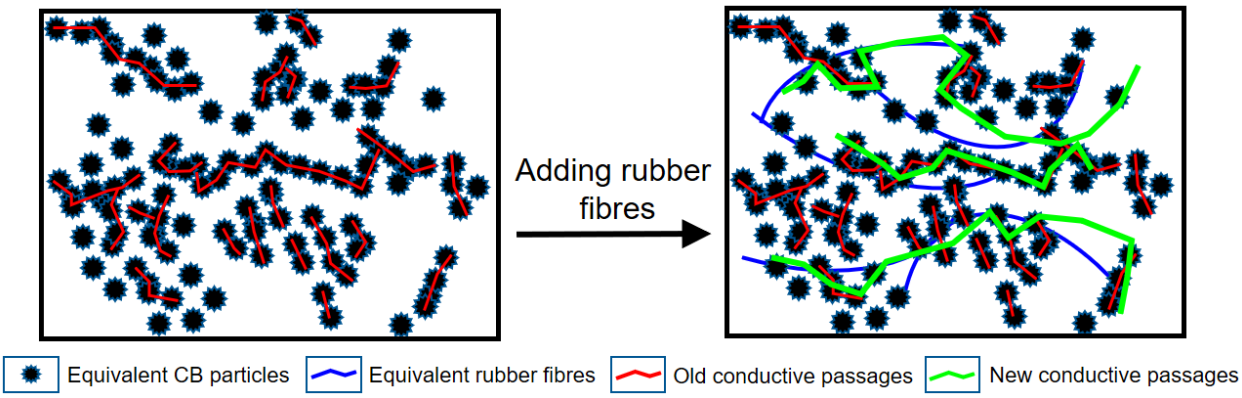

Figure 5.2. Schematic diagram of the functionality of conductive rubber fibres on CB/cement composites.

On the other hand, apart from the aforementioned conductive mechanism along the fibres longitudinal direction, special conductive passages could be established through the rubber fibres from different layers. In the transversal surface of the CB/rubber filled composite, different kinds of conductive passages could be created by the two conductive phases' linkage of rubber fibres to the dispersed CB particles, rubber fibres to CB agglomerations or the interconnections between rubber fibres, CB particles and agglomerations themselves. Predictably, the vertical conductive paths could not only lower the volume resistivity, but somewhat improve the conductivity in the direction of rubber fibres. Overall, it was the electrical conductivity amelioration on both longitudinal and transversal directions by conductive rubber fibres that improve the conductivity and reduce the percolation of the CB/cement composites.

5.1.2 Piezoresistivity behaviours

5.1.2.1 Composites with 0.5 wt.% CB

Figure 5.3 illustrates the fractional changes of resistivity for the composites filled with 0.5 wt.% CB and embedded by different amount of conductive rubber fibres. The selection of approximately 2000 με as the ultimate strain is to ensure that the composites at the elastic stages, which outputs a more stable strain to determine the fractional changes of resistivity and

gauge factor. Among them, positive correlation between fractional changes of resistivity and strain could be observed. Moreover, since the loading process was stress-controlled compression, it could be observed that the composites with larger rubber content reached the preset strain quickly because of the lower stiffness and elastic modules induced by conductive rubbers.

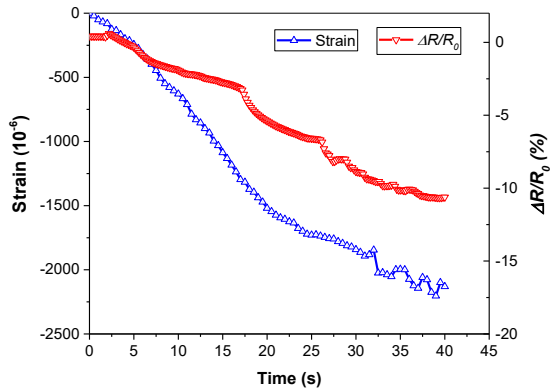

(a) Composite without rubber

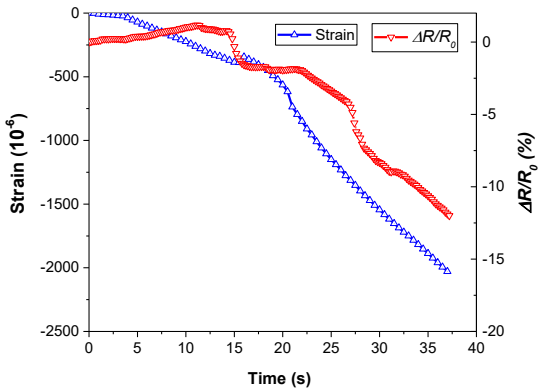

(b) Composite with 20 rubber fibres (0.32 vol.%)

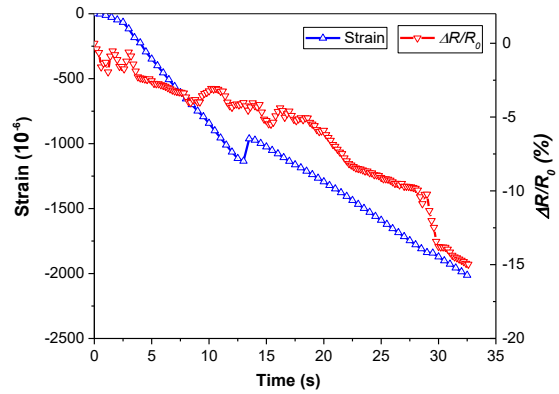

(c) Composite with 40 rubber fibres (0.64 vol.%)

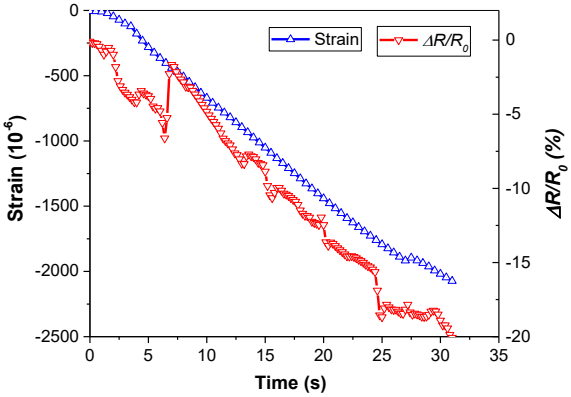

(d) Composite with 80 rubber fibres (1.27 vol.%)

Figure 5.3. Fractional changes of resistivity for 0.5 wt.% CB/cement cementitious composites.

For the composites without rubber, more stable outputs of fractional changes of resistivity were observed, with the ultimate changes reaching 10.6%. The gentle resistivity increase at the beginning was owing to the polarization of composites, which could be negligible compared with the resistivity reduction caused by the compressive strain. For the composites with 20 rubber fibres (0.32 vol.%) embedded, whose fractional changes of resistivity were fluctuated

with compressive strain, was provided with slightly better piezoresistivity to 12.5%. Furthermore, when the rubber content increased to 40 (0.64 vol.%) and 80 (1.27 vol.%) fibres, the maximal fractional changes of resistivity rose to 15.0% and 20.1%, respectively, which were accompanied by more vulnerable fractional changes of resistivity, and both with sudden decreases. In general, there were two main reasons responsible for the resistivity fluctuation, including cracks and pores inside specimens and the interference from the conductive rubber. The distinguish of these two factors for resistivity fluctuation could be carried out by means of compressive strain observation, which was often smooth and continual in the process of loading for the dense and compact composite, but followed by sudden changes if there were cracks and pores inside the composite. In terms of the effect by conductive rubber, the existing contacted nearby rubber fibres might be detached or the separated ones might be connected in the process of loading, which greatly affects the electrical resistivity of the composites.

Although the changes of resistivity unstably increased with strain, especially for the composites embedded with rubber fibres, similar increase patterns could be seen from both strain and fractional changes of resistivity for all the composites. To better understand their relationship and the gauge factor, Figure 5.4 depicts the correlation between compressive strain and the fractional changes of resistivity for different rubber contents embedded composites, where specially established linear fitting formulas for the composites to show their gauge factors. It could be observed that the fractional changes of resistivity to strain curves were almost straight lines for both composites, especially when eliminating the sudden resistivity changes caused by the pores/cracks. Hence, in consideration of the elastic loading regime during compression, it could be indicated that the CB/rubber cement-based composite possess acceptable performances to self-monitor its compressive strain. As shown in Figure 8, the slopes of the fitting lines represented the gauge factors to evaluate the piezoresistive sensitivity of CB/rubber cementitious composite (The following figures are deviations). For the

composites without rubber and the counterparts embedded with rubber contents from 20 (0.32 vol.%), 40 (0.64 vol.%) to 80 (1.27 vol.%) fibres, their gauge factors were 51, 59, 61 and 91, respectively. In comparison to the composites only filled with CB, positive effects could be seen that the gauge factors of CB filled composites embedded with conductive rubber were significantly increased with the growth rate reaching 15.7%, 19.6% and 78.4%, with 20 (0.32 vol.%), 40 (0.64 vol.%) to 80 (1.27 vol.%) rubber fibres, respectively.

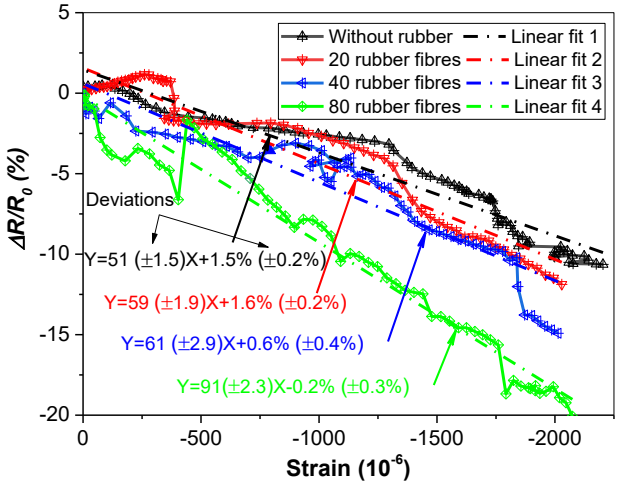

Figure 5.4. Correlation between fractional changes of resistivity and compressive strain and their linear fits for the 0.5% CB/cement composites with/without rubber fibres.

To compared the results with other studies, Monteiro et al. (Monteiro, Cachim & Costa 2017) investigated the CB filled cementitious composite and obtained the gauge factor of approximately 25 under 10 cycles of cyclic compressive loading. It was achieved higher gauge factor of 45 by using better CB dispersion technology of sonication (Monteiro et al. 2017). Furthermore, Li et al. (Li, Xiao & Ou 2006; Li, Xiao & Ou 2008) obtained gauge factor of approximately 55 for CB composite, and their CB dispersion method was through water reducing agent and deformer rather than sonication. Generally, one reason for their gauge factors discrepancy probably is due to the different CB content, and the CB cementitious composite from Li et al. (Li, Xiao & Ou 2008) seems to have better electrical conductivity and thus possesses a higher gauge factor. Another reason is the aggregates, which obviously

decreased the gauge factors in Monteiro et al. (Monteiro et al. 2017). In this study, the gauge factor of the cementitious composite only filled with 0.5 wt.% CB was 51, similar to the other values. The instable outputs were possibly due to the lack of drying process, and the higher gauge factor might be due to the positive effects by silica fume. Overall, the gauge factor amelioration of the CB filled cementitious composite was achieved by the embedded conductive rubber fibres, which increased to the value of 91 when the composite was embedded with 80 rubber fibres (1.27 vol.%).

5.1.2.2 Composites with 1.0 wt.% CB

Cementitious composites filled with 1.0 wt.% CB were really close to reach the percolation threshold, where slight variations of conductive fillers might result in considerable resistivity changes. Similarly, it could be foreseen that there existed significant fractional changes of resistivity if the phenomenon of percolation took place simultaneously when the composite subjects to external loadings. Given the lack of description of piezoresistivity during electrical percolation, new definition on the word of "piezoresistive percolation" was proposed, to represent the sudden increase of fractional changes of resistivity or piezoresistivity and distinguish from the concept of generally used electrical percolation.

For the 1.0 wt% CB filled composites without rubber fibres, higher fractional changes of resistivity were observed than that filled with 0.5 wt.% CB, reaching approximately 22% as shown in Figure 5.5(a). Furthermore, a rapid decrease of resistivity which was defined as piezoresistive percolation was emerged when the strain got close to the ultimate value. Considering that the content of 1.0 wt.% CB were close to the percolation threshold of CB cementitious composites, where small concentration changes of conductors could result in tremendous electrical signal fluctuation, the significant conductivity amelioration was very likely owing to the higher conductor's concentration in the composites under larger compressive strain, because of the compressed pores, cracks and the specimen itself.

As for the same composites embedded with 20 rubber fibres (0.32 vol.%), whose final fractional changes of resistivity reached nearly 49%, a small piezoresistive percolation occurred in the early compression stage in Figure 5.5(b). It was considered that the sudden resistivity reduction was mainly originated from the rubber fibres, which might be connected with each other in a small proportion of composite, due to the fact that the compressive strain was small and the impacts from conductor's concentration could be neglected. Moreover, the conductive rubber fibres in the length of approximately 30 mm were nearly equal to the distance of two electrodes. Although these were flexible materials which can be curved or folded, the resistivity reduction caused by the rubber fibres was still faster than that by the compressive strain.

Similarly, three piezoresistive percolations are illustrated for the 1.0 wt.% CB filled composite with 40 rubber fibres (0.64 vol.%) in Figure 5.5(c), with the fractional changes of resistivity increasing to nearly 10% at the first piezoresistive percolation, approximately 40% at the second piezoresistive percolation, and slight higher than 80% at the last percolation. The first and second piezoresistive percolations were mainly due to the touch and connections between the rubber fibres, and the last piezoresistive percolation which led to a larger fractional changes of resistivity, was due to the combined actions of both rubber fibres and higher conductor's concentration under larger compressive strain. However, different from the other composites, a much severe piezoresistive percolation occurred for the composites with 80 rubber fibres (1.27 vol.%), by the fractional changes of resistivity increasing from 10% to 100% in the middle stage of compression, then followed by a resistivity increase to the value of approximately 80%, as shown in Figure 5.5(d). Even the composite with 80 rubber fibres (1.27 vol.%) was provided with excellent conductivity, it can be seen that the significant resistivity reduction is because of the more connection between rubber fibres to form shortest conductive passages in the composite. Moreover, closer contact between the rubber fibres also resulted in

a lower contact resistance and brought better conductivity. In terms of the reduced fractional changes of resistivity, one reason was related to the cracks which altered compressive strain values synchronously, and another one came from the dislocation and detach between rubber fibres, since the high compressive strain might destroy the already connected rubber fibres and increase the resistivity.

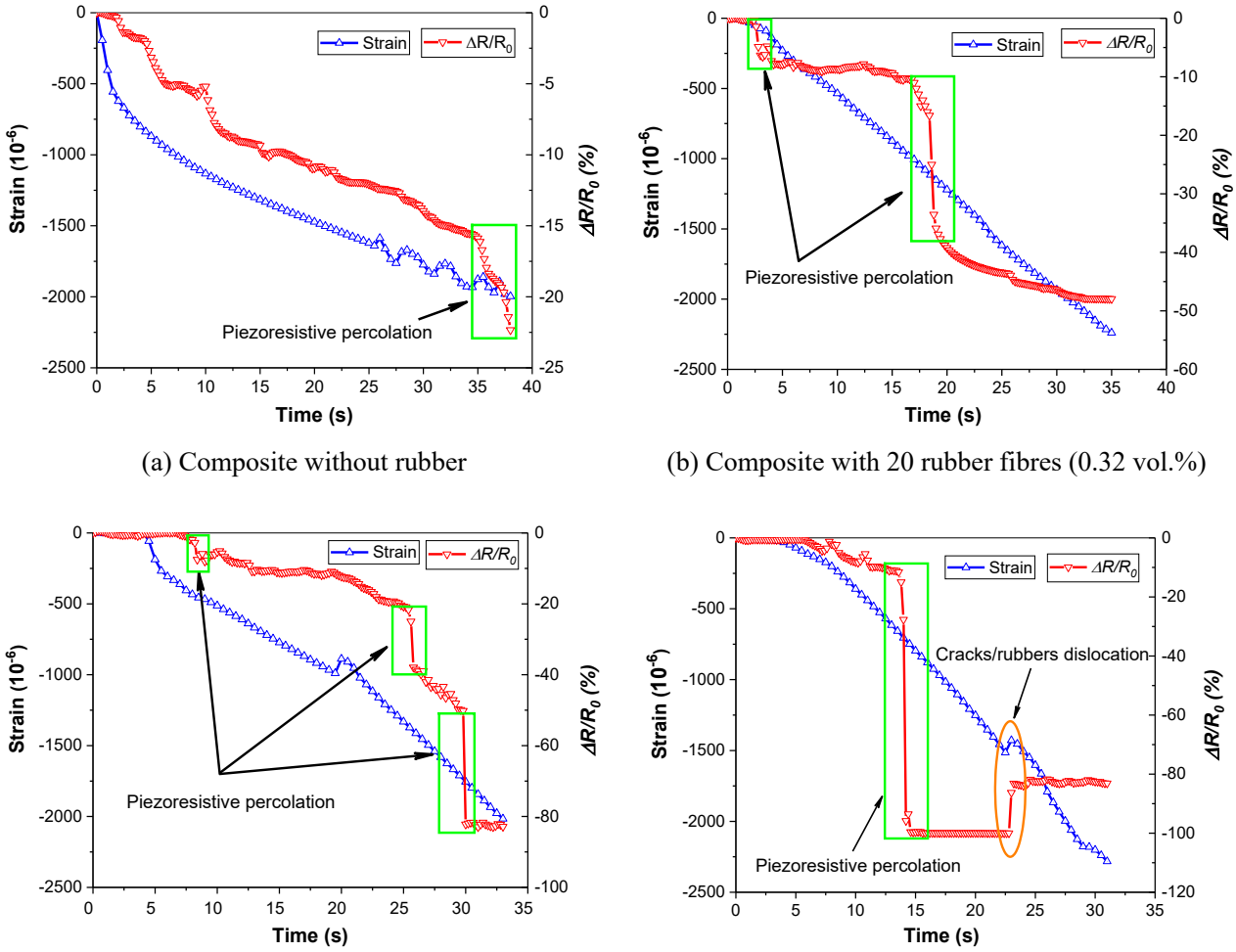

(a) Composite without rubber

(b) Composite with 20 rubber fibres (0.32 vol.%)

(c) Composite with 40 rubber fibres (0.64 vol.%)

(d) Composite with 80 rubber fibres (1.27 vol.%)

Figure 5.5. Fractional changes of resistivity for 1.0 wt.% CB filled cementitious composites.

Figure 5.6 represents the fractional changes of the resistivity as a function of compressive strain for the 1.0 wt.% CB filled composites with/without rubber. It indicates that the composite only filled with 1.0 wt.% CB performed close linear relationship between fractional changes

of resistivity and strain, while the composites embedded with rubber fibres had abrupt changes in the resistivity because of conductive rubber interference. As for the piezoresistive sensitivity, according to the linear fits, much higher gauge factors were observed, reaching the values of 114, 251, 375 and 482 for the composites without rubber, and the counterparts with 20 (0.32 vol.%), 40 (0.64 vol.%) and 80 (1.27 vol.%) rubber fibres, respectively. In comparison to the usually dried cementitious composites filled with CB, which possess average gauge factor of 50, the experimental results were at least twice of that value, and even improved by eight times for the composite with 80 rubber fibres (1.27 vol.%). Moreover, compared with the commercial strain gauge, which has gauge factor of 2, the piezoresistive sensitivity was increased by hundreds of times.

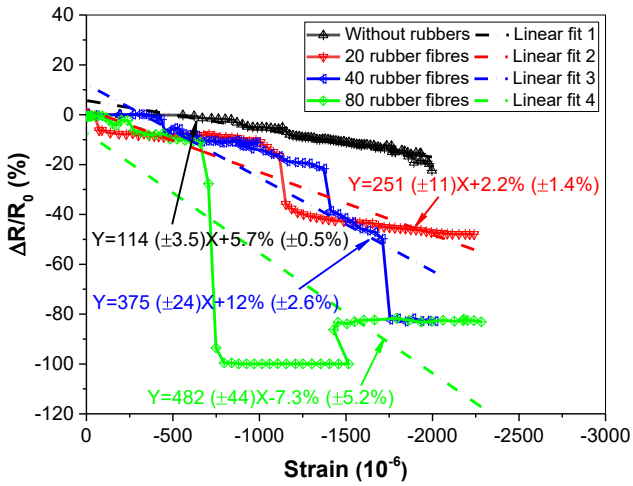

Figure 5.6. Correlation between fractional changes of resistivity and compressive strain and their linear fits for the 1.0 wt.% CB filled composites with/without rubber fibres.

Different from the CB filled cementitious composites in other studies, whose fractional changes of resistivity possessed approximate linear characteristics to strain, but instead were often provided with low piezoresistive sensitivity. Despite the poor linear relationship to the compressive strain due to the piezoresistive percolation, their gauge factors were greatly improved by several times for the composites with conductive rubber fibres. It means that the former sensor could obtain the exact values of strain/deformation by measuring the minor

changes of resistivity, and the latter sensor with higher gauge factor out of piezoresistive percolation, had a capacity to acquire the ranges of strain/deformation values by a considerable resistivity changes. However, what is particularly worth mentioning is that the resistivity is various due to many factors, including ambient temperature and humidity, corrosions, input current and so on (Teomete 2016), which are common problems in real projects to confuse the sensor results. The larger gauge factor means the misunderstandings from the other factors could be negligible. Furthermore, because of the brittleness of cementitious materials, sometimes a rough value of strain/deformation could indicate the health condition of structures and elements, rather than a specific output.

5.1.2.3 Composites with 2.0 wt.% CB

As illustrated in Figure 5.7, the fractional changes of resistivity for the 2.0 wt.% CB filled cementitious composites showed smooth increase with the compressive strain when compared with the composites filled with 1.0 wt.% CB. For all composites, the maximum fractional changes of resistivity reached approximately 20%. The composites filled with 2.0 wt.% CB were in the range of after percolation threshold, which possessed better electrical conductivity with a resistivity of several hundred Ω·cm. Hence, the conductivity amelioration by the conductive rubber was relatively small for more formed conductive passages by CB particles. In other words, when the composites were subjected to loadings, the contact between the rubber fibres could not greatly decrease the resistivity, thus the rubber interference on the fractional changes of resistivity was weakened, with only slight fluctuations for the composite with rubber content of 80 fibres (1.27 vol.%).

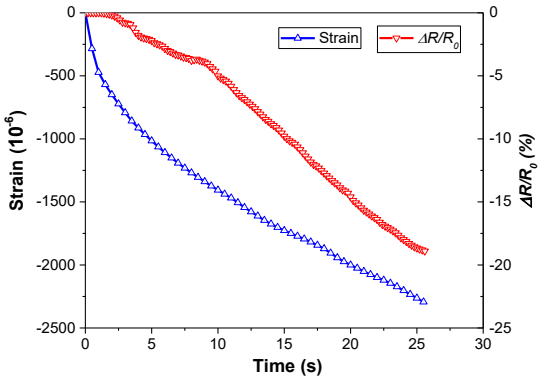

(a) Composite without rubber

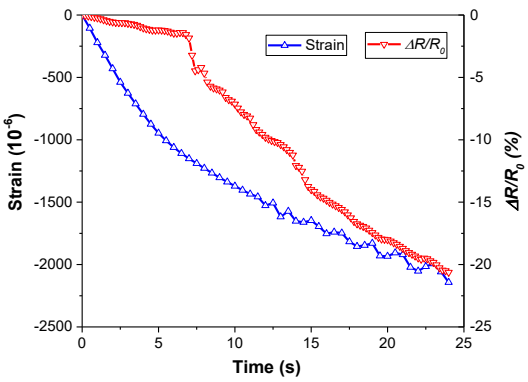

(b) Composite with 20 rubber fibres (0.32 vol.%)

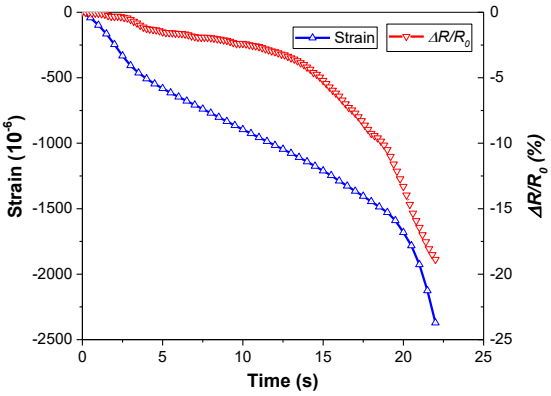

(c) Composite with 40 rubber fibres (0.64 vol.%)

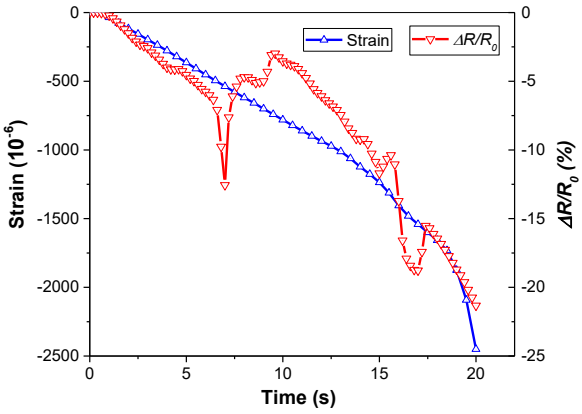

(d) Composite with 80 rubber fibres (1.27 vol.%)

Figure 5.7. Fractional changes of resistivity for 2.0 wt.% CB filled cementitious composites.

Figure 5.8 illustrates the relationships between the fractional changes of the resistivity and the compressive strain of the 2.0 wt. % CB filled cementitious composite. Except for the composites embedded with 80 rubber fibres (1.27 vol.%), all of the composites exhibited continual and nearly linear fractional changes of the resistivity with regard to the compressive strain. However, it seems that the gauge factors had no direct relationship to the rubber content, and the values reached 105, 119, 86 and 92 for the composites without rubber and with 20 (0.32 vol.%), 40 (0.64 vol.%) and 80 (1.27 vol.%) rubber fibres, respectively. The reasons were explained previously, for the already formed conductive passages by CB rather than conductive rubber fibres. In addition, compared to similar studies focusing on CB particles, the improved

sensitivity for the 2.0 wt.% CB filled composites was most likely caused by the effects of silica fume and the pore solutions in the composites which had never been dried (Nam, Kim & Lee 2012; Zhang et al. 2019). Moreover, the composites without rubber or embedded with 20 rubber fibres (0.32 vol.%) achieved the best gauge factors of 105 and 119, while it was decreased with the increasing number of rubbers. This might be due to the negativities caused by more content of conductive rubber fibres, which cause more cracks and gaps in the composites to decrease the gauge factors. Also, detach between connected rubber fibres reduced conductivity and damaged gauge factor as well.

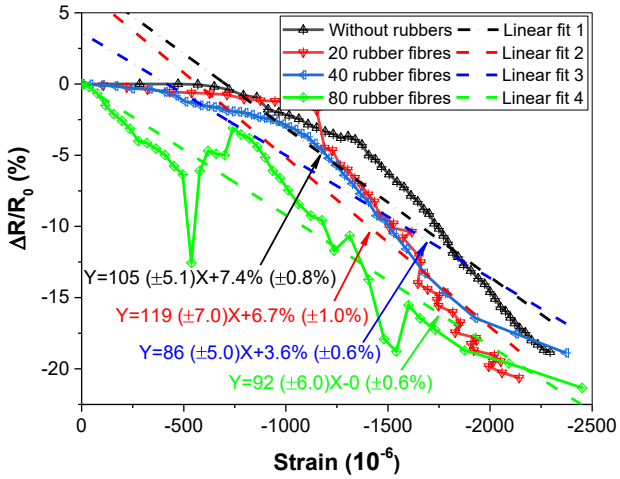

Figure 5.8. Correlation between fractional changes of resistivity and compressive strain and their linear fits for the 2.0 wt.% CB filled composites with/without rubber fibres.

5.2 Effect of PP fibres

In this study, different dosages of carbon black (CB) and polypropylene (PP) were added to manufacture cementitious composite, trying to improve the conductivity and piezoresistivity of cement-based sensors.

5.2.1 Electrical resistivity

Figure 5.9 shows the electrical resistivity of the CB filled cementitious composites with different contents of PP fibres. It could be observed that the electrical resistivity dramatically decreased by more than one order of magnitude for the composites filled with 0.1 wt.% PP

fibres. Afterwards, with the increase of PP fibres, the electrical resistivity of the cementitious composite decreased at a slow rate and reached the value of 3.4×10^5 Ω·cm at the dosage of 0.4 wt.% PP fibres. With the presence of well-dispersed CB nanoparticles, it shows that the PP fibres at a small concentration of 0.4 wt.% to the weight of binder have the capacity to decrease the electrical resistivity of the CB cementitious composite by approximately two orders of magnitude.

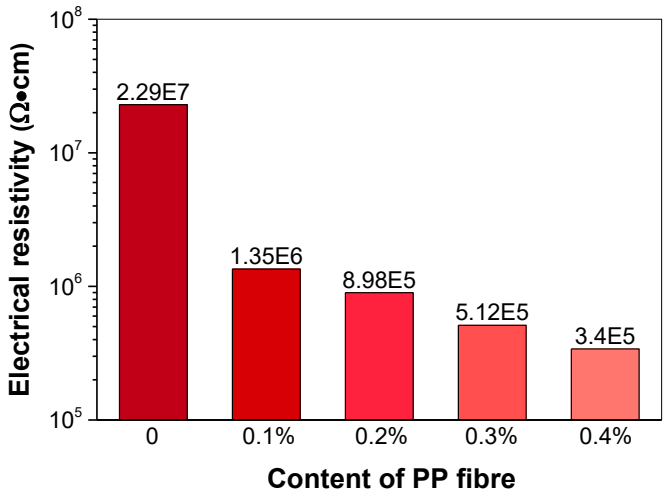

Figure 5.9. Electrical resistivity for CB/cementitious composite with various contents of PP fibre.

To elucidate the phenomenon of decreased electrical resistivity, Figure 5.10 shows the micromorphology of PP fibres with four different magnifications in the CB filled cementitious composite. Generally, it could be detected that the PP fibres were surrounded by the cement hydration products and CB nanoparticles. The nonconductive hydration products made no differences on the electrical resistivity of PP fibres, while the enclosed CB nanoparticles could generate the conductive passages through their contacts and greatly decrease the electrical resistivity of the PP fibres. Previous studies had demonstrated that the conductive fibrous fillers had better performance to enhance the electrical conductivity of the cementitious composite than the spherical fillers. The high aspect ratio PP fibres with improved conductivity are just

similar to the conductive fibrous fillers, which can stimulate the electrical conductivity of the whole cementitious composite by the inner connection among PP fibres. Secondly, in comparison to the density of CB distribution in the PP fibres and cement matrix, it seems that the CB nanoparticles had higher possibility to be absorbed in the surface of PP fibres, rather than spread in the cement matrix. It has been proposed that the CB preferentially distributed in the epoxy with high polarity (Tchoudakov et al. 1996). Generally, the CB possesses the hydrophobic groups in the surface such as aryl group, ether group and ester group (Donnet 1982), that is why the CB nanoparticles having the difficulties to disperse in the aqueous solution. However, it seems that the nonpolar PP fibres had much higher lipophilicity than cement matrix and aqueous solution, hence CB nanoparticles were tended to be absorbed by the surface of PP fibres. In other words, the addition of PP fibres led to the directional distribution of CB nanoparticles in the cement matrix, especially along with the PP fibres, which was beneficial for the creation of conductive passages and decreased the electrical resistivity of the cementitious composite. However, the high concentration of CB nanoparticles on the surface of PP fibres represented decreased CB concentration in the cement matrix, which actually had a detrimental effect on the conductivity of cementitious composite. From the above experimental results, the conclusion can be drawn that the positive effect by CB enclosed PP fibres on the electrical conductivity of CB filled cementitious composite overwhelmed the negativity brought by lower CB concentration in cement matrix. More discussions on the reduced CB concentration in cement matrix will be presented in the following section.

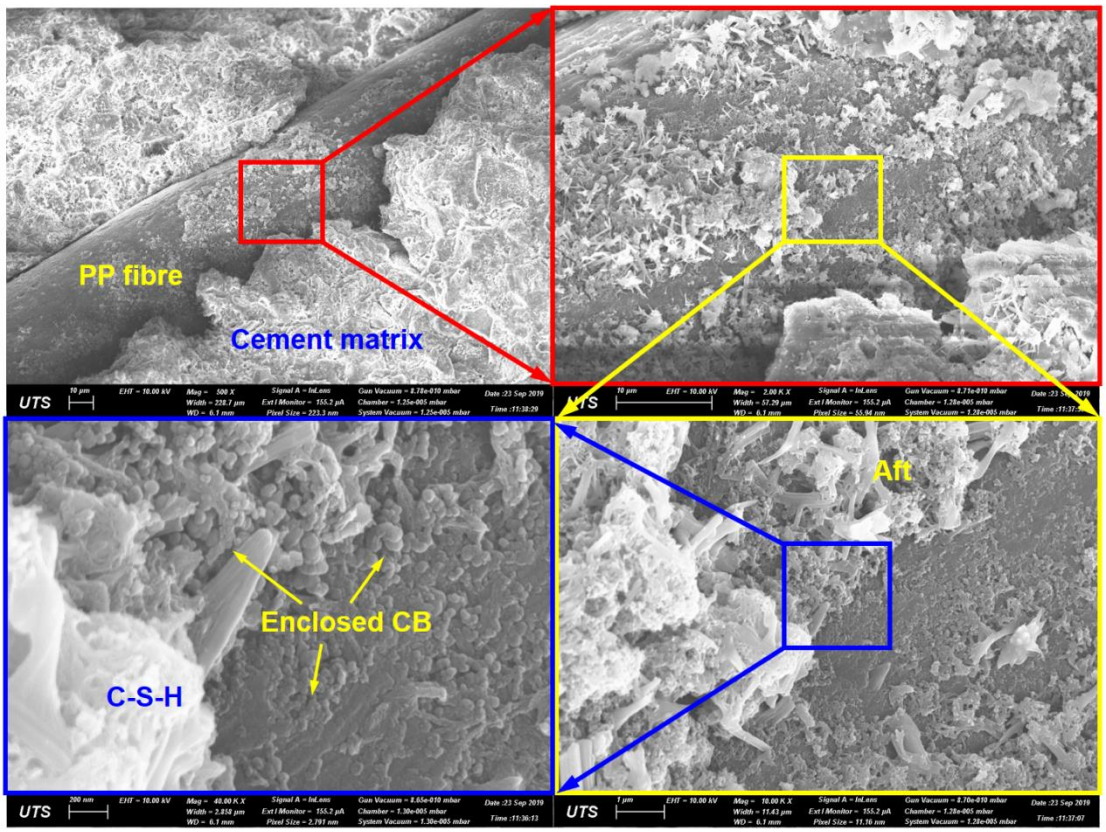

Figure 5.10. Microstructure of PP fibres in CB/cement matrix and functional groups in CB surface.

5.2.2 Piezoresistivity behaviours

The compressive strength sensing ability is to assess the potential of CB filled cementitious composite with PP fibres as a stress/strain sensor, while the flexural failure sensing ability is to evaluate its application potential to be a self-sensing concrete beam.

5.2.2.1 Compressive stress monitoring

Figures 5.11(a) to 5.11(c) illustrate the fractional changes of resistivity (FCR) as a function to compressive stress for the composites with various contents of PP fibres under various loading rates. For all composites, the FCR (absolute value, the same below) increased with the increment of compressive stress and decreased when the stress returned to zero, and performed good piezoresistivity. Linear fittings of these results were attached, showing that the relationship between FCR changes and compressive strength was almost linear. Moreover, the

overlapped or very close curves in the loading and unloading process indicated that the piezoresistivity of composite showed good repeatability. Therefore, it could be deduced that the CB filled cementitious composite with/without PP fibres were both eligible to be a stress sensor, regardless of the loading rates. Generally, the tendency of FCR changes was similar under various loading rates, which demonstrated that the loading rates almost possess no impact on the piezoresistivity. Since the loading rates in reality are always unpredictable and multiple, the results lay the foundation of applying the CB/PP fibres filled cementitious composite into the real engineering project. In terms of the piezoresistive sensitivity, the composite without PP fibres reached the FCR peaks of approximately 2% at the stress magnitude of 5 MPa. However, it seems that the increasing rate of FCR increased with the increased content of PP fibres, and the largest FCR nearly 8% occurred for the composite filled with 0.4 wt.% PP fibres at the same stress magnitude. The results showed that the CB cementitious composite filled with 0.4 wt.% PP fibres could improve the piezoresistive sensitivity by three times more than those without PP fibres. The SEM images have showed that the PP fibres were enclosed with conductive CB nanoparticles, and the higher FCR mainly originated from the conductive PP fibres, which were more easily connected to form conductive passages given their high aspect ratio. Howbeit, the CB nanoparticles were much more difficult to contact with each other due to the spherical properties, and that was why the FCR changes were lower for the CB cementitious composite without PP fibres when subjected to identical compressive stress.

Figure 5.11(d) illustrates the ratios of FCR to compressive stress as a function to the content of PP fibres. The ratio of FCR changes by unit stress can be a coefficient to evaluate the piezoresistive sensitivity. Regardless of the loading rates applied, the fitting curve showed that the piezoresistive sensitivity of CB cementitious composite possessed linear relationship with the added dosage of PP fibres. Therefore, the fitting curve can be used to predict the

compressive stress sensing efficiency for the CB cementitious composite filled with different contents of PP fibres. Generally, the Eq. (8) to predict the compressive stress based on the statistical results in Figure 5.11(d) is listed as follows:

$$\sigma_c = \frac{100FCR}{3.2X + 0.36} \tag{8}$$

Incorporating the Eq. (8), the expression to calculate the compressive stress is:

$$\sigma_c = \frac{100\Delta R}{R_0(3.2X + 0.36)} \tag{9}$$

where σ_c the compressive stress (MPa); R_0 the initial electrical resistance of the composite; ΔR the electrical resistivity changes out of compressive stress; the constant 100 presents that the magnified values of resistivity changes during fitting (i.e. 10% resistivity changes equal to 0.1); X the content of PP fibres to the weight of binder in percentage (i.e. 0.1 wt.% PP fibres equals to 0.1). Based on the derived fitting formula, the compressive stress on the CB filled cementitious composite with/without PP fibres could be evaluated. In addition, the rough compressive stress could also be obtained for the composite filled with more than 0.4 wt.% PP fibre.

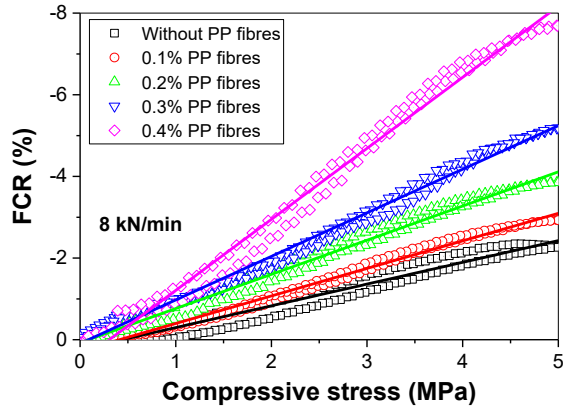

(a) Loading rate of 8 kN/min

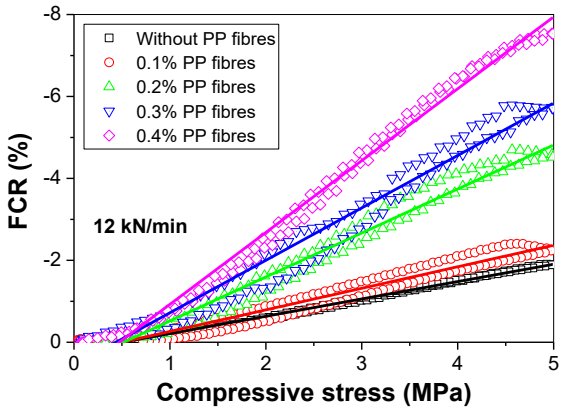

(b) Loading rate of 12 kN/min

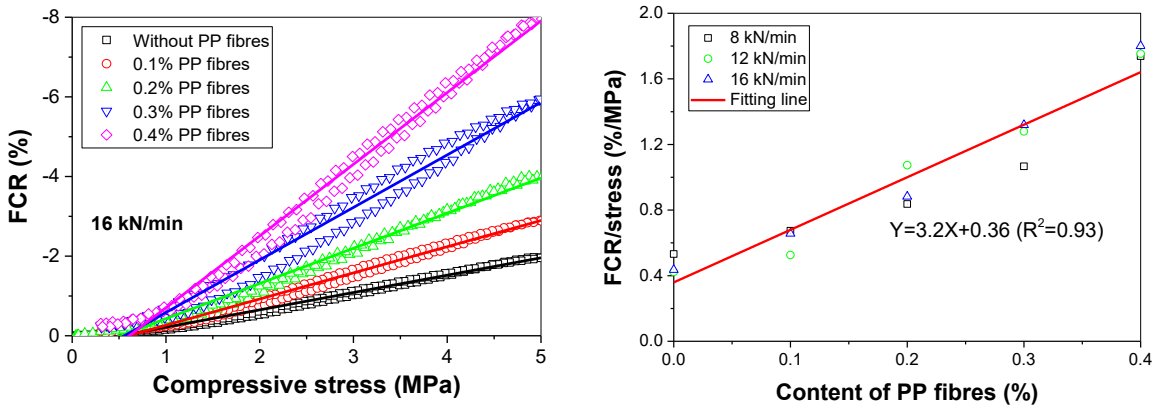

(c) Loading rate of 16 kN/min (d) ratio of FCR to stress

Figure 5.11. Fractional changes of resistivity as a function of compressive stress under various loading rates and ratio of FCR to stress with various PP contents.

Figure 5.12 illustrates the distribution of CB nanoparticles and PP fibres in the cementitious composite, as well as the contact points that lead to the improved piezoresistivity. For the composite without PP fibres, the CB nanoparticles have the capacity to connect with each other to form conductive points, which can be linked subjected to external forces and reduce the electrical resistivity. However, it is found that limited contact points can be observed due to the spherical properties of CB nanoparticles, as shown in Figure 5.12(a). That is why the piezoresistive performance of CB filled cement-based sensors is normally lower than the counterparts filled with fibrous conductors. On the one hand, with the addition of 0.1 wt.% PP fibres, the CB concentration in cement matrix is decreased because a proportion of CB nanoparticles are attached on the surface. As a result, it leads to the decreased contacts points formed by CB nanoparticles and somewhat weakens the piezoresistivity. On the other hand, the conductive PP fibres enclosed with CB nanoparticles can significantly increase the contact points in the composite, because of their fibrous properties and high aspect ratio. The improved piezoresistivity indicates that the increased contact points by PP fibres overwhelm the decreased contact points, as plotted in Figure 5.12(b). In addition, with the further increase of PP fibres to 0.4 wt.%, more contact points by PP fibres can be observed. However, it is found

that the contact points generated by CB nanoparticles almost disappeared, due to the greatly decreased CB concentration in the cement matrix. In summary, based on the piezoresistive results and the SEM images of PP fibres and cement matrix, the concentration of CB in the cement matrix decreased with the increase of PP fibres. The improved piezoresistivity demonstrates that the contact points are easily formed by PP fibres, rather than CB nanoparticles. Importantly, the number of contact points almost linearly increases with the increased PP fibres, which can be deduced from the linear altered ratios of FCR to stress with the increase of PP fibres.

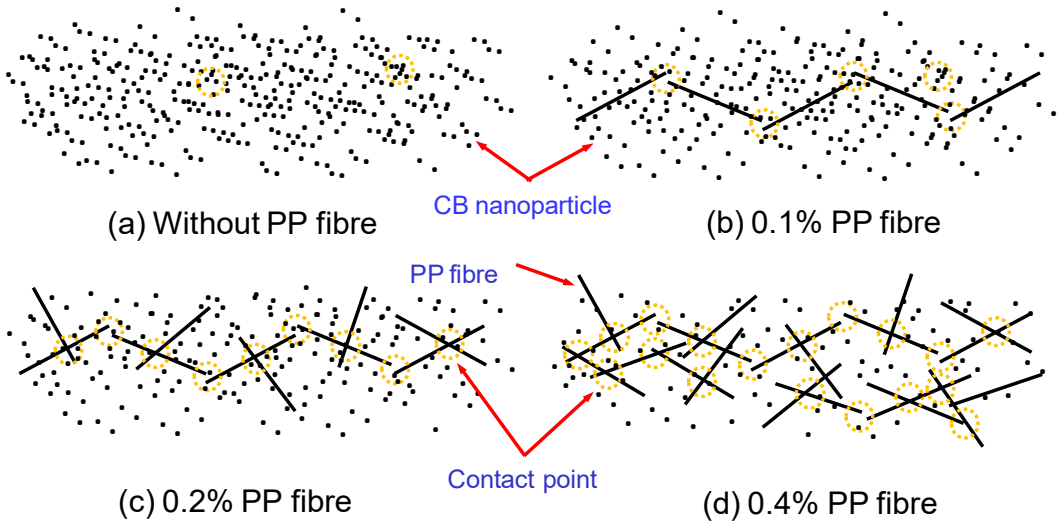

Figure 5.12. Schematic diagram of CB, PP fibres and potential contact points in cementitious composite.

5.2.2.2 Flexural failure monitoring

The results of FCR as a function to flexural stress by three-point-bend test until failure are displayed in Figure 5.13(a). Similarly, the electrical resistivity of the composite decreased with the increase of flexural stress, even though the FCR were much smaller than the values under the same stress of uniaxial compression. In addition to the mentioned improved flexural strength of composite, it was found that the flexural stress sensing ability increased with the increased PP fibres, by the FCR increased from 0.23% to 2.35% when the dosage of PP fibres

reached 0.4 wt.%. The more than 10 times higher FCR is mainly attributed to the more contact points induced by PP fibres. As for the failure detection, it could be found that the FCR rapidly increased at the failure point. This is easy to understand because of the brittleness of cementitious composite, the permanent cracks are firstly generated from the central loading point. The bridging effect of PP fibres maintained the decreased electrical resistivity even there are existing micro-cracks. Still, the cracks can suddenly run through the beam when the stress exceeds flexural strength, thus the PP fibres are failed to maintain the conductive passages and that is why the electrical resistivity rapidly increases.

Figure 5.13(b) shows the flexural stress sensing efficiency by plotting the relationship between the ratios of FCR to flexural stress and the content of PP fibres. It seems that the flexural stress sensing efficiency increased with the increase of PP fibres. Similarly, the fitting curve is proposed to assess the piezoresistive sensitivity to the content of PP fibres. Based on the fitting formula, the flexural stress can be calculated by Eq. (10):

$$\sigma_f = \frac{100\Delta R}{R_0(1.27X + 0.01)} \tag{10}$$

where σ_f represents the flexural stress (Unite: MPa); R_0 means the initial electrical resistance of the composite; ΔR is the electrical resistivity changes out of flexural stress; X the content of PP fibres (0.1 wt.% PP fibres equals to 0.1). Likewise, for the CB cementitious composite filled with more PP fibres, the exact flexural stress can be forecasted through the measurement of electrical resistance during three-point-bend test.

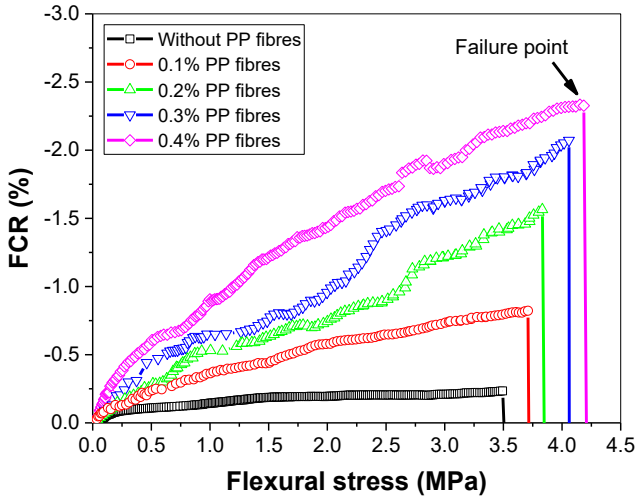

(a) FCR changes to flexural stress

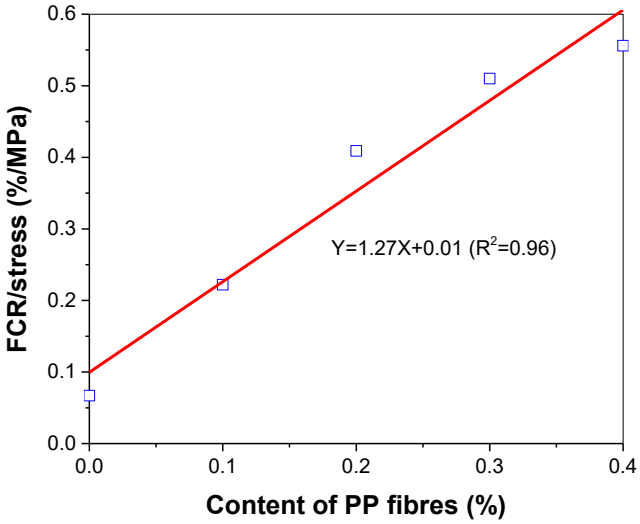

(b) Flexural stress monitoring efficiency

Figure 5.13. FCR changes during flexural failure test and flexural stress sensitivity at various of PP fibres.

5.3 Effect of silica fume

The effects of different cement replacement rates by condensed silica fume (SF) ranging from 0 to 20% on physicochemical, microstructure, mechanical and piezoresistive properties of CB-cementitious composites are investigated in this study.

5.3.1 Physicochemical properties

The impact of silica fume on the setting time of CB-cementitious composites is illustrated in Table 5.1. When the dosage of SF ≤ 10%, it could be observed that both the initial and final setting time enlarged with the increase of SF. Also, it seems that the increasing rate was slightly reduced with the rising SF. Therefore, it demonstrated that the appropriate concentration of SF could prolong the setting time of CB-cementitious composites and showed the delayed effect. However, for the composites with 20% SF, the initial setting time was significantly decreased to lower than that of the composite without SF. Since the w/b ratio was unchangeable for all composites, the reduced initial setting time is probably due to the false setting of composites , because the silica fume could consume an amount of water and affect the cement hydration. The final set of the composites with 20% SF was more significant than the plain one, but the duration decreased in comparison to the composites with 10% SF, which was attributed to the combined effects by the delayed effect and the false setting.

Table 5.1 Physicochemical properties of CB-cementitious composite with various SF.

CB content (%)	Content of silica fume (%)	Setting time (min)		Flowability (mm)	Rate of water absorption (%)	Electrical resistance (Ω)
		Initial	Final			
2	0	135	225	213.6	7.5	1600
2	5	155	245	201.2	6.7	175
2	10	165	260	188.5	5.9	122
2	20	115	255	170.0	6.5	85

As for the workability of CB-cementitious composites, it shows that the flowability monotonously decreased with the increase of SF. The reduction rate significantly increased when the content of SF increased from 10 to 20%. It has been proposed that the water reducer had a significant impact on the flowability of the cementitious composites with SF . The smaller flowability under identical content of water reducer demonstrated that the SF could cause

disadvantages on the workability of the composites. This is mainly due to the small size and high specific surface of SF, which could not only absorb the water from cement particles but also fill the channels that might lead to water bleeding in the composites.

The water absorption ability can evaluate the microstructures and compactness of the cementitious composites. The rate of water absorption firstly decreased with the increase of SF to 10%, and then slightly increased when the content increased to 20%. It indicated that the effect of SF on the resistance of water penetration depended on the dosage of SF. The moderate SF could fill the pores and channels to compact the microstructures. On the other hand, the high concentration of SF might agglomerate and form clusters in the composites, which could block the water content to hinder cement hydration .

The electrical resistance of the cubic composites decreased with the increase of SF, ranging from 1600 to 85 Ω. Previous studies have mentioned that the conductive fillers can be better dispersed by the addition of SF, thus enhance the electrical conductivity of the cementitious composites . The experimental results in Table 5 further demonstrated that only a small dosage of SF was beneficial to uniformly disperse CB nanoparticles, and significantly decreased the electrical resistance. Afterward, with the increase of SF whose concentration even up to 20%, the electrical resistance still reduced, but at a lower rate. The results mentioned above showed that the SF had the capacity to fill the pores and cracks in the cementitious composites because of its small particle size. Based on the rate of water absorption, it seems that the composites filled with 20% SF possessed worse microstructures and compactness than the counterparts with 10% SF. The still improved electrical conductivity might be attributed to the better dispersion of CB nanoparticles for the composites with 20% SF.

5.3.2 Mechanical and micro properties

5.3.2.1 Compressive and flexural strengths

Figure 5.14 illustrates the compressive and flexural strengths of the CB-cementitious composites filled with various contents of SF. Generally, significant reinforcement effect by SF could be observed both on the ultimate compressive strength and flexural strength. It showed that the compressive strength considerably increased by 22% to 41.2 MPa when the CB-cementitious composites filled with 5% SF. The highest compressive strength occurred for the composites filled with 10% SF, reaching approximately 43.4 MPa. Afterward, the compressive strength decreased to 40.7 MPa as the SF concentration reached 20%, while the strength was still larger than the CB-cementitious composites without SF reinforcement. In terms of the flexural strength, which experienced similar development with the increase of SF, the most substantial strength of 3.1 MPa generated for the composites filled with 10% SF with the increasing rate reaching nearly 48%. Since there were no aggregates in the composites, the improved flexural strength was mainly attributed to the denser microstructures and better compactness . Similarly, the flexural strength decreased for the composites filled with 20% SF to only 2.5 MPa. Overall, it shows that the flexural strength was more volatile to the dosage of SF than the compressive strength. The microstructures of CB-cementitious composites with various content of SF will be analyzed to elucidate the strength evolution.

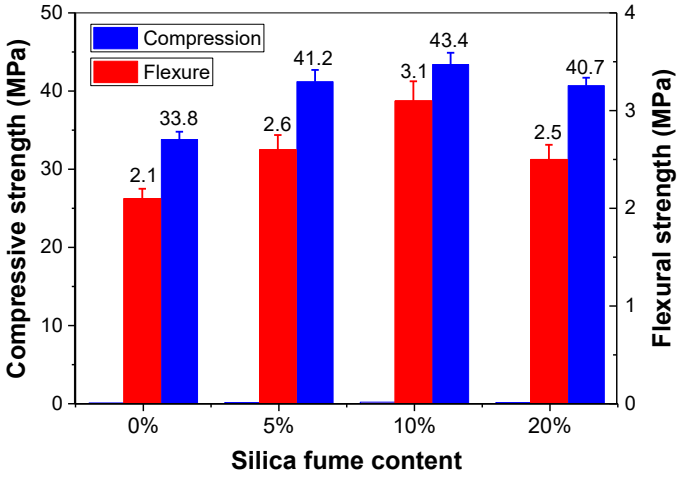

Figure 5.14. Compressive and flexural strengths of CB-cementitious composite with various content of SF.

5.3.2.2 Micromorphology

Figure 5.15 illustrates the microstructural morphology of the CB-cementitious composites without SF, where the micropores and the distribution of CB agglomerations could be observed. Moreover, the compactness and the density of the composites could also be qualitatively assessed through the morphology analysis. The CB-cementitious composites without SF were provided with loose microstructures partially due to the excessive CB nanoparticles absorbed the water content to hinder the cement hydration . As a consequence, a considerable number of micropores emerged in the composites, which greatly limited the mechanical properties. In addition to the restricted cement hydration, due to the absence of defoamer in the mixing procedure, there was the possibility that some of the micropores were induced by the enclosed air bubbles. These micropores were considered responsible for the highest water absorption of the composites without SF in Table 5. Furthermore, the CB nanoparticles having high surface energy could easily agglomerate and form clusters, as shown in Figures 5.15(c) and 5.15(d). These CB agglomerations have worse resistance to external forces and reduce the improvement efficiency of electrical conductivity, which explained why the CB-cementitious composites without SF had the lowest compressive and flexural strength, as well as the highest electrical resistance.

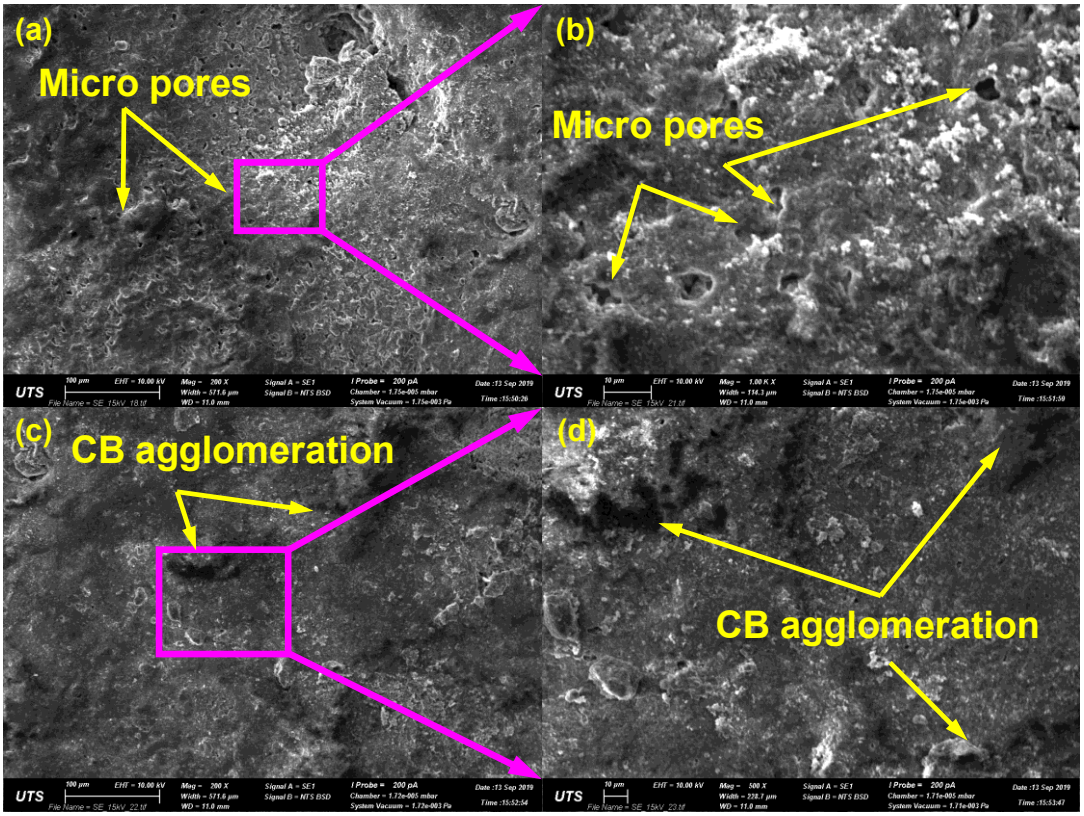

Figure 5.15. Micromorphology and agglomeration in CB-cementitious composite without SF.

The micromorphology of CB-cementitious composites reinforced with 5%, 10% and 20% SF is shown in Figure 5.16. Different from the aforementioned porous microstructures, it could be observed that the CB-cementitious composites filled with 5% SF possess much denser microstructures with very fewer micropores. It seems that the majority of CB nanoparticles were well-dispersed in the cement matrix, and that is why the electrical resistance of the composites strongly decreased. Still, as illustrated in Figure 5.16(a), a small amount of CB agglomerations could be detected. Anyway, it could be deduced that the SF did have the capacity to disperse nanoparticles in cementitious composites. According to the remained small proportion of CB agglomeration, it seems that the concentration of SF was of importance to disperse the CB nanoparticles thoroughly. As for the microstructures in Figure 5.16(b), fewer pores and cracks could be observed in the SEM images with large magnifications. There are two functionalities that the SF takes effect to reduce the porosity, with the first one by the

filling effect of SF and the second by the stimulated generation of cement skeleton. The former is mainly owing to the smaller particle size of SF than cement particles; thus the SF could fill the micropores or cracks among the unhydrated cement particles. The latter is due to the continually stimulated C-S-H gel by SF, which could fill the pores and make the CB-cementitious composites denser.

Figures 5.16(c) and 5.16(d) depict the microstructures of CB-cementitious composites filled with 10% SF. The micromorphology was very similar to that of the composites filled with 5% SF, with less micropores and dense structures. It could also be observed that the most CB nanoparticles were evenly distributed in the cement matrix without agglomerations. However, with the increasing of SF, it seems that there appeared the problem of SF agglomeration rather than CB agglomeration. Since the SF is a small particle with high specific surface, the high concentration of SF can cause the clusters of SF, as shown in Figure 5.16(d). It was found that the SF agglomerations were accompanied by micropores which probably damage the physical and mechanical properties of CB-cementitious composites. Howbeit, the improved electrical conductivity, water impermeability and mechanical strengths demonstrated that the dosage of 10% SF is still beneficial to the CB-cementitious composites.

The micromorphology of the CB-cementitious composites filled with 20% SF is displayed in Figures 5.16(e) and 5.16(f). For the excessive SF, it seems that the CB nanoparticles tended to mix with SF or the agglomerations, as illustrated in Figure 5.16(e). In particular, it seems that the filling effect of SF might be affected by the CB nanoparticles, and thus more micropores were observed than the composites filled with 10% SF. This can explain why the water absorption for the composites filled with 20% SF was higher than that of the composites with 10% SF. In addition to the filling effect, the CB/SF agglomerations might affect the cement hydration process, since both of them could absorb a large amount of water because of their high specific surface. Therefore, both the compressive and flexural strength of the

composites decreased compared with the composites with 10% SF. Interestingly, the electrical resistance of the composites decreased when the SF content increased to 20%, indicating that the conductivity of the composites was improved even with the CB/SF agglomerations. This is probably due to the improved conductivity of pores and cracks, which are filled with CB/SF agglomerations.

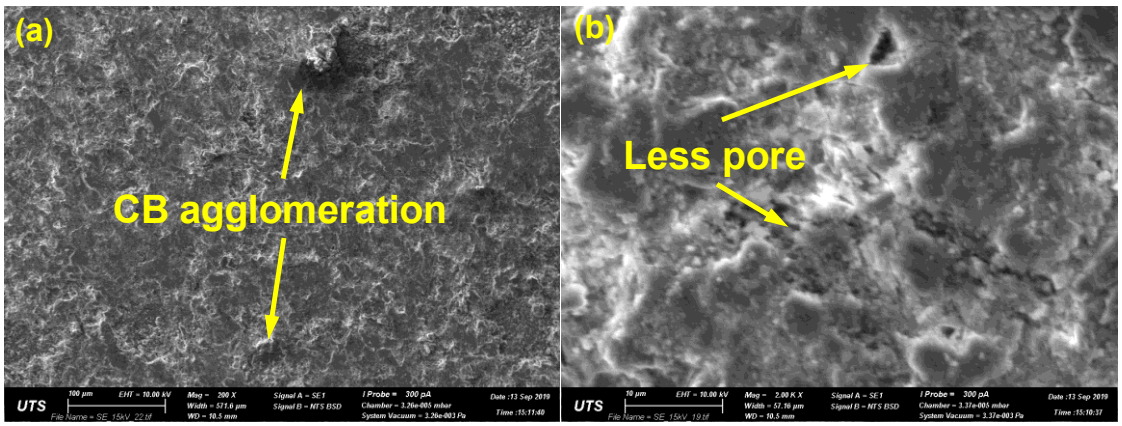

(a) and (b) 5% SF

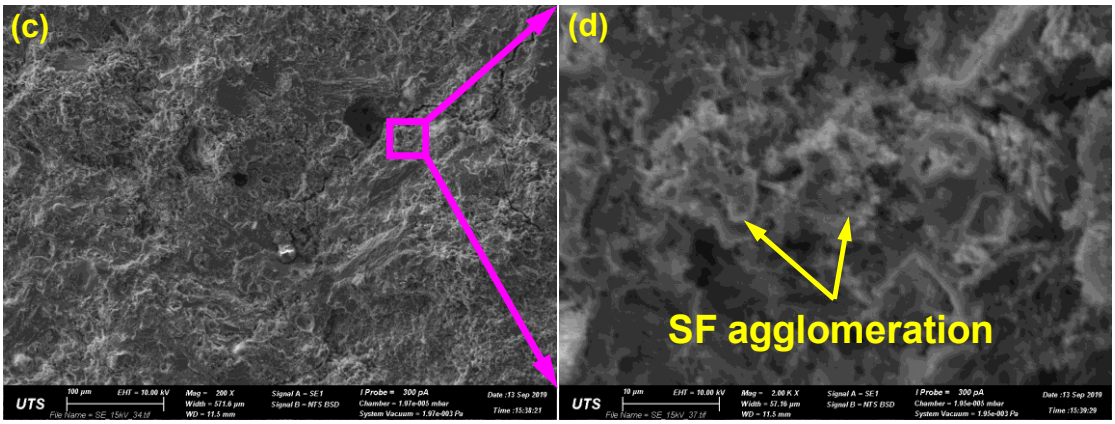

(c) and (d) 10% SF

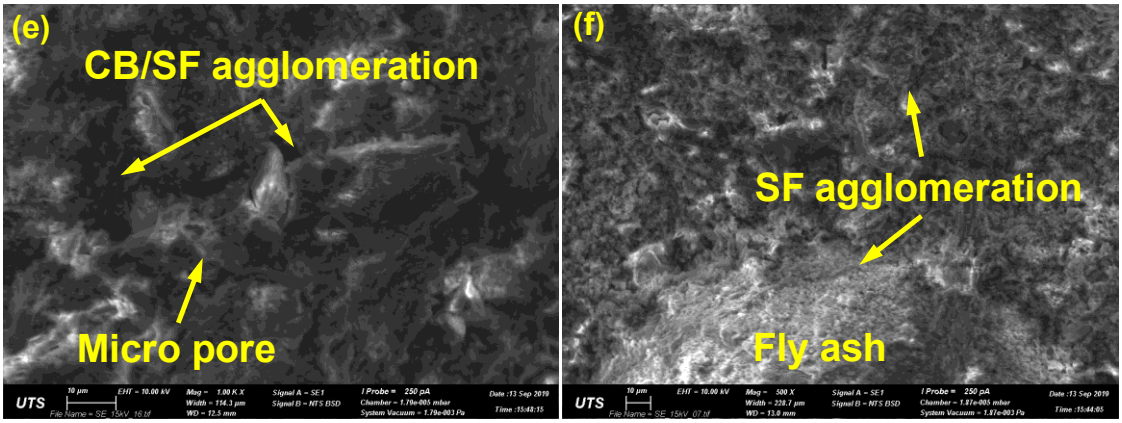

(e) and (f) 20% SF

Figure 5.16. Micromorphologies and agglomeration of CB-cementitious composite with different SF contents.

5.3.3 Crystal phases and nanostructure

5.3.3.1 Thermal gravity

The relationships between TGA and DSC to the increased temperature are displayed in Figure 5.17. Although the composites contain 2% CB, it seems that the CB makes no differences on the results due to the environment of nitrogen atmosphere. For the TGA results, in addition to the gradually decreased mass due to the dehydration of C-S-H, there are three sharp declines at the temperature ranges of 65-120 °C, 420-450 °C and 660-730 °C, respectively representing the decomposition of ettringite, dehydration of portlandite and the decarbonisation of calcium carbonate. Since the small dosage of SF (5% and 10%) could stimulate the cement hydration, the slight higher mass reduction in the beginning was mainly owing to the dehydration of C-S-H. It means that the effect of SF on the ettringite cannot be judged only based on the TGA results. On the contrary, it could be observed that the amount of portlandite and calcium carbonate was decreased with the increase of SF. Moreover, the final mass reduction reduced with the rise of SF, it is considered that the less involved water should be responsible for this phenomenon, as well as the less portlandite and calcium carbonate. The above deductions could be further demonstrated by the DSC results, where the enthalpy change presented the decomposition of various phases. For the composites with 20% SF, a dramatic reduction on the endothermic peak could be observed in comparison to the counterparts with less SF. The discrepancy on the first and second endothermic peaks is challenging to distinguish among the composites filled with ≤ 10% SF, while it could be observed the decreased heat absorption for the third endothermic peaks, which indicated the lowered calcium carbonate for the composites filled with increased SF.

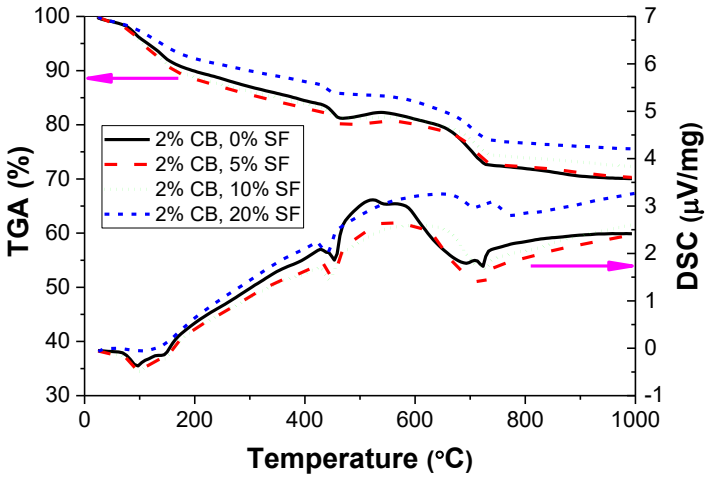

Figure 5.17. TG/DSC curves of CB-cementitious composite with different contents of SF.

5.3.3.2 XRD

The results of XRD test is illustrated in Figure 5.18, to further distinguish the crystal phases of composites filled with various contents of SF. The ettringite is formed in the presence of gypsum during the hydration of C_3A. It could be observed that the addition of SF decreased the formation of ettringite given the more calcium ions converted into the stable compound of calcium silicate. Another reason is probably due to the attenuated hydration rate, the addition of CB nanoparticles and excessive SF could absorb water content, and that is why the ettringite even disappeared for the composites filled with 20% SF. As for the second phases of monocarboaluminate, investigations have found that the monocarboaluminate can be rapidly formed as the OPC clinkers interground with limestone during hydration . This is due to the reduced concentration of calcium ions with an increase of SF. Similarly, the less stable calcium carbonate can be progressively converted into the calcium silicate in the early stage; thus, the formation of monocarboaluminate in the composites decreased with the increased SF. In addition, the most significant reduction occurred in the phases of portlandite, which was mainly attributed to the pozzolanic reaction between SF and calcium hydroxide. Since the test is conducted after 28 days hydration, the composites might get carbonized in the air atmosphere.

Moreover, the limestone might remain in the composites. Even though, the XRD results demonstrated that the calcite was less generated on the composites with a higher content of SF.

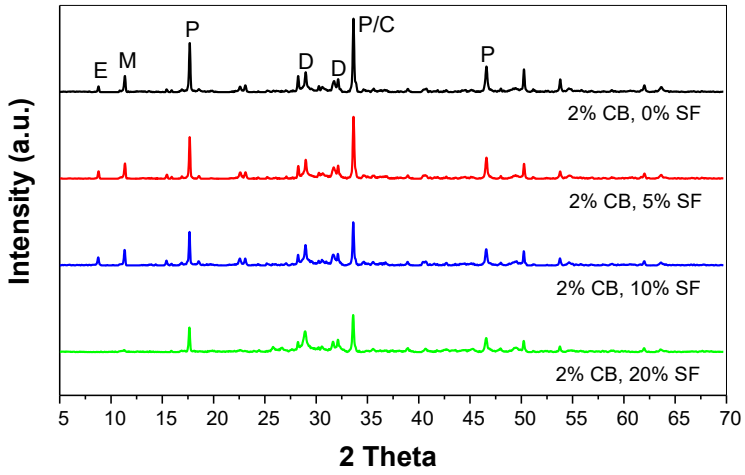

Figure 5.18. XRD analysis for CB-cementitious composite with various amounts of SF (E = Ettringite; M= Monocarboaluminate; P = Portlandite; C= Calcite; D = OPC clinkers).

5.3.3.3 Hydration heat

Figure 5.19 illustrates the rate of hydration heat and the total cumulative heat of hydration for the plain cement paste and the cement paste with different contents of SF from 5 to 20% substitution rates to cement. Generally, it could be observed that the SF decreased the cement hydration rate in the acceleration period (accelerated heat evolution before the first peak) and prolonged the dormant period (relatively low heat evolution). For the cement paste with 20% SF, the rate of hydration heat decreased by 22.5% from 4.0 mW/g to 3.1 mW/g, as well as the lower accumulative hydration heat within 72 hr. Moreover, the second hydration peaks after the acceleration period were more visible with the increase of SF. The results are consistent with the previous studies, which claimed that the impeded hydration rate was due to the lower W/B ratios. The extremely fine particles of SF compared to the cement particles can not only absorb water content, but also form agglomerations that enclose the cement particles to hinder their hydration process. However, within the first 6 hr of the hydration process, the SF did enhance the hydration rate of the composites. The primary reason is due to the nucleation sites

provided by the SF, which improve the hydration rate when the water content is still high. Also, since the Ca^{2+} and alkali ions are released from cement ingredients at the beginning of hydration, the second reason is because the Ca^{2+} is considerably consumed by the increase of SF, thus the cement hydration can be further stimulated in the alkaline environment .

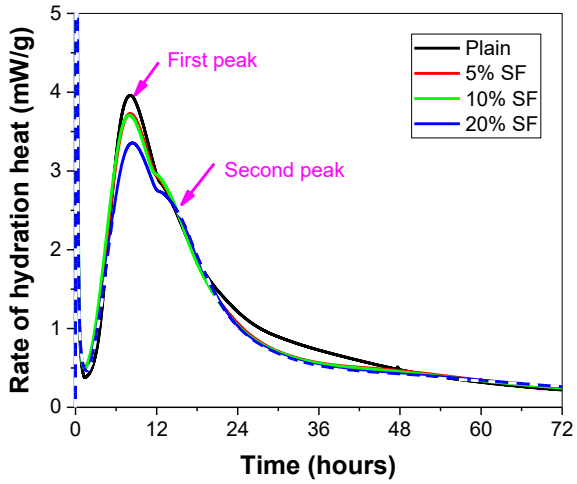

(a) Hydration released heat rate

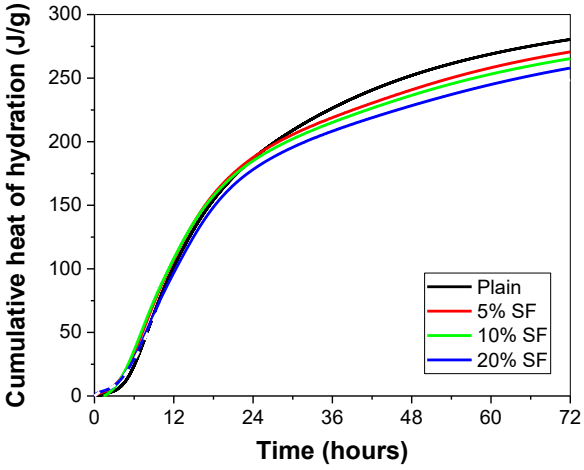

(b) Cumulative hydration heat

Figure 5.19. Rate of hydration heat and cumulative heat of hydration for cement paste with various SF contents.

5.3.3.4 Nanostructure characterization

Figure 5.20 illustrates the nanostructures of CB-cementitious composites without SF and filled with 10% SF, from which the discrepancy among the composites on the nanoscale can be

clearly seen. For the composites without SF, it could be found that the CB nanoparticles were easily clustered to form agglomerations. Given the CB agglomerations have strong water absorption ability and poor cohesion, they tended to be companied by capillary pores and weak interfaces to cement matrix, as shown in Figures 5.20(a) and 5.20(b). Based on the SEM images, the sizes of the CB agglomerations were in the ranges of hundreds of nanometres to 1 μm. It seems that the neighbouring pores and cracks possessed similar sizes to the CB agglomerations, and they generated either along with the CB agglomerations or in the boundaries between the agglomerations to the cement matrix. The observation can explain the decreased mechanical properties for the cementitious composites filled with CB nanoparticles from the nanoscopic point of view. In addition, it could be observed that these pores and cracks were empty without fillers because of the absence of SF; hence it is believed that the porous nanostructures of the cementitious composites without SF led to the reduced compressive and flexural strengths. Different from the composites without SF, much fewer pores and cracks were observed for the CB-cementitious composites filled with 10% SF. Moreover, the filling effect of SF could be deduced from the fresh fracture surface of composites, in which there were cement hydration products, such as calcite (CH) and ettringite (Aft). Generally, it could be found that the SF particles filled tightly in the pores and thus both the size and quantity of porosity were greatly reduced. Furthermore, the SF particles were observed in the gaps between CH and Aft. It seems that the SF particles had the capacity to avoid the clusters and fill the gaps and pores among the CH and Aft. In addition to the filling effect, the separation effect of CH and Aft might be another reason leading to the denser microstructures and the better mechanical properties.

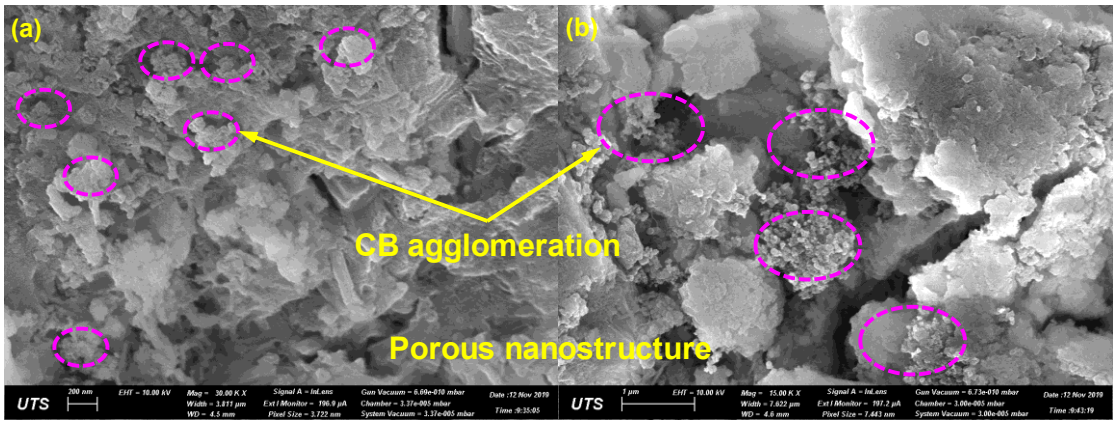

(a) and (b) without SF

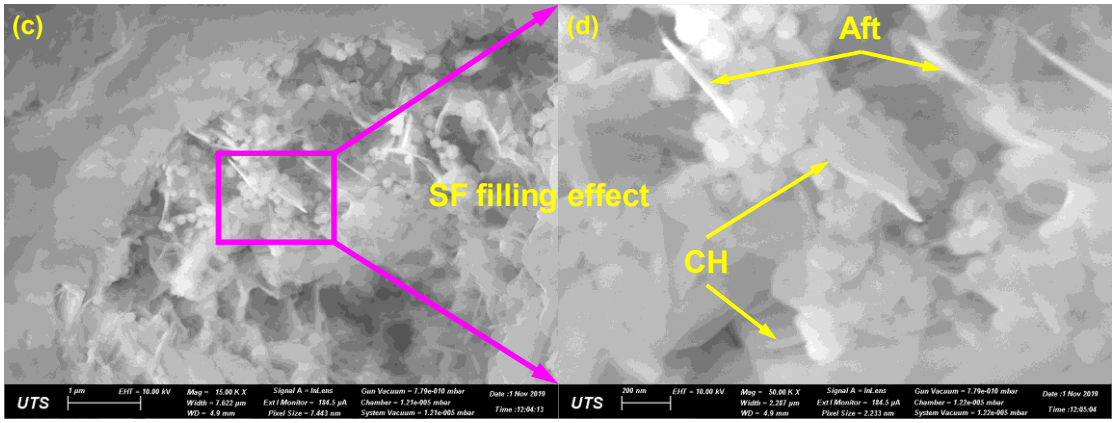

(c) and (d) with 10% SF

Figure 5.20. Microstructures of CB-cementitious composites with different SF contents.

With the increase of SF, it has been mentioned that there generate the CB/SF agglomerations, especially for the composites filled with 20% SF as illustrated in Figure 5.21. The diameter of the SF particle is at least five times larger than that of CB nanoparticles; therefore, it could be seen that the SF particles were enclosed by the CB nanoparticles. The CB nanoparticles tended to cause capillary pores and gaps in the cementitious composites, while the SF having the filling effect could fill these pores. Hence, the effect of SF particles in the CB agglomerations is similar to the "reinforcements", which are able to increase the density and mechanical strengths of the agglomerations, in comparison to the single CB agglomerations. Further, previous studies have demonstrated that the size of CNTs agglomerations declined with the addition of SF . Similarly, the number and size of CB agglomerations decreased with incorporated SF

because the SF intermixed with CB nanoparticles and disrupted the formation of agglomerations. The strengthened CB agglomerations were beneficial to the denser micro and nanostructures of the composites, such as the composites filled with 10% SF, whose mechanical properties reached the highest values. However, because of the high specific surface of SF, they also tended to cluster with CB nanoparticles and absorb nearby water content to affect the cement hydration process. This deduction can be testified by the above hydration heat and thermogravimetry results. As a result, even though the CB agglomerations reinforced by SF particles had higher mechanical strengths and denser microstructures, the affected cement hydration and the induced capillary pores and gaps caused more negativities on the mechanical properties of the CB-cementitious composites. This can be a reason for the decreased mechanical strengths for the composites filled with 20% SF in a nanoscale.

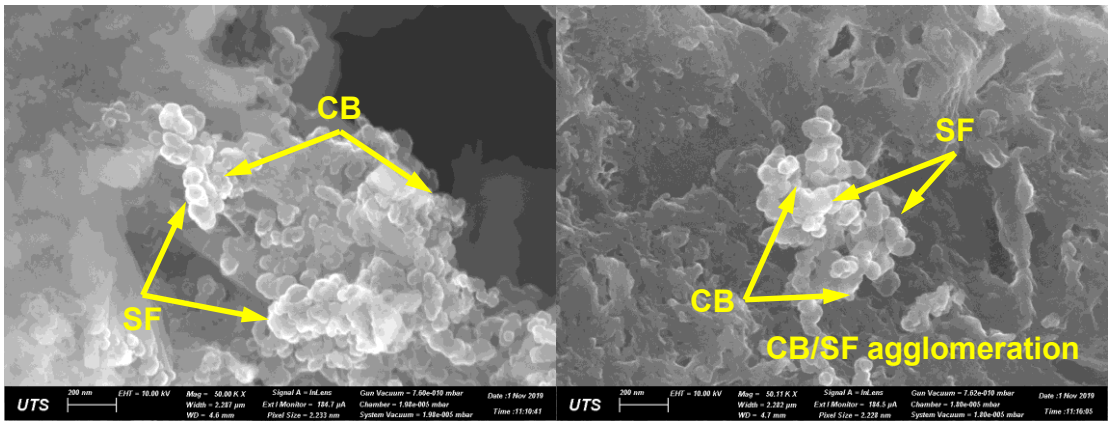

Figure 5.21. Morphology of CB/SF agglomerations in cementitious composite.

5.3.4 Piezoresistivity behaviours

Figure 5.22 illustrates the applied compressive stress and the *FCR* for the 2% CB filled cementitious composites with various contents of SF. For the composites without SF, the FCR values were still consistent with the altered compressive stress, which decreased with the increase of stress and increased when the stress returned. It could be seen that the FCR peaks at the stress magnitudes of 4 and 8 MPa reached approximately 0.4% and 0.8%, respectively. Previous micro and nanostructures of the CB-cementitious composites without SF have shown

their high porosity and the severe CB agglomerations. It seems that the applied stress is mainly converted into the deformation of micropores and CB agglomerations, rather than changing the relative positions among CB nanoparticles dispersed in the cement matrix; thus the electrical resistivity of the composites is rarely changed. Even though, it was found that the composites without SF showed good linearity between the FCR and compressive stress, as well as excellent repeatability. It implied that the composites under the stress magnitudes of 8 MPa were still in the elastic range. Moreover, almost unchangeable FCR was found for the composites under the ladder-shaped loading maintaining at the stress amplitude of 4 MPa. In comparison, the slightly increased FCR were observed at the stress amplitude of 8 MPa. This is due to the more unstable microstructures caused by higher compressive stress than the small stress intensity for all the composites.

Figures 5.22(b) to 5.22(d) illustrate the piezoresistivity for the CB-cementitious composites with 5%, 10% and 20% SF, respectively. The FCR values increased by 20 times and tenfold, respectively at the stress peaks of 4 and 8 MPa for the composites with 5% SF. It could be deduced that the reduced porosity and denser microstructures were responsible for the increased FCR. However, it was found that the FCR changed rapidly at the beginning of the loading, and the changing rate gradually slowed down with the increase of compressive stress. As mentioned that the composites possessed fewer pores and better microstructures due to the SF filling effect, the small stress could lead to the altered positions of conductive CB nanoparticles and result in the rapid resistivity changes. With the increase of compressive stress, the microstructures of composites became denser and the porosity filled with SF started to be unstable, and that was why the FCR changes were reduced. In terms of the composites filled with 10% and 20% SF, similar FCR alterations could be found to that of the composites with 5% SF. The FCR values significantly increased and reached 20% and 25% for the composites with 10% SF at the stress amplitude of 4 and 8 MPa. However, for the SF dosage of 20%, the

FCR values were decreased in the range of 10% to 15% but still higher than that of the composites with 5% SF.

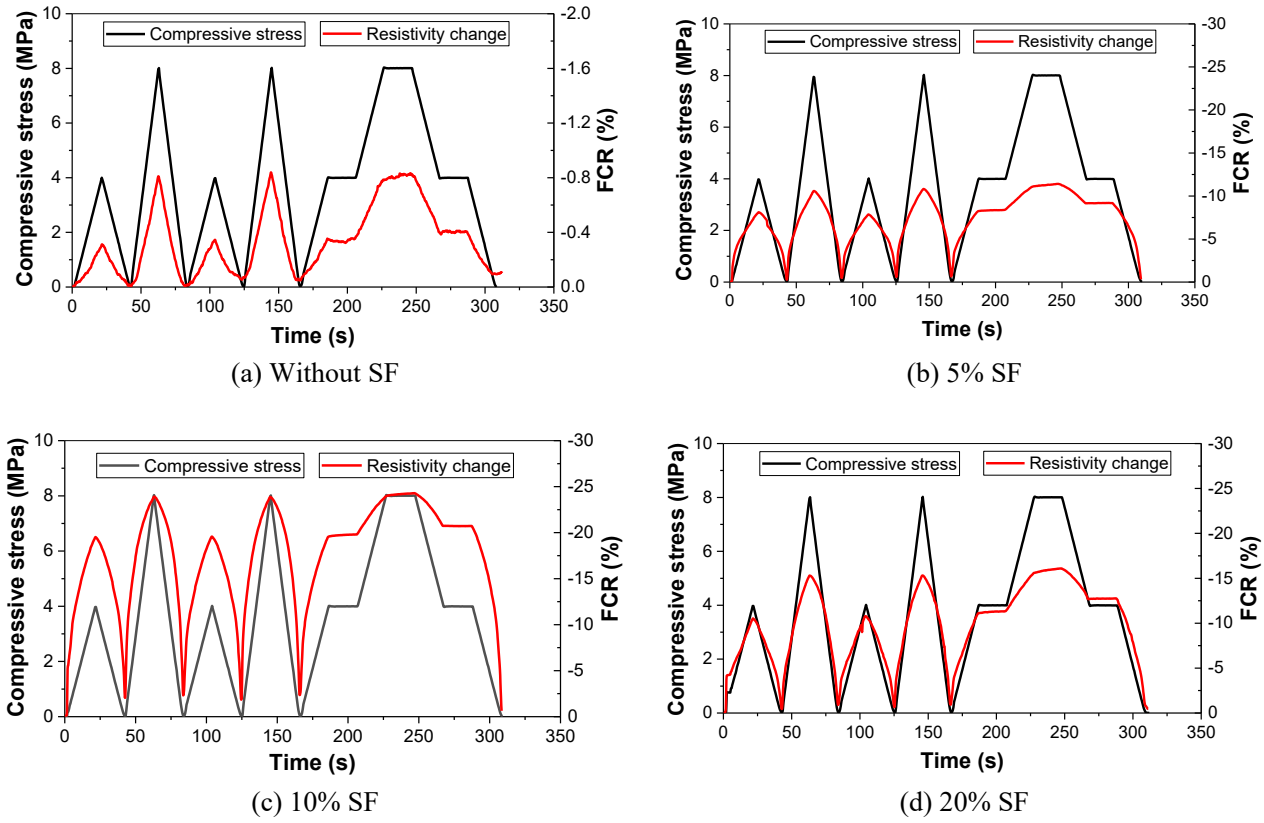

(a) Without SF (b) 5% SF

(c) 10% SF (d) 20% SF

Figure 5.22. Fractional changes in electrical resistivity for CB-cementitious composite with different SF contents.

To evaluate the stress monitoring efficiency of the CB-cementitious composites filled with different contents of SF, Figures 5.23(a) and 5.23(b) illustrates the relationships among FCR and compressive stress in the triangle-shaped and the ladder-shaped loading modes, respectively. Generally, it could be observed that the SF could make the CB-cementitious composites more sensitive to the compressive stress, and the concentration of 10% SF could achieve the composites with the highest sensing efficiency. As for the composites with 20% SF, the SEM images of the composites have demonstrated that their existed CB/SF agglomerations. Because of the larger size of SF than CB nanoparticles, it seems that the CB nanoparticles were blocked by the excessive SF particles, which may partially lead to the

reduction of FCR under compressive stress. Also, the FCR to compressive stress curves were nearly identical for the composites under the triangle-shaped and ladder-shaped loading patterns, which demonstrated that the loading modes made no differences on the stress sensing behaviours. It is worthy to note that the electrical resistivity stability is of significance to the CB-cementitious composites for SHM. The resistivity fluctuation of the composites with different SF contents at the constant stress of 4 MPa was shown in Figure 5.23(b), where the fluctuated electrical resistivity reached approximately < 0.1%, 1.4%, 1.5% and 2.0% could be observed for the composites with 0, 5%, 10% and 20% SF, respectively. The maintained compressive stress is liable to cause fatigue damages inside the CB-cementitious composites. Therefore, the less fluctuated electrical resistivity during the maintained stress represented the better resistance of the composites to fatigue damages. Since the composites without SF possessed extremely low FCR, the fluctuated resistivity was lower than 0.1%. Otherwise, it seems that the CB-cementitious composites filled with 5% or 10% SF were provided with the best stability to fatigue damages, since the excessive content of 20% SF increased the fluctuated resistivity by nearly 33%.

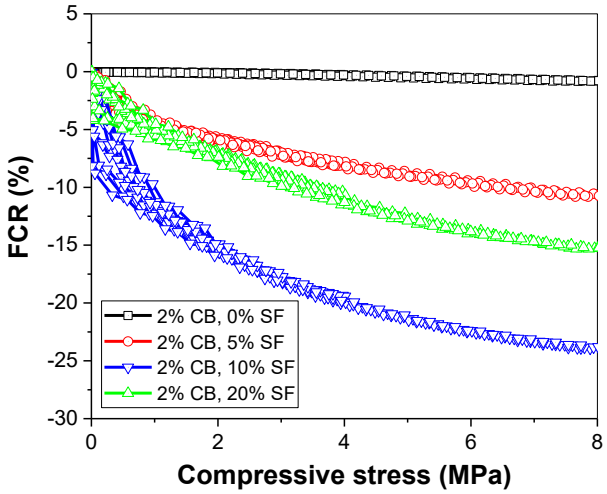

(a) Triangle-shaped loading mode

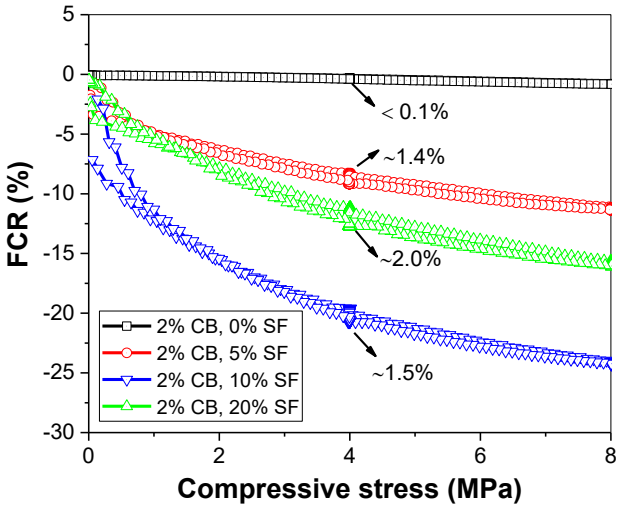

(b) Ladder-shaped loading mode

Figure 5.23. FCR as a function to compressive strength for CB-cementitious composite with various SF contents.

5.4 Summary

The conductive rubber fibres, PP fibres and silica fume are added in the smart cementitious composites as additives, to enhance the electrical conductivity and piezoresistive performances. The specific conclusions can be listed as follows:

(1) The electrical conductivity of the CB/cementitious composites was improved by the conductive rubber fibres. The more rubber fibres, the better conductivity is. The percolation threshold was clearly decreased for the 0.5–1.0 wt% CB/cementitious composites embedded with 80 rubber fibres (1.27 vol%).

(2) Conductive rubber had capacity to improve the gauge factor of 0.5 wt% CB/cementitious composites, by the growth rate of 78.4% compared to the results from other literatures; for 1.0 wt % CB/cementitious composites, the gauge factor significantly increased to hundreds of times higher than commercial strain gauge but with worse linearity to compressive strain, because of the phenomenon of piezoresistive percolation; Since the better conductivity for the

composites with 2 wt% CB, conductive rubber rarely influenced its conductivity and piezoresistivity.

(3) Although the PP fibres were electrically insulative, the enclosed CB nanoparticles on the surface could increase the conductive passages through PP fibres, thus the electrical conductivity of the cementitious composite was enhanced with the increase of PP fibres.

(4) The flexural stress sensing ability was much weaker than that of compressive stress, and the sensing efficiency dramatically increased by nearly 6 times when the added PP fibres reached 0.4 wt%. Similarly, the flexural stress as a function to resistivity changes and contents of PP fibres was established.

(5) Micropores and CB agglomerations were found in CB-cementitious composites without SF, while denser microstructure and well-dispersed CB nanoparticles could be observed with 5% and 10% addition of SF. Nano/microscale porous structures along with CB agglomerations could be clearly seen without the addition of SF. On the contrary, less pores due to the physical filling effect of SF could be obtained with 10% SF.

(6) Piezoresistivity of CB-cementitious composites was significantly improved with the addition of SF, especially with 10% SF. The FCR values altered rapidly in the initial loading stage, and then gradually slowed down with the increased compressive stress. The specimen with 5 and 10% SF exhibited better piezoresistivity under the constant stress compared to the one with 20% SF.

CHAPTER 6: PIEZORESISTIVITY INTERFERENCE FROM WORKING ENVIRONMENT

In this chapter, the effects of environments ranging from temperature, water content, freeze-thaw cycle, acid erosion and impact loading on the performance of cement-based sensors were explored.

6.1 Effect of temperature

Sections 6.1.1 and 6.1.2 present the piezoresistivity of CB cementitious composites under the temperatures ranging from -20 °C to 100 °C. The section 6.1.3 presents the piezoresistivity of CNT cement-based sensors after elevated temperatures of 300 °C and 600 °C treatment.

6.1.1 Effect of thermal exchange

Figure 6.1 illustrates the *FCR* variation of CB cementitious composites exposed in the ambient environment of 20 °C and 60% relative humidity without any external forces. It represented an opposite tendency among the heated and the frozen composites, with the increased resistivity by the heated specimens and the decreased resistivity by the frozen ones. Based on the theory of thermal exchange, this phenomenon is owing to their different exchange patterns. Since the composites under high temperature tended to emit heat into the ambient and decreased the temperature until reaching equilibrium, the resistivity of composite decreased gradually with the exposure time. On the contrary, the frozen composites had a trend to absorb heat from the ambient environment and increased the temperature to decrease their electrical resistivity.

Generally, curves of the relationship between *FCR* and exposure time from both thermal radiation and absorption of the CB/cementitious composite are in linear relationship, with the slope fluctuation as low as 10^{-5} in Figure 6.1. After 15 min of air exposure, the *FCR* changes for the thermal absorption reached higher than 30%, while the values even higher for the composites under thermal radiation and achieved nearly 40%. The results are probably out of

their different degree of temperature deviations to the room temperature, which reach at 80 °C for the heated composites (under 100 °C) and only 40 °C for the frozen ones (under -20 °C). In other words, the fractional changes of resistivity for the CB/cementitious composites are highly depended on the temperatures. Thus, unless the compression tests on these high/subzero temperature CB/cementitious composites were carried out in the incubator with identical environmental temperature, the *FCR* alterations induced by the thermal exchanges was not excluded in the next section of piezoresistive test on the CB/cementitious composite under various temperatures.

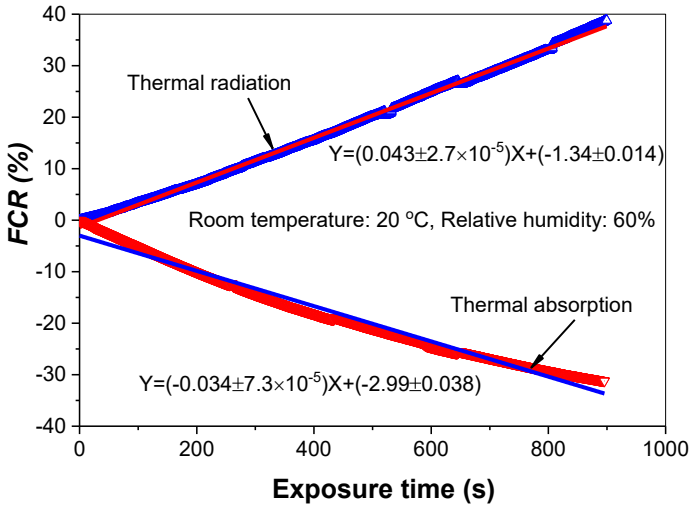

Figure 6.1. Relationship between thermal radiation/absorption and *FCR* of dry CB cementitious composites under temperature of 20 °C and relative humidity of 60%.

6.1.2 Piezoresistivity at low temperatures

Under the loading regime of three cycles and the stress magnitude of 2 MPa as loading limit, Figure 6.2 shows the *FCR* and strain development of composites at different temperatures of -20 °C, 20 °C, 60 °C and 100 °C. It was observed that only the specimens at the room temperature of 20 °C exhibited excellent repeatability on electrical resistance, while all the other cementitious composites at the higher or lower temperatures performed gradual increase or decrease in the loading process and led to the irreversible *FCR* changes. Based on the aforementioned results, the original *FCR* changes (dotted red lines) were generated from the

combined action of both cyclic compressive stress and the thermal exchange. Therefore, to eliminate the effect of thermal radiation and absorption on the irreversible resistivity of cementitious composites, the calibrated *FCR* (red lines) on the basis of the decreasing or increasing *FCR* of untreated specimens in the ambient environment were carried out. Overall, after the temperature calibration of *FCR* to remove the effect of thermal exchange, all the heated or frozen CB filled cementitious composites showed good synchronicity and repeatability to compressive stress. The results illustrated that the temperatures themselves from -20 °C to 100 °C can't affect the repeatability of CB/cementitious composites. However, under the extreme circumstances with fire attacks, concrete infrastructures embedded with CB cementitious sensors might undergo temperature higher than 450 °C. The repeatability of CB/cementitious composites is still unknown for the both reduced conductor content because of the oxidized carbon black particles and the damaged C-S-H gels.

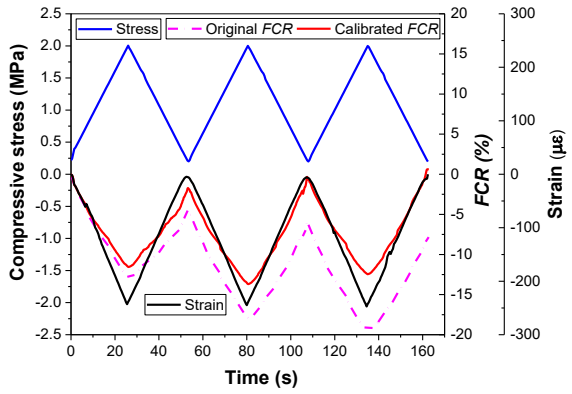

(a) At temperature of -20 °C

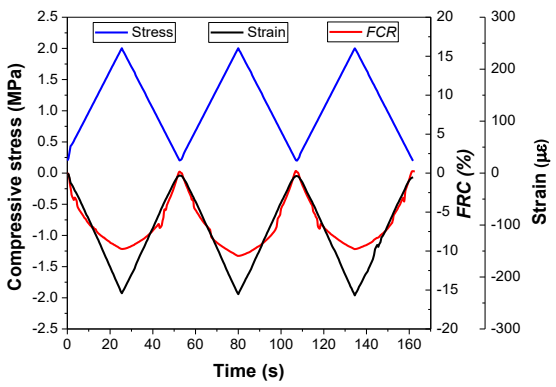

(b) At temperature of 20 °C

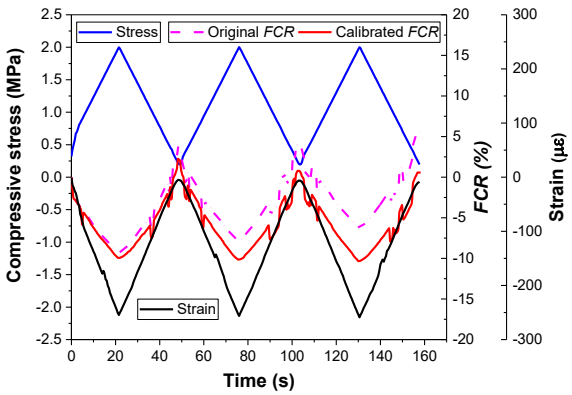

(c) At temperature of 60 °C

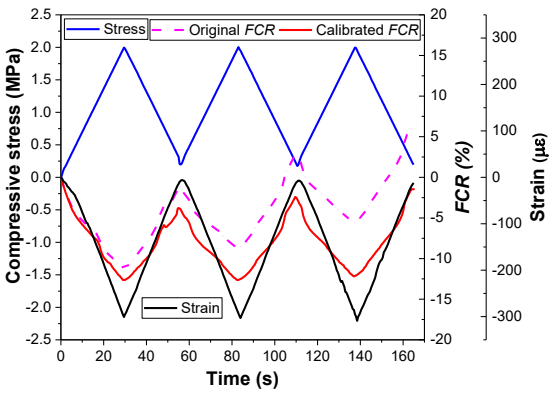

(d) At temperature of 100 °C

Figure 6.2. The *FCR* of dry CB cementitious composite at different temperatures under cyclic compression.

The sensitivity of CB cementitious composites under different temperatures were conducted through the *FCR* alterations by per unit strain which is also known as the gauge factor. It indicates that during a loading process, both the changes of *FCR* and compressive strain are of importance to the sensitivity of cementitious composites. Figure 6.3 compares the relationship between their strain and *FCR* changes among CB/cementitious composites at different temperatures. The composites under 100 °C were provided with largest *FCR* of 12.6% as well as producing the largest strain values. However, both smallest *FCR* changes and compressive strain were generated for the composites at the room temperature.

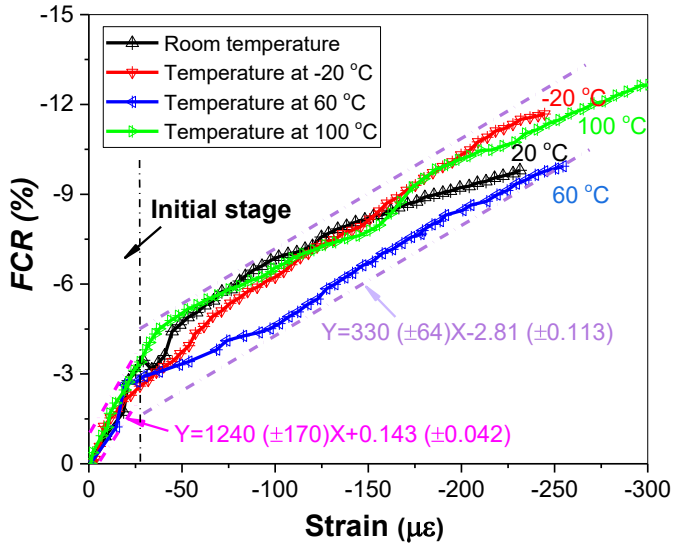

Figure 6.3. Relationship between *FCR* and strain for CB cementitious composites under various temperatures.

Even though there were small differences between composites at different temperatures, two sections could be divided according to the curves of *FCR* to strain. It seems that higher fractional changes of resistivity occurred at low strain, while the resistivity changes decreased when the compressive strain reached the limit of 30×10^{-6}. This is consistent to the

investigations by Pang et al. (Dai Pang et al. 2014) who proposed that the reduced interfacial distance between conductive fillers and cement matrix was responsible for the swift resistivity alterations during initial loading. To describe their differences on the gauge factor and sensitivity, the fitting formulas of these curves in the two sections were plotted in Figure 6.3. Their fitting errors were also followed in the formulas. It shows that in the initial loading stage, much higher gauge factor reaching 1240 was achieved, which demonstrates the ultra-high sensitivity of CB/cementitious sensor with small deformations. However, with the increase of strain, the increasing rate of *FCR* was greatly reduced and the gauge factor of approximately 330 was obtained. There are several potential reasons for the decreased gauge factor or sensitivity. The first reason is probably owing to the higher CB content and the excellent electrical conductivity of cementitious composites, where exists uneven CB agglomerations which could be connected and decrease the resistivity with very small deformations. The second is because of the minor pores in the CB/cementitious composites, where physical and electrical properties were nonlinear and vulnerable to the deformations, and led to the damaged microstructures and decreased gauge factor. Furthermore, as mentioned above, the sudden resistivity reduction was likely due to the easier reduced interfacial distance between CB particles to cement matrix.

Overall, the experimental results illustrate that both the repeatability and sensitivity of 3% CB filled cementitious composites makes no differences on account of different application temperatures from -20 °C to 100 °C. However, the temperature changes or thermal exchange during the service of cement-based sensors affected its electrical characteristics and must be calibrated. In addition, the sensitivity was influenced by different loading stages, with the much higher sensitivity at the initial loading stage and the relatively lower but more stable sensitivity in the later loading stage (Dong, Li, Tao, et al. 2019).

6.1.3 Piezoresistivity at high temperature

6.1.3.1 Composites reinforced with 0.25% MWCNT

Figures 6.4(a) to 6.4(c) illustrates the cyclic compressive stress, strain and the fractional changes of resistivity of 0.25% MWCNT reinforced composites without treatment, after 300 °C and 600 °C heat treatments, respectively. Generally, a decreased electrical resistivity in the loading process and an increased resistivity in the unloading process could be observed for all composites. For the composites without heat treatment, the fractional changes of resistivity reached 6.2%, 9.4%, 12.1% and 14.5% respectively at the stress magnitudes from 4 MPa, 6 MPa, to 8 MPa and up to 10 MPa, exhibiting acceptable linearity and excellent reversibility in Figure 6.4(a). It demonstrated that the MWCNT reinforced cementitious composites are capable to serve as cement-based sensors for SHM.

However, for the elevated temperatures treated composites, considerable increases of fractional changes of resistivity were observed in Figures 6.4(b) to 6.4(c), with resistivity plunges and leaps in the beginning and end of loading. Afterwards, the fractional changes of resistivity were similar to that of untreated MWCNT/cement composites and showed almost linear alterations with compressive stress. In the loading peak, it was seen that the sharp reduction of resistivity reached from 25% to 33% for the composites in different stress magnitudes after 300 °C heat treatment, which greatly overwhelmed the later fractional changes of resistivity with increase of loadings, since the total fractional changes of resistivity was in the range of 40% to 50%. Furthermore, the irreversibility was gradually increased with loading cycles and stress magnitudes, with the average permanent resistivity reduction by 5.2%, 8.9%, 13.5% and 16.2% in the stress magnitudes of 4 MPa, 6 MPa, 8MPa and 10 MPa. In terms of the composites after 600 °C heat treatment, similar results were observed on the sudden resistivity changes when small forces applied and the later more stable and linear resistivity changes. Nevertheless, both the total fractional changes of resistivity and the sharp alterations

were less in comparison to the counterparts after 300 °C heat treatment, with the former in the scope of 30% to 40% at the stress peak and the latter within 20% to 30% based on different stress magnitudes.

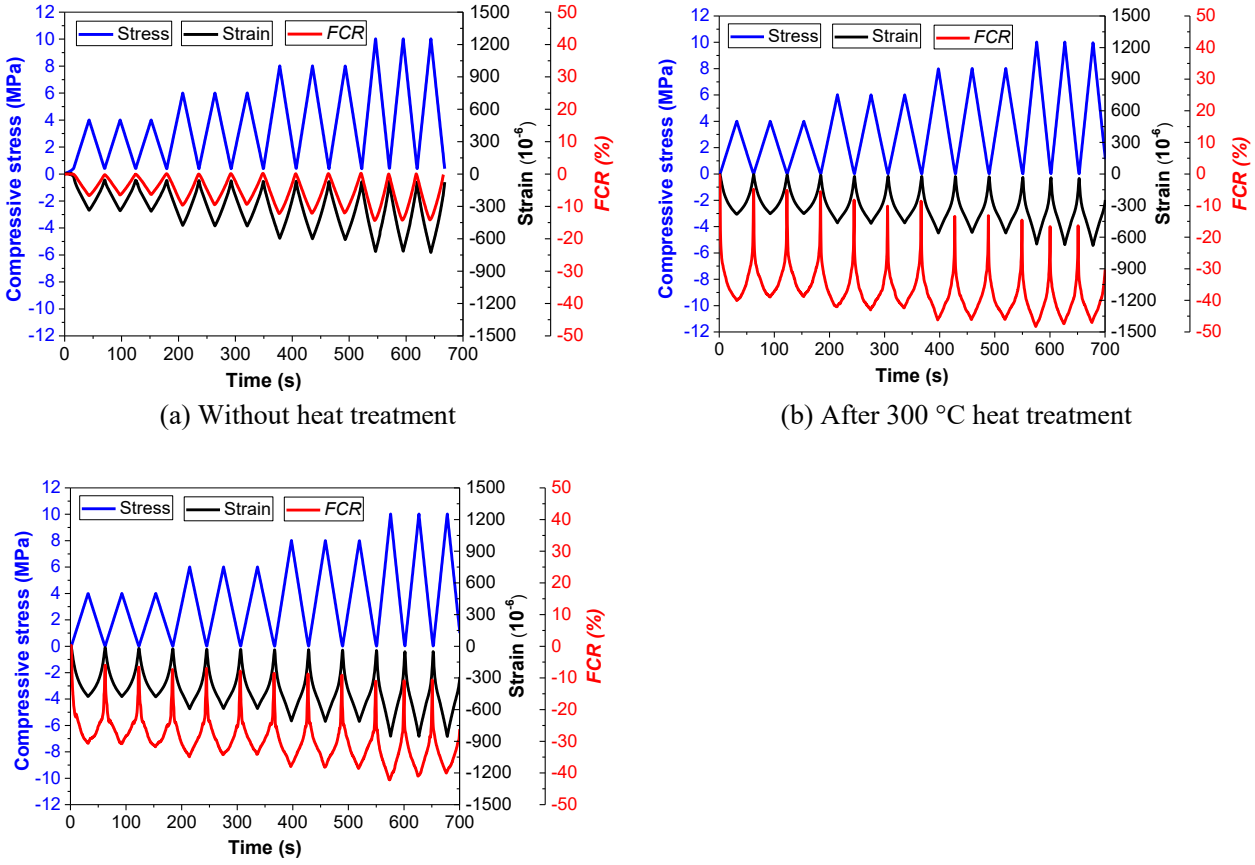

(a) Without heat treatment

(b) After 300 °C heat treatment

(c) After 600 °C heat treatment

Figure 6.4. Fractional changes of resistivity of 0.25% MWCNT/cementitious composites related to compressive stress and strain.

To further understand the alteration patterns of fractional changes of resistivity, and evaluate the effects of these sharp changes on the piezoresistive sensitivity, Figure 6.5(a) exhibits the fractional changes of resistivity of MWCNT reinforced cementitious composites under different heat treatments as a function to compressive strain. The values of fractional changes of resistivity and compressive strain were both in absolute values. Each curve consists of 12 loops of resistivity changes to strain, because of four different stress magnitudes each possessing three cycles. The piezoresistive sensitivity was represented by the value of gauge

factor, which expresses as the fractional changes of resistivity per unit strain. For the MWCNT/cement composites without heat treatments, the fractional changes of resistivity illustrated good linearity to compressive strain, and the gauge factor achieved approximately 228, such as slope of the green fitting line in Figure 6.5(a). Moreover, it was observed that the untreated composites maintained well both on the electrical resistivity and compressive strain, with the irreversible resistivity less than 0.50% and the irreversible strain of approximately 50 $\times 10^{-6}$.

As for the heat treated MWCNT reinforced composites, before the reluctantly linear relationship between fractional changes of resistivity and the compressive strain, a significant nonlinearity was observed in the ranges with small strain. It demonstrated that the sensitivity at the beginning was extremely high, which gradually slowed down until to the linear part. Generally, it was found that the threshold value for transforming worse linearity to the better linearity was approximately 200×10^{-6} for the composites after 300 °C heat treatment, which slightly increased to 250×10^{-6} for the counterparts after 600 °C heat treatment. In the aspect of linear portion of the heat treated composites, the gauge factors were calculated based on their fitting curves as shown in Figure 6.5(b), with the values of 380 shown in slope of the red fitting line in Figure 6.5(b) and 322 shown in slope of the blue fitting line in Figure 6.5(b) for the composites after 300 °C and 600 °C heat treatments, respectively. Obviously, the gauge factors of the linear portion for the heat treated MWCNT reinforced cementitious composites were higher than that without heat treatment, demonstrating the better piezoresistive sensitivity in the larger strain regions for the composites after the heat treatment. The results indicate that the heated MWCNT/cement composites at the temperature of 300 °C were provided with best sensitivity.

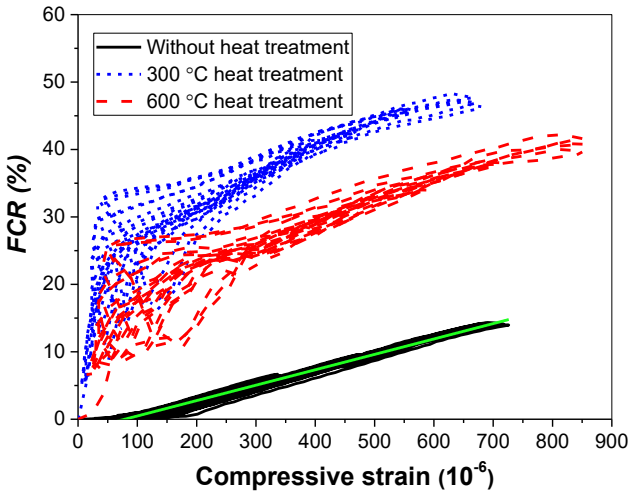

(a) Complete curves of *FCR* to compressive strain

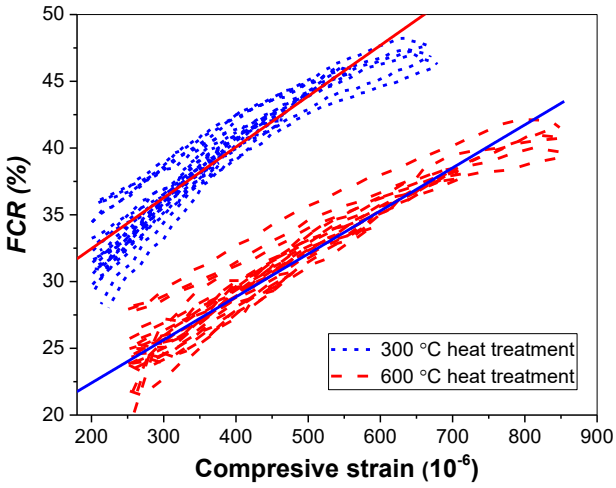

(b) Linear part of *FCR* to compressive strain

Figure 6.5. Fractional changes of resistivity as a function to compressive strain of cementitious composites incorporating 0.25% MWCNT after heat treatments.

6.1.3.2 Composites with 0.50% MWCNT

Figure 6.6 displays the fractional changes of resistivity for the 0.50% MWCNT reinforced cementitious composites to the applied cyclic compressive loading. Generally, in comparison to that of 0.25% MWCNT, smaller fractional changes of resistivity and gentler resistivity jumps were observed for the 0.50% MWCNT reinforced cementitious composites subjected to identical loadings and heat treatment. In particular, it was found that the fractional changes of resistivity reached 6.8%, 8.8%, 10.8% and 12.5%, respectively at stress peaks of 4 MPa, 6 MPa,

8MPa and 10 MPa for the composites without heat treatment. Although the fractional changes of resistivity in the first three cycles were relatively higher achieving 6.8% than 6.2%, the later increment of fractional changes of resistivity for the composites with 0.25% MWCNT were considerably weakened for the composites with 0.50% MWCNT. Similar to composites with 0.25% MWCNT, the composites with 0.50% MWCNT still maintained stable piezoresistivity, and exhibited satisfactory repeatability.

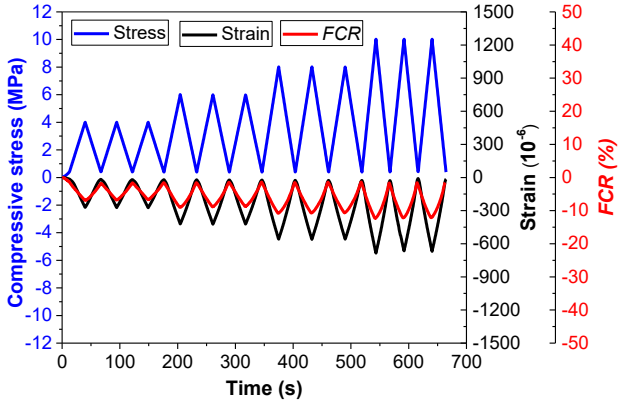

(a) Without heat treatment

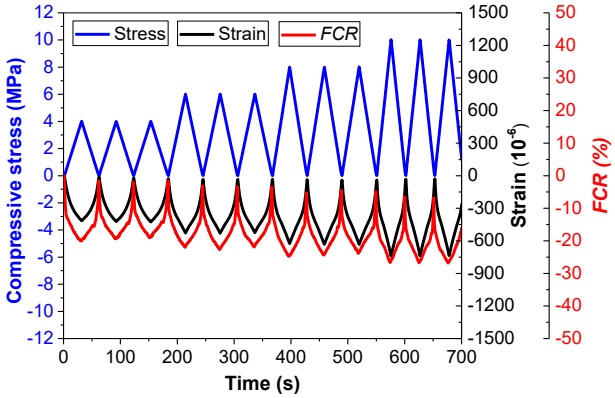

(b) After 300 °C heat treatment

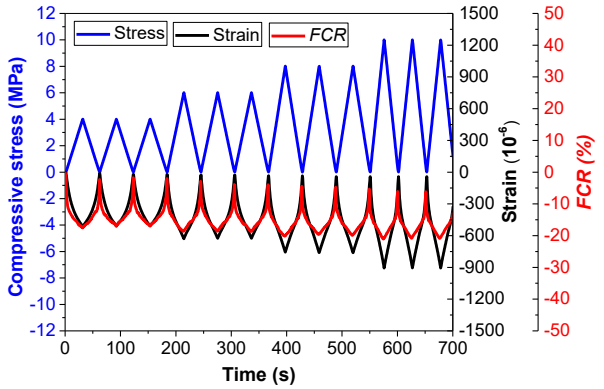

(c) After 600 °C heat treatment

Figure 6.6. Fractional changes of resistivity of 0.50% MWCNT/cementitious composites related to compressive stress and strain.

For the 0.50% MWCNT reinforced composites after heat treatment, much smaller total fractional changes of resistivity were observed since reduced sharp alterations at the beginning and end of loading. Also, it was observed that the composites after 600 °C heat treatment possessed both lower total fractional changes of resistivity and sharp reduction than the

composites after 300 °C heat treatment. The results showed the sudden changes narrowing down to approximately 18% and less than 15% for the composites after 300 °C and 600 °C heat treatments, respectively. Furthermore, in terms of the irreversibility of the 0.50% MWCNT reinforced composite, similar tendency could be detected by the increased irreversible resistivity with the increased stress magnitudes and cycles. Compared to the counterparts with 0.25% MWCNT, the irreversible resistivity was reduced by both lower than 10% for the composites with 0.50% MWCNT after 300 °C and 600 °C heat treatments.

Similarly, to reveal the relationship between fractional changes of resistivity to compressive strain and uncover the piezoresistive sensitivity, Figure 6.7 depicts the fractional changes of resistivity as a function to compressive strain. For the composites without treatment, excellent linearity could be observed with the gauge factor of 168 shown in slope of the green fitting line in Figure 6.7(a). However, dramatic nonlinearity in the region with small strain was observed for the heat treated composites, just as mentioned for the composites with 0.25% MWCNT. Therefore, the linear parts of these curves were chosen to evaluate the piezoresistive efficiency after different temperatures heat treatment. The gauge factor for the composites after 300 °C heat treatment reached 263 shown in slope of the red fitting line in Figure 6.7(b) in the linear part, while the values significantly decreased to 137 shown in slope of the blue fitting line in Figure 6.7(b) for the 600 °C heated composites. Overall, the composite after 300 °C heat treatment seems possessing better piezoresistive sensitivity than that without treatment and that after 600 °C heat treatment. Because of the sharp alterations in the beginning and end of loading, the linearity only occurred in the regions with larger compressive stress. It demonstrated that the appropriate heat treatment on the MWCNT reinforced cementitious composites possibly has capacity to increase the piezoresistive sensitivity.

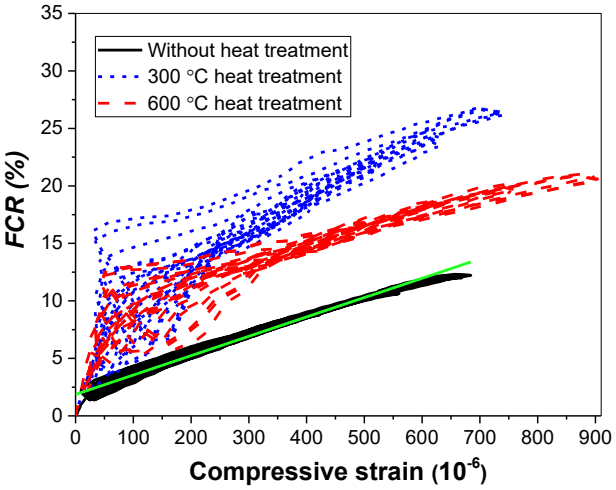

(a) Complete curves of *FCR* to compressive strain

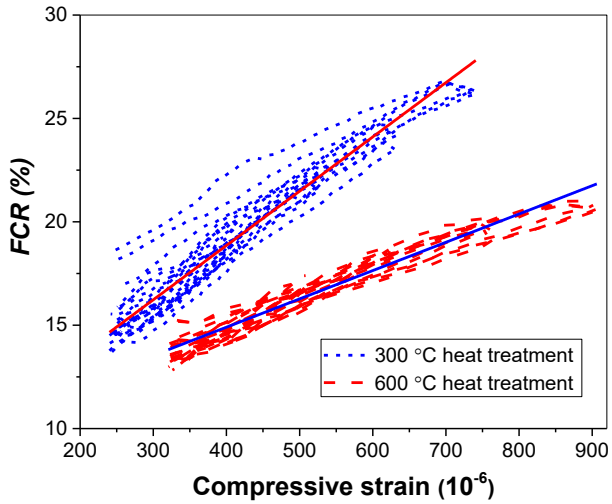

(b) Linear part of *FCR* to compressive strain

Figure 6.7. Fractional changes of resistivity as a function to compressive strain of cementitious composites incorporating 0.50% MWCNT after heat treatments.

6.1.3.3 Mechanism of piezoresistivity

To elucidate the sharp alterations and increased fractional changes of resistivity of the heat-treated MWCNT reinforced composites, Figure 6.8 displays four possible transformations of MWCNT and cement matrix after heat treatment, named MWCNT purification, MWCNT destruction, cement matrix destruction and agglomerates destruction. Since the cementitious composites had been dried before heat treatment, the effects of pore solutions and conductive ions that significantly affect the electrical resistivity and piezoresistivity will not be mentioned

here. The manufacturing of MWCNT is always accompanied by introducing metal catalysts, and the final MWCNT products often possess more or less impurities, such as residual metal particles, carbon nanofibers, graphite and amorphous carbon, which somewhat influence their electrical properties. The weight loss of as received CNTs in high temperature includes the oxidation of carbonaceous impurities . It has been proposed that the temperature ranges of gas phase oxidative purification of CNTs are from 225 °C to 760 °C under an oxidizing atmosphere . The temperatures of 300 °C and 600 °C in this study did have the capacity to eliminate a proportion of carbonaceous impurities and affect the electrical conductivity of MWCNT. In addition, by means of TGA and electron dispersion X-ray (EDX), Porro et al. observed the presence of iron and oxygen in CNTs due to the generation of Fe_2O_3. Since these conductive metal particles were attached into the surface of nanotube, the oxidation in nanotube bodies must affect the electrical conductivity. This could be further demonstrated by the different electrical conductivity for the annealed MWCNT with different weight losses. Since the intact MWCNT have higher oxidation temperature, fewer impurities were found on the mixtures after the severe oxidation process by heat treatment over 500 °C. As shown in Figure 6.8(a), the impurities attached in the external surface of MWCNT might block the electrical contact between nearby MWCNT, while the heat treatment could eliminate some of impurities and make the MWCNT easier to contact with each other, which to some extent contribute to the higher fractional changes of resistivity under same loadings.

As for the MWCNT destruction in Figure 6.8(b), based on the SEM morphology of MWCNT without and after the heat treatments, significant MWCNT destruction was observed, especially for the composites subjected to 600 °C heat treatment. The disconnected MWCNT may be due to its initial structural defects or the weakened properties induced during ultrasonication . Even though the disconnected MWCNT could cause higher electrical resistivity for the cementitious composites, more contact points were created to generate the conductive passages between new

formed MWCNT. It means that small external loading might reconnect these disconnected MWCNT and decrease electrical resistivity, and that was one of reasons for the generation of sharp resistivity changes in the beginning and end of loading after heat treatments. In other words, the nonlinearity of the fractional changes of resistivity to compressive strain in the beginning and end of loading was partially due to the reconnection of disconnected MWCNT.

As shown in Figure 6.8(c), the third potential factor that influenced the piezoresistivity is the cement matrix destruction during heat treatment. It has been reported that the high pressure steam could be generated inside the composites during heat treatment, which caused inner stress to larger the cracks and pores . In addition, the decomposition of C-S-H gel could also soften the MWCNT/cement composites under high temperature treatment, which could be supplemented by the SEM images and the increased compressive strain under the same loading. Both of these factors caused the destruction of cement matrix and lower the strength of composites, and the "softer" composites might contribute to the easier altered fractional changes of resistivity during the compression.

Another potential factor that may affect the piezoresistive performance is the features of MWCNT agglomerates after the heat treatment. As briefly illustrated in Figure 6.8(d), the morphology of MWCNT agglomerates before the heat treatment looked like a firm and completely conductive cluster. However, owing to the disconnected MWCNT or other oxidized conductive impurities induced cracks or gaps, the agglomerates with defects have possibility to become non-conductive phase or the clusters with much higher resistivity. It was proposed that crystal particles could be vaporised from CNTs agglomerates in high heating rates for CNTs purification. Hence, it was deduced that the electrical resistivity of MWCNT agglomerates could be affected after high temperature treatment. In addition, this could be further demonstrated by the disconnection of MWCNT after heat treatment, which could be occurred in the agglomerates to increase the electrical resistivity. Since the agglomerates

possessed worse resistance to external loadings , a small compressive stress/strain might cause the reconnection between agglomerated MWCNT and greatly reduced the fractional changes of resistivity. Furthermore, the MWCNT used in this study was relatively in lower qualities (Purity higher than 95 wt.%), for the sake of lower costs especially when extensively applied in engineering project, there inevitably existed impurities in the MWCNT and agglomerates. It can be deduced that the gaps/cracks due to the oxidization and disconnection of impurities or MWCNT were large enough to ensure the separation between some of MWCNT in the unloading process, since the sharp increases on the resistivity on this stage.

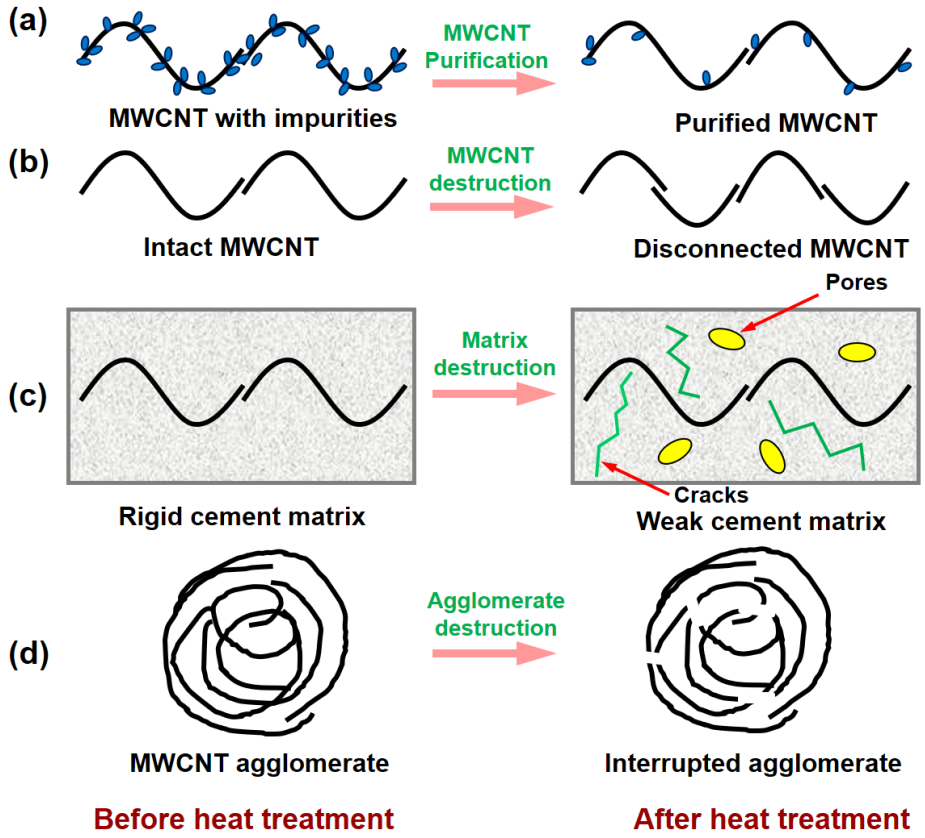

Figure 6.8. Mechanisms for improved fractional changes of resistivity for MWCNT/cementitious composites after heat treatments.

6.2 Effect of water content

6.2.1 Piezoresistive properties at various water contents

Figure 6.9 depicts the *FCR* and compressive strain changes of CB/cementitious composites at different water contents under the same cyclic compression. It could be observed that the *FCR* changes showed excellent repeatability when the CB cementitious composites contained water contents lower than 12%, which was only accompanied with a small fluctuation on resistivity changes. Also, it represents that the CB/cementitious composites containing water content of 4% and 8% expressed larger *FCR* changes than that with 12% water content and the dry specimens. However, for the saturated specimens and the composites containing water content of 16%, it depicts that the composites not only showed lower *FCR* changes, but along with more volatile and fluctuated *FCR* alterations. One reason for these fluctuations is because of the polarization effect in pore solutions, where exists movements of ions in electric filed until reaching electrical potential balance. Another reason is that the water content affects the concentration and the number of solution filled pores, the touch and detach of nearby pore solutions also increased the curve volatility .

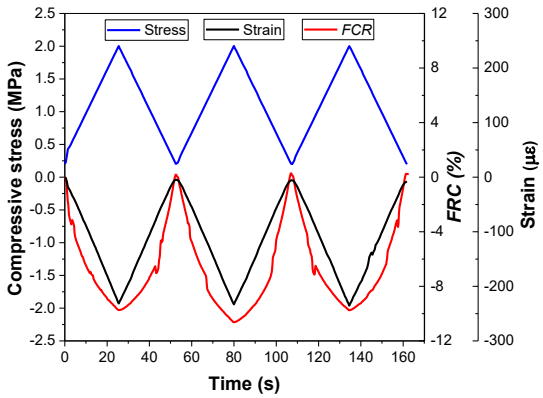

(a) Dry state

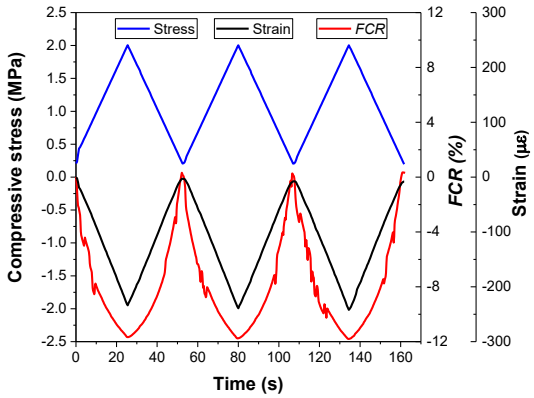

(b) 4% water content

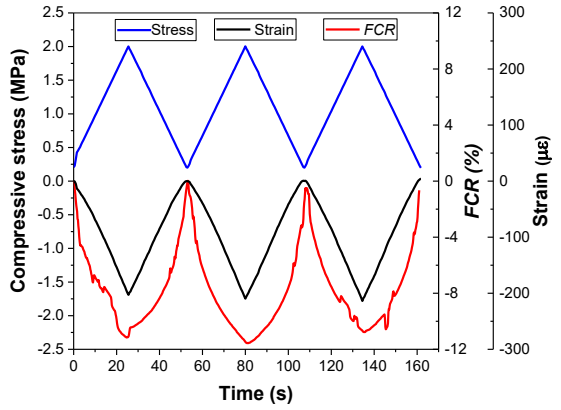

(c) 8% water content

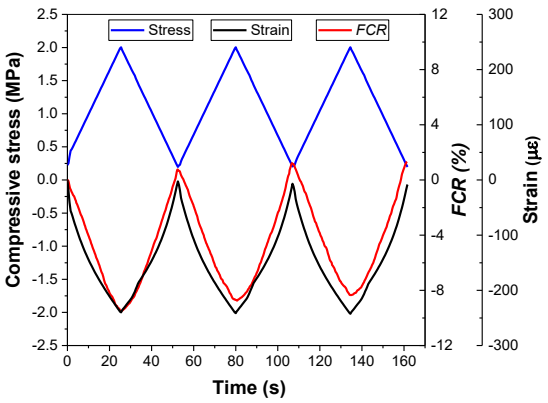

(d) 12% water content

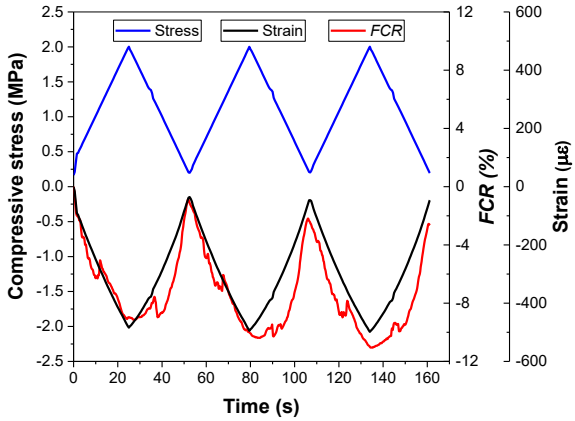

(e) 16% water content

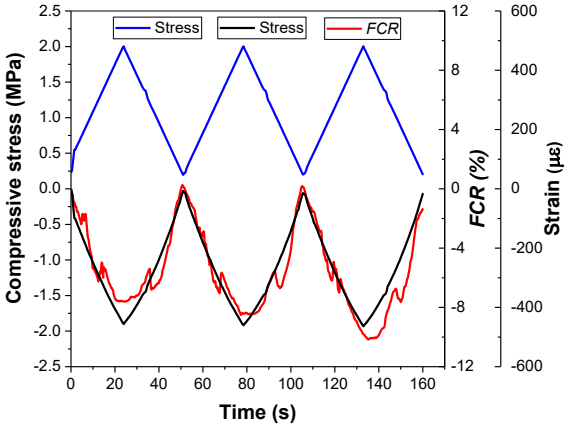

(f) Saturation state

Figure 6.9. The *FCR* of CB cementitious composites with different water contents under cyclic compression.

Figure 6.10 plots the dependence of *FCR* to the compressive strain for cementitious composites with different water contents. It was observed that the sensitivity of CB/cementitious composites firstly increased and then decreased with rise of water content. For the composites at the saturation state, the piezoresistivity experienced the lowest sensitivity with the gauge factor of approximately 150. Then the gauge factor slightly increased to nearly 175 for the composites cooperating 16% water content. The composites at dry state and that with 12% water content showed nearly identical gauge factor of 400, with small discrepancy on the rapid growth in the early stage for the former and in the late stage for the latter. The rough evaluation of optimal water content for CB/cementitious composites was approximately

at 8%, with the gauge factor reaching the value of 488. To acquire more precise optimum value of water content in the CB/cementitious composites, more tests are needed to narrow down the interval of water content in the composites.

In terms of the tendency of individual curve, it was seen that for the dry specimens and the composites with water content of 4% and 8%, their growth rates of *FCR* (gauge factor) gradually decreased with the loading process. However, for the composites at saturated state and that with 12% and 16% water content, their *FCR* growth rates were well maintained (saturated specimens and that with 16% water content) and even gradually increased (composites with 12% water content). This is probably out of the easier contact between CB particles without the interferences from water content, and the detailed explanation will be presented in the next section. In summary, the water content influenced both repeatability and sensitivity of CB/cementitious composites. Based on the current experimental results and previous studies, the potential mechanisms will be discussed in the next section.

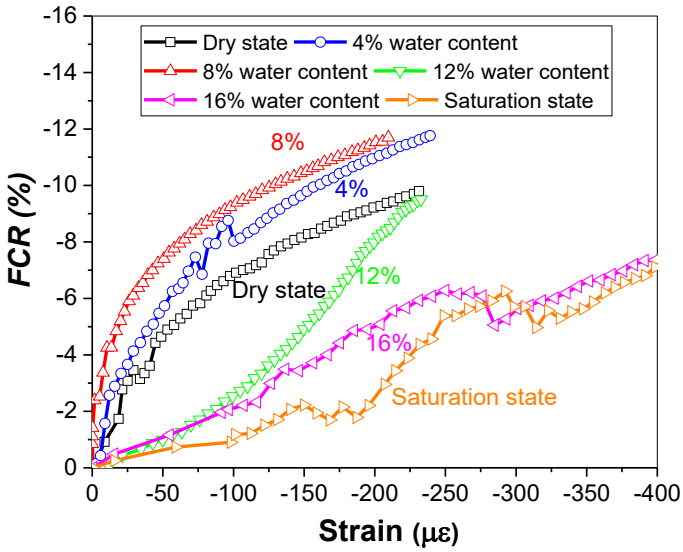

Figure 6.10. The *FCR* of CB cementitious composites at different water contents as a function of compressive strain.

6.2.2 Mechanism discussion

As mentioned above, the increase of water content affects the sensitivity of CB cementitious composites, by firstly increasing then decreasing the gauge factor. Figure 6.11 shows the electrical resistance changes of composites with different water contents, and relative positions between CB particles in different stages on account of water content, striving to explain the relationship between the CB particles, water content, electrical resistance and the aforementioned piezoresistivity. Different stages from *A* to *D* represent the dry stage, less-water stage, medium-water stage and the large-water stage, respectively (Dong, Li, Zhu, et al. 2021). The CB particles enclosed by water layer demonstrated transformation among different conductive mechanisms, due to the increase of water content in the CB/cementitious composites. It was observed that the electrical resistance of cementitious composites increased with the water content, from approximately 102 Ω for the dry composites to nearly 620 Ω for the saturated ones. One possibility for the increased electrical resistance was due to the decreased conductivity of the water enclosed CB particles. Also, the higher water content resulted in severe polarization effect during the resistance measurement and caused larger measuring errors, especially for the cementitious composites under high temperatures.

It is widely known that the electrical conductivity includes electronic conductivity, which is generated from the movement of free electrons, and the ionic conductivity that produced out of ions' movement. In the dry stage (Figure 6.11-A), the electrical conductivity mainly came from the contacts between CB particles, which possessed the electrical resistivity of lower than 0.43 Ω·cm. It seems that the direct contact between CB particles could provide a very low resistance to the electrons' movement and improve the conductivity of cementitious composites. As for the piezoresistivity, the *FCR* changes were only due to the contact between CB particles to reduce electrical resistance, while the cement hydration products with worse conductivity rarely altered the resistance and the *FCR*.

With the increase of water content, the composites came to the less-water stage (Figure 6.11-B), where some CB particles were enclosed by water layers. It blocked the direct connections among CB particles by thin water film to reduce the electrical conductivity. Interestingly, the piezoresistivity in this stage was improved, just like the composites with 4% and 8% water content, respectively. This is because the *FCR* changes were not only due to the contact of CB particles, there also were resistance reduction because of the ions movements such as Ca^{2+}, OH^- and SO_4^{2-} in the water layers. Owing to the limited water content, most of the *FCR* changes still came from the CB particles, and brought the largest gauge factors.

The followed medium-water stage (Figure 6.11-C) had higher electrical resistance just as the composites with 12% and 16% water content. In this stage, increased CB particles were covered by the water layers, which considerably increased the contact resistance between CB particles. Although the *FCR* changes from the ions conductivity was stimulated, the electrical responses from the contact of CB particles were weakened due to the water layer decreased conductivity. According to the reduced gauge factor, it was deduced that the negative effect on the electronic conductivity of CB particles and the induced piezoresistivity overwhelmed the positive effect brought by water content introduced ionic conductivity.

In the case of saturated cementitious composites, it was found from Figure 6.11-D that the CB particles or small CB agglomeration were entirely surrounded by water layers. In this circumstance, the ions conductivity had predominance on the electrical conductivity than the electrons conductivity and led to highest electrical resistivity. Since the CB particles totally inside the water layers, the applied load firstly caused the deformation of composites and then delivered to the deformation of water layers, and finally transmitted to the location alterations of CB particles. As plotted that the saturated composites and the composites with water content of 12% and 16% had lower gauge factor at the initial loading stage and relatively higher gauge factor in the later stage, just because the *FCR* changes were firstly induced by ion conductivity,

and then produced by the electrons conductivity. Even if the *FCR* changed by water layers increased, it greatly decreased the *FCR* changes by the contact of CB particles, and then reduced the whole sensitivity. Moreover, the intensity of ionic conductivity mainly depended on the ion concentration of pore solutions and water layers, which was hardly altered during the compression process and failed to improve the *FCR* changes and piezoresistivity.

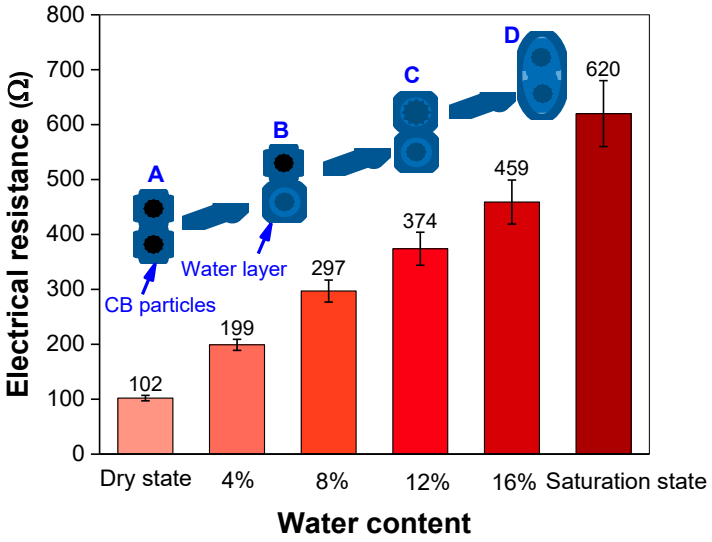

Figure 6.11. Resistance of CB cementitious composites to water content and the relative positions between CB particles on account of water layers.

6.3 Effect of freeze-thaw cycle

6.3.1 Resistivity development under different cycles

Figure 6.12 illustrates the resistance changes of dry CB cementitious composites in two patterns of heating and cooling cycles. The small diagram at top right is the heating and cooling process without water freezing, and the larger one involves the subzero temperatures called the freeze-thaw cycles. Both patterns included 10 cycles of heating and cooling process. It was found that only a small discrepancy were observed among electrical resistances in different cycles at the same temperature, and showed good repeatability even in the process of freeze-thaw cycles. For the dry specimens without free water, the resistance changes of CB/cementitious composites under various temperatures mainly come from the bound water.

It could be altered in viscosity and ionic activity of solutions with temperatures to change the electrical resistance of cementitious composites. However, the bound water can't be eliminated under the drying condition of 100 °C , hence it can be deduced that the resistance repeatability of dry CB/cementitious composites are immune from the freeze-thaw cycles, regardless of the heating and cooling processes with or without the freezing stage. This phenomenon is easy to understand for the lack of free water which fails to get frozen and expand its volume to damage the microstructures of cementitious composites (Duan, Jin & Qian 2011; Mu et al. 2002; Özgan & Serin 2013; Polat et al. 2010; Shang, Song & Qin 2008; Sun et al. 2002; Sun et al. 1999; Wang et al. 2019; Zhang, Wittmann, et al. 2017).

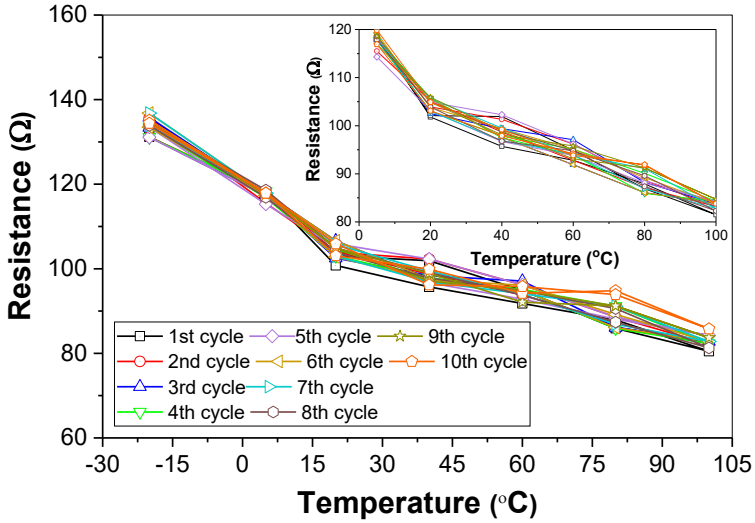

Figure 6.12. Electrical resistance development of dry CB cementitious composites with or without subzero temperature exposures.

Figure 6.13 shows the resistance development of CB cementitious composites under the same treatment of heating and cooling patterns in the saturation state. Compared to that of dry specimens, the electrical resistance of saturated cementitious composites were more sensitive to the temperature changes, because of a great amount of free water in the composites. The resistance drops with increase of temperature were partially due to the worse viscosity of solution resistance, while the main reason is because of the activated ions in the pore solution

to greatly reduce the electrical resistance. For the cycles without the subzero temperature, small divergence on the resistance was measured at the same temperature and showed good repeatability. In comparison to the similar results from the dry specimens, the deduction could be proposed that the temperature cycles above the zero had no impacts on the electrical resistance of CB cementitious composites, no matter how much water content they contained. In terms of the freeze-thaw cycles on the saturated specimens, an obvious larger resistance discrepancy was generated with the increase of freeze-thaw cycles, especially the resistance of composites at the temperature of -20 °C. This can be explained by the effect of water freezing and expansion on the micro conductive network in the CB/cementitious composites, which might be permanently destroyed and result in higher resistance with freeze-thaw cycles.

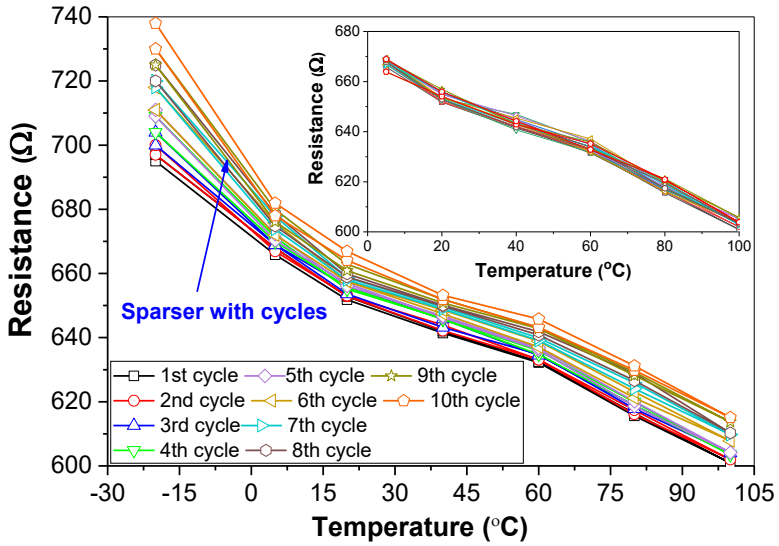

Figure 6.13. Electrical resistance development of saturated CB cementitious composites with or without subzero temperature exposures.

6.3.2 Piezoresistivity after freeze-thaw cycles

Figure 6.14 illustrates the changes of compressive strain and *FCR* before and after 10 cycles of freeze-thaw treatment for the dry CB cementitious composites under the same cyclic compression. The dotted lines are the results before the freeze-thaw cycles and the solid lines represent the same composites after the freeze-thaw cycles. It was observed that the composites

before the freeze-thaw cycles exhibited excellent repeatability and sensitivity with compressive strain, while for the composites after the freeze-thaw cycles, slightly higher *FCR* were observed in the second cycle and a bit lower *FCR* were occurred in the first and third cycle. The average of largest *FCR* was similar before and after freeze-thaw cycles, and the small discrepancy could be attributed to the minor differences in microstructures between composites. Hence, it could be considered that the freeze-thaw cycles made no differences on the electrical resistivity of the dry CB cementitious composite, which was consistent well with the repeatable resistance in Figure 6.14. On the other hand, as for the compressive strain of CB cementitious composites, higher deformation by compression was observed after the freeze-thaw cycles, with the ultimate strain increasing by approximately 11.9%. As a result, the sensitivity parameter of gauge factor was decreased owing to the maintained *FCR* values but the increased strain. Generally, the piezoresistive repeatability of the dry CB cementitious composites was well preserved with gentle fluctuation after the freeze-thaw cycles. As the piezoresistive sensitivity depended on the both electrical and mechanical properties, and freeze-thaw cycles might weaken the mechanical properties of composites by enlarging the compressive strain, the dry CB cementitious composites still expressed a reduced gauge factor by a rough approximation of 11.9% (equal to the increased strain) after the freeze-thaw cycles.

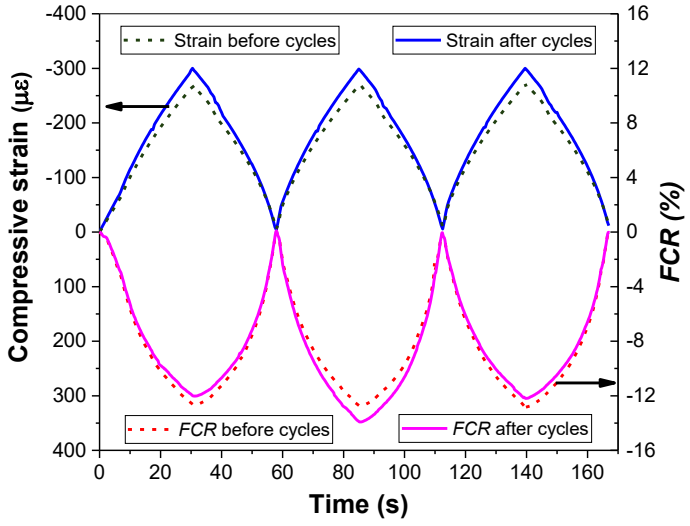

Figure 6.14. The *FCR* changes of dry CB cementitious composites with compressive strain before and after the freeze-thaw cycles.

In the aspect of saturated CB cementitious composites, their *FCR* and compressive strain changes before and after the freeze-thaw cycles were more complicated than that of dry CB/cementitious composites, since the volume expansion of pore solutions generated stress concentration and damaged the microstructures of composites. As mentioned before that the saturated CB/cementitious composites without freeze-thaw cycles could provide the relatively high *FCR* but with worse linearity and repeatability, just as the pink dotted line in Figure 6.15. However, after the treatment of freeze-thaw cycles, much more significant fluctuations on the resistivity output and the lower *FCR* could be observed for the saturated CB cementitious composites. The aforementioned reasons for the resistivity fluctuations were mainly due to the impacts by the connection of pore solutions, however, in this section, the extreme volatility was not only attributed to the interferences by pore solutions, but was determined by the microstructural damages of cement matrix, which might establish the conductive passages agian in cementitious composites and greatly affect the electrical resistivity. As for the reasons for the decreased peak values of *FCR*, the elastic part of the microstructures in cementitious composites which brought about the repeat resistivity in a cyclic compression was vulnerable and limited. The freeze-thaw cycles induced stress concentration inside the composites could permanently destroyed the microstructures and caused lower resistivity changes of the cementitious composites. Furthermore, the compressive strain of the saturated CB/cementitious composite was slightly larger than that of dry specimens which increased by 14.6%. In the case of the second compressive cycle that possessed relatively smooth *FCR* changes to evaluate the sensitivity reduction, the gauge factor for saturated CB/cementitious composite after the freeze-thaw cycles dropped by approximately 30.7%.

Both the dry and saturated CB cementitious composites showed weakened piezoresistive properties after the freeze-thaw cycles, because of the either increased compressive strain or the decreased *FCR*. The dry CB/cementitious composites possessed better resistance to the freeze-thaw cycles by smaller variations on the electrical resistivity, while the saturated CB/cementitious composites were sensitive to the freeze-thaw cycles due to the damages caused by volume shrinkage and expansion of pore solution. Overall, it demonstrated that the CB/cementitious sensors have limitations on the real applications in the environment with subzero temperatures, since the relatively weak mechanical properties and the poor frost resistance of CB particles.

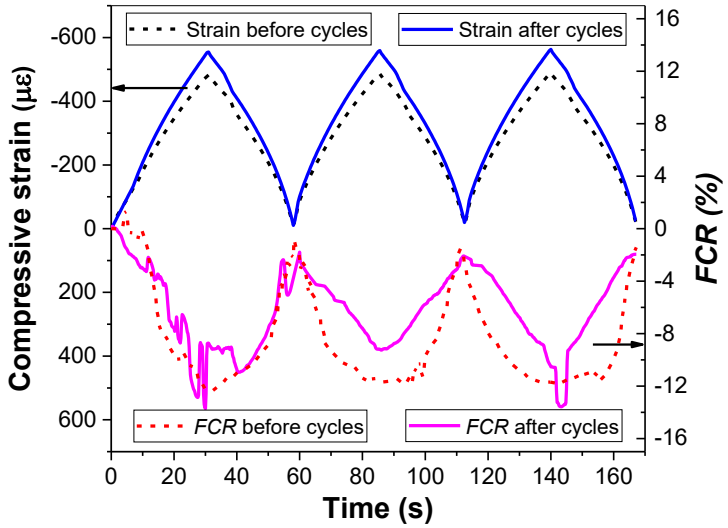

Figure 6.15. The *FCR* changes of saturated CB cementitious composites with compressive strain before and after the freeze-thaw cycles.

6.4 Effect of acid erosion

In this section, the cement-based sensors incorporating GNP are proposed and explored relative to their mechanical, microstructural and piezoresistive performances after exposure up to 3% sulphuric acid for up to 180 days duration to simulate an aggressive environment under accelerated conditions of sulphate attack. The effect of acid concentration and exposure duration on the compressive strength and piezoresistivity of cementitious composites are

reported. Disseminated findings of this study are expected to enhance the application of cement-based sensor technologies in environments of an aggressive nature (Chang et al. 2005; Hewayde et al. 2006; Li, Xiong & Yin 2009; Pacheco-Torgal & Jalali 2009).

6.4.1 Mass loss

Figure 6.16 shows the mass change of GNP filled cementitious composites after 90 and 180 days storage in 0%, 1%, 2% and 3% H_2SO_4 for a normalized axis. Mass change data reported with a positive sign indicates mass gain whereas mass change data reported with a negative sign indicates a mass loss. Both 90 and 180-day specimens stored in water are observed to show similar mass growth by 1.7% and 2.0%, respectively. This increase in mass is probably due to hydration and densification of the cement matrix resulting over time with the rate of mass gain decreasing with age (Dong, Li, Vessalas, et al. 2020; Fattuhi & Hughes 1988). In contrast, H_2SO_4 specimens were observed to increase the mass loss with an increased acid concentration and immersion time. Since the cement clinker chemistry and the hydration products can readily react with H_2SO_4 to form gypsum and ettringite related phases, these materials can easily exfoliate without cohesion to the substrate surfaces of the cementitious composites.

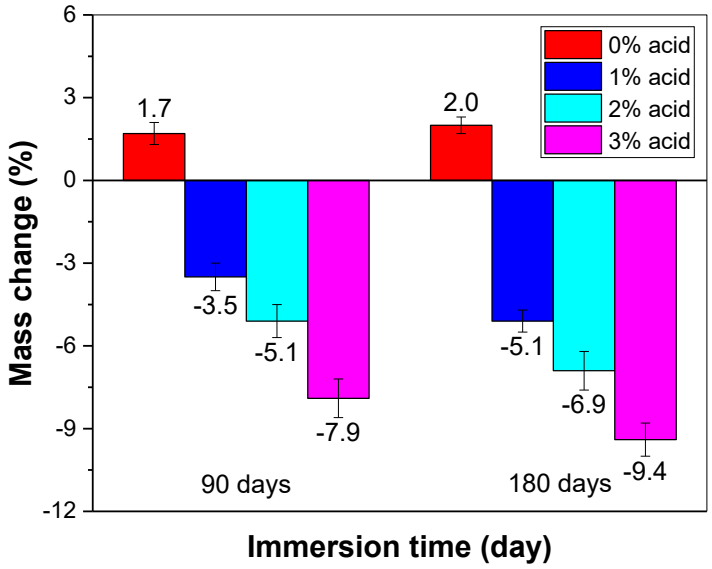

Figure 6.16. Mass change of GNP cementitious composites stored in 0%, 1%, 2% and 3% H_2SO_4 after 90 and 180 days.

6.4.2 Compressive strength

Figure 6.17 shows the maximum compressive strength of GNP filled cementitious composites after 90 and 180 days storage in H_2SO_4. The compressive strength of specimens immersed in water after 90 and 180 days were found to be similar, 49.5 MPa and 49.2 MPa, respectively. This similarity in strength implies that continuous hydration has contributed to no strength development of the cementitious composite between 90 to 180 days. This feature may be due to the replenishing of the solution after the first 90 days with clean water. As calcium hydroxide (CH) would have leached into the storage solution, replacing this solution would also mean a fresh supply of CH arising from continued hydration of these specimens. For the specimens stored in H_2SO_4, the compressive strength was observed to decrease with an increase in acid concentration and storage age. Specifically, the compressive strength reached 47.5 MPa, 40.3 MPa, and 35.8 MPa, respectively, for 1%, 2%, and 3% H_2SO_4 exposure after 90 days. The reduction in strength was found to be 4%, 19%, and 28%, respectively, as a function of increasing sulphuric acid concentration. Similarly, for specimens stored in the sulphuric acid solution for 180 days, the compressive strengths were 45.1 MPa, 33.6 MPa, and 29.6 MPa, respectively, for the 1%, 2%, and 3% concentrations. The reduction in strength was noted to be higher than the control specimen with 8%, 32%, and 40% decreases noted in strength. There are several reasons for the noted decrease in strength. The C-S-H can react with acid to form low-strength phases. In addition, the CH reacting with sulphate radical ions could also generate gypsum, which expands and damages the layered network of the C-S-H matrix. The gypsum can also further react with hydrated calcium aluminate to form ettringite, which possesses a similar expansion index to gypsum. As for the lower compressive strength observed after 180 days compared to after 90 days, the longer period of exposure to sulphuric acid solution has

also contributed to less compressive strength. Furthermore, given the sulphuric acid has been replenished after the first 90 days, the deposited products on the specimen surfaces have also been removed. This could in turn aggravates the severity of the acid attack by exposing fresh specimen surfaces to the acid solution for the next 90 days, which leads to further compressive strength loss after 180 days in total.

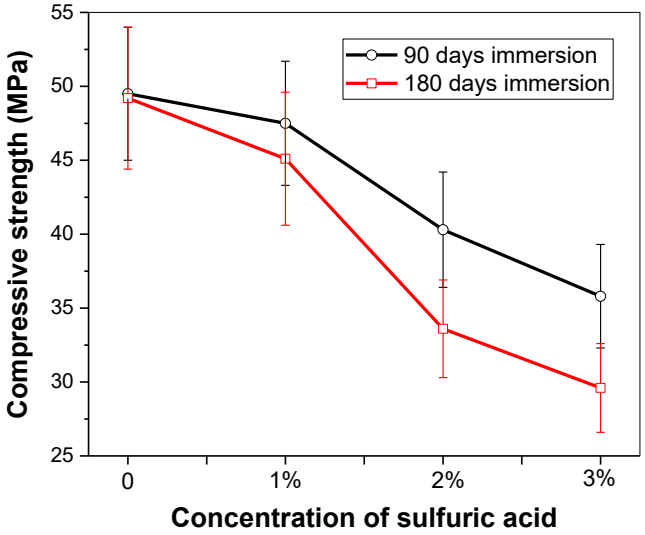

Figure 6.17. Compressive strength of GNP filled CBS stored in 0%, 1%, 2% and 3% H_2SO_4 after 90 and 180 days.

6.4.3 Microstructural analysis

Figure 6.18 depicts the microstructure of the GNP and the distinct features of different products formed in the cement matrix collected from cementitious composites after 180 days storage in 0%, 1%, 2% and 3% H_2SO_4. Figures 6.18(a) and 6.18(b) illustrate the presence of GNP in silicate sheet-like layers and the inclusion of needle-like material found in the deposited product. This need-like material is reminiscent of the formation of later age ettringite . The uniformly dispersed nature of the GNP particles in the cement matrix has contributed to enhanced piezoresistivity performance, as reported further in Section 3.5. The next SEM images were taken from specimens exposed to 0%, 1%, 2%, and 3% H_2SO_4. For the specimen exposed to water, Figure 6.18(c), a dense and impervious microstructure is observed. This

feature is most likely due to the hydration of cement, contributing to the formation of more interlayered C-S-H products . In terms of the specimen exposed to 1% H_2SO_4, Figure 5(d), a relatively dense microstructure is apparent; however, there also appears to be the formation of a sporadically generated pore structure. Further, in Figure 6.18(e), a higher volume of pores is apparent for the specimen exposed to 2% H_2SO_4. The highest volume of pores though is observed for the specimen exposed to 3% H_2SO_4.

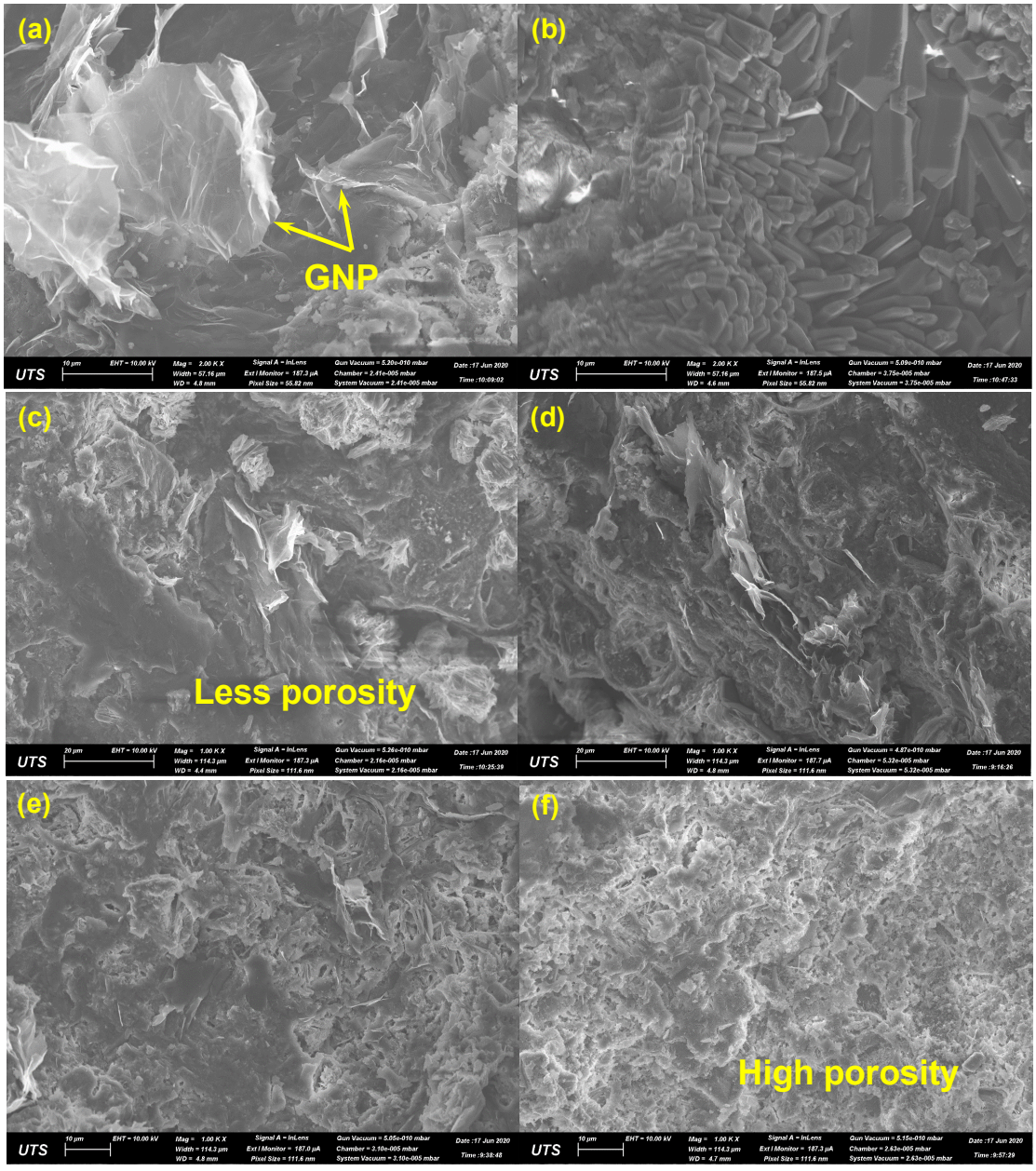

Figure 6.18. Microstructural morphology: (a) GNP in cement matrix; (b) Erosion products and GNP filled cementitious composite subjected to (c) 0%; (d) 1%; (e) 2% and (f) 3% H_2SO_4 solution.

Figure 6.19 illustrates the EDX data of the elements of Ca, Si, Al, Na and S for cementitious composite specimens stored in 0%, 1%, 2%, and 3% H_2SO_4 after 180 days. The amount of sulphur found in specimens was observed to increase as a function of increasing sulphuric acid concentration. This result is consistent with the microstructural features reported in Section 3.4. The presence of more sulphur incorporating the other elements also suggests the formation of more sulphate-bearing hydration products such as gypsum and ettringite. Further, the appearance of these later age hydration products can lead to expansion and cause distress in the cement matrix. This distress can also contribute to a higher pore volume and interconnectivity between these pores leading to higher permeability arising from the sulphuric acid attack.

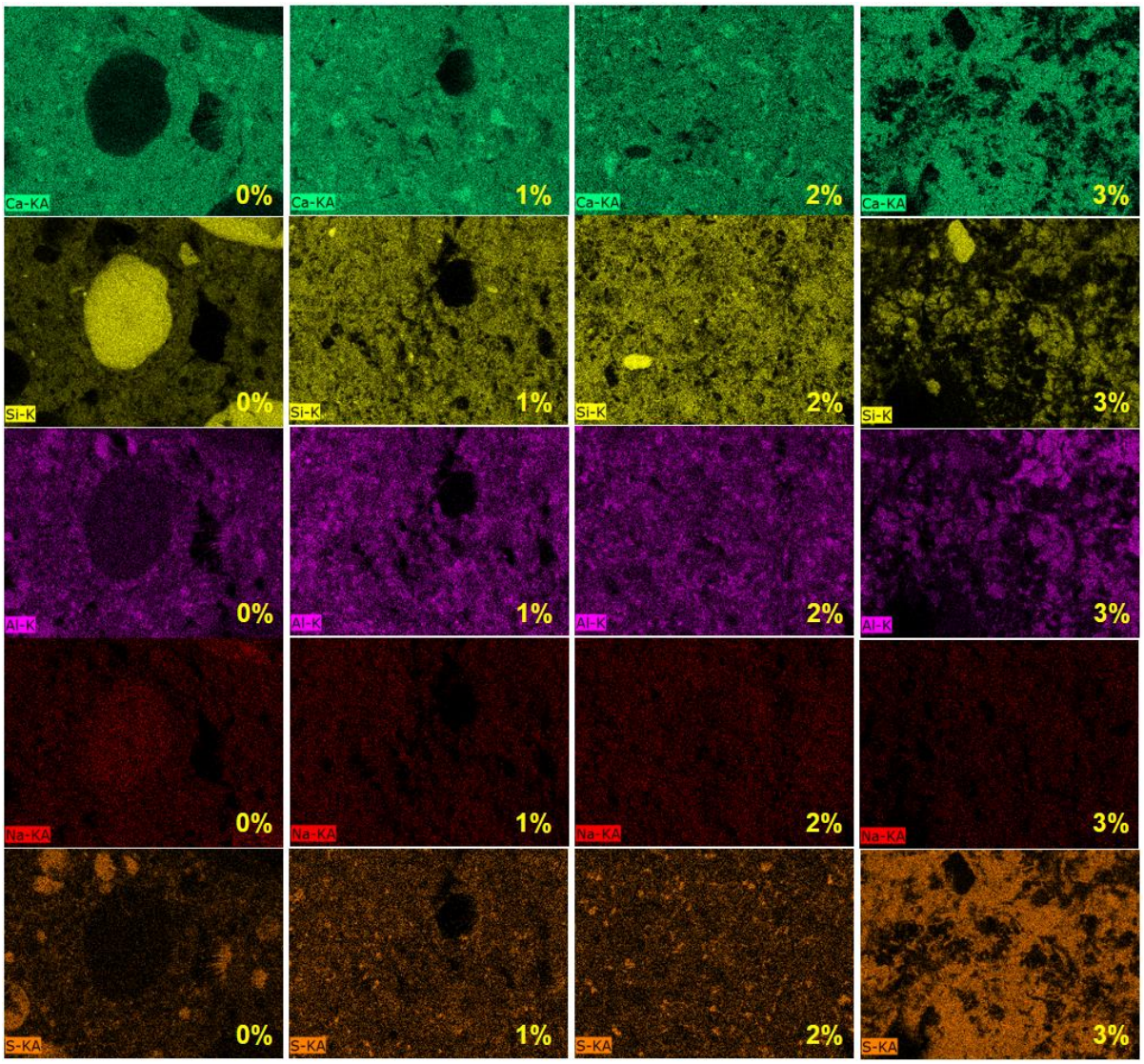

Figure 6.19. EDX analysis on elements of Ca, Si, Al, Na and S in the GNP filled cementitious composite subjected to 0%, 1%, 2% and 3% H_2SO_4 solutions after 180 days.

6.4.4 Piezoresistivity behaviours

6.4.4.1 Initial specimens without erosion

Two different loading patterns are carried out to assess the stress sensing performance of CBS with GNP. The constant amplitude-loading (CAL) pattern is conducted to assess the repeatability of the sensors, while the varied amplitude-loading (VAL) pattern is applied to estimate the combined effect of cyclic loading and stress amplitude on the piezoresistivity. Figures 6.20(a) and 6.20(b) show the FCR of initial specimens subjected to CAL and VAL

patterns. The FCR altered linearly to the cyclic compression, with the decreased FCR at the loading stage and the increased FCR at the unloading stage. For the specimens under CAL pattern, the average FCR at the stress magnitude of 2 MPa reached 11.8%. The irreversible FCR values after the first cyclic load could be observed, which was mainly attributed to the brittleness of cementitious composites and the permanent deformations of weak microstructures and pores. Afterward, the irreversibility of FCR was strongly weakened under identical loading patterns. It indicates that the GNP filled cement-based sensors are capable of replacing traditional sensors to monitor the forces on structures, as long as the irreversible performance of piezoresistivity can be eliminated by applying preloading. Moreover, the FCR values at the zero stress slightly increased with the cyclic load because of the gentle polarization during the test. It demonstrated that some conductive solutions with movable ions were still preserved in the closed pores after 3 days of drying. This implied that the cement-based sensors should be dried entirely before practical application. Otherwise, the AC rather than the DC should be applied to capture the electrical signal alterations during the piezoresistivity test. Similar FCR to compressive stress changes could be found for the initial specimens subjected to VAL pattern. The largest FCR values at the stress peaks of 4 MPa and 2 MPa reached 22.8% and 11.9%, respectively. The linearity of specimens was very similar, with the FCR values achieved 11.8% and 11.9%, respectively under CAL and VAL patterns. However, compared to the specimens under the CAL pattern, the larger applied stress amplitude led to higher irreversible FCR values. The stable irreversibility of FCR occurred after several cycles of loadings, implying that CBS with GNP monitoring high stress should be previously loaded with large cyclic loadings to achieve both the stable linearity and reversibility.

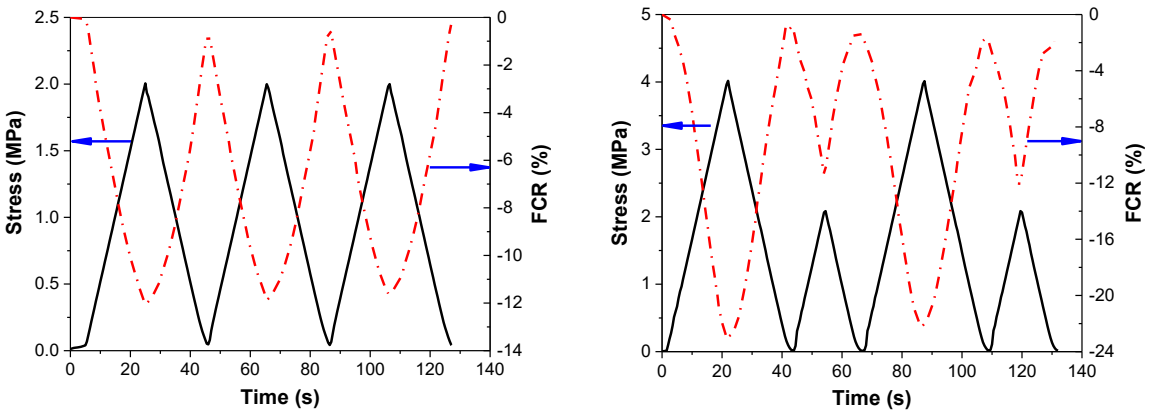

(a) CAL pattern (b) VAL pattern

Figure 6.20. Piezoresistivity of GNP-filled cement-based sensor without sulphuric acid immersion.

Figure 6.21 displays the relationship between FCR and the compressive stress for the initial specimens under CAL and VAL patters. The linear fitting curves were also plotted, based on the correlation of FCR values to compressive stress. The slope of fitting curves indicates the FCR changes under unit compressive stress, which also means stress sensing efficiency. It was found that the two fitting curves were almost parallel to each other, with the slopes of -6.08 and -5.98. The small discrepancy of the slopes is mainly due to the unstable or weak cementitious structures that possess different bearing capacities under multiple loading amplitudes. It leads to changes in the microstructures and conductive passages, and slightly affects the piezoresistivity. Anyway, it showed that the stress sensing efficiency of GNP filled cement-based sensors was nearly a constant under the CAL and VAL patterns. Further, the deviations of these fitting curves R_C^2 and R_V^2 show the larger value of 0.973 for the CAL pattern and lower value of 0.966 for the VAL pattern, demonstrating the relatively poor linearity for the specimens subjected to VAL pattern. The VAL pattern consists of higher stress amplitudes, higher loading rates, and more complicated stress conditions than those of CAL pattern. The poorer linearity of specimens under the VAL pattern indicated that the linearity of piezoresistivity might worsen with the complexity of external loading forces. Although the

linearity of specimens after the VAL pattern was still acceptable, much more in-depth analysis of the minor changes of piezoresistivity under complicated loadings should be further explored.

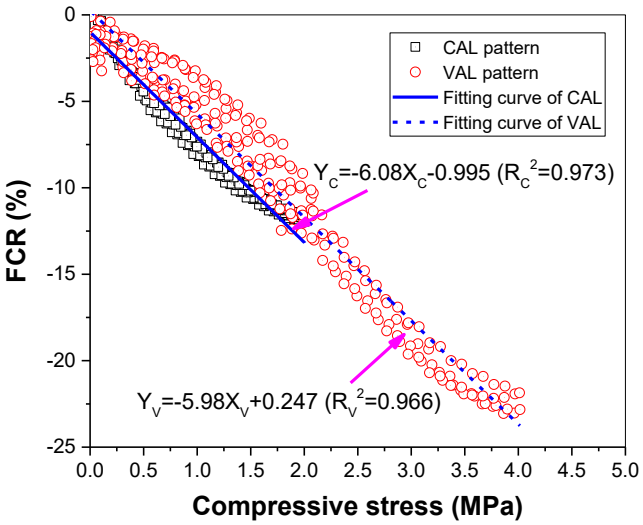

Figure 6.21. FCR as a function to compressive stress for the initial CBS under CAL and VAL patterns.

6.4.4.2 Specimens after erosion

Figure 6.22 illustrates the piezoresistive performance of cementitious composites after 90 days of storage in sulphuric acid solutions, subjected to CAL patterns for the piezoresistivity test. The FCR values showed satisfactory linearity to the compressive stress for the specimens in 0% H_2SO_4. In comparison to the initial counterpart without treatment, the water stored specimens showed smaller FCR values of 9.4% at the stress peak of 2 MPa. As mentioned previously, the further hydration of specimens could occur during long-term water immersion. The slightly lower FCR values might be due to the denser structures of specimens after water storage. For the specimens in 1% H_2SO_4 solutions, the piezoresistive stability seemed to be slightly affected, with the small fluctuation on FCR values. This is because the erosion of the cement matrix led to some weak areas and increased the inhomogeneity of cement-based sensors. Moreover, it could be found that the largest FCR increased to approximately 13.5%. The erosion of cementitious composites by H_2SO_4 is similar to a specimen softening process, making the

conductive filler of GNP easier to connect with each other to create a larger electrical resistivity change under the same specific force. Even so, the linearity of FCR to compressive stress could still be observed for the specimens in 1% H_2SO_4. In terms of the specimens immersed in 2% and 3% H_2SO_4, the linearity among FCR and compressive stress was wholly destroyed, as plotted in Figures 6.22(c) and 6.22(d). Take the specimens in 2% H_2SO_4 for example, the FCR at the stress peak of 2 MPa finally attained to 20.5%, while the values at the first 1 MPa nearly reached 19.7%, indicating that the later applied forces almost made no differences on the electrical resistivity of the cement-based sensors. Further, it was found that the FCR values could mostly recover to the initial values, implying the moderate repeatability of the cement-based sensors after erosion treatment. With this, the conclusion can be proposed that the piezoresistive linearity possess no relationship to the repeatability. The excellent repeatability of cement-based sensors cannot ensure acceptable piezoresistivity, linearity, and serviceability. In addition to the worse linearity, Figure 6.22(d) shows the gradually decreased FCR values with cyclic compressive stress. It demonstrated that the corroded specimens under external compression were subjected to permanent damages on the microstructures. For instance, CBS might be forced to close their pores and cracks to decrease the electrical resistivity. Also, the conductive GNP could get closer and connected in this process.

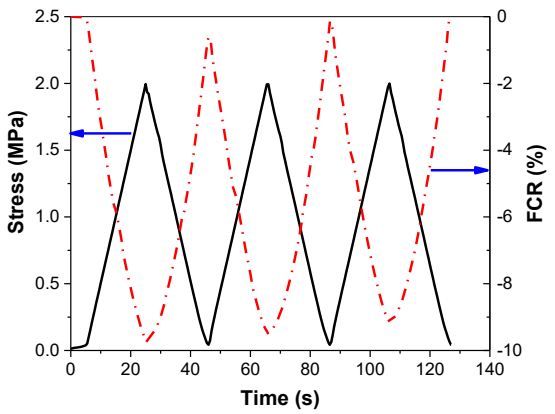

(a) 0% H_2SO_4 solution

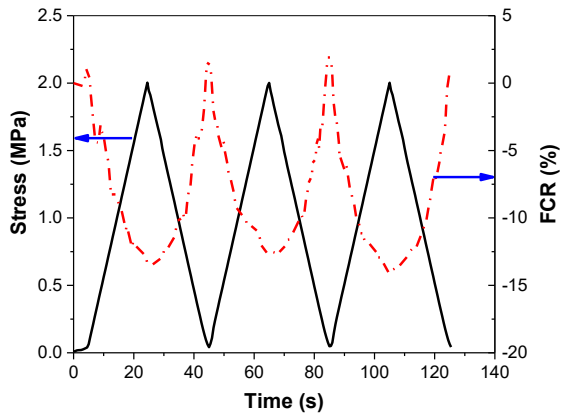

(b) 1% H_2SO_4 solution

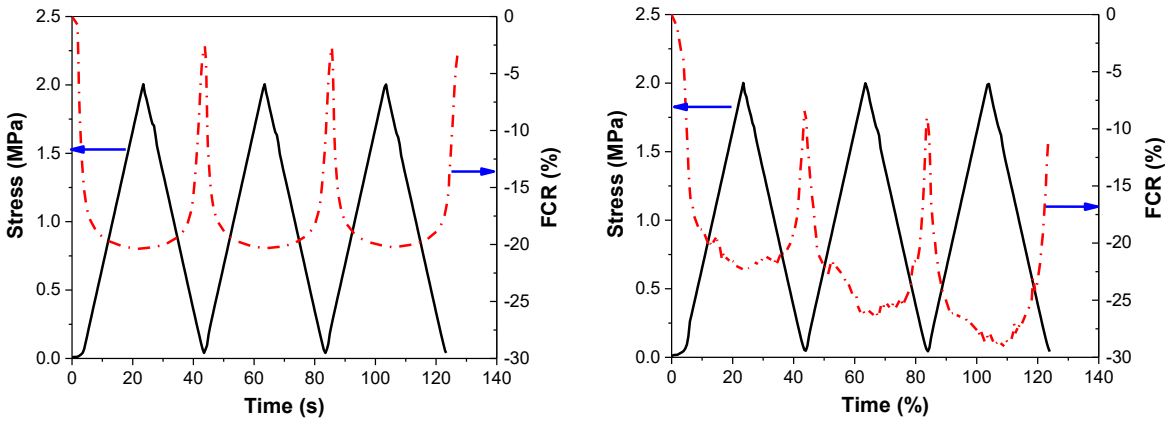

(c) 2% H_2SO_4 solution (d) 3% H_2SO_4 solution

Figure 6.22. Piezoresistivity of GNP filled CBS after 90 days sulphuric acid storage subjected to CAL pattern.

The piezoresistivity of cementitious composites after 180 days of storage in sulphuric acid solutions subjected to VAL patterns is shown in Figure 6.23. Being different from the specimens after 90 days of water storage, both the linearity and largest FCR values were altered after 180 days of immersion in 0% H_2SO_4. It indicates that long-term storage of cement-based sensors in water can greatly affect the piezoresistivity. It seems that the water can also change the micro conductive passages in the cement-based sensors through slow but continuous hydration of cement. The denser microstructures caused the FCR values to strongly decrease even subjected to the larger compressive stress of 4 MPa. It implied that the future practical application of cement-based sensors should ensure their excellent hydrophobicity and water repellency, to get rid of the effects of humidity or water vapour from working environments. For the specimen exposure to 1% and 2% H_2SO_4, worse piezoresistive repeatability and linearity were observed compared to the specimens after 90 days of storage. This is because the severer damaged microstructures and GNP formed conductive networks, leading to the more suddenly changed FCR values. The phenomenon is significant for the specimens exposed to 3% H_2SO_4 for 180 days. The FCR arrived at nearly 67.0% when the stress reached 1 MPa, which then slowly increased to 75.5% at the stress magnitude of 4 MPa. Previous studies have

mentioned that the formation of sulphate compounds, e.g., gypsum and ettringite possess less resistance to external forces than the cement matrix. At the beginning of loading, the soft compositions are firstly compressed to alter the electrical resistivity; this leads to the swift changes on the FCR values. Afterward, the rigid cement matrix starts to hold the increased external forces to decrease the alteration of FCR values. In summary, the experimental results implied that CBS with GNP were damaged both on the piezoresistive sensitivity and repeatability when they were subjected to a highly corrosive environment.

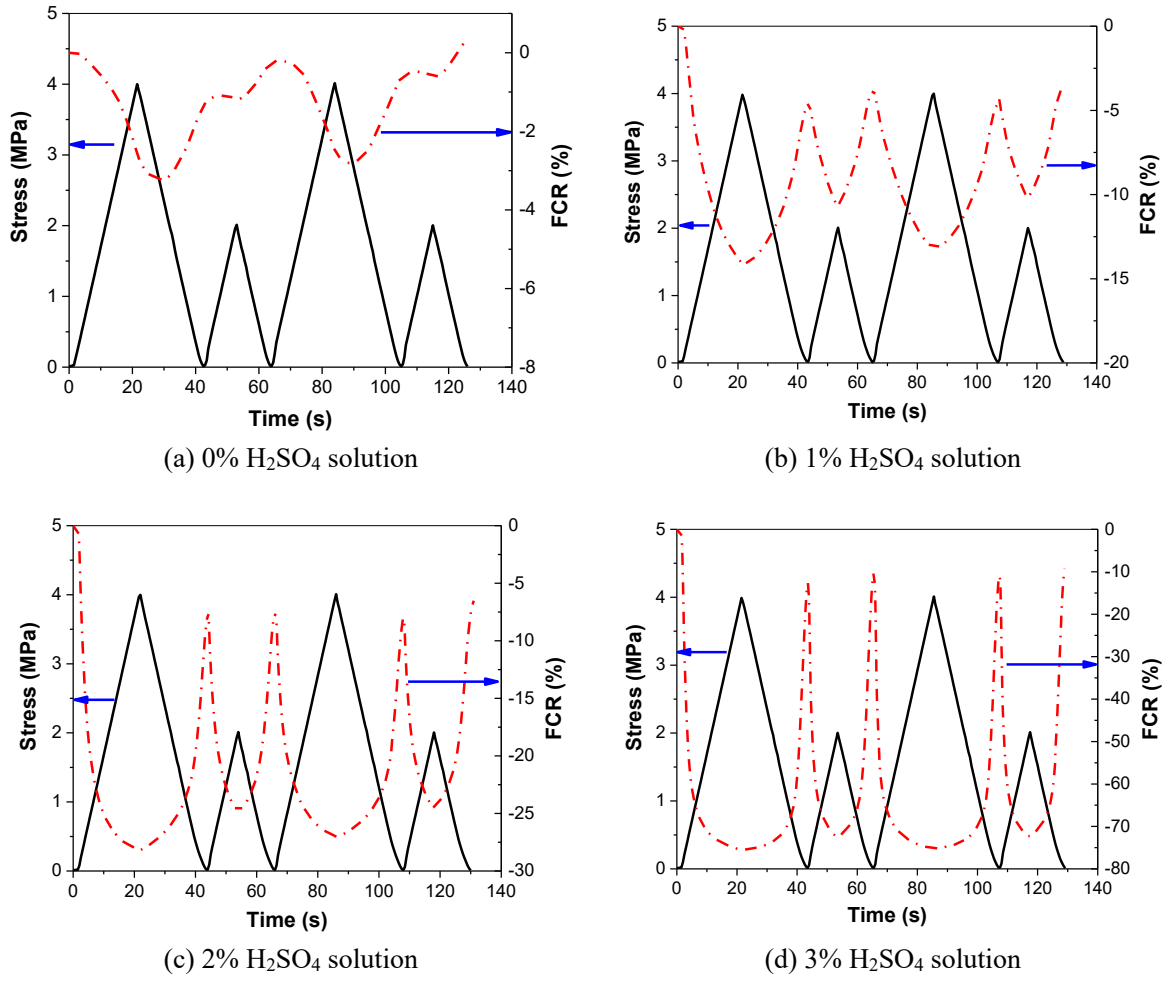

(a) 0% H_2SO_4 solution (b) 1% H_2SO_4 solution

(c) 2% H_2SO_4 solution (d) 3% H_2SO_4 solution

Figure 6.23. Piezoresistivity of GNP filled CBS after 180 days sulphuric acid immersion subjected to VAL pattern.

6.4.4.3 Mechanism discussion

Figure 6.24 schematically plots the solid phases, pores and conductive passages alterations in GNP filled CBS in the process of loading, to illustrate the piezoresistive performances of specimens after different degrees of sulphuric acid attack. Based on the SEM images and the compressive strength, the initial GNP filled CBS have limited porosity and a well-preserved cement matrix. However, for the specimens exposed to H_2SO_4, increased porosity, and deteriorated cement matrix appear. The high concentration of H_2SO_4 leads to a highly degraded cement matrix and generates more pores filled with erosion products. The erosion products of gypsum and silica gel possess weak resistance to force and deformations, which attributes to their easier compressed porosity than the specimens without erosion. In terms of establishing conductive passages, the GNP randomly distributing in the specimens decreases the electrical resistivity of composites by their direct contact or tunnel effect. The compressed porosity is beneficial to the connection between GNP and stimulates the formation of the conductive passage. That can explain the increased FCR values of specimens after erosion. As for the sudden FCR changes of highly corroded specimens at the beginning of loading of a small force, this can be interpreted by the different bearing capacities of porosity containing erosion products and the well-preserved cement matrix. The porosity is induced by the sulphuric acid erosion of the cement matrix, and it can be easier compressed than the uncorroded cement matrix. Therefore, mainly because of the compressed porosity, the new conductive passages by GNP can be generated at a small force at the beginning of loading and significantly alter the electrical resistivity of the composite. Once most pores are compressed to become dense and stable structure, it will be harder to change the conductive passages from the deformation of pore structures. At this stage, even the force increases to larger values; the specimen with depressed porosity only displays small FCR changes because the well-preserved cement matrix has higher force resistance, which is more challenging to vary the conductive passages and

electrical resistivity. That is why the composite rapidly changes the FCR values at the beginning of loading, and then slowly alters the FCR values under high-stress magnitude.

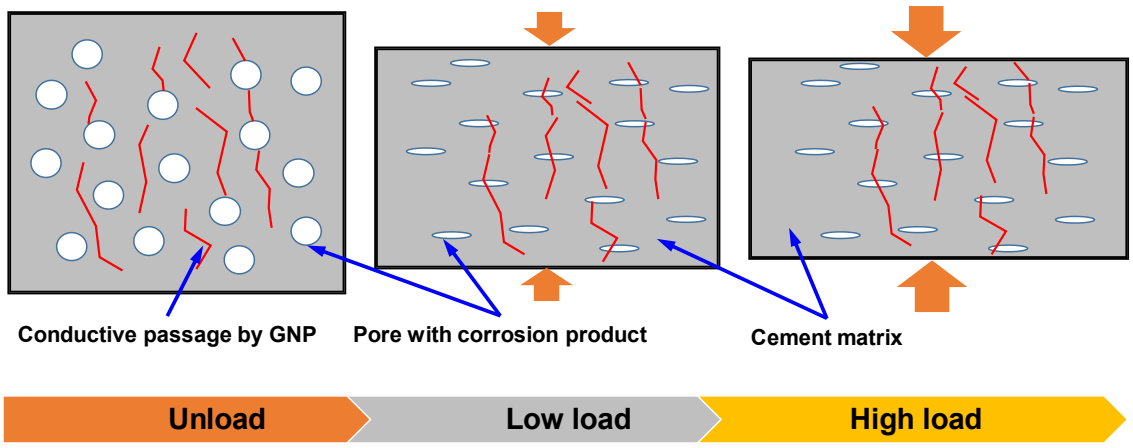

Figure 6.24. Schematic diagram of conductive passage alteration of highly porous GNP filled cementitious composite under loading.

6.5 Effect of drop impact

In this section, the cyclic compression and four series of fixed magnitude impact loads with an increment of 50 times were conducted alternatively on the 0.1% carbon nanotubes (CNTs) reinforced cementitious composites, to evaluate the piezoresistive sensitivity and repeatability of composites after the drop impact energy of 6.24×10^{-4}, 12.48×10^{-4} and 18.72×10^{-4} J/cm^3 (Barr & Baghli 1988; Feng et al. 2018; Iqbal, Kumar & Mittal 2019; Kumar, Iqbal & Mittal 2018; Rao, Bhattacharyya & Barai 2011).

6.5.1 Piezoresistivity behaviours

Figure 6.25 shows the relationship between the compressive stress and fractional changes of the resistivity during alternating cyclic compression and the impact load of 6.24×10^{-4} J/cm^3 for the 0.1% CNTs reinforced cementitious composites. For the composites before impact, the fractional changes of resistivity illustrated unstable alterations by the gradually decreased summits with the compressive cycles of the same stress amplitude. The reason for the relatively higher resistivity changes in the first cycle is possibly due to the brittleness of the cementitious

composites. There is irreversible plastic deformation when the composite is compressed in the beginning of compression test. Therefore, the average fractional changes of the resistivity reached approximately 2.4% and 3.8%, respectively for the stress amplitudes of 4 MPa and 8 MPa. After the first 50 times of impact, there was a resistivity growth of approximately 0.24% for the CNTs reinforced cementitious composites (The distance between two blue dotted curves), which was caused by the permanently created micro-cracks or voids. It was found that the fractional changes of the resistivity after the first impact treatment expressed little discrepancy to the counterpart without treatment, which showed similar resistivity changes. In terms of the composites subjected to further 50 times of impact (100 times of impact in total), the resistivity increases rose to 0.46%. It means an incremental increase in damage than the previous composites after 50 times of impact. The results indicate that the weak microstructures which were easier deformed under forces still hold a certain proportion after the first regime of impact, and got further damaged in the second regime of impact. However, in comparison to the composites without impact or under 50 times of impact, more equal and stable outputs of the resistivity changes in each cycles were observed, which may be attributed to the reduced unstable and weak microstructures in the cementitious composites . Furthermore, the fractional changes of the resistivity of the CNTs reinforced cementitious composites after 150 and 200 times of impact showed similar changes to compressive stress, and illustrated excellent stability and repeatability as well. It is worth noting that the increase rate of the resistivity growth gradually narrowed with the increased times of impact, with the irreversible resistivity reaching 0.31% and 0.23% for the composites under 150 and 200 times of impact, respectively. It was considered that the reduced weaker microstructures in the composites under impact load can be attributed to the decreased resistivity jumps. As compared to all the results without impact or under different times of impact load of 6.24×10^{-4} J/cm^3, it seems that the impact load induced irreversible damages in the microstructures could bring a gentle reduction in the fractional

changes of the resistivity, because of the decreased values of nearly 2.2% and 3.6% for the last two cyclic compressions.

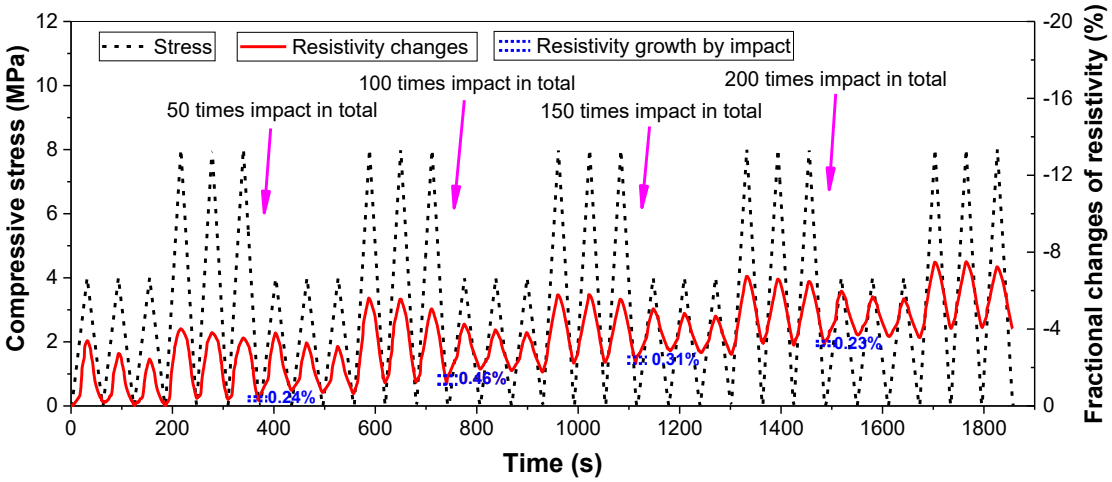

Figure 6.25. Fractional changes of resistivity of 0.1% CNT/cementitious composites under cyclic compression after different times of impact with energy of 6.24×10^{-4} J/cm^3.

Figure 6.26 presents the resistivity output for the CNT/cementitious composites under the cyclic compression without impact and after 50, 100, 150 and 200 times of impact at the impact energy of 12.48×10^{-4} J/cm^3. Similarly, the composites without impact exhibited slightly higher fractional changes of resistivity in the front cycles for each stress amplitude, with the average values of 1.6% and 3.3%, at 4 MPa and 8 MPa, respectively. After 50 times of impact, the resistivity growth was higher than the counterparts under smaller impact energy and reached 0.29%. In addition, irreversible resistivity emerged after the cyclic compression for the impact treated composites. In comparison to the results of composites subjected to lower impact energy, where very low irreversible resistivity occurred after impact load, the higher irreversibility of composites under cyclic compression indicated that new weak microstructures formed in the process of impact, even though the weak microstructures were damaged at the same time. Studies have proposed the solution of electrical resistivity detection to monitor the impact damage on conductive cementitious composites. Similarly, by analysing the irreversible resistivity, it can be deduced that the impact energy of 12.48×10^{-4} J/cm^3 could cause micro-

cracks or gaps inside the composites after at least 50 times of impact. As for the composites after 100, 150 and 200 times of impact, their electrical resistivity suddenly increased by 0.58%, 0.31% and 0.21%, respectively. The reason for the gradually "improved impact resistance" is similar to the above situation at the impact energy of 6.24×10^{-4} J/cm^3. Although new weak microstructures such as micro-cracks and voids were created after impact, the following cyclic compression could decrease their numbers as revealed by the irreversible resistivity. In other words, not only the impact reduced the weak microstructures, the cyclic compression also caused denser microstructures to improve the resistance to later impact. In terms of piezoresistive sensitivity, the resistivity changes slightly increased with slow down increasing rate as the increase of impact, and arrived at the values of 2.4% and 4.4% under the final compression. The improved sensitivity of CNTs filled cementitious composites by the impact energy of 12.48×10^{-4} J/cm^3 were irreconcilable with the reduced sensitivity for the composites by the impact energy of 6.24×10^{-4} J/cm^3, which demonstrated the electrical anisotropy of cementitious composites . Nevertheless, more stable and equal resistivity in each cycle was achieved to improve the accuracy of the deformation or damage monitoring.

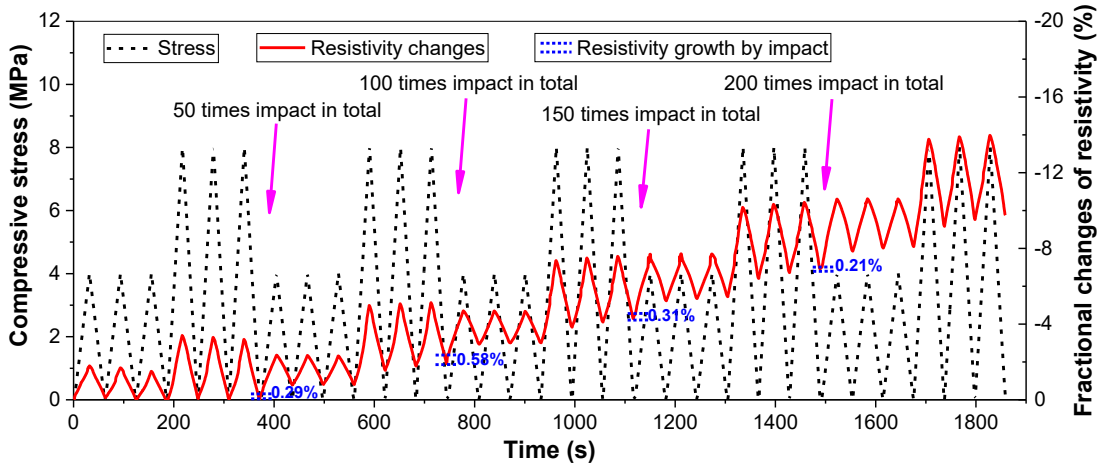

Figure 6.26. Fractional changes of resistivity of 0.1% CNT/cementitious composites under cyclic compression after different times of impact with energy of 12.48×10^{-4} J/cm^3.

The fractional changes of resistivity of CNTs reinforced cementitious composites under alternating compression and impact loads of 18.72×10^{-4} J/cm^3 are illustrated in Figure 6.27. Different from the previous curves, composites after being impacted for hundreds of times showed rapid resistivity reduction in the beginning and end of cyclic compression, which can be illustrated by the distance between these two green dashed curves. For the composites after 50 times of impact, the resistivity growth reached 0.45%, while the rapid resistivity reduction for the followed compression reached 0.56%. It could be assumed that the rapid reduction of the resistivity was partially sourced from the resistivity growth caused by impact treatment. The impact energy of 18.72×10^{-4} J/cm^3 on the CNTs reinforced cementitious composites did cause irreversible microstructural damages and led to the permanent resistivity growth, while the created micro-cracks or voids could be easily recovered under small external forces and result in the sudden resistivity reduction under cyclic compression. After 100 times of impact treatment, much clearer resistivity growth and reduction could be observed, with the variation rate of 1.16% and 1.06%, respectively. Also, for the curves under identical stress amplitude, it was found that the fractional changes of the resistivity at different cycles illustrated smaller discrepancy than the composites without impact or with 50 times of impact, which was consistent to the above conclusions of more stable resistivity output after impact treatment. In terms of the composites after 150 and 200 times of impact, very similar curves of fractional changes of the resistivity were obtained, with the resistivity growths being approximately 1.82% for the former and 1.65% for the latter, respectively.

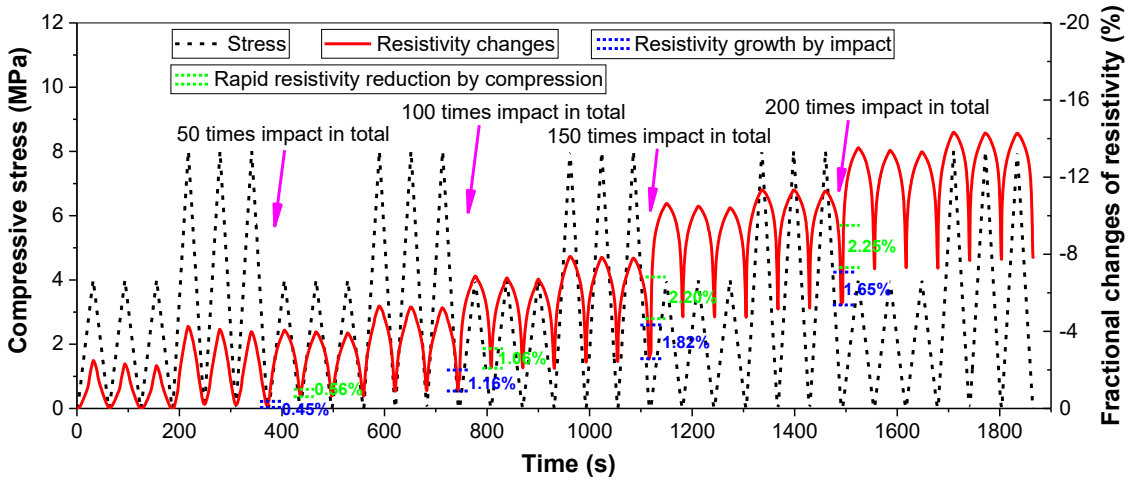

Figure 6.27. Fractional changes of resistivity of 0.1% CNT/cementitious composites under cyclic compression after different times of impact with energy of 18.72×10^{-4} J/cm^3.

It could be observed that the piezoresistive performances of the initial 0.1% CNT reinforced cementitious composites without impact were slightly different among three impact regimes. This is because the different individuals were applied here to eliminate the effect of loading history. It is easy to understand that the larger irreversible resistivity growth is due to the higher impact energy. In addition, it was predicted that the resistivity growth would gradually decrease with more impacts just like the situation under lower impact energy. However, the largest resistivity growth happened after 150 times of impact at the impact energy of 18.72×10^{-4} J/cm^3 rather than the aforementioned 100 times of impact at the impact energy of 6.24×10^{-4} J/cm^3, indicating that more numbers of impact should be applied for the "improved impact resistance" under the conditions of higher impact energy. As for the rapid resistivity reduction by compression, their values increased up to 2.20% and 2.25%, respectively for the composites after 150 and 200 times of impact, which almost accounted for one half of the total fractional changes of resistivity. In that case, the nonlinear part of the fractional changes of the resistivity to stress will cause false evaluation on the monitored stress and deformations, if the effects of impact forces are underestimated or ignored.

6.5.2 Mechanism discussion

To simply describe the resistivity growth by impact and rapid resistivity reduction in the beginning of compression, Figure 6.28 illustrates the development of micro-cracks inside the CNT/cementitious composites with the increase of impact numbers, although the fibres could prohibit the cracks growth and propagation. It can be seen that the impact treatment could enlarge the initial cracks and create new micro-cracks, which led to the sudden resistivity growth. On the other hand, during the impact treatment, some already connected CNTs might get detached, especially for the CNTs playing the bridging effect. The reconnection between these CNTs due to the closed cracks in the compression partially contributed to the rapid resistivity reduction. In addition, even for the cracks without CNTs, the easier compressed cracks could also result in the decrease of electrical resistivity.

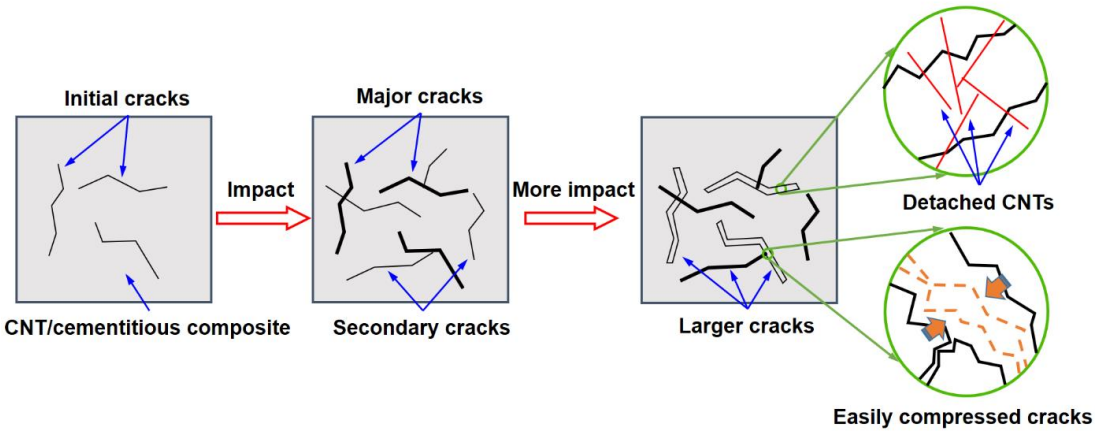

Figure 6.28. Schematic diagram of micro-cracks initiation and propagation in CNT/cementitious composites after impact treatment.

6.6 Summary

This section explored the effects of temperature, humidity, freeze-thaw cycles, acid erosion and drop impact on the performance of cement-based sensors. The key conclusions are listed as follows:

(1) The FCR of CB/cement-based sensors greatly varied if there were extreme temperature differences between the sensors and working environments, due to the severe thermal exchanges. Therefore, the real application of CB/cementitious composites should be accompanied by a temperature compensation circuit or other special treatments for thermal insulation. After removing the heat exchanges interference, the piezoresistive properties of CB/cementitious composites were independent from the temperature variations ranging from -20 ℃ to 100 ℃, and showed both satisfactory sensitivity and repeatability of piezoresistivity.

(2) With the increase of water content, in addition to the increased electrical resistivity, the piezoresistive sensitivity of CB/cementitious composites firstly increased but then decreased, and the optimal water content was found out around 8%. Moreover, the high water content in the cementitious composites could make the resistivity behaviours fluctuate widely.

(3) The freeze-thaw cycles exhibited limited impacts on the electrical resistivity of dry CB/cementitious composites, but the induced higher compression strain still caused reduced gauge factor and slightly lower piezoresistive sensitivity with reduction of 11.9%. However, both the electrical and mechanical properties of saturated CB/cementitious composites were greatly affected by the freeze-thaw cycles, which resulted in the decreased piezoresistive sensitivity by 30.7%.

(4) The intact GNP/cementitious composite before erosion exhibited excellent piezoresistivity for SHM as cement-based sensors. However, after 90 and 180 days of sulphuric acid erosion, the piezoresistivity was strongly affected with less linearity and repeatability. In particular, after subjected to 3% H 2 SO 4 solutions, the FCR changes under low and high loads presented extremely high and low, respectively.

(5) The mechanism of altered piezoresistivity is due to the mechanical and microstructural properties of corroded GNP/cementitious composite. The erosion-induced porous structure filled with erosion products was easily compressed during the beginning of load, which led to

the connection of GNPs and decreased the electrical resistivity. With the increase of load, the compressed porosity maintained unchanged and the intact cement matrix took responsibility for the further deformation, and then the FCR changes decreased with the increase of load.

(6) Impact load caused sudden resistivity growth for CNTs/cementitious composites, the higher impact energy applied, the larger resistivity increase composites were. The impact resistance was improved with the increase of impact times accompanied by the progressively reduced resistivity growth after the same times of impact.

(7) Wider and longer cracks were produced based on microstructural characterization. Along with the major cracks in CNTs/cementitious composites, secondary cracks were produced with more times of impact treatment. It concluded that wider cracks were more likely to be compressed, which led to the sudden resistivity reduction.

CHAPTER 7: SELF-SENSING CEMENTITIOUS MATERIALS WITH MULTIFUNCTIONALITY

In this chapter, the multifunctional cementitious materials were proposed with combined self-sensing and self-healing properties, self-sensing and hydrophobic properties, and the integrated self-sensing, superhydrophobic and self-cleaning properties.

7.1 Combined self-sensing and self-healing properties

7.1.1 Experimental program

Smart cementitious composite with integrated self-healing and self-sensing properties is developed using microencapsulation of nano-carbon black (NCB) to enclose slaked lime (SL). The binder used is commercially available General purpose cement, and 10 wt.% of which is replaced by silica fume to improve the microstructure of cement paste. For the control group without SL, the water, water reducer and NCB to binder ratios are 0.45, 0.8% and 1.0%, respectively. For the experimental group, the content of SL is 2.0%. For the composite with SL, the SL was dry pre-mixed with half NCB first until the white coloured SL powder turned to grey NCB/SL mixture. Then the NCB/SL mixture was poured into the binder, and mixed with the well-dispersed solutions containing another half of NCB for 3 min to achieve the uniform composites. Subsequently, the moulds at the size of 50 mm ×50 mm ×50 mm were cast and cured in the curing chamber. The specimens were demolded after 1 day of curing, and were cured for another three months to decrease the autogenous healing.

The characterization of crack closure was applied to evaluate the autonomous healing properties of cementitious composites with/without NCB/SL mixture. To induce cracks, the composites were preloaded to 60% of their maximum strength, with a steel bar between the specimen and the compression platens. Then the surface with cracks was placed into the sonication bath for 3 min to eliminate the attached NCB and expose the SL particles.

Afterwards, the composites were placed into the standard curing chamber with a temperature of 23 °C and relative humidity of 90% for the autonomous healing. Water spray was carried out twice a day during the self-healing process (Hu et al. 2018; Luo et al. 2018; Souradeep & Kua 2016; Van Tittelboom et al. 2016; Wang et al. 2014; Xu & Yao 2014). In terms of the self-sensing ability, fractional changes of resistivity (FCR) of composites under cyclic compression were evaluated.

7.1.2 Autonomous crack healing

Figure 7.1 illustrates the crack healing features of the NCB filled cementitious composites with/without SL at different curing ages. For the composite without SL, there still existed the self-healing characteristics after 7 and 14 days of curing, as shown in region 1 of Figure 7.1(a). This feature is likely due to combined effect of further hydration of unhydrated cement particles (CP) and the carbonation of calcium hydroxide. However, the efficiency of autogenous healing was observed to decrease with increasing age and crack width. That is why only the cracks with the average width of 0.121 mm were partially healed, while the other cracks with a width of 0.198 mm almost maintained constant width. For the composites with NCB enclosed SL, dramatic autonomous crack healing could be found with the curing ages, as illustrated in Figure 7.1(b). Regions 1-3 could clearly show the gradually healed cracks in various widths with the increase of curing days. The comparable results indicated the potential application of SL enclosed with NCB for self-healing cementitious composites.

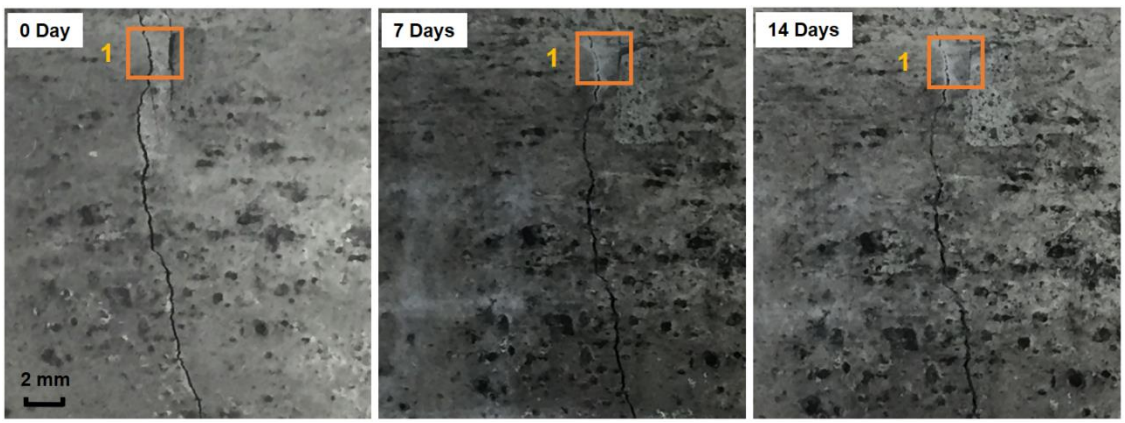

(a) Composite without SL

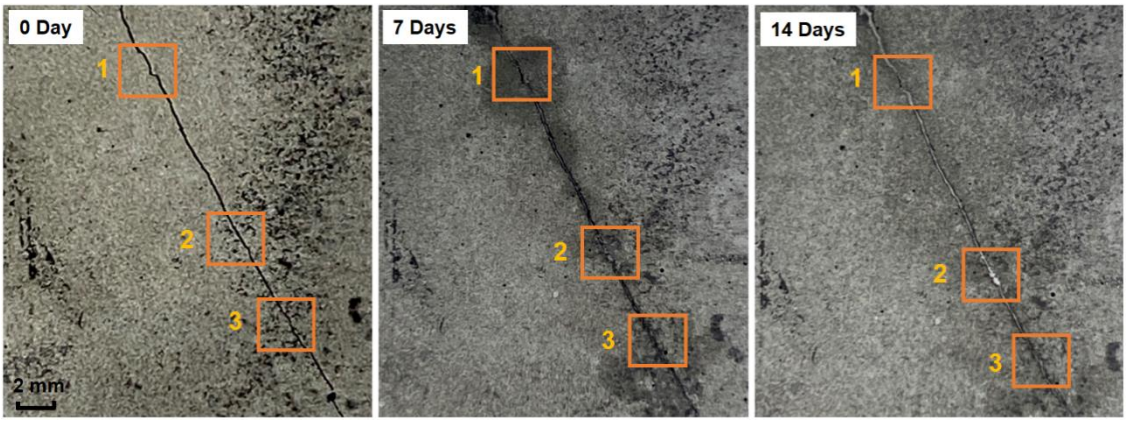

(b) Composite with 2% SL

Figure 7.1. Crack closure of NCB/cementitious composites with/without SL at various curing ages (Dong, Li, Shen, et al. 2021).

7.1.3 Self-sensing capacity

The stress sensing capacity of NCB cementitious composites originates from the electrical conductivity of NCB. Figure 7.2 illustrates the FCR of composites under cyclic compression from 0 to 5 MPa. The initial NCB cementitious composites expressed satisfactory piezoresistivity, regardless of the content of SL. It seems that the composites with SL possessed higher FCR values. After the healing process, much higher FCR values were observed because of micro cracks. However, the composites without SL possessed worse repeatability, while the composites with 2% SL are provided with more stable piezoresistivity.

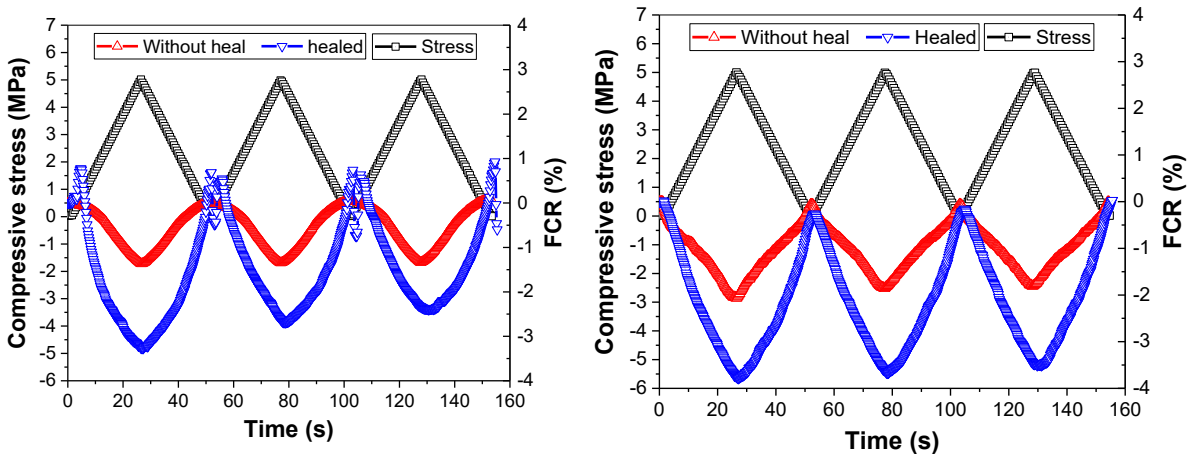

(a) Without SL (b) With 2% SL

Figure 7.2. Stress sensing performances of the NCB cementitious composites with/without SL.

7.1.4 Mechanism discussion

Figure 7.3 illustrates the micromorphology of the boundary interface between SL to cement matrix. It could be found that the NCB particles were separating the SL from cement matrix, because the NCB were attached to the surface of SL. Due to the excellent conductivity of NCB, their relative positions and contact states are altered under compression, which is contributed to the piezoresistivity. Figure 7.4 depicts the microencapsulation of NCB containing SL filled composites, and the schematic diagrams of the composites for self-healing preparations. Since the SL particle is in micro size of < 75 μm and the NCB is the nanoparticles with an approximate size of 20 nm, thousands of NCB were attached to the surface of SL during the pre-mixing process, due to the high surface energy of NCB. Therefore, a proportion of SL was preserved from the initial cement hydration and the later air carbonation. Similarly, some CP (< 10 μm) could be enclosed by NCB during mixing. These preserved self-healing agents provide the opportunity of the self-healing cementitious composites.

In addition, the pre-cracked composites exposed the SL and NCB that had access to humidity and carbon dioxide from air atmosphere. However, given that some SL particles and unhydrated CP were still encapsulated by NCB nanoparticles even though the specimens were previously compressed to create cracks, the self-healing efficiency of composites could be significantly weakened. Therefore, with the cracked surface immerging into the solution, the sonication bath was applied to reduce and eliminate the number of NCB particles onto the surface of SL and CP particles. In the case of exposed SL and unhydrated CP, the self-healing products include the $CaCO_3$, C-S-H and $Ca(OH)_2$ that sourced from the carbonation of SL and rehydration of CP.

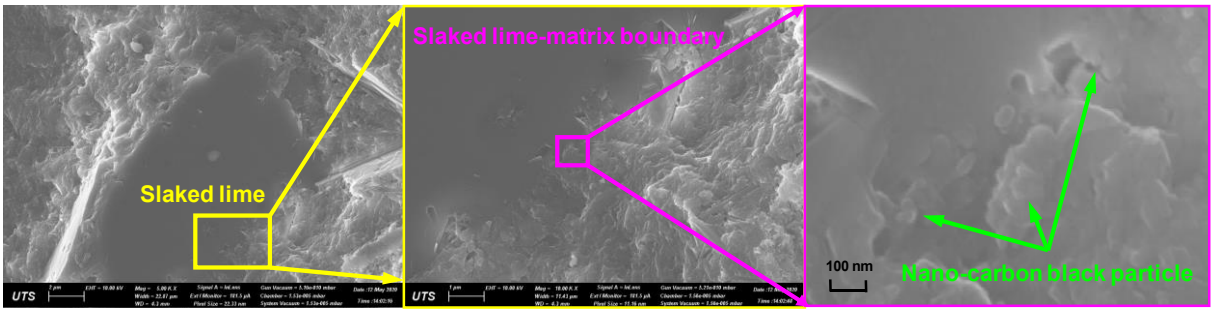

Figure 7.3. Microstructural morphology of NCB enclosed SL in cement matrix.

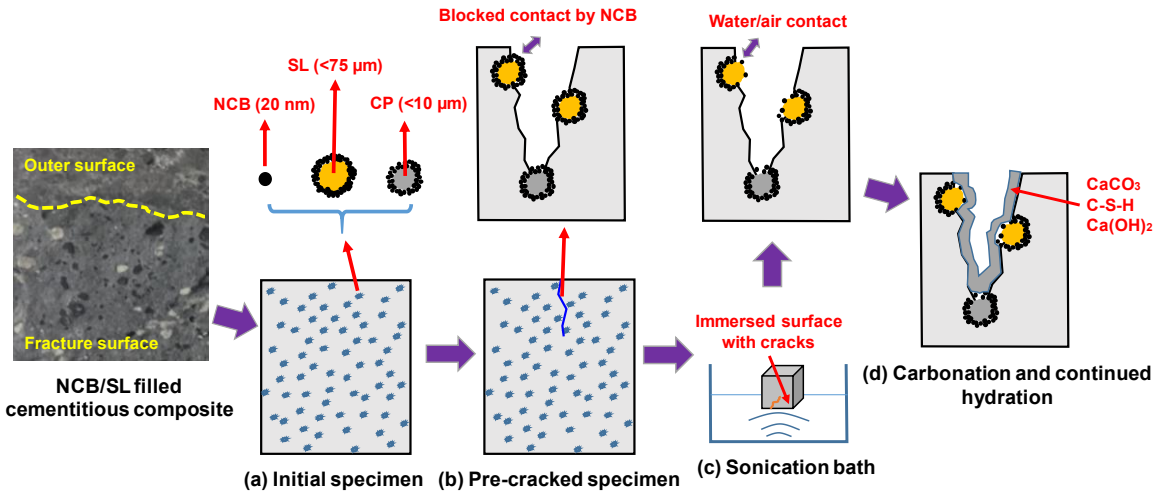

Figure 7.4. Schematic diagram of the released slaked lime after sonication bath for cracks self-healing.

7.2 Combined self-sensing and hydrophobic properties

In this section, the multifunctional cementitious composites with integrated self-sensing and hydrophobicity abilities were firstly developed and investigated using conductive graphene nanoplate (GNP) and silane hydrophobic powder (SHP) (Gao et al. 2018; Geng et al. 2020; Horgnies & Chen 2014; Husni et al. 2017; Lei et al. 2020; She et al. 2018; Yin et al. 2020). The GNP and SHP are mixed together with binders and water to produce cementitious composites.

7.2.1 Water absorption and surface wettability

7.2.1.1 Capillary water absorption

The water absorption of the cementitious composite as a function of time (square root of second) with various GNP is displayed in Figures 7.5(a) to 7.5(c), in the case of the SHP contents at 0, 1% and 2% respectively. For the specimen without SHP, the water absorption shapely increased in the first 6 hr, and then the increasing rate gradually slowed down until to a constant at the fourth day. However, for the specimen filled with SHP, the water absorption increased at a prolonged rate in the first several hours, and continually increased at a much slower rate till the end. In comparison to the absorption values of the specimen with/without SHP, it could be found that the SHP possessed positive influences on the water permeability by greatly decreasing the water absorption. The final water absorption of the specimen after 4 days of water immersion was nearly decreased by 10 times for the specimen with 1% SHP and 15 times for the specimen with 2% SHP. The final water absorption (I_t) reached approximately 0.44 mm, 0.31 mm and 0.37 mm, respectively for the 2% SHP filled cementitious composites with 0, 1% and 2% GNP. This phenomenon is mainly due to the filling effect of SHP and the reduction of porous structures in the specimen. In addition, the hydrophobic surface of cementitious composite can be built because of the addition of silicon powders, which also block the entrance of water into the specimen.

As for the effect of GNP, previous studies proposed that the plate-like structures of GNP could increase the permeation path of invasive solutions, and improve the impermeability of cementitious composite. Moreover, it was found that the pores of specimen could be transformed into smaller pores and decrease the water absorption. In this study, the results showed that the GNP could reduce the water absorption capacity of cementitious composite, no matter how much the dosages of SHP specimen possessed. The best water impermeability of the specimen occurred for the composite reinforced with 1% GNP, and the reduction on

water absorption was slightly decreased when the GNP concentration increased to 2%. This phenomenon might be attributed to the nano-size effect of GNP, which possess high surface energy and could agglomerate with each other.

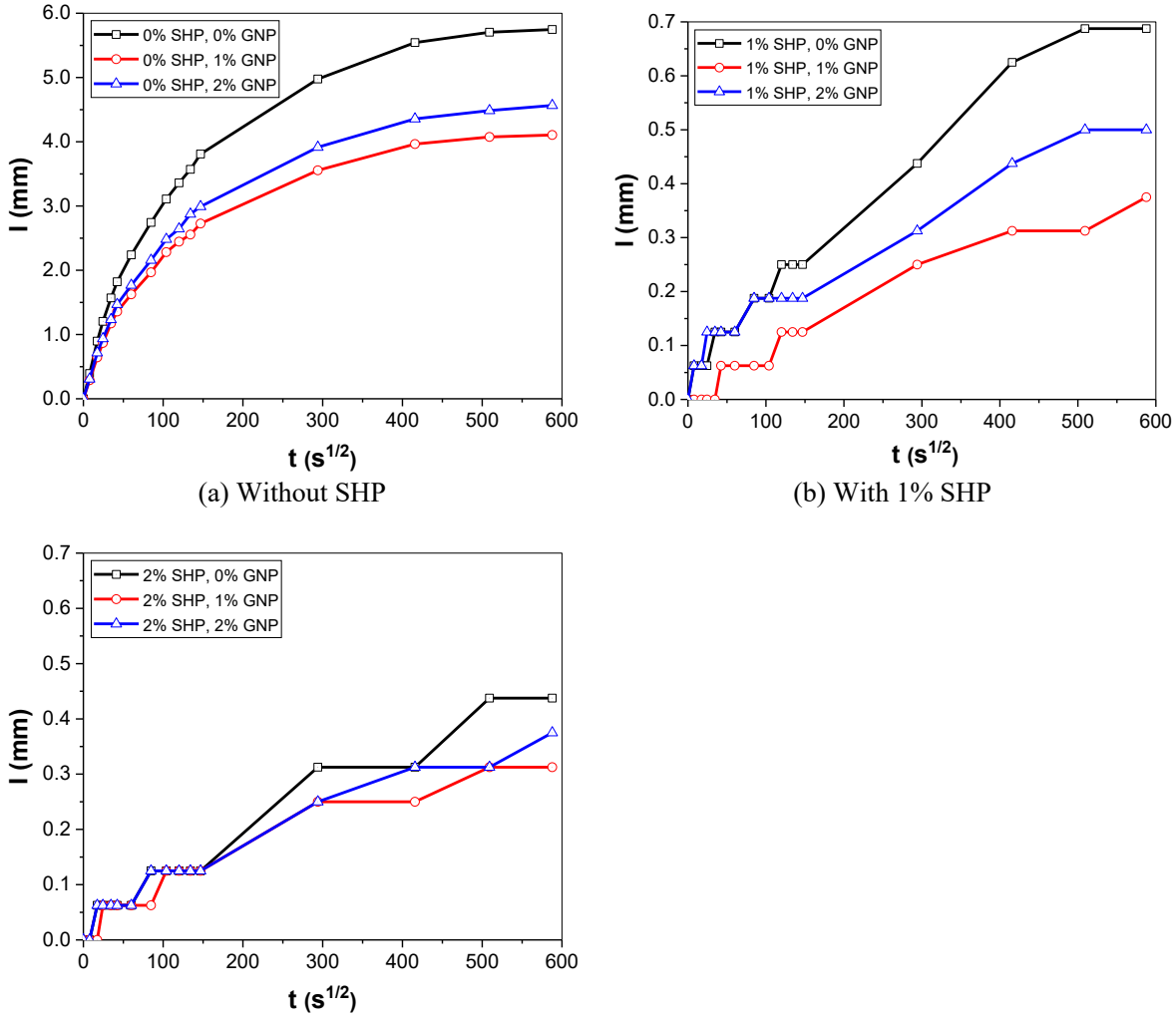

(a) Without SHP

(b) With 1% SHP

(c) With 2% SHP

Figure 7.5. Water absorption of cementitious composites with various contents of GNP and SHP.

7.2.1.2 Water contact angle

The water contact angle of cementitious composite relates to the capillary porosity and the surface tension. The results of the specimen reinforced with various concentrations of SHP and GNP are exhibited in Figures 7.6(a) to 7.6(i). For the plain cement paste without GNP, the water contact angle considerably increased from 53.5 ° to 79.4 ° with 1% SHP. Subsequently,

with the increase of SHP to 2%, the water contact angle decreased to 70.3 ° but still higher than that of the plain specimen without SHP. Even for the specimen in the presence of GNP, the effect of SHP on the water contact angle showed a similar tendency with the optimal concentration of 1%. The results are consistent to the above discussed water absorption, because the SHP particles could fill the micropores and reduce the water movement from capillary passages. Moreover, the silane/resin based composition of SHP could greatly improve the hydrophobicity of the specimen and increase the water repellency. As for the decreased water contact, it might be attributed to the affected cement hydration and the more created capillary pores under a high concentration of SHP.

In terms of the effect of GNP on the water contact angle of specimen, the results of the specimen without SHP showed an increased water contact angle with the added GNP from 53.5 ° to 63.2 °. The optimal concentration of GNP was 1%, while the largest water contact angle reached 67.9 °. However, for the specimen with 1% SHP, the addition of GNP showed opposite functionalities. It was found that the 1% GNP increased the water contact angle from 79.4 ° to 86.4 °, while the addition of 2% GNP strongly decreased the contact angle to 68.2 °. This might be due to the aforementioned poor dispersion of high concentrated GNP, which instead decreased the water contact angle of the specimen. As for the specimen with 2% SHP, the effect of GNP seemed to be negligible. The contact angle increment by GNP was much smaller than the counterparts filled with ≤ 1% SHP and reached only 6.2 °. It implied that the effect of GNP on the water contact angle of cementitious composite could be weakened in the presence of excessive SHP. In addition to the filling effect by GNP, the nano-size GNP could improve the hydrophobicity of specimens and increase their surface tension, which also resulted in the increased water contact angle.

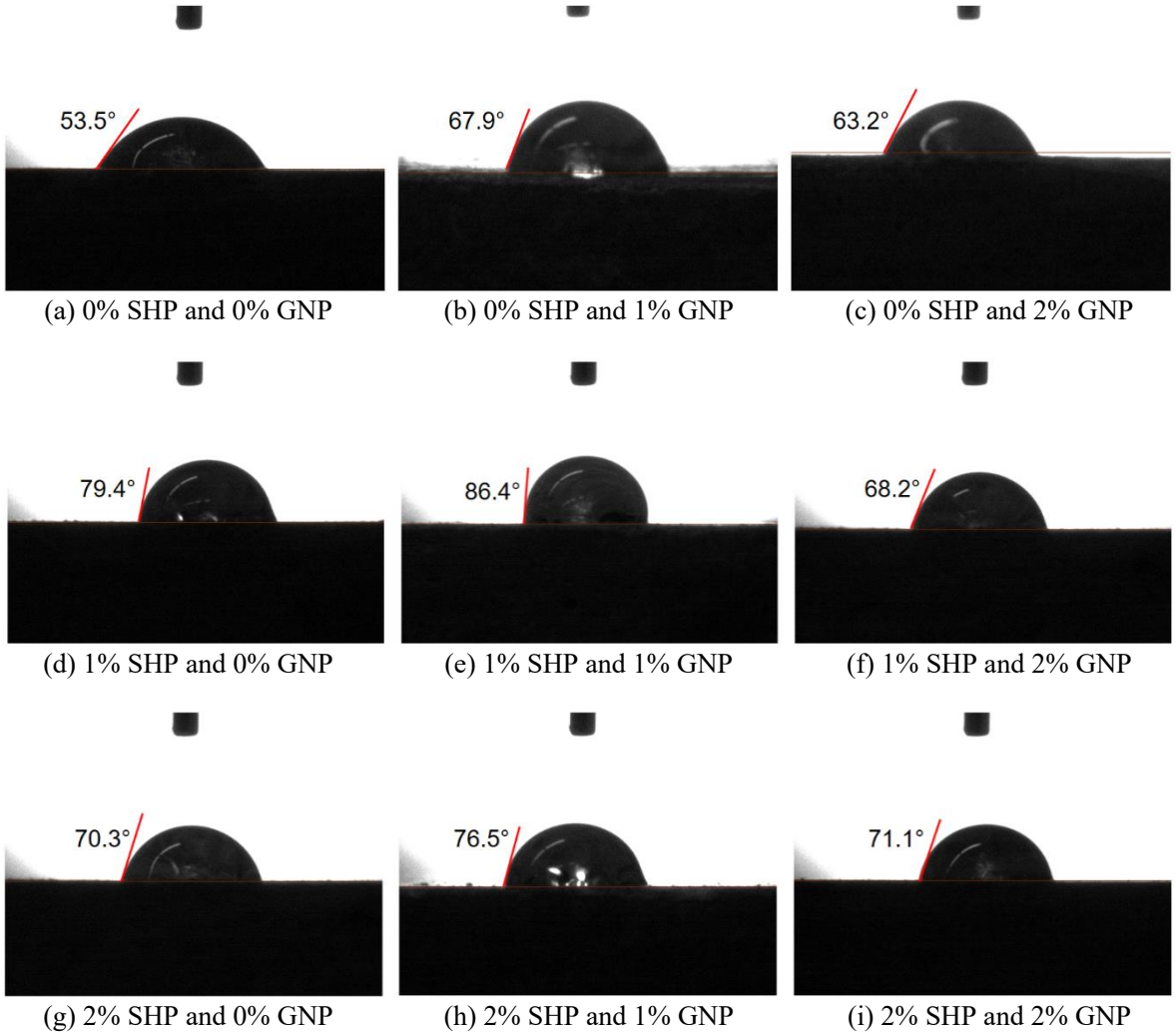

(a) 0% SHP and 0% GNP (b) 0% SHP and 1% GNP (c) 0% SHP and 2% GNP

(d) 1% SHP and 0% GNP (e) 1% SHP and 1% GNP (f) 1% SHP and 2% GNP

(g) 2% SHP and 0% GNP (h) 2% SHP and 1% GNP (i) 2% SHP and 2% GNP

Figure 7.6. Water contact angle in fracture surface of cementitious composite with SHP and GNP.

7.2.2 Piezoresistive behaviours

7.2.2.1 Load rate and magnitude

Figure 7.7 illustrates the alteration of electrical resistivity changes and compressive strain of the cementitious composite subjected to compressive stress, attempting to figure out the piezoresistive behaviours under various loading rates and magnitudes. Generally, the fractional changes of resistivity and strain increased/decreased with the increase/decrease of loading magnitudes. Their values at the stress peaks were linearly fitted, and the square deviation of fitting curves was plotted, with R_1^2 and R_2^2 representing the deviation of fractional changes of

resistivity and compressive strain, respectively. Since different compressive cycles possessed various loading rates and magnitudes, the square deviation of 0.999 and 0.992 indicates that these figures of resistivity changes had an excellent linear relationship to the compressive stress, regardless of their loading rates and magnitudes. In addition, it was found that the compressive strain of specimen experienced similar linearity to compressive stress. However, the linearity is poorer than that of fractional changes of resistivity, with the deviation values of 0.991 and 0.970, respectively. The nonlinearity might be due to the accumulated microdefects in the cementitious composite during each compression. To specifically reveal the effect of stress magnitude, Table 7.1 shows the square deviation of the cementitious composites under various stress magnitudes based on the linear regression. It could be found that both fractional changes of resistivity and the compressive strain showed worse linearity under small stress magnitude, in comparison to those under large stress magnitude. This might be due to the unstable porous structures and microstructures of cementitious composites that affect the conductive passages and electrical resistivity. Under small stress conditions, the altered electrical resistivity is small and the FCR is easily disturbed by the resistivity changes originated from unstable structures. On the contrary, the large FCR values under high-stress conditions are much more stable and free from the interferences by unstable resistivity changes. It means that the cementitious composite is more appropriate to measure the compressive stress/strain under large external forces. Under a low-stress environment, nonlinearity induced deviation might occur on the cement-based sensors and affect the accuracy.

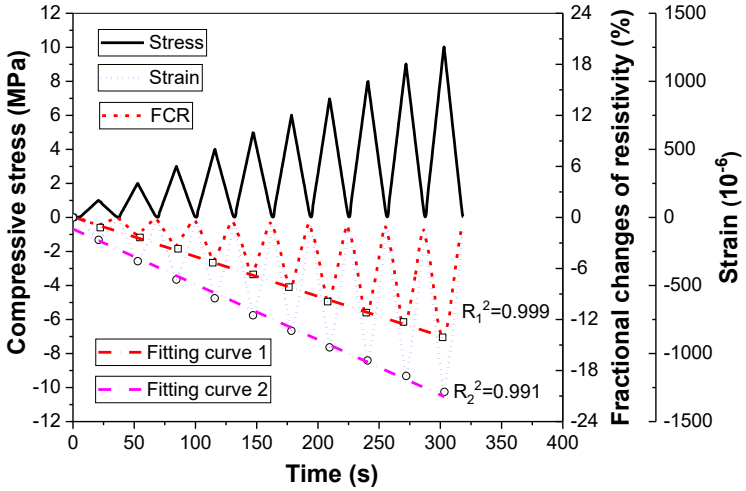

(a) 1% GNP and 2% SHP

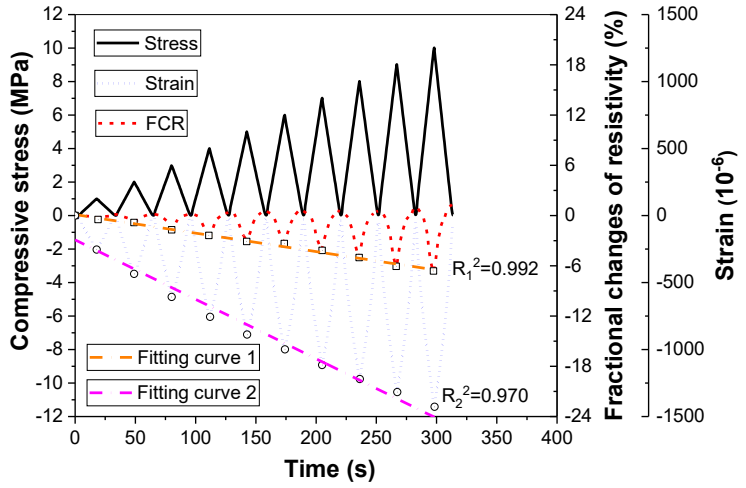

(b) 2% GNP and 2% SHP

Figure 7.7. *FCR* as a function of compressive stress and strain of cementitious composite with 2% SHP.

Table 7.1 Square deviation of cementitious composite under various stress magnitudes

Group	Square deviation	Ranges of stress magnitudes		
		$0 \leq \sigma \leq 5$ MPa	$5 \leq \sigma \leq 10$ MPa	$0 \leq \sigma \leq 10$ MPa
1% GNP and 2% SHP	R_1^{2*}	0.998	0.999	0.999
	R_2^{2*}	0.989	0.998	0.991
	R_1^2	0.993	0.994	0.992

2% GNP and 2% SHP	R_2^2	0.966	0.999	0.970

Note*: R_1^2 means the square deviation of the *FCR*; R_2^2 represents the square deviation of compressive strain.

Similar to the commercially available foil strain gauge which has a constant gauge factor of 2, the well maintained gauge factor of the cementitious composite under altered loading rates and magnitudes is a crucial factor in ensuring their practical application. Previous study have demonstrated that the stress magnitude is more significant than loading rate to affect the gauge factor. As a consequence, based on the above results, the gauge factors of the cementitious composite under different loading magnitudes were displayed in Figure 7.8. It presented that the gauge factor firstly increased with the loading magnitude, and then became stable with a much lower increasing rate when the loading magnitudes were larger than 8.0 MPa. The results implied that the sensing ranges of the cementitious composite should be larger than 8.0 MPa, to have the constant gauge factor in the measurement.

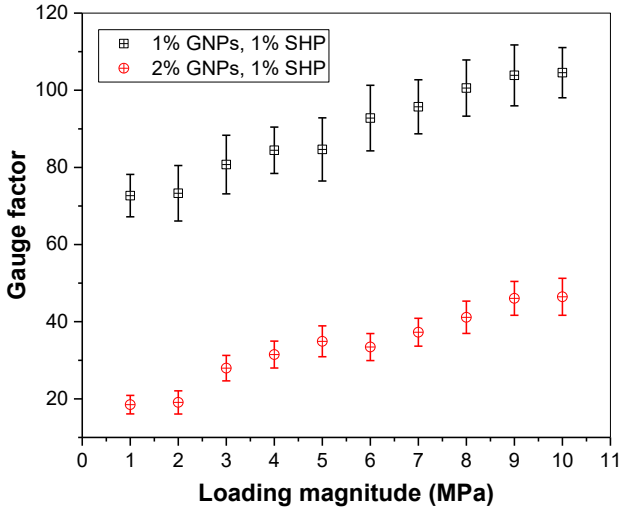

Figure 7.8. Gauge factor variation under coupled effects of loading rate and load magnitude.

7.2.2.2 Water immersion

Figure 7.9 shows the *FCR* of the cementitious composite without SHP subjected to cyclic compression, before and after 1 day water immersion treatment. For the specimen filled with 1% GNP in Figure 7.9(a), the initial *FCR* exhibited an excellent consistency to compressive stress, and the largest FCR reached approximately 14.4% at the stress magnitude of 10 MPa. As for the piezoresistive repeatability, the irreversible *FCR* was as low as 2.0% after 10 cycles of compression. The irreversibility was partially due to microdefects in the cementitious composite, which retarded the electrons' transport and increased the electrical resistivity of specimen. Moreover, because of the movement of free ions in residual solutions under the electric field, which was also known as polarization effect, the electrical resistivity of specimen could gradually increase with the duration of measurement. In this study, the specimens were dried previously before the piezoresistive test; hence, the polarization effect was considered not significant. However, after the immersion treatment, the fractional changes of resistivity showed different patterns by a considerable increase in resistivity during the piezoresistive test. The resistivity reduction still occurred in the process of loading, but the decreasing rate was overwhelmed by the increasing rate. It led to the positive values of *FCR* in compression test, except the values in the beginning. Moreover, it was observed that the irreversibility of *FCR* reached 19.5% which was almost 10 times higher than that of the dried specimen. This phenomenon was mainly due to the effect of water content, which penetrated into the specimen and brought the polarization effect. Figure 7.9(b) illustrates the FCR alterations of the specimen filled with 2% GNP. Previous results demonstrated that the specimen possessed similar water absorption to the counterparts with 1% GNP, and it was found the influenced *FCR* values because of the introduction of water content. The irreversible *FCR* accounted for 0.5% and 3.5% respectively before and after water immersion, which is magnified by 7 times. In addition, not only the piezoresistive repeatability, the *FCR* intensity altered as well under the influence of

water content. The original *FCR* value was approximately 5.9% at the stress magnitude of 10 MPa, while the new value increased to approximately 7.8%. Dong et al. explored the effect of water content on the piezoresistive sensitivity, and found that there was optimal water content to achieve the best piezoresistivity. In this case, the absorption of water content improved the piezoresistive sensitivity for the dried cementitious composite filled with 2% GNP.

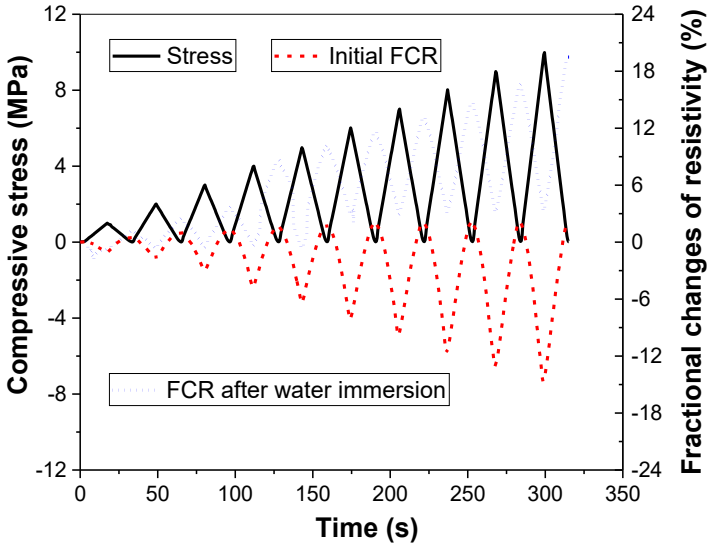

(a) 1% GNP and 0% SHP

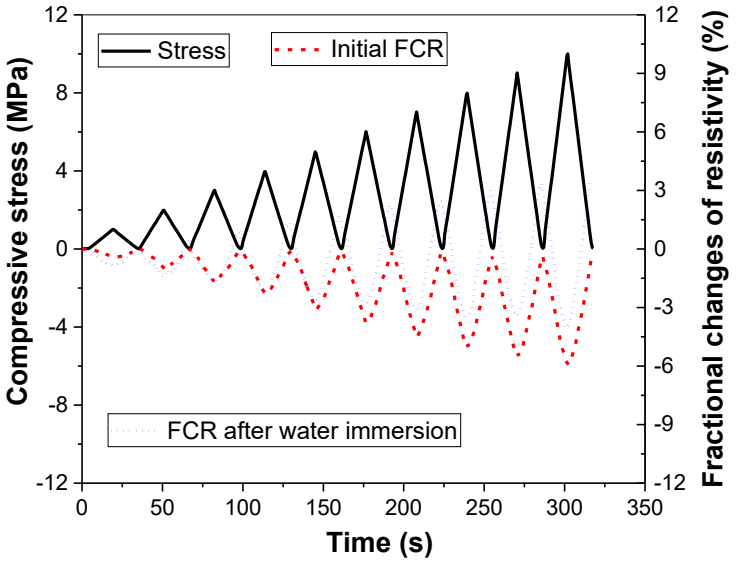

(b) 2% GNP and 0% SHP

Figure 7.9. *FCR* of cementitious composite without SHP before/after water immersion treatment.

The piezoresistive performance of specimen filled with 1% SHP before and after water immersion is shown in Figure 7.10. To estimate the hydrophobicity and water repellency, the specimens were water immersed for 7 days. For the specimen with 1% GNP, it could be observed that the *FCR* after water immersion was approximately identical to the original values, except for the alterations at the beginning of compression. Similarly, in comparison to the specimen without SHP, a much low discrepancy on the *FCR* occurred for the specimen filled with 2% GNP. The results should be attributed to the failed entrance of water, since the water absorption was greatly decreased from 4 to 0.5 mm after the application of SHP in the cementitious composite. Even though, a proportion of water had the potential to penetrate the near-surface area or remain in the surface of specimen, and affect the generation of conductive passages. That is why the piezoresistive performances of the cementitious composite slightly fluctuated after the water immersion. Overall, in comparison to the piezoresistive performance of specimen without SHP after 1 day of water immersion, more stable and consistent piezoresistivity could be found for the specimen with SHP even after 7 days of water immersion.

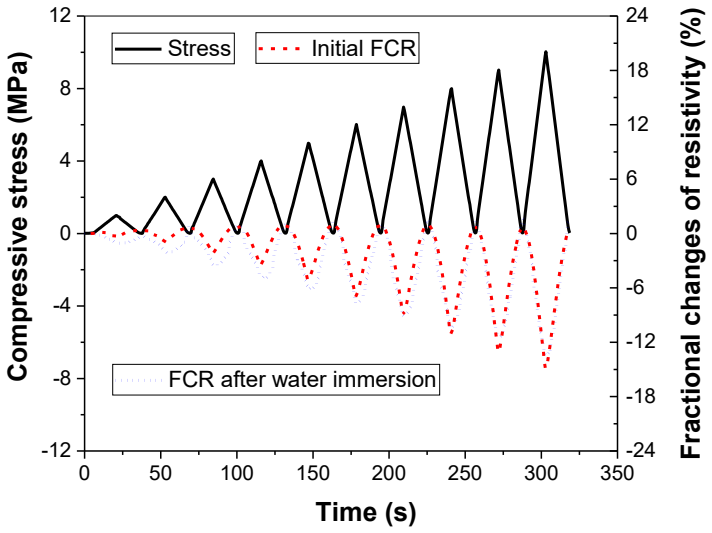

(a) 1% GNP and 1% SHP

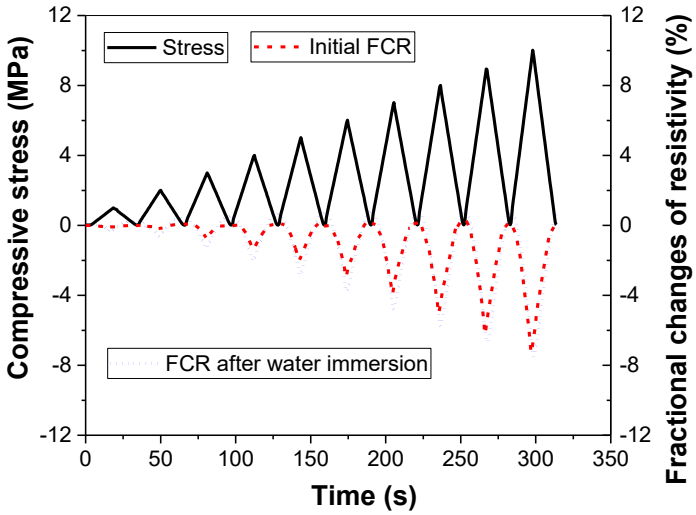

(b) 2% GNP and 1% SHP

Figure 7.10. *FCR* of cementitious composite with 1% SHP before/after water immersion treatment.

7.2.2.3 Mechanism discussion

The affected piezoresistive behaviours by water immersion were consistent well with the performance of water absorption of the cementitious composite. In the case of water immersion of cementitious composite, the aforementioned results indicated that the amount of penetrated water played a critical role in the development of piezoresistivity. Figure 7.11 schematically depicts the functionality of GNP and SHP in cementitious composite, and the potential channels of water penetration, attempting to elucidate the mechanism behind the cementitious composite reinforced with incorporated GNP and SHP. For the plain cement paste, because of the microcracks and pores, water can easily penetrate into the cement paste and lead to high water absorption. With the addition of GNP, the pores and cracks are reduced to resist the water absorption, and the plate-like structures of GNP also benefit the water impermeability. It was found that the GNP has the capacity to block the water channel and retard the further penetration of water content. Furthermore, according to the previous studies, the length of water penetration passages can be increased with the intervention of GNP which also weakens the ability of water absorption. However, combining the results of water absorption of the

cementitious composites only filled with GNP, the conclusion can be drawn that a large proportion of water penetrates into the specimen even the water absorption is decreased by more than 30%. In other words, some pores might not be penetrated from the external water due to the GNP, but there exist water-saturated pores close to the surface and unsaturated pores because of the super long channels. The electrical resistivity of specimen is very sensitive to the water content changes, and that is why the piezoresistive behaviours of specimen filled with GNP altered considerably after the water immersion.

For the cementitious composite filled with combined GNP and SHP, in addition to the isolation effect of GNP, the SHP helps to establish a hydrophobic film in the surface of specimen, GNP, pores and cracks. The hydrophobic film on the surface of pores and cracks represents that the cement hydration products possess hydrophobicity. In comparison to the specimen only filled with GNP, the entered water content is greatly decreased. Moreover, the water channels that might work in the specimen with GNP are further blocked by the enclosed hydrophobic film. Even if the water is successful in penetrating through the channels, the attached hydrophobic film can greatly limit their entrance into the pores, as shown in Figure 7.11. This contributes to the small water absorptions and stable piezoresistive performances of the cementitious composite.

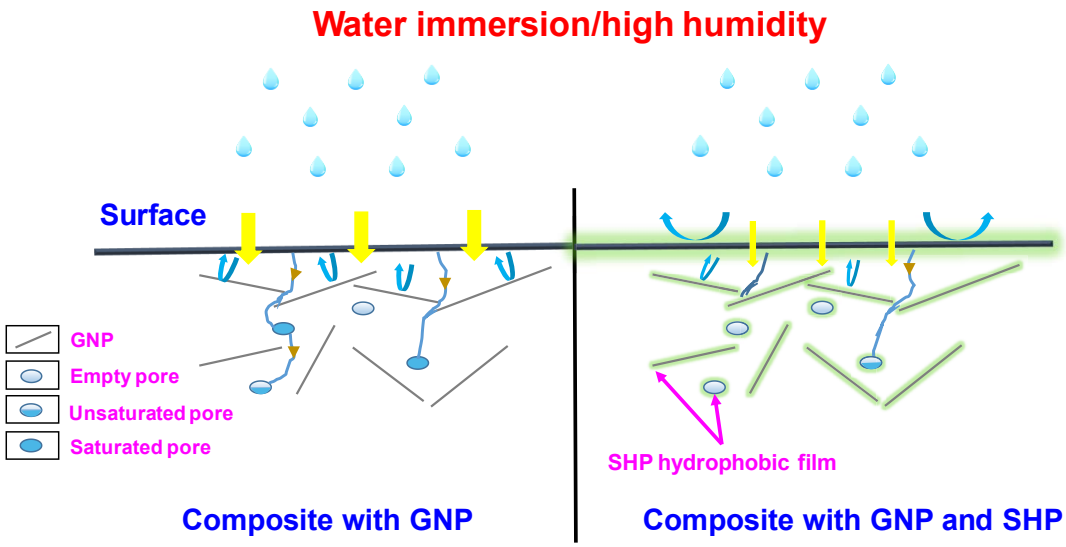

Figure 7.11. Schematic diagram of water penetration into GNP/cementitious composite with/without SHP.

7.3 Combined self-sensing, hydrophobic and self-cleaning properties

In this section, a multifunctional cementitious composite was synthesized to possess integrated superhydrophobicity, self-cleaning and self-sensing functions. The synthesis was carried out by penetrating a precast graphene nanoplate filled cement-based sensors with silane/isopropanol solution.

7.3.1 Silane treatment

Cement-based sensors were cast in a mould of 10 mm × 10 mm × 60 mm after 28 days of curing. The silane treatment is carried out when the cement-based sensor is hardened after 28 days of curing. As shown in Figure 7.12, the trichloro-silane is firstly poured into the solvent of isopropanol with mechanical stirring for dissolution, and the silane to isopropanol ratio is 4% by volume. Afterwards, the cleaned cement-based sensors are immersed in the silane/isopropanol solution. After 2 hours, the sensors are taken out and moved to an oven for 4 hours drying with the temperature of 50°C. The immersion and followed drying procedures are conducted twice to ensure the sufficient entry of silane into cement-based sensors.

To prepare the specimens for piezoresistivity-based self-sensing test, four copper meshes are embedded in the cementitious composites during casting as electrodes. The hydrophobicity is assessed through the water contact angle (CA) test with the deionized water as test liquid. The self-cleaning performance is assessed using visual inspections of carbon dust and food stains' removing efficiency before and after the sensor surfaces were rinsed with deionized water. For each specimen, a total amount of deionized 10ml water was spread on the surfaces using an injector. The self-cleaning performance of cement-based sensor without any treatment is compared to the experimental group after silane surficial enhancement.

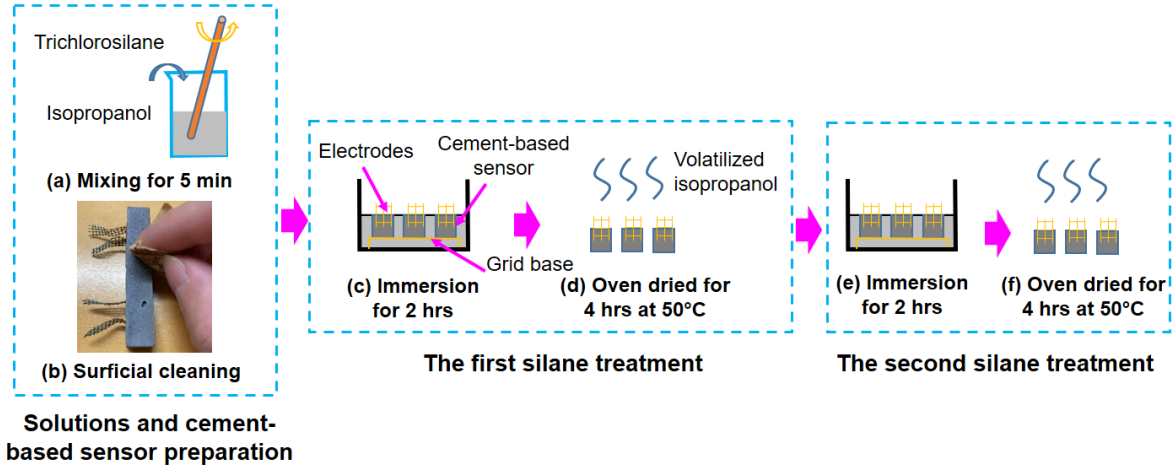

Figure 7.12. Schematic plots of the detailed procedures of surficial enhancement on cement-based sensors.

7.3.2 Self-sensing performance

Figures 7.13(a) to 7.13(b) shows FCR of cement-based sensor as a function to compressive stress and strain, respectively. It could be found that the compressive stress and strain had a linear correlation to FCR, which decreased as the stress or strain increased and recovered as the load was removed. Given the stress magnitude applied within the elastic range of cement-based sensors, the gauge factor can be obtained through the fitting curves between FCR and compressive strain. Gauge factor means the FCR changes in unit strain that evaluate the sensing efficiency of piezoresistivity-based sensors. In this study, the graphene nanoplate filled cement-based sensor after silane treatment achieved a gauge factor of 141.8, which was nearly 72 times higher than that of commercially available strain gauge. The results implied that the cement-based sensors after silane treatment still possessed a satisfactory piezoresistivity.

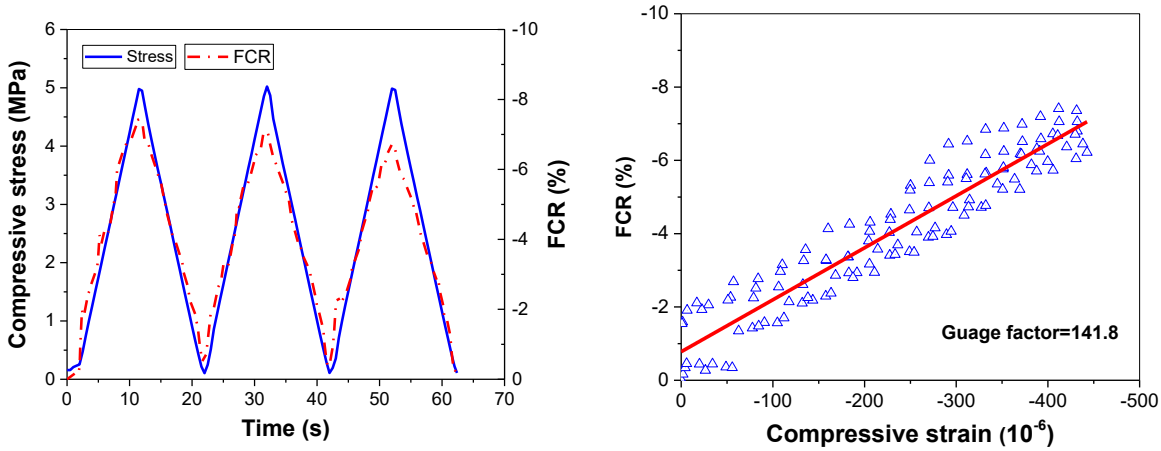

(a) Stress monitoring (b) Strain monitoring

Figure 7.13. Self-sensing performance of cement-based sensor after silane treatment.

7.3.3 Water contact angle

Figures 7.14(a) to 7.14(c) show water CA of cement-based sensors after silane treatment. The CA values of intact surface, destructed surface with scratches and the cross section of cement-based sensors are measured and compared. For the intact silane-treated surface shown in Figure 7.14(a), the average CA reached the highest value of 163°. It demonstrated that the cement-based sensor had a superhydrophobic surface after immersion in silane/isopropanol solution owing to the invasion of hydrophobic silane. Previous studies have proposed the hydrophobic cementitious composites coupled with silane-based materials, but the CA values are usually lower than 150° because of the hydrophilic cement matrix. The ultrahigh CA values obtained in this study are probably due to the additional filler of graphene nanoplate as conductive filler in cement-based sensor, given that the graphene nanoplate is beneficial for the hydrophobicity.

To simulate the situation of concrete structures damaged with man-made scratches, the silane treated cement-based sensors were engraved by pen knife to create scratches on the surface, as shown in Figure 7.14(b). The experimental results indicated a smaller CA value than that of intact surface, reaching approximately 148°. There are mainly two possible reasons responsible for the weakened hydrophobicity and reduced CA values. The first reason is the damaged micro

papillae that reduce the surface energy of cementitious composites, and the second reason is the fall of hydrophobic silane and graphene nanoplate. In addition, as displayed in Figure 7.14(c), the contact angle test of cross section of cement-based sensors showed the smallest CA value of 142° compared to the CA values of surfaces. The results demonstrated that the inner parts of cement-based sensors was also hydrophobic. This property can significantly enhance the water repellency of cement-based sensors and increase the serviceability of sensors by reducing the interference of electrical resistivity from pore solutions. In general, the hydrophobicity of internal cement-based sensors should be benefit from relatively small size and the two cycles of immersion/drying for silane treatment. In that circumstance, the silane/isopropanol solutions can be entered into inner porosity easily through capillary suction.

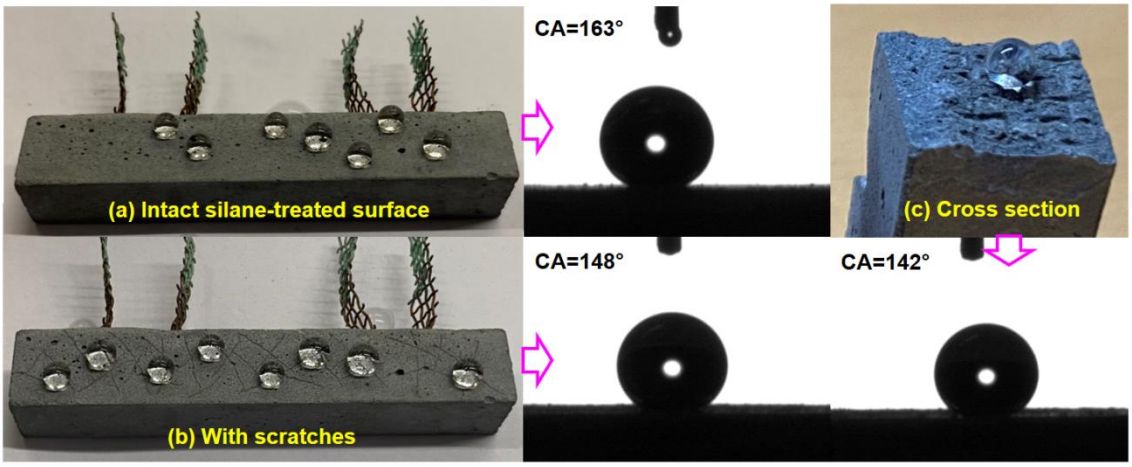

Figure 7.14. Water contact angle of silane-treated cement-based sensor: (a) intact silane-treated surface; (b) with scratches and (c) in the cross section.

7.3.4 Self-cleaning performance

The carbon dust, as well as two sauces of tomato sauce and barbecue sauce with different stickiness are applied to observe the dust and food stains' removing efficiency by 10 ml deionized water, in order to assess the self-cleaning performance. Figures 7.15(a) to 7.15(c) show the removing efficiency of cement-based sensors before and after the silane treatment. For the carbon dust sprinkled on the surface of cement-based sensors, the silane-treated sensor

showed a very clean surface without leftover but the untreated sensor still had the residuals after the water drops rolling from upper part of sensors. The experimental results are very similar to the previous studies, which found that the hydrophilic carbon dust was easily adhered and absorbed to the water drops . Subsequently, the water drops removed the carbon dust for the silane-treated cement-based sensor. However, for the hydrophilic untreated cement-based sensor, water drops could penetrate into the cement matrix with carbon dust and that was why there left dark spots on the surface. As for the water drops removing efficiency regarding to tomato and barbecue sauces, the experimental results showed similar tendency of less residuals on the surface of cement-based sensors after silane treatment. In comparison to carbon dust, the sauces were more lipophilic rather than hydrophilic, and they could not completely adhered to the rolled water drops. Because the barbecue sauce was more sticky than tomato sauce, it could be found that the barbecue sauce was much difficult to be removed, and tiny sauces still remained even for the treated cement-based sensor. In addition, the experimental results implied that the silane-based surficial treatment reduced the adhesion between cement matrix and lipophilic materials such as sauces, and enhanced the self-cleaning property.

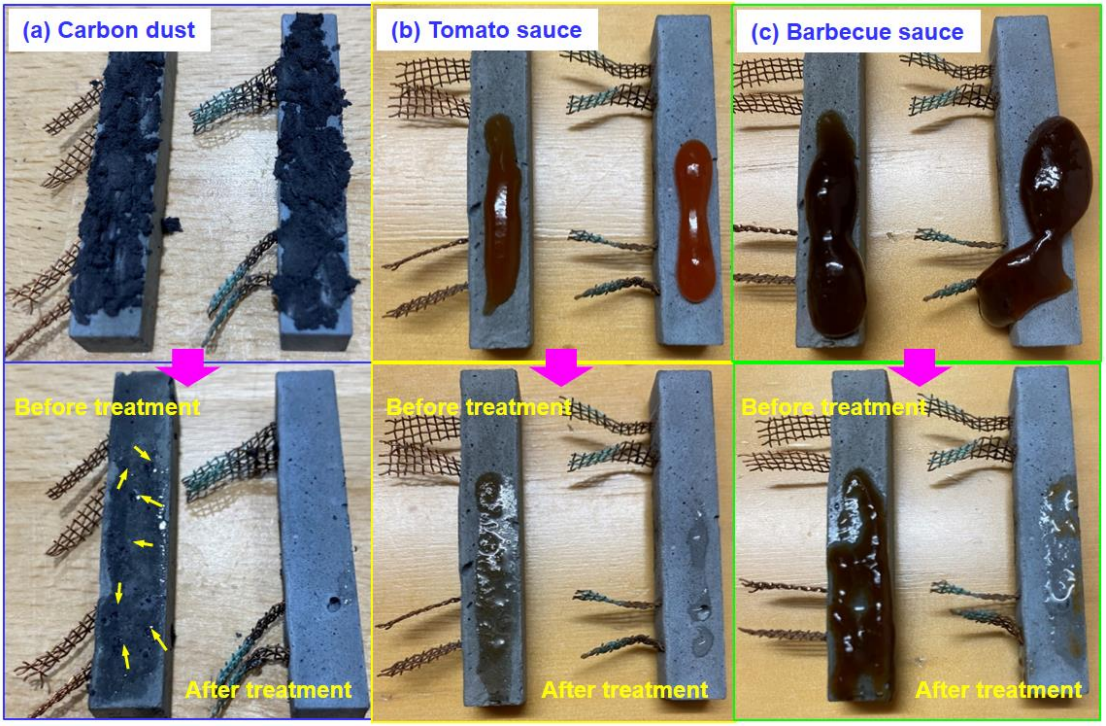

Figure 7.15. Dust and food stain self-cleaning performance of cement-based sensors before/after silane treatment.

7.4 Summary

The piezoresistive, self-healing, superhydrophobic and self-cleaning capacities of multifunctional cementitious composites as novel cement-based sensors were developed and investigated in this study. The main conclusions can be drawn as follows:

(1) Novel microencapsulation of nano-carbon black (NCB) enclosing slaked lime was applied for multifunctional cementitious composite with integrated self-healing and self-sensing capacities. The piezoresistivity was achieved by the excellent conductivity of NCB. Since the preserved SL particles were released after the generation of cracks, and the cracks self-healing occurred. The results provide a novel microencapsulation of NCB containing self-healing agent of SL to improve the self-sensing and self-healing performances of smart cementitious composite.

(2) The water absorption of cementitious composites decreased with the addition of GNP, and specimen with 1% GNP exhibited slightly better impermeability than that with 2% GNP. The usage of SHP greatly decreased the water absorption, especially for the specimen with 2% SHP, which reduced the water absorption by more than 15 times. The water contact angle of the plain cement paste was only 53.5°, while the highest contact angle of 86.4° was found for the specimens with 1% GNP and 1% SHP.

(3) Regardless of the GNP contents, treatment of water immersion significantly affected the piezoresistive performances of cementitious composites without SHP, because of the penetrated water and induced polarization effect. But with addition of SHP, the influence was controlled with minor fluctuations. The hydrophobic films were established on the surface of specimen, GNP, cracks and pores, which prohibited further water movements.

(4) The superhydrophobic behaviours with highest water CA of 163.4° and 142° were achieved on the surface and interior of cement-based sensors after the twice coating by 4% silane with isopropanol. The once coated cement-based sensor exhibited slightly worse performance than that of the twice coated counterparts. The cement-based sensors after 100% silane treatment without isopropanol showed hydrophobic behaviours only on the surface but hydrophilic behaviours interior.

(5) The self-cleaning performance of the sensor, assessed with visual inspection of carbon dust and sauce stain removing subjected to water rinsing, was much superior to the sensor without silane treatment, especially on the hydrophilic carbon dust cleaning.

CHAPTER 8: APPLICATION OF CEMENT-BASED SENSORS

In this chapter, we applied the cement-based sensors in unreinforced concrete beams and mortar slabs to evaluate their monitoring capacity in large-scale concrete structures. Because the embedded cement-based sensors normally would not touch the reinforcements in reinforced concrete beams, the conclusions obtained from concrete beams without reinforcement could also applied to the reinforced concrete structures.

8.1 Cement-based sensors in concrete beams

8.1.1 Configuration of cement-based sensors

Figure 8.1 depicts three embedding configurations of CB filled cement-based sensor (CBCS) in the small scale unreinforced beams (40 mm× 40 mm× 160 mm) for three-point-bending test. The piezoresistive-based sensing performances of CBCS were investigated in both the compression and tension zones. Since the distribution of stress was various based on the distance to load point, the effects of embedding locations of sensors in unreinforced beams were also considered. Figure 8.1(a)-1 shows the first sensors configuration in compression zone, where the distance of CBCS-1 and CBCS-2 to centre of beams is 10 mm, and very close to the load applied point. Another sensor configuration (CBCS-3 and CBCS-4) in the compression zone is conducted by longer distance of 20 mm to the load point, as shown in Figure 8.1(a)-2. Generally, it could be considered that the former one was in the high stress concentration zone, while the latter one was in the low stress distribution zone. The sensors in these regions were subjected to both compressive and tensile stresses. As for the CBCS in the tension zone, the sensors only embedded in the central section (CBCS-5) were investigated in Figure 8.1(b), because of the largest tensile stress in the beams and the relatively weak sensing ability of

cement-based sensors for the tensile stress monitoring (Gupta, Gonzalez & Loh 2017; Lu et al. 2013; Qin, Lu & Li 2010; Ubertini, Laflamme, et al. 2014).

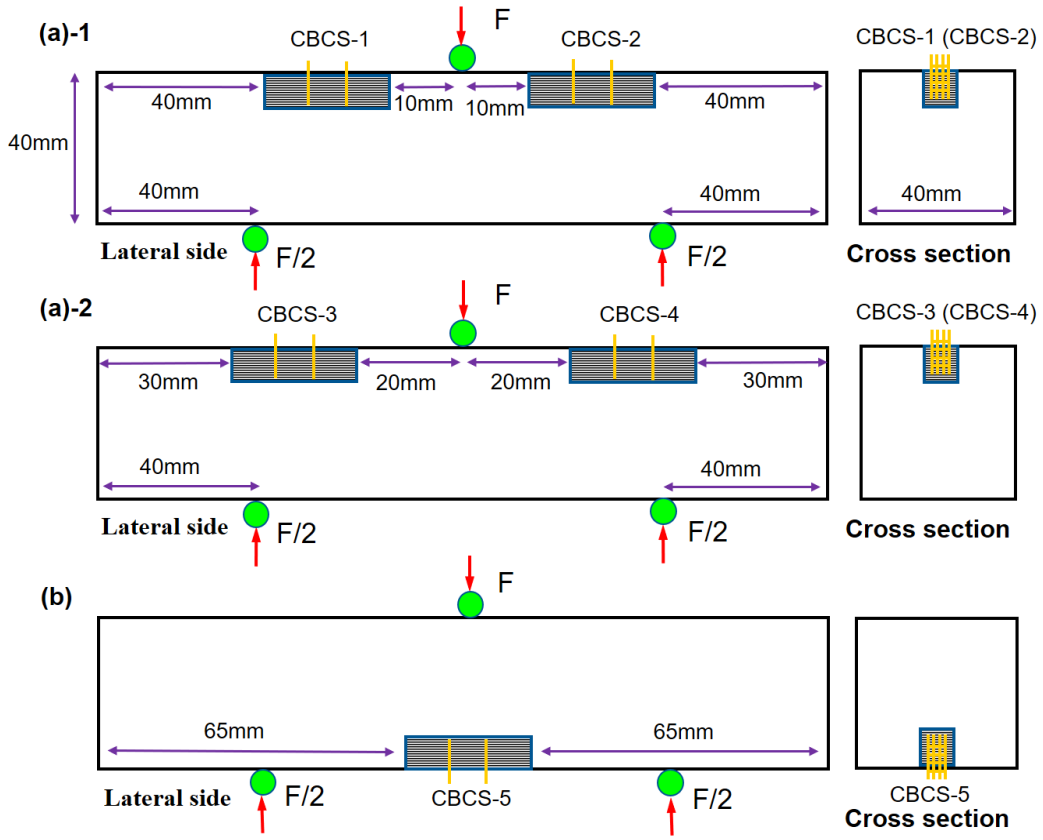

Figure 8.1. Configuration of CBCS embedded in different zones of unreinforced beam under three-point-bending.

8.1.2 Beam failure monitoring

Investigations demonstrated that the brittleness cementitious composites often exhibit the destruction by sudden failure and dramatically decreased of bearing capacity, but rare studies reported the electrical resistivity changes during the failure process. In this section, the embedded CBCS both in the compression and tension zones of unreinforced beams were proposed to investigate the electrical resistivity changes of embedded sensors in the flexural failure process of concrete beams, and attempt to establish the relationship between the electrical resistivity changes of embedded sensors to the health condition and damages of monitored beams. The flexural failure means the largest flexural stress that the specimens could

be hold under three-point-bending. Especially, the results can provide the self-sensing signal of concrete beams in the long-term service life based on the resistivity performances of CBCS.

8.1.2.1 Compression zone

Figure 8.2 shows the FCR values of CBCS in the longer distance (lower stress distribution zones) to the central load point in the compression zone during the bending test. Three different kinds of CBCS with various CB contents of 0.5% (CBCS05), 1% (CBCS1) and 2% (CBCS2) illustrated similar tendencies on the FCR decreases as the increase of loading. Generally, since the intrinsic embedded CB/cementitious sensors had much less negative impacts on the mechanical properties of monitored concrete beams, it was observed that the beams with CBCS05, CBCS1 and CBCS2 displayed very close ultimate flexural strength, reaching approximately 2.59 MPa, 2.87 MPa and 2.73 MPa, respectively. After the peak flexural strength, the stress was dramatically decreased almost to zero which implied the flexural failure of unreinforced concrete beams.

In terms of electrical resistivity variations for different CBCS, it seems that the FCR values decreased consistently to the flexural stress and increased almost at the same time when the flexural failure occurred. This is due to the CBCS under compression in the compression zone of unreinforced concrete beams to reduce their electrical resistivity and the excellent cohesion and dense interface between CBCS and beams. Also, it was seen that both the increasing rate and ultimate values of FCR increased with the increase of CB content, with the ultimate FCR at the flexural failure point rising from 0.51%, 0.65% to 0.71% for the CBCS05, CBCS1 and CBCS2, respectively. However, even with highest piezoresistive sensitivity to bending failure monitoring, it was observed that the CBCS2 exhibited the worst resistivity repeatability compared to those of CBCS05 and CBCS1. The slightly decreased electrical resistivity is mainly originated from the permanent compressed CBCS and the constant stress situation in the compression zones even at the bending moment of flexural failure. As previous studies

found that the CB particles could lower the mechanical properties of cementitious composites, the reason for the worst resistivity repeatability of CBCS2 is due to its relatively lower bearing capacity and the more compression deformations in the bending process. Overall, for the CBCS embedded at a longer distance (lower stress distribution zone) to the loading point in three-point-bending concrete beams, the minor changes of electrical resistivity can still alternatively to monitor the health of the beams in their service life.

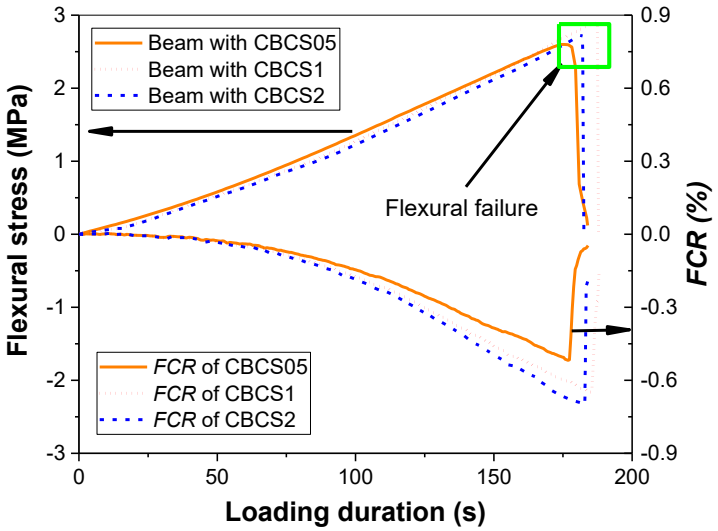

Figure 8.2. Resistivity of CBCS containing various CB contents with long distance to the central loading point in compression zone.

For the CBCS embedded in the closer distance (stress concentration zone) to the load point, apart from the similar alteration patterns for the flexural stress of beams and the electrical resistivity of CBCS as shown in Figure 8.2, much higher values of FCR were observed in Figure 8.3 compared to the above mentioned ones with longer distance from the loading point. In general, the CBCS2 once again performed the best piezoresistive sensitivity by the larger changes of FCR, which was followed by the moderate sensitivity of CBCS1 and the worst piezoresistive performances by CBCS05. Compare to the counterparts embedded in the long distance zone, the FCR values of CBCS05 nearly trebled and surged to 1.44%, and the values increased sharply to 1.82% and 1.96% for the CBCS1 and CBCS2, respectively in the flexural

failure. It indicates that the close distance areas were subjected to higher stress and deformation in the three-point-bending test, and thus the CBCS embedded in these zones can be more efficient to monitor the damage and health conditions of concrete structures to achieve excellent performances of cement-based sensors. However, it should be emphasized that the irreversible electrical resistivity also increased significantly, especially for the CBCS2, whose irreversibility increased from less than 0.3% to the values of higher than 0.5%. This may be attributed to the lower bearing capacity and the larger compression deformations induced by higher stress and closer distances among conductive CB particles, which could permanently decrease the electrical resistivity of CBCS. In comparison to the CBCS under uniaxial compression, whose final resistivity were increased after reaching 4.0 MPa cyclic compression, the results demonstrated that the embedded CBCS in unreinforced concrete beams never generated irremediable damages or cracks for the permanently increase in electrical resistivity.

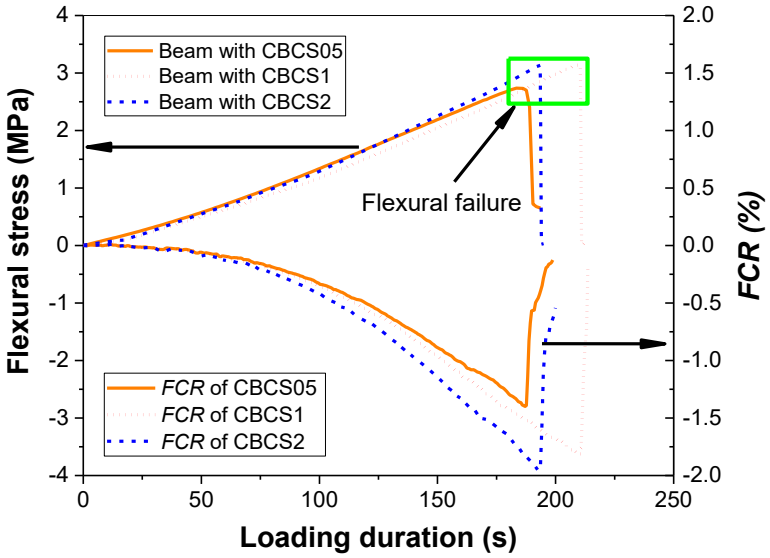

Figure 8.3. Resistivity of CBCS containing various CB contents with close distance to the central loading point in compression zone.

8.1.2.2 Tension zone

The CBCS embedded in the tension zone of three-point-bending beams were right below the loading point where presented the largest tensile stress concentration. Figure 8.4 displays the

electrical resistivity changes of embedded CBCS with the flexural stress development of unreinforced concrete beams. Compare to the CBCS in the compression zones, the embedded CB/cement-based sensors in the tension zone caused severe negativities on the ultimate flexural strength of the unreinforced concrete beams. The flexural strength of the beams embedded with CBCS05 reached 2.91 MPa, which considerably decreased to only 2.65 MPa and 2.48 MPa for those beams with sensors of CBCS1 and CBCS2 embedded, respectively. The low tensile capacity of cementitious composites and the stress concentration in the tension zones during three-point-bending test , demonstrating the need of high bearing capacity of beams in the tension zones, such as adding longitudinal reinforcements in concrete beams. Therefore, since the CB/cement-based sensors had poor mechanical properties as the increase of CB content, the CBCS with higher CB content were probably responsible for the reduced bending strength of the beams because of the poor tensile strength of CBCS themselves.

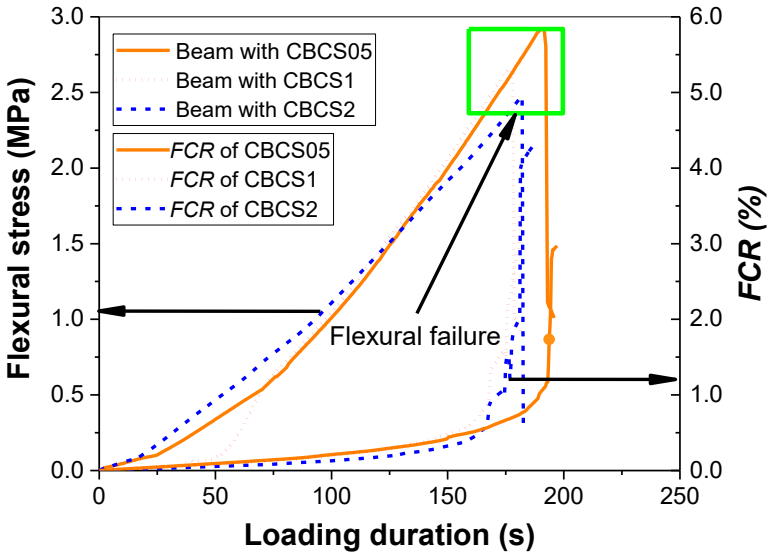

Figure 8.4. Resistivity of CBCS containing different CB contents in tension zone during three-point bending.

As for the electrical resistivity changes of CBCS in the tension zones, it showed completely opposite trend of FCR to the sensors in the compression zones. It was observed that the electrical resistivity increased with the flexural stress, especially with a sharp increase on FCR

at the moment of flexural failure of beams. This can be explicated by the conductive fillers of CBCS in tension, whose distances among CB particles are widened and thus increase the electrical resistivity. Similar to that of the CBCS in compression zones, the sensors with 2% CB (CBCS2) were provided with largest piezoresistivity of nearly 4.2% increase of FCR, and values of 3.4% and 3.1% were observed for the CBCS1 and CBCS05, respectively.

Another finding is that the electrical resistivity of CBCS never returned to the original values, once the beams were damaged by cracks. As mentioned above, the bending strength of unreinforced concrete beams partially depended on the bearing capacity of CBCS in the tension zone. In this circumstance, the CBCS were firstly destroyed when the beams came to the flexural loading capacity, and that is why the electrical resistivity was permanently increased in tension zone. On the contrary, the CBCS in the compression zones with lower stress were relatively intact even if the cracks throughout the beams occurred.

8.1.3 Beam stress monitoring

8.1.3.1 Compression zone

Figure 8.5 presents the FCR changes of the embedded sensors of CBCS05 (orange lines), CBCS1 (red lines) and CBCS2 (blue lines) subjected to cyclic flexural bending with the longer distance to the central load point in the compression zone. Generally all the sensors performed similar trends by the decreased electrical resistivity in the loading stage and increased resistivity in the unload process. It seems that the sensors of CBCS2 were given the highest monitoring sensitivity with the FCR linearly increased from 0.1% to 0.21% as the stress increased from 0.47 MPa to 0.94 MPa. The second is the CBCS1 which got a moderate sensitivity, but acquired a relatively unstable and fluctuated resistivity especially under the stress of lower stress magnitudes. Since 1% CB is in the range of percolation threshold for the CB/cementitious composites, which caused significant electrical resistivity alterations with minor changes of conductor contents and microstructures, and hence be responsible for the

fluctuated curves of CBCS1 in the initial stage. As for the sensors of CBCS05, the lowest sensitivity with FCR values of 0.08% and 1.5% for the stress magnitudes of 0.47 MPa and 0.94 MPa were observed, respectively. Generally, the stress monitoring ability of these sensors embedded in unreinforced concrete beams were competent for their self-sensing behaviours and flexural failure monitoring capacity.

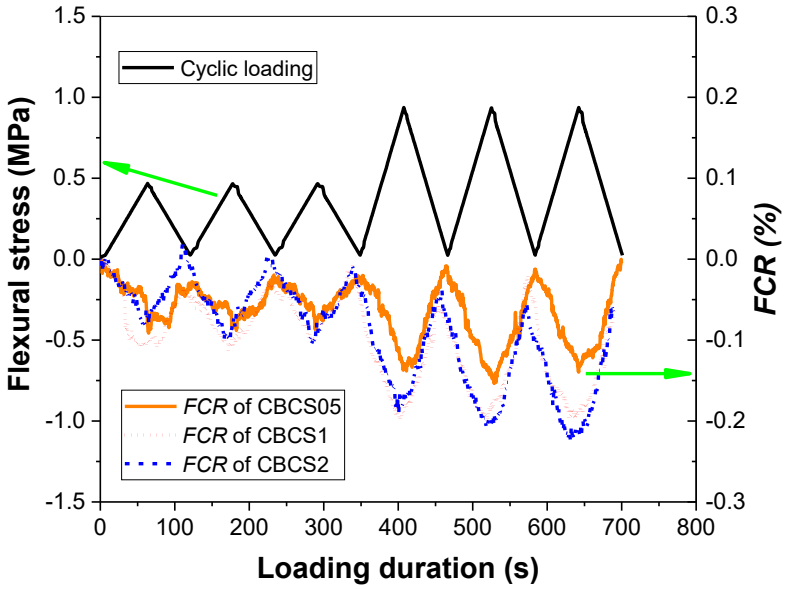

Figure 8.5. The FCR variations of embedded CBCS with the long distance to central load point in compression zones under cyclic flexural loading.

On the other hand, all the sensors expressed cyclic resistivity alterations on account of applied flexural stress on concrete beams. Even possessed worst sensitivity, the sensors CBCS05 were observed with best resistivity repeatability as the electrical resistivity almost returned to the initial values, while the electrical resistivity for both the CBCS1 and CBCS2 sensors permanently decreased by approximately 0.5% after the cyclic loading. This can be explained by the decreased mechanical properties of CB cementitious composites with increase of CB content, which became “softer” and easier to cause more deformations of sensors and closer distances among conductive CB particles to decrease the resistivity. Meanwhile, the phenomenon of reduced rather than increased electrical resistivity demonstrated that these

sensors were not destroyed to generate cracks in the compression. Moreover, slight electrical resistivity increases were arisen for the CBCS2 in the initial loading stage. Since the high content CB cementitious composites are more likely to agglomerate together to produce defects or weak zones in the composites, the initial resistivity increases were probably due to the densification on the CB agglomeration defects and weak zones by compression.

In terms of the sensors embedded with close distance to the load point in the compression zones of unreinforced concrete beams, their electrical resistivity changes under cyclic flexural stress were displayed in Figure 8.6. Compare to the sensors long distance to the load point, higher FCR values were observed for all CBCS with the FCR values of CBCS2 gradually increased from 0.2% to 0.4%, which were also doubled for the sensors CBCS05 and CBCS1. Similar to the CBCS1 with the long distance to load point, much more severe resistivity fluctuations were observed for the same sensors embedded with close distance to the loading point. The reason is identical to the above mentioned instability since the 1% CB is in the range of percolation threshold for CB/cementitious composites. In addition, Figure 8.6 represents that the sensors went through small stress magnitude exhibited excellent resistivity repeatability, while clear FCR irreversibility occurred when the stress magnitudes doubled. The irreversible FCR for CBCS1 reached 0.1% for CBCS05 and CBCS02, and higher than 0.2%. It demonstrates that the sensors maintained good performances under the stress magnitude of 0.47 MPa. However, high compressive stress, microcracks initiation and connected conductors occurred close to the loading point by the doubled stress magnitude. Furthermore, the especially severe irreversibility by CBCS1 is also probably due to the effect of slight percolation in the cementitious composites.

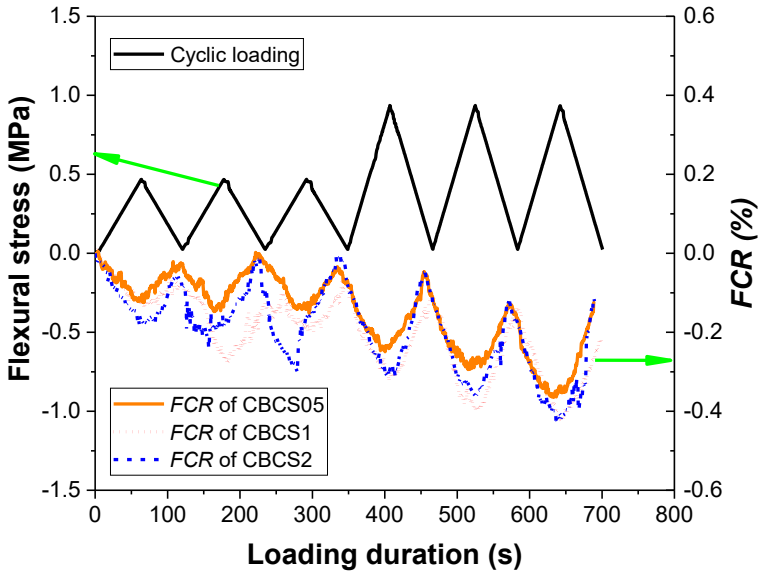

Figure 8.6. FCR alterations of embedded CBCS with close distance to the central loading point in compression zones under cyclic flexural loading.

Overall, for the majority of concrete structures with known load points, such as concrete beams and columns, the sensors close to the load point exhibit higher changes in electrical resistivity and seems easier to capture compared to the sensors far from the loading point. However, the drawbacks of slightly decreased repeatability and more fluctuated resistivity of sensors with high content of carbon black, especially for CBCS1 and CBCS2, should be particularly resolved in the future.

8.1.3.2 Tension zone

Figure 8.7 shows the electrical resistivity changes of embedded various CBCS in the tension zones under cyclic flexural stress. Contrary to the sensors in compression zones, those in tension zones showed increased electrical resistivity with the increase of flexural stress and decreased resistivity as the stress returned to the original level, indicating the tensile stress induced in the embedded sensors and the longer distance between carbon black particles in the tension zones. Generally, the sensors with 2% CB (CBCS2) possessed highest FCR values of slightly over 0.5% in the first three cycles and boomed to approximately 2% when the stress magnitudes doubled to 0.94 MPa. For the stress magnitude at 0.47 MPa, the sensors CBCS05

ranked the second sensitivity by the average FCR values reaching approximately 0.5% which were superior to that of CBCS1. This phenomenon is partially contributed to the gradually decreased resistivity in the loading process, which can be explained in Figure 8.7. However, when the applied stress increased to 0.94 MPa, the electrical resistivity changes of CBCS1 were consistent to the results in compression zone and gently higher than the FCR of CBCS05, with the values both approached to 0.18%.

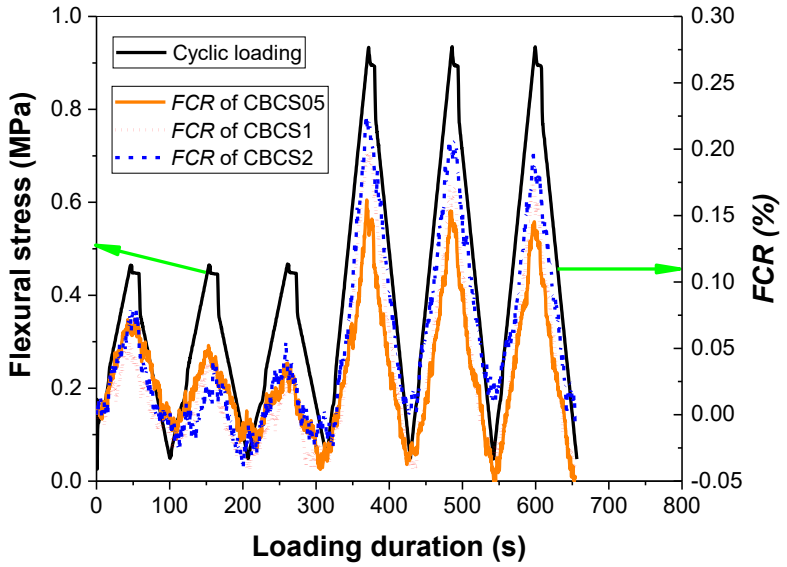

Figure 8.7. FCR alterations of embedded CBCS in tension zones of unreinforced concrete beams under cyclic flexural loading.

Even with the highest average FCR values for CBCS2, the tendency was observed that the gradually decreased electrical resistivity occurred for the sensors under the stress in low magnitudes. Similar phenomenon was observed for the CBCS1, which were responsible for the aforementioned smaller FCR values than that of CBCS05. To explicate the decreased electrical resistivity in tension zones, Figure 8.8 illustrates the stress conditions of sensors and the potential distributions of conductive CB particles and their agglomerations in the tension zones under flexural stress. Unlike the sensors under axial tension where the electrical resistivity increased gradually, the cement-based sensors in tension zone of beams subjected to bending moment still had partial regions under compression. It indicates that the electrical

resistance of sensors were dependent on the coupled actions of both compression and tension zones between two electrodes, and the actual resistivity was the combination of the resistivity decreases in the region under compression and the resistivity increases in the region under tension. For the sensors with high CB contents (CBCS1 and CBCS2), the compression zone was relatively easy to be compressed to cause the microcracks. Thus, the decreased electrical resistivity might compensate the resistivity increase in the tension zones and decrease the bulk electrical resistivity.

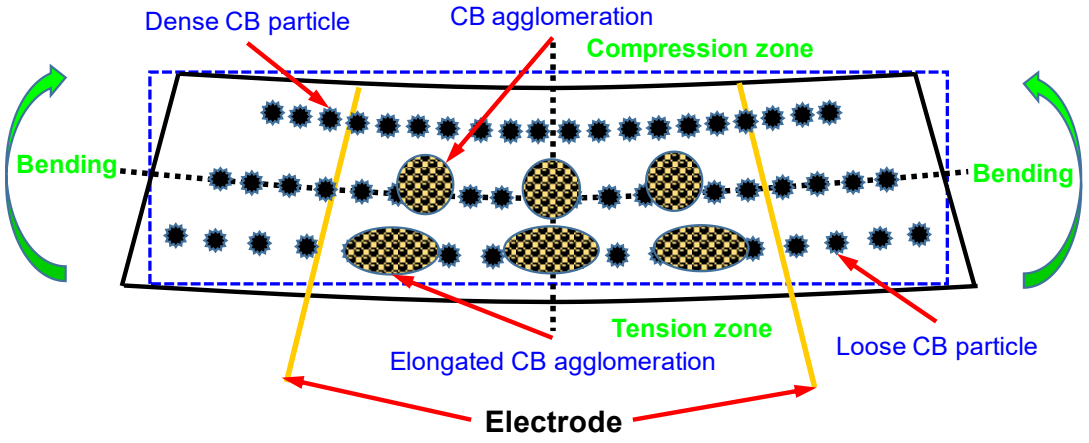

Figure 8.8. Potential distribution of conductive CB particles and agglomerations in CBCS embedded in the tension zones of unreinforced concrete beams.

Figure 8.9 depicts the micromorphology of CBCS by SEM. In particular, in spite of an appropriate treatment of ultrasonic dispersion, a small amount of CB agglomerations still was observed in the composites. These agglomerations had worse cohesion compared to hydration products, therefore, another reason for the decreased resistivity is owing to the deformation of CB agglomerations in the sensors with high CB contents, which were stretched and elongated in the direction of conductive paths during the bending test but could not returned back in the unloading process to perpetually decrease the bulk electrical resistivity . Moreover, since the cementitious composites are more sensitive to tensile stress because of their brittleness and low tensile strength , the electrical resistivity of cement-based sensors are more likely to increase

rather than decrease. Therefore, the slight resistivity reduction for CBCS in the tension zones may serve as an indicator to recognize no obvious damages happened in the tension zones.

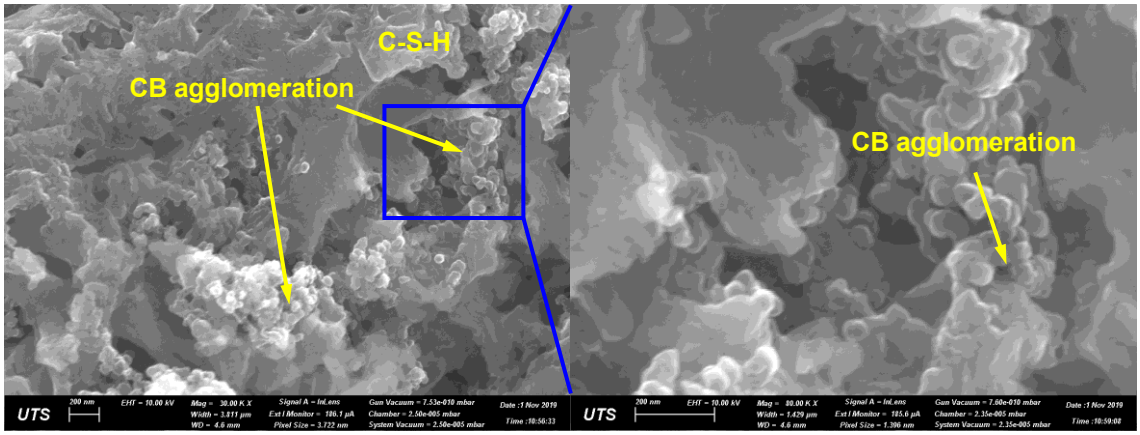

Figure 8.9. Morphology and microstructures of CBCS and the CB agglomerations.

8.2 Cement-based sensors in mortar slabs

8.2.1 Pre-connection of cement-based sensors

Different from direct load applied on the cement-based sensors, the embedded sensors are subjected to smaller distributed load because the surrounded cement matrix bears the majority of load, to affect the force transmission and sensing efficiency of cement-based sensors. As a consequence, the cement-based sensors connected in series are proposed to magnify the sensing ranges and electrical resistivity changes, through collecting the resistivity changes from all cement-based sensors in multiple locations under compression. As shown in Figure 8.10, multiple cement-based sensors are connected through electrical soldering on the joints, which were then coated by insulated glue to eliminate the influence from pore solutions after being embedded into cement mortar slab.

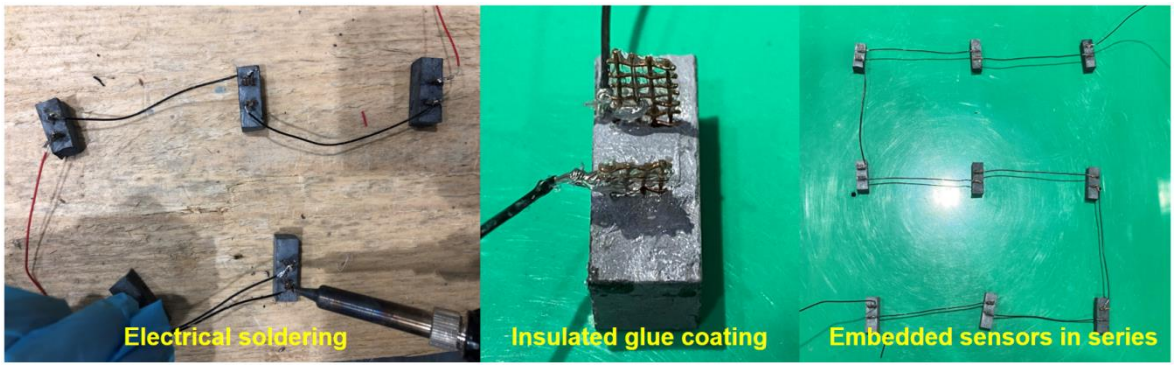

Figure 8.10. The joint connection, insulated glue coating and final cement-based sensors in series

8.2.2 Cement mortar slab and sensors embedding

The cement mortar is manufactured with identical mix proportion to that of cement-based sensor, expect for the addition of conductive filler. Then the sand to binder ratio of 2.0 is chosen for all mortar slabs. The embedding of cement-based sensors are carried out after the preparation of fresh cement mortar and during its casting process, as shown in Figure 8.11. The size of mould prepared for the mortar slab is 450 mm ×450 mm ×120 mm. After casting the mould to the height of approximately 70 mm, the cement-based sensors connected in series are manually inserted into the cement mortar one by one with the plane of the electrode being parallel to the up/down surface of mortar slab. It should be noted that the casting and sensors embedding procedures are better conducted in the vibration table and accompanied with moderate vibration, in order to reduce air pores of cement mortar slab and improve interfacial transition zones (ITZ) among cement-based sensors and mortar slab.

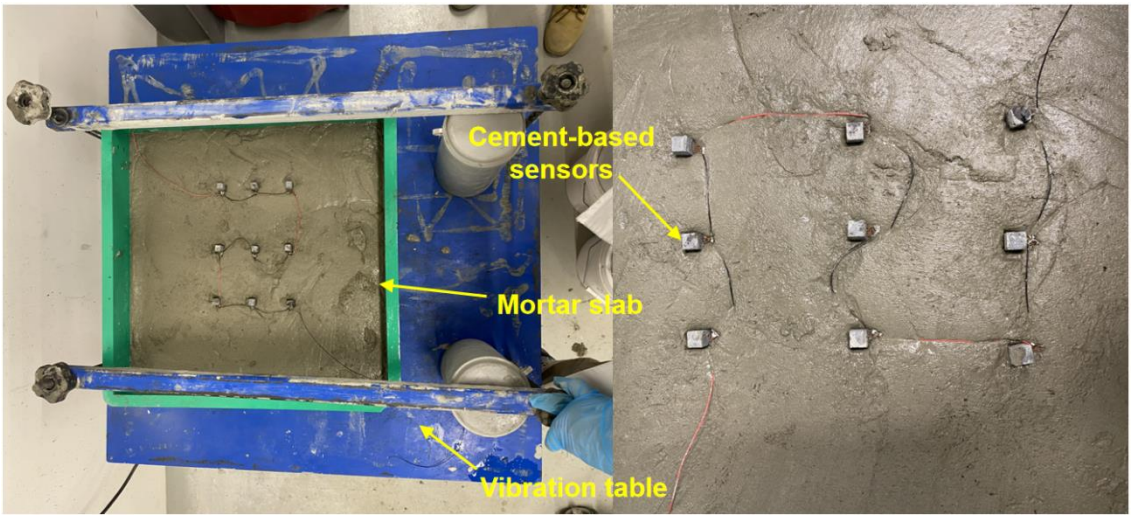

Figure 8.11. Insertion of cement-based sensors to cement mortar slab during casting.

8.2.3 Application of cement-based sensors for human motion detection

8.2.3.1 Feet up or down test

The application of cement-based sensors for human motion detection is a key step for future smart infrastructures. It has wide application potential, including people counting, crowd flow monitoring, housing security, and even body weighing. Figure 8.12 shows the electrical resistivity changes of cement mortar slab with the human motions of feet up and feet down. It could be found that the FCR possessed a clear relationship with the human motion of feet up or down. The largest FCR was in the range from -1.3% to -1.0% in the first 10 cycles when the feet were totally on the slab, and the smallest FCR was around -0.15% as the feet down the mortar slab. The average FCR was approximately -1.09% at the peaks. For the second 10 cycles, the average FCR was gently decreased to -0.92%, indicating the released irreversibility after preloading. It should be noted that the FCR could almost return to the initial value after the feet up and down tests, indicating that the human weight will not greatly affect the inner structures of cement-based sensors and maintain an intact conductive passages.

It was observed that the FCR values failed to turn back to the original values during human motions of feet up and down test. Two potential reasons were responsible for the irreversibility.

Firstly, the 10 cycles of feet up and down were carried out in 22 seconds (2.2 s for each cycle). Different from the static compression test, the irreversible FCR might be enhanced in the dynamic loading because of the hysteresis behaviour of cement-based sensors. Secondly, the data collection rate in this study is five datums per second, increasing the rate of electrical resistance acquisition might reduce the FCR irreversibility during human motion detection. In addition, it could be observed the noise of FCR especially in the step of feet down test. Given nine cement-based sensors were connected in series and embedded in the mortar slab, the noise was mainly depended on the exact location of feet landing on the cement mortar slab. To improve the accuracy and serviceability of cement-based sensors, the relationships between FCR changes and weight location on the cement-based sensors should be further investigated.

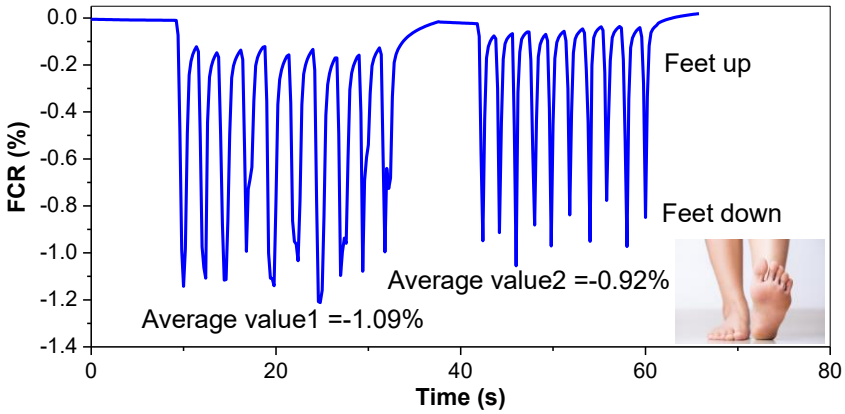

Figure 8.12. Self-sensing performance of cement mortar slab under human motion of feet up and down.

8.2.3.2 Jump motion test

Figure 8.13 displays the electrical resistivity changes of embedded cement-based sensors when the mortar slab subjected to human jump load. Totally three cycles with each cycle containing of 10 times of jump were carried out. It should be noted that the FCR of cement-based sensors did not return to the initial value during jumping, because of the pushing force in the beginning of jumping and the hysteresis behaviour of cement-based sensors. Therefore, different from the motion of 'up-down' feet, the red and green regions with an irreversible FCR and different

FCR peaks could be observed, respectively. As aforementioned that the body weight was applied on the mortar slab all the time during jumping, it could be found that the FCR changes of cement-based sensors out of body weight were around -1% in red region. This value is very close to the above-mentioned FCR changes of cement-based sensors exposure to motion of 'up-down' feet, when all the body weight was applied on the mortar slab. During jumping on the mortar slab, two dynamic loads by pushing off mortar slab and the following drop impact can be produced. The sudden impact load can generate larger FCR peaks as shown in the green regions. These peaks are changeable in the ranges of -2% to -3%, due to the changes of drop point. In addition, in comparison to the stable output of 'up-down' feet test, the more violent fluctuations were also related to the multiple jumping heights and the gravity centres of human body. Overall, the experimental results of this study showed a potential of smart concrete structures with embedded self-sensing cement-based sensors to detect human motions.

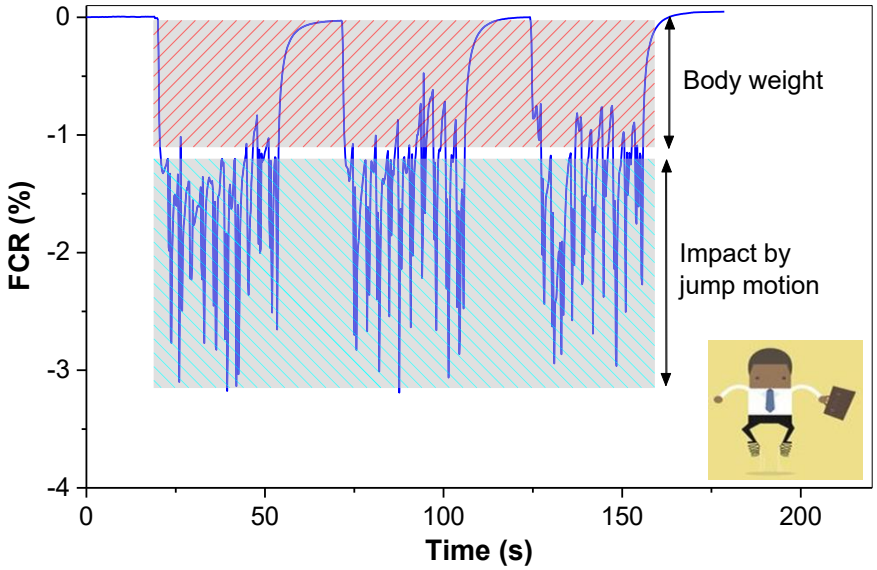

Figure 8.13. Self-sensing performance of cement mortar slab under human motion of jump up/down.

8.2.4 Application of cement-based sensors for vehicle speed detection

8.2.4.1 Self-sensing ability in different vehicle speeds

Figure 8.14(a) to (h) shows the output electrical signal of cement mortar slab with a car driving over in multiple speeds ranging from approximately 2.0 km/h to 40 km/h. Two peaks could be observed in the output electrical signal, respectively are the front wheel and back wheel of the tested car applying on the cement mortar slab. Therefore, based on the simple Eq. (1):

$$V = \frac{L}{t} \tag{1}$$

where: L the distance between front and back wheels, which is a constant value of 2.775 m in this study; t the time interval between two obtained electrical peaks, and we can easily calculate the V of car speed.

Regarding to the output FCR of cement mortar slab, several phenomena are worthy to be discussed. Firstly, the FCR peaks are different among front and back wheels, with the FCR values of front wheel are always larger than that of back wheel. The 2013 Toyota Camry Altise is a front-wheel-drive car which powered by an engine in the front. Therefore, the larger FCR of front wheel is mainly attributed to the fact that the position of gravity centre of the car is closer to the front wheels, so that the car load applied on the mortar slab is larger than that by back wheel. Secondly, with the increasing car speed, the second peak of FCR was becoming harder to distinguish, particularly for the car speeds of 30 km/h and 40 km/h. Therefore, to detect high-speed vehicles, the advanced data acquisition system with a higher data collection rate should be applied. For instance, the time interval is approximately 0.1 s for the tested car at the speed of 100 km/h. It means that at least 10 electrical signals should be collected to ensure the capture of FCR peaks under front and back wheels. Thirdly, it could be observed the changed baseline of FCR before and after car driving over test, especially for the car load with high speed. Given the cement mortar slab is moveable and just placed in the pavement rather than embedded and fixed into the pavement, the high-speed passing car can drag and

mobilize the mortar slab to affect the electrical signal output. Fortunately, this problem can be easily solved in a practical application by embedding or fixing cement-based sensors or mortar slabs to detected concrete infrastructures such as pavements and bridges.

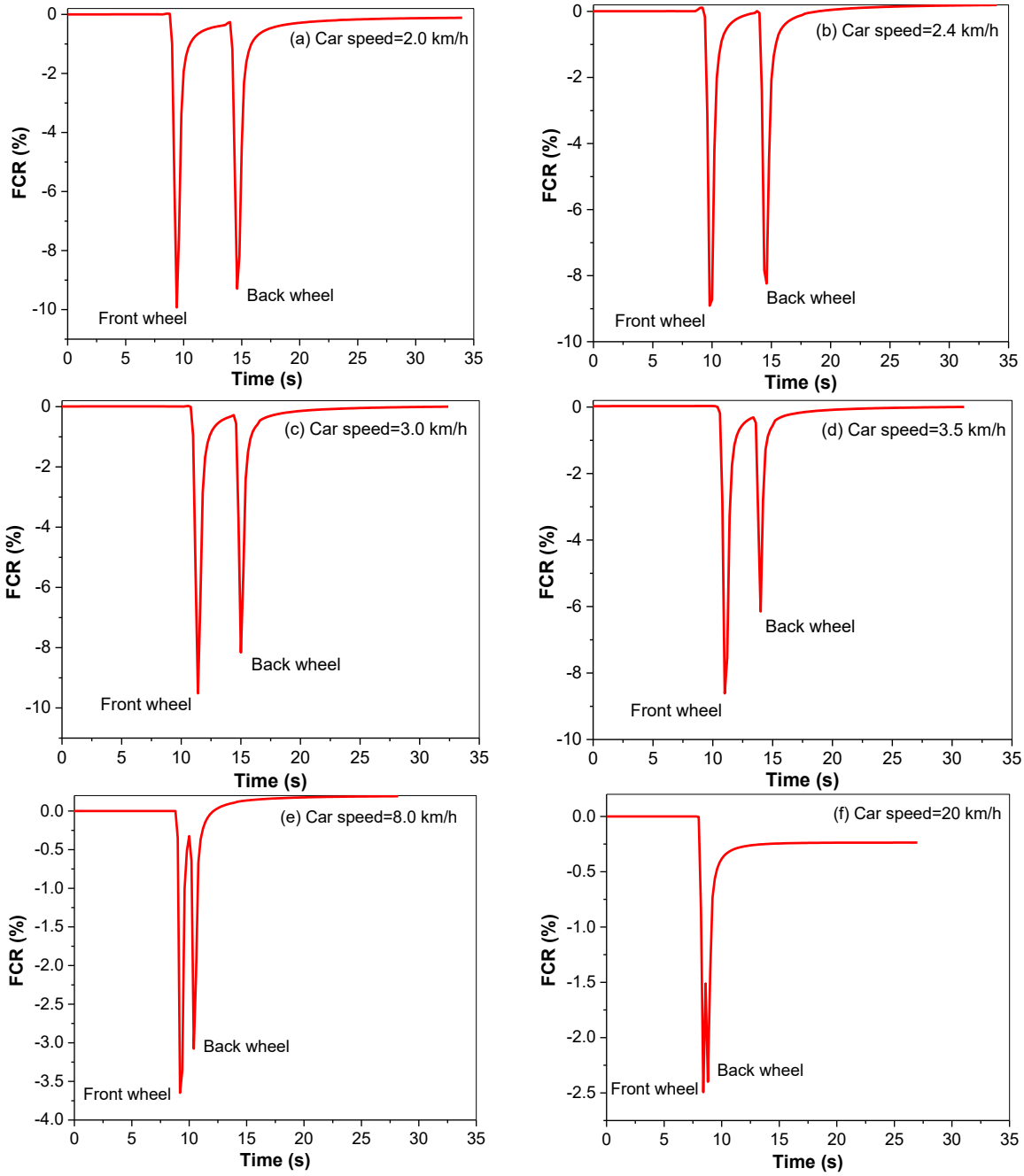

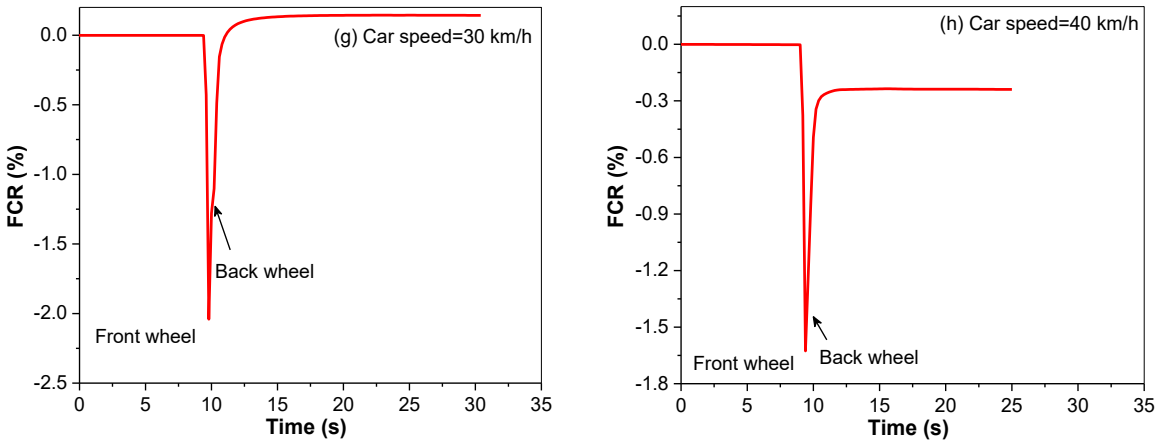

Figure 8.14. Self-sensing performance of cement mortar slab under traffic load with different speeds.

Above figures have showed the FCR peaks under the speed of 2.0, 2.4, 3.0, 3.5, 8.0, 20, 30, and 40 km/h based on the speed indicator. Figure 8.15 compares the car speed between indicator and calculated speed based on the FCR peaks. It could be found that the calculated speed from FCR peaks have high degree similarity to the speed from indicator, indicating that the cement-based sensors embedded cement mortar slab was capable of monitoring the traffic volume and vehicle speed. Limited to the laboratory space and the multimeters, the largest car speed tested is approximately 40 km/h. As mentioned previously, the larger car speed monitoring can be achieved in full-scale pavement test with matched data acquisition system.

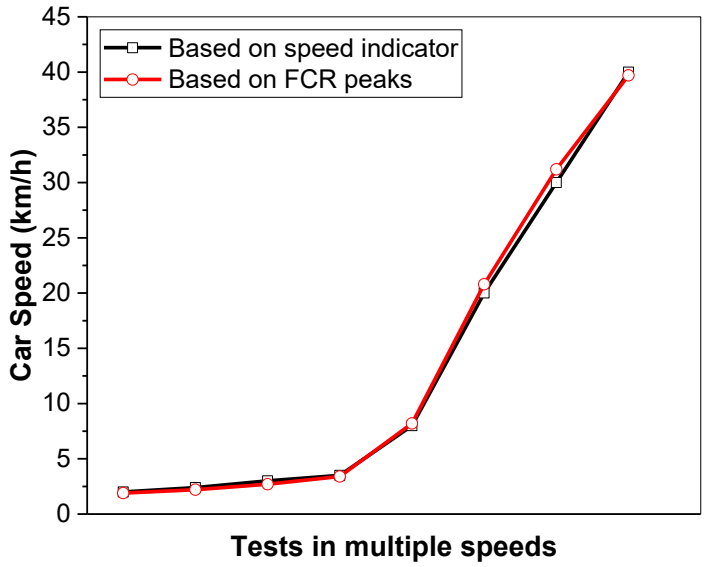

Figure 8.15. Car speed discrepancy based on the speed indicator of car and the FCR peaks.

8.2.4.2 Relationship between FCR to vehicle speed

This study firstly observed the decreased FCR peaks with increasing car speed. Figure 8.16 displays the largest FCR values of front and back wheels as a function of car speed. The reduction of FCR with increasing speed can be explained by the following reason, based on the Bernoulli equation:

$$p + \frac{1}{2}\rho v^2 + \rho g h = C \quad (2)$$

where: p the intensity of pressure; ρ the fluid density; v the fluid speed; C is a constant; g the acceleration of gravity and h the height. With increasing car speed, the air above car moves faster than the air under the car, which results in a larger air pressure under the car. Therefore, the main reason could be the reduced carload applying on the cement mortar slab, because of the generated lift force by high-speed moved air.

In particular, the relationship between largest FCR and vehicle speed could be another index to predict the car speed, to adjust the obtained car speed based on the FCR peaks. According to the character of obtained data, the three-parameter logarithmic fitting was determined to predict relationship among largest FCR to car speed. The fitting curves and formulas are attached with the obtained data as shown in Figure 8.16(a) and (b). On the one hand, the vehicle speed higher than 40 km/h was not tested due to limited lab space, the fitting curves enabled to predict the largest FCR of cement-based sensors and detect the vehicle speed exceeding 40 km/h. On the other hand, in the case of missing data of either front wheel or back wheel, the fitting curves could be another way to evaluate the vehicle speed.

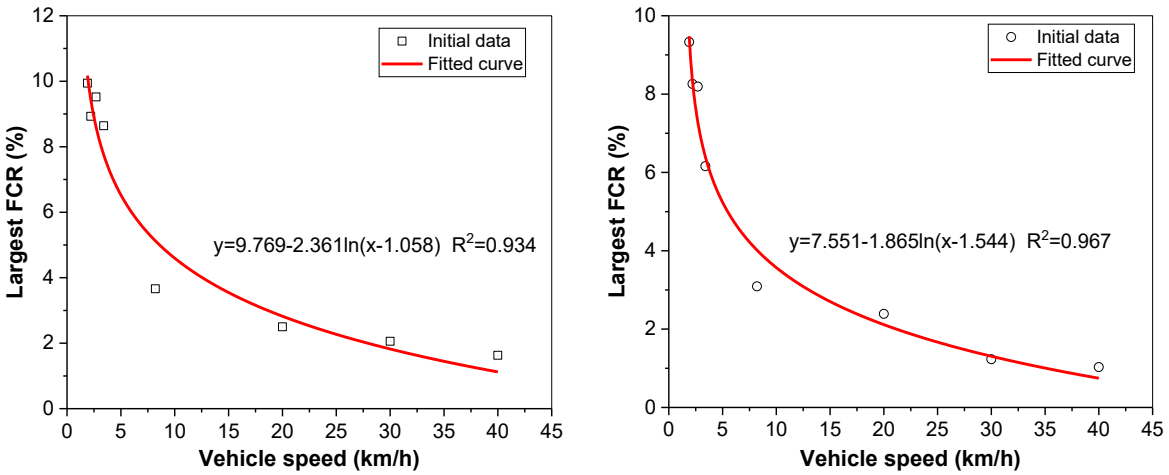

(a) Front wheel (b) Back wheel

Figure 8.16. Relationship between largest FCR of wheels and vehicle speed under logarithmic fitting.

8.3 Summary

The Self-sensing properties of cement-based sensors embedded in both compression and tension zones of concrete beams were investigated to monitor the stress magnitude and failure process. In addition, the cement-based sensors were embedded in mortar slab to evaluate the capacity of monitoring human motion and traffic speed. The main conclusions could be drawn up as follows:

(1) Cement-based sensors with 0.5%, 1% and 2% CB contents (weight of binder) performed high FCR changes under direct uniaxial compression, and the sensors with 2% CB exhibited the best fractional changes of resistivity and monitoring sensitivity compared to those with 0.5% and 1% CB. In addition, the cement-based sensors can successfully monitor the stress magnitude and failure initiation in the concrete beam under three-point bending load. Similarly, the best performances are achieved by the sensors with 2% CB.

(2) The embedded cement-based sensors with close distance to the loading point presented higher electrical resistivity changes in the concrete beam under three-point-bending because of the higher stress magnitude than that embedded with long distance to the loading point.

(3) Cement-based sensors in the compression zones of the beam exhibit gradual decrease in electrical resistivity but then suddenly returned to their initial resistivity values when approaching the flexural failure. However, the counterparts in the tension zones experienced an increase in electrical resistivity followed a further abrupt jump near the flexural failure.

(4) CB/cement-based sensors in the tension zones showed increased electrical resistivity with the increase of flexural stress, and then decreased resistivity as the flexural stress returned to its original values. This indicates there are tensile micro cracks and elongated distances among carbon black particles in the tension zones.

(5) In the 'up-down' feet test, the FCR showed a peak at the feet down, and then returned to the initial values at the feet up. The small irreversible FCR could be due to the low data collection rate of multimeter. The results demonstrated that the smart mortar slab with the existence of cement-based sensors could be used to detect human traffic.

(6) In the jump movement test, in addition to the human weight induced FCR, the dynamic loads by pushing off mortar slab in the beginning of jumping and the following drop impact can generate another FCR peaks. It can be an index for the smart mortar slab to detect several specific human movements.

(7) The exact vehicle speed can be calculated based on the two peaks induced by the front and back wheels. With increasing vehicle speed, the FCR gradually decreased because the lift force on the bottom of vehicle increased to decrease the applied vehicle load.

CHAPTER 9: CONCLUSIONS AND RECOMMENDATIONS

Multiple experiments have been conducted regarding the piezoresistivity of cement-based sensors containing conductive rubber products and carbon nanomaterials. Subsequently, the cement-based sensors with enhanced conductivity and piezoresistivity under the assist of additives have been developed. Then, the effects of working environments on the performance of cement-based sensors were explored, followed by the development of multifunctional cementitious materials with integrated self-sensing, self-healing, self-cleaning and superhydrophobicity properties. The last section involves the practical application of cement-based sensors in concrete beams and mortar slabs, for the evaluation of self-sensing performances in concrete structures. The specific conclusions and recommendations of each chapter are listed below:

9.1 Conductive rubber products as fillers in cement-based sensors

- The electrical conductivity of the CB/cementitious composites was improved by the conductive rubber fibres. The more rubber fibres, the better conductivity is. The percolation threshold was clearly decreased for the 0.5–1.0 wt% CB/cementitious composites embedded with 80 rubber fibres (1.27 vol%).
- The improved gauge factor indicated the great application potential for the application of CB/conductive rubber cement-based composites to monitor concrete structural health or pavement traffic conditions in low cost and high sensitivity.
- Four conductive and piezoresistive mechanisms based on experimental results were proposed for the rubber/cement composites, including the conductive passages created by penetrated pores, connected rubber fibres and pores. Among them, the conductive

rubber fibres played a dominant role to influence the electrical conductivity and piezoresistivity.

- The percolation never generated for the modified cement mortar filled with different conductive rubber crumbs from 10 to 40%, as a result of separately distributed rubber crumbs in the composites. It seems that the larger particle sizes of rubber crumbs compared to the commonly used conductive nanoparticles were responsible for this phenomenon.

9.2 Carbon nanomaterials as fillers in cement-based sensors

- For composites filled with 0.1 wt%, 0.5 wt%, 1.0 wt%, 2.0 wt% and 4.0 wt% CB, the w/b ratios of 0.31, 0.32, 0.34, 0.4 and 0.5, respectively, could provide the composites with similar and excellent workability. The compressive strength of cementitious composites was more sensitive to the CB content, and decreased to approximately 15 MPa for the 4.0 wt% CB/composites.
- The sizes of CNT agglomerations in the LDCC were in the ranges of several microns to dozens of microns. The smaller sized agglomerations had smoother boundaries and became more spherical. In contrast, the larger sized agglomerations possessed worse roundness and led to more similar shaped pores, which might cause stress concentration in cementitious composites and reduce mechanical properties.
- The cementitious composites with CNT (both UDCC and LDCC) were provided with intrinsic stress-sensing ability. The UDCC possessed excellent stability, repeatability, as well as satisfactory sensing efficiency. For LDCC, although the sensing efficiency increased with the increase of CNT layers, the increased CNT layers exacerbated the irreversibility and deviation of resistivity output.
- For the UDCC and LDCC with similar piezoresistivity, the dosage of CNT used is significantly reduced for LDCC. The CNT in LDCC2 only accounted for approximately

2.2% for the total amount of CNT in UDCC. Therefore, the self-sensing cementitious composite with layered CNT for piezoresistive capacity could greatly reduce the cost of CNT.

9.3 Enhanced conductivity and piezoresistivity with additives

- Conductive rubber had capacity to improve the gauge factor of 0.5 wt% CB/cementitious composites, by the growth rate of 78.4% compared to the results from other literatures. For 1.0 wt% CB/cementitious composites, the gauge factor significantly increased to hundreds of times higher than commercial strain gauge but with worse linearity to compressive strain, because of the phenomenon of piezoresistive percolation; Since the better conductivity for the composites with 2 wt% CB, conductive rubber rarely influenced its conductivity and piezoresistivity.
- Although the PP fibres were electrically insulative, the enclosed CB nanoparticles on the surface could increase the conductive passages through PP fibres, thus the electrical conductivity of the cementitious composite was enhanced with the increase of PP fibres.
- The compressive stress sensing efficiency linearly increased with the increase of PP fibres, regardless of the various loading rates. The higher sensitivity was attributed to more contact points, which was much easier generated by conductive PP fibres rather than the spherical CB nanoparticles.
- Electrical resistance and the flowability of CB-cementitious composites monotonically decreased with the increase of SF. The water absorption of the composites reached the lowest value when reinforced with 10% SF. The setting time firstly increased with the SF and then decreased when SF dosage reached 20%.
- Piezoresistivity of CB-cementitious composites was significantly improved with the addition of SF, especially with 10% SF. The FCR values altered rapidly in the initial loading stage, and then gradually slowed down with the increased compressive stress.

The specimen with 5 and 10% SF exhibited better piezoresistivity under the constant stress compared to the one with 20% SF.

9.4 Piezoresistivity interference from working environment

- After removing the heat exchanges interference, the piezoresistive properties of CB/cementitious composites were independent from the temperature variations ranging from -20 °C to 100 °C, and showed both satisfactory sensitivity and repeatability of piezoresistivity.
- With the increase of water content, in addition to the increased electrical resistivity, the piezoresistive sensitivity of CB/cementitious composites firstly increased but then decreased, and the optimal water content was found out around 8%. Moreover, the high water content in the cementitious composites could make the resistivity behaviours fluctuate widely.
- The freeze-thaw cycles exhibited limited impacts on the electrical resistivity of dry CB/cementitious composites, but the induced higher compression strain still caused reduced gauge factor and slightly lower piezoresistive sensitivity with reduction of 11.9%. However, both the electrical and mechanical properties of saturated CB/cementitious composites were greatly affected by the freeze-thaw cycles, which resulted in the decreased piezoresistive sensitivity by 30.7%.
- The intact GNP/cementitious composite before erosion exhibited excellent piezoresistivity for SHM as cement-based sensors. However, after 90 and 180 days of sulphuric acid erosion, the piezoresistivity was strongly affected with less linearity and repeatability. In particular, after subjected to 3% H_2SO_4 solutions, the FCR changes under low and high loads presented extremely high and low, respectively.
- Under the impact energy of 18.72×10^{-4} J/cm^3, cementitious composites after hundreds of times impact exhibited a swift resistivity reduction under low loads during cyclic

compression. This is due to the emerged micro-cracks and voids that could be compressed and closed during cyclic compression at low stress magnitude.

9.5 Self-sensing cementitious composites with multifunctionality

- Novel microencapsulation of nano-carbon black (NCB) enclosing slaked lime (SL) was applied for multifunctional cementitious composite with integrated self-sensing and self-healing capacities. The piezoresistivity was achieved by the excellent conductivity of NCB. As the preserved SL particles were released after the generation of cracks, and the cracks self-healing occurred. The results provide a novel microencapsulation of NCB containing self-healing agent of SL to improve the self-sensing and self-healing performances of smart cementitious composite.
- The water absorption of cementitious composites decreased with the addition of GNP, and specimen with 1% GNP exhibited slightly better impermeability than that with 2% GNP. The usage of SHP greatly decreased the water absorption, especially for the specimen with 2% SHP, which reduced the water absorption by more than 15 times. The water contact angle of the plain cement paste was only 53.5°, while the highest contact angle of 86.4° was found for the specimens with 1% GNP and 1% SHP.
- Regardless of the GNP contents, treatment of water immersion significantly affected the piezoresistive performances of cementitious composites without SHP, because of the penetrated water and induced polarization effect. But with addition of SHP, the influence was controlled with minor fluctuations. The hydrophobic films were established on the surface of specimen, GNP, cracks and pores, which prohibited further water movements.
- A trichloro-silane penetrated graphene nanoplate filled cement-based sensor was developed. It was found that this sensor possessed integrated superhydrophobicity, self-cleaning and self-sensing properties. It had a high stress/strain sensing ability with a

gauge factor of 141.8. The water contact angle of the intact sensor surfaces reached 163°, indicating an excellent hydrophobic behaviour. The self-cleaning performance of the sensor, assessed with visual inspection of carbon dust and sauce stain removing subjected to water rinsing, was much superior to the sensor without silane treatment, especially on the hydrophilic carbon dust cleaning.

9.6 Cement-based sensors in small concrete beams and mortar slabs

- The embedded cement-based sensors with close distance to the loading point presented higher electrical resistivity changes in the concrete beam under three-point-bending because of the higher stress intensity than that embedded with long distance to the loading point.
- Cement-based sensors in the compression zones of the beam exhibit gradual decrease in electrical resistivity but then suddenly returned to their initial resistivity values when approaching the flexural failure. However, the counterparts in the tension zones experienced an increase in electrical resistivity before a further abrupt jump near the flexural failure.
- For the cement-based sensors with high CB content (CBCS2), the electrical resistivity in the compression zone after cyclic flexural bending had possibility to decrease. This may be due to the connections of the elongated CB agglomerations in the direction of electronic movement because of the compressive stress.
- CB/cement-based sensors in the tension zones showed increased electrical resistivity with the increase of flexural stress, and then decreased resistivity as the flexural stress returned to its original level. It indicates the tensile microcracks and enlarged distances among carbon black particles in the tension zones.
- In the ‘up-down’ feet test, the FCR showed a peak at the feet down, and then returned to the initial values at the feet up. The small irreversible FCR could be due to the low

data collection rate of multimeter. The results demonstrated that the smart mortar slab with the existence of cement-based sensors could be used to detect human traffic.

- In the jump movement test, in addition to the human weight induced FCR, the dynamic loads by pushing off mortar slab in the beginning of jumping and the following drop impact can generate another FCR peaks. It can be an index for the smart mortar slab to detect several specific human movements.
- The exact vehicle speed can be calculated based on the two peaks induced by the front and back wheels. With increasing vehicle speed, the FCR gradually decreased because the lift force on the bottom of vehicle increased to decrease the applied vehicle load.

9.7 Recommendations for future works

- Cement-based sensors have been developed for more than 20 years, but their commercial applications are still very limited. To make a breakthrough, sensors are required to have high piezoresistivity effectiveness, sensitivity, and accuracy. Further studies on the sensor composites should be focused on the optimisation of matrices and additives.
- More investigations shall be carried out to study the layout of sensors for concrete structures so as to find desirable locations for sensors to capture the characteristics of concrete in field services. Consequently, a sensor network for concrete structures may be further investigated.
- Future challenges on the practical application of functional cement-based sensors include the effect of environmental factors, electrical signal collection, sensors calibration, and the understanding of their long-term behaviours and so on.
- In addition to the piezoresistivity explorations on the cementitious composites with various conductors, more attempts should be focused on how to promote the application of cement-based sensors toward smart structural health monitoring.

REFERENCES

Aghlara, R. & Tahir, M.M. 2018, 'Measurement of strain on concrete using an ordinary digital camera', *Measurement*, vol. 126, pp. 398-404.

Al-Dahawi, A., Sarwary, M.H., Öztürk, O., Yıldırım, G., Akın, A., Şahmaran, M. & Lachemi, M. 2016, 'Electrical percolation threshold of cementitious composites possessing self-sensing functionality incorporating different carbon-based materials', *Smart Materials and Structures*, vol. 25, no. 10, p. 105005.

Andrawes, B. & Chan, L.Y. 2012, 'Compression and tension stress-sensing of carbon nanotube-reinforced cement', *Magazine of Concrete Research*, vol. 64, no. 3, pp. 253-8.

Azhari, F. 2008, 'Cement-based sensors for structural health monitoring', University of British Columbia.

Azhari, F. & Banthia, N. 2012, 'Cement-based sensors with carbon fibers and carbon nanotubes for piezoresistive sensing', *Cement and Concrete Composites*, vol. 34, no. 7, pp. 866-73.

Baeza, F.J., Galao, O., Zornoza, E. & Garcés, P. 2013a, 'Effect of aspect ratio on strain sensing capacity of carbon fiber reinforced cement composites', *Materials & Design*, vol. 51, pp. 1085-94.

Baeza, F.J., Galao, O., Zornoza, E. & Garcés, P. 2013b, 'Multifunctional cement composites strain and damage sensors applied on reinforced concrete (RC) structural elements', *Materials*, vol. 6, no. 3, pp. 841-55.

Banthia, N., Djeridane, S. & Pigeon, M. 1992, 'Electrical resistivity of carbon and steel micro-fiber reinforced cements', *Cement and Concrete Research*, vol. 22, no. 5, pp. 804-14.

Barr, B. & Baghli, A. 1988, 'A repeated drop-weight impact testing apparatus for concrete', *Magazine of Concrete Research*, vol. 40, no. 144, pp. 167-76.

Buoso, A., Coppola, L. & Corazza, F. 2011, 'Electrical properties of carbon nanotubes cement composites for monitoring stress conditions in concrete structures', *Applied Mechanics and Materials*, vol. 82, Trans Tech Publ, pp. 118-23.

Butler, L.J., Gibbons, N., He, P., Middleton, C. & Elshafie, M.Z. 2016, 'Evaluating the early-age behaviour of full-scale prestressed concrete beams using distributed and discrete fibre optic sensors', *Construction and Building Materials*, vol. 126, pp. 894-912.

Cai, H. & Liu, X. 1998, 'Freeze-thaw durability of concrete: ice formation process in pores', *Cement and Concrete Research*, vol. 28, no. 9, pp. 1281-7.

Cao, J. & Chung, D.D.L. 2002, 'Damage evolution during freeze–thaw cycling of cement mortar, studied by electrical resistivity measurement', *Cement and Concrete Research*, vol. 32, no. 10, pp. 1657-61.

Chacko, R.M., Banthia, N. & Mufti, A.A. 2007, 'Carbon-fiber-reinforced cement-based sensors', *Canadian Journal of Civil Engineering*, vol. 34, no. 3, pp. 284-90.

Chang, Z.-T., Song, X.-J., Munn, R. & Marosszeky, M. 2005, 'Using limestone aggregates and different cements for enhancing resistance of concrete to sulphuric acid attack', *Cement and Concrete Research*, vol. 35, no. 8, pp. 1486-94.

Chen, B., Wu, K. & Yao, W. 2004, 'Conductivity of carbon fiber reinforced cement-based composites', *Cement and Concrete Composites*, vol. 26, no. 4, pp. 291-7.

Chen, P.-W. & Chung, D. 1995, 'Improving the electrical conductivity of composites comprised of short conducting fibers in a nonconducting matrix: The addition of a nonconducting particulate filler', *Journal of Electronic Materials*, vol. 24, no. 1, pp. 47-51.

Chen, P.-W. & Chung, D. 1996, 'Concrete as a new strain/stress sensor', *Composites Part B: Engineering*, vol. 27, no. 1, pp. 11-23.

Chen, S., Collins, F.G., MacLeod, A.J.N., Pan, Z., Duan, W. & Wang, C.M. 2011, 'Carbon nanotube–cement composites: A retrospect', *The IES Journal Part A: Civil & Structural Engineering*, vol. 4, no. 4, pp. 254-65.

Chuah, S., Pan, Z., Sanjayan, J.G., Wang, C.M. & Duan, W.H. 2014, 'Nano reinforced cement and concrete composites and new perspective from graphene oxide', *Construction and Building Materials*, vol. 73, pp. 113-24.

Chung, D. 2005, 'Dispersion of short fibers in cement', *Journal of Materials in Civil Engineering*, vol. 17, no. 4, pp. 379-83.

Costa, P., Silva, J., Ansón-Casaos, A., Martinez, M., Abad, M.J., Viana, J. & Lanceros-Méndez, S. 2014, 'Effect of carbon nanotube type and functionalization on the electrical, thermal, mechanical and electromechanical properties of carbon nanotube/styrene–butadiene–styrene composites for large strain sensor applications', *Composites Part B: Engineering*, vol. 61, pp. 136-46.

Cutler, H.E., Wang, K., Schaefer, V.R. & Kevern, J.T. 2010, 'Resistance of Portland cement pervious concrete to deicing chemicals', *Transportation Research Record*, vol. 2164, no. 1, pp. 98-104.

Dai Pang, S., Gao, H.J., Xu, C., Quek, S.T. & Du, H. 2014, 'Strain and damage self-sensing cement composites with conductive graphene nanoplatelet', *Sensors and Smart Structures Technologies for Civil, Mechanical, and Aerospace Systems 2014*, vol. 9061, International Society for Optics and Photonics, p. 906126.

Dai, Y., Sun, M., Liu, C. & Li, Z. 2010, 'Electromagnetic wave absorbing characteristics of carbon black cement-based composites', *Cement and Concrete Composites*, vol. 32, no. 7, pp. 508-13.

Dalal, S.P. & Dalal, P. 2021, 'Experimental investigation on strength and durability of Graphene Nanoengineered concrete', *Construction and Building Materials*, vol. 276, p. 122236.

De Backer, H., De Corte, W. & Van Bogaert, P. 2003, 'A case study on strain gauge measurements on large post-tensioned concrete beams of a railway support structure', *Insight-Non-Destructive Testing and Condition Monitoring*, vol. 45, no. 12, pp. 822-6.

del Carmen Camacho, M., Galao, O., Baeza, F.J., Zornoza, E. & Garcés, P. 2014, 'Mechanical properties and durability of CNT cement composites', *Materials*, vol. 7, no. 3, pp. 1640-51.

Devi, S. & Khan, R. 2020, 'Effect of graphene oxide on mechanical and durability performance of concrete', *Journal of Building Engineering*, vol. 27, p. 101007.

Dimov, D., Amit, I., Gorrie, O., Barnes, M.D., Townsend, N.J., Neves, A.I., Withers, F., Russo, S. & Craciun, M.F. 2018, 'Ultrahigh performance nanoengineered graphene–concrete composites for multifunctional applications', *Advanced Functional Materials*, vol. 28, no. 23, p. 1705183.

Ding, Y., Chen, Z., Han, Z., Zhang, Y. & Pacheco-Torgal, F. 2013, 'Nano-carbon black and carbon fiber as conductive materials for the diagnosing of the damage of concrete beam', *Construction and Building Materials*, vol. 43, pp. 233-41.

Ding, Y., Huang, Y., Zhang, Y., Jalali, S. & Aguiar, J. 2015, 'Self-monitoring of freeze–thaw damage using triphasic electric conductive concrete', *Construction and Building Materials*, vol. 101, pp. 440-6.

Ding, Y., Liu, G., Hussain, A., Pacheco-Torgal, F. & Zhang, Y. 2019, 'Effect of steel fiber and carbon black on the self-sensing ability of concrete cracks under bending', *Construction and Building Materials*, vol. 207, pp. 630-9.

Dong, W., Guo, Y., Sun, Z., Tao, Z. & Li, W. 2021, 'Development of piezoresistive cement-based sensor using recycled waste glass cullets coated with carbon nanotubes', *Journal of Cleaner Production*, vol. 314, p. 127968.

Dong, W., Li, W., Guo, Y., He, X. & Sheng, D. 2020, 'Effects of silica fume on physicochemical properties and piezoresistivity of intelligent carbon black-cementitious composites', *Construction and Building Materials*, vol. 259, p. 120399.

Dong, W., Li, W., Long, G., Tao, Z., Li, J. & Wang, K. 2019, 'Electrical resistivity and mechanical properties of cementitious composite incorporating conductive rubber fibres', *Smart Materials and Structures*, vol. 28, no. 8, p. 085013.

Dong, W., Li, W., Lu, N., Qu, F., Vessalas, K. & Sheng, D. 2019, 'Piezoresistive behaviours of cement-based sensor with carbon black subjected to various temperature and water content', *Composites Part B: Engineering*, vol. 178, p. 107488.

Dong, W., Li, W., Luo, Z., Guo, Y. & Wang, K. 2020, 'Effect of layer-distributed carbon nanotube (CNT) on mechanical and piezoresistive performance of intelligent cement-based sensor', *Nanotechnology*, vol. 31, no. 50, p. 505503.

Dong, W., Li, W., Shen, L. & Sheng, D. 2019, 'Piezoresistive behaviours of carbon black cement-based sensors with layer-distributed conductive rubber fibres', *Materials & Design*, vol. 182, p. 108012.

Dong, W., Li, W., Shen, L., Sun, Z. & Sheng, D. 2020, 'Piezoresistivity of smart carbon nanotubes (CNTs) reinforced cementitious composite under integrated cyclic compression and impact', *Composite Structures*, vol. 241, p. 112106.

Dong, W., Li, W., Shen, L., Zhang, S. & Vessalas, K. 2021, 'Integrated self-sensing and self-healing cementitious composite with microencapsulation of nano-carbon black and slaked lime', *Materials Letters*, vol. 282, p. 128834.

Dong, W., Li, W., Tao, Z. & Wang, K. 2019, 'Piezoresistive properties of cement-based sensors: Review and perspective', *Construction and Building Materials*, vol. 203, pp. 146-63.

Dong, W., Li, W., Vessalas, K., He, X., Sun, Z. & Sheng, D. 2021, 'Piezoresistivity deterioration of smart graphene nanoplate/cement-based sensors subjected to sulphuric acid attack', *Composites Communications*, vol. 23, p. 100563.

Dong, W., Li, W., Vessalas, K. & Wang, K. 2020, 'Mechanical and conductive properties of smart cementitious composites with conductive rubber crumbs', *ES Materials & Manufacturing*.

Dong, W., Li, W., Wang, K., Guo, Y., Sheng, D. & Shah, S.P. 2020, 'Piezoresistivity enhancement of functional carbon black filled cement-based sensor using polypropylene fibre', *Powder Technology*, vol. 373, pp. 184-94.

Dong, W., Li, W., Wang, K., Han, B., Sheng, D. & Shah, S.P. 2020, 'Investigation on physicochemical and piezoresistive properties of smart MWCNT/cementitious composite exposed to elevated temperatures', *Cement and Concrete Composites*, vol. 112, p. 103675.

Dong, W., Li, W., Wang, K., Luo, Z. & Sheng, D. 2020, 'Self-sensing capabilities of cement-based sensor with layer-distributed conductive rubber fibres', *Sensors and Actuators A: Physical*, vol. 301, p. 111763.

Dong, W., Li, W., Wang, K., Vessalas, K. & Zhang, S. 2020, 'Mechanical strength and self-sensing capacity of smart cementitious composite containing conductive rubber crumbs', *Journal of Intelligent Material Systems and Structures*, vol. 31, no. 10, pp. 1325-40.

Dong, W., Li, W., Zhu, X., Sheng, D. & Shah, S.P. 2021, 'Multifunctional cementitious composites with integrated self-sensing and hydrophobic capacities toward smart structural health monitoring', *Cement and Concrete Composites*, vol. 118, p. 103962.

Donnet, J. 1982, 'Structure and reactivity of carbons: from carbon black to carbon composites', *Carbon*, vol. 20, no. 4, pp. 267-82.

Du, H., Gao, H.J. & Dai Pang, S. 2016, 'Improvement in concrete resistance against water and chloride ingress by adding graphene nanoplatelet', *Cement and Concrete Research*, vol. 83, pp. 114-23.

Duan, A., Jin, W. & Qian, J. 2011, 'Effect of freeze–thaw cycles on the stress–strain curves of unconfined and confined concrete', *Materials and Structures*, vol. 44, no. 7, pp. 1309-24.

Fattuhi, N. & Hughes, B. 1988, 'The performance of cement paste and concrete subjected to sulphuric acid attack', *Cement and Concrete Research*, vol. 18, no. 4, pp. 545-53.

Feng, J., Sun, W., Zhai, H., Wang, L., Dong, H. & Wu, Q. 2018, 'Experimental study on hybrid effect evaluation of fiber reinforced concrete subjected to drop weight impacts', *Materials*, vol. 11, no. 12, p. 2563.

Ferraris, C.F., Obla, K.H. & Hill, R. 2001, 'The influence of mineral admixtures on the rheology of cement paste and concrete', *Cement and Concrete Research*, vol. 31, no. 2, pp. 245-55.

Fu, X. & Chung, D. 1995, 'Contact electrical resistivity between cement and carbon fiber: its decrease with increasing bond strength and its increase during fiber pull-out', *Cement and Concrete Research*, vol. 25, no. 7, pp. 1391-6.

Fu, X. & Chung, D. 1996a, 'Submicron carbon filament cement-matrix composites for electromagnetic interference shielding', *Cement and Concrete Research*, vol. 26, no. 10, pp. 1467-72.

Fu, X. & Chung, D.D.L. 1996b, 'Self-monitoring of fatigue damage in carbon fiber reinforced cement', *Cement and Concrete Research*, vol. 26, no. 1, pp. 15-20.

Fu, X. & Chung, D.D.L. 1997, 'Effect of curing age on the self-monitoring behavior of carbon fiber reinforced mortar', *Cement and Concrete Research*, vol. 27, no. 9, pp. 1313-8.

Fu, X., Lu, W. & Chung, D.D.L. 1998, 'Improving the Strain-Sensing Ability of Carbon Fiber-Reinforced Cement by Ozone Treatment of the Fibers 11Communicated by D.M. Roy', *Cement and Concrete Research*, vol. 28, no. 2, pp. 183-7.

Galao, O., Baeza, F.J., Zornoza, E. & Garcés, P. 2014, 'Strain and damage sensing properties on multifunctional cement composites with CNF admixture', *Cement and Concrete Composites*, vol. 46, pp. 90-8.

Gao, Y., Qu, L., He, B., Dai, K., Fang, Z. & Zhu, R. 2018, 'Study on effectiveness of anti-icing and deicing performance of super-hydrophobic asphalt concrete', *Construction and Building Materials*, vol. 191, pp. 270-80.

Garcia-Macias, E., D'Alessandro, A., Castro-Triguero, R., Pérez-Mira, D. & Ubertini, F. 2017, 'Micromechanics modeling of the electrical conductivity of carbon nanotube cement-matrix composites', *Composites Part B: Engineering*, vol. 108, pp. 451-69.

García-Macías, E., D'Alessandro, A., Castro-Triguero, R., Pérez-Mira, D. & Ubertini, F. 2017, 'Micromechanics modeling of the uniaxial strain-sensing property of carbon nanotube cement-matrix composites for SHM applications', *Composite Structures*, vol. 163, pp. 195-215.

García, Á., Schlangen, E., van de Ven, M. & Liu, Q. 2009, 'Electrical conductivity of asphalt mortar containing conductive fibers and fillers', *Construction and Building Materials*, vol. 23, no. 10, pp. 3175-81.

Geng, Y., Li, S., Hou, D., Zhang, W., Jin, Z., Li, Q. & Luo, J. 2020, 'Fabrication of superhydrophobicity on foamed concrete surface by GO/silane coating', *Materials Letters*, vol. 265, p. 127423.

Ghazizadeh, S., Duffour, P., Skipper, N.T. & Bai, Y. 2018, 'Understanding the behaviour of graphene oxide in Portland cement paste', *Cement and Concrete Research*, vol. 111, pp. 169-82.

Gong, H., Li, Z., Zhang, Y. & Fan, R. 2009, 'Piezoelectric and dielectric behavior of 0-3 cement-based composites mixed with carbon black', *Journal of the European Ceramic Society*, vol. 29, no. 10, pp. 2013-9.

Güneyisi, E., Gesoğlu, M. & Özturan, T. 2004, 'Properties of rubberized concretes containing silica fume', *Cement and Concrete Research*, vol. 34, no. 12, pp. 2309-17.

Gupta, S., Gonzalez, J.G. & Loh, K.J. 2017, 'Self-sensing concrete enabled by nano-engineered cement-aggregate interfaces', *Structural Health Monitoring*, vol. 16, no. 3, pp. 309-23.

Han, B., Guan, X. & Ou, J. 2007, 'Electrode design, measuring method and data acquisition system of carbon fiber cement paste piezoresistive sensors', *Sensors and Actuators A: Physical*, vol. 135, no. 2, pp. 360-9.

Han, B., Han, B. & Yu, X. 2010, 'Effects of the content level and particle size of nickel powder on the piezoresistivity of cement-based composites/sensors', *Smart Materials and Structures*, vol. 19, no. 6, p. 065012.

Han, B., Yang, Z., Shi, X. & Yu, X. 2013, 'Transport properties of carbon-nanotube/cement composites', *Journal of Materials Engineering and Performance*, vol. 22, no. 1, pp. 184-9.

Han, B., Yu, X. & Kwon, E. 2009, 'A self-sensing carbon nanotube/cement composite for traffic monitoring', *Nanotechnology*, vol. 20, no. 44, p. 445501.

Han, B., Yu, X., Kwon, E. & Ou, J. 2012, 'Effects of CNT concentration level and water/cement ratio on the piezoresistivity of CNT/cement composites', *Journal of Composite Materials*, vol. 46, no. 1, pp. 19-25.

He, Y., Lu, L., Jin, S. & Hu, S. 2014, 'Conductive aggregate prepared using graphite and clay and its use in conductive mortar', *Construction and Building Materials*, vol. 53, pp. 131-7.

Hewayde, E., Nehdi, M., Allouche, E. & Nakhla, G. 2006, 'Effect of geopolymer cement on microstructure, compressive strength and sulphuric acid resistance of concrete', *Magazine of Concrete Research*, vol. 58, no. 5, pp. 321-31.

Horgnies, M. & Chen, J. 2014, 'Superhydrophobic concrete surfaces with integrated microtexture', *Cement and Concrete Composites*, vol. 52, pp. 81-90.

Hou, Y., Wang, D., Zhang, X.-M., Zhao, H., Zha, J.-W. & Dang, Z.-M. 2013, 'Positive piezoresistive behavior of electrically conductive alkyl-functionalized graphene/polydimethylsilicone nanocomposites', *Journal of Materials Chemistry C*, vol. 1, no. 3, pp. 515-21.

Hu, Z.-X., Hu, X.-M., Cheng, W.-M., Zhao, Y.-Y. & Wu, M.-Y. 2018, 'Performance optimization of one-component polyurethane healing agent for self-healing concrete', *Construction and Building Materials*, vol. 179, pp. 151-9.

Hughes, B. & Fattuhi, N. 1977, 'Load–deflection curves for fibre-reinforced concrete beams in flexure', *Magazine of Concrete Research*, vol. 29, no. 101, pp. 199-206.

Husni, H., Nazari, M., Yee, H., Rohim, R., Yusuff, A., Ariff, M.A.M., Ahmad, N., Leo, C. & Junaidi, M. 2017, 'Superhydrophobic rice husk ash coating on concrete', *Construction and Building Materials*, vol. 144, pp. 385-91.

Iqbal, M., Kumar, V. & Mittal, A. 2019, 'Experimental and numerical studies on the drop impact resistance of prestressed concrete plates', *International Journal of Impact Engineering*, vol. 123, pp. 98-117.

Irshidat, M.R., Al-Nuaimi, N., Ahmed, W. & Rabie, M. 2021, 'Feasibility of recycling waste carbon black in cement mortar production: Environmental life cycle assessment and performance evaluation', *Construction and Building Materials*, vol. 296, p. 123740.

Khaloo, A.R., Dehestani, M. & Rahmatabadi, P. 2008, 'Mechanical properties of concrete containing a high volume of tire–rubber particles', *Waste Management*, vol. 28, no. 12, pp. 2472-82.

Kim, G., Yang, B., Ryu, G. & Lee, H.-K. 2016, 'The electrically conductive carbon nanotube (CNT)/cement composites for accelerated curing and thermal cracking reduction', *Composite Structures*, vol. 158, pp. 20-9.

Kim, G.M., Yang, B.J., Cho, K.J., Kim, E.M. & Lee, H.K. 2017, 'Influences of CNT dispersion and pore characteristics on the electrical performance of cementitious composites', *Composite Structures*, vol. 164, pp. 32-42.

Kim, H., Park, I. & Lee, H.-K. 2014, 'Improved piezoresistive sensitivity and stability of CNT/cement mortar composites with low water–binder ratio', *Composite Structures*, vol. 116, pp. 713-9.

Konsta-Gdoutos, M.S. & Aza, C.A. 2014, 'Self sensing carbon nanotube (CNT) and nanofiber (CNF) cementitious composites for real time damage assessment in smart structures', *Cement and Concrete Composites*, vol. 53, pp. 162-9.

Konsta-Gdoutos, M.S., Metaxa, Z.S. & Shah, S.P. 2010a, 'Highly dispersed carbon nanotube reinforced cement based materials', *Cement and Concrete Research*, vol. 40, no. 7, pp. 1052-9.

Konsta-Gdoutos, M.S., Metaxa, Z.S. & Shah, S.P. 2010b, 'Multi-scale mechanical and fracture characteristics and early-age strain capacity of high performance carbon nanotube/cement nanocomposites', *Cement and Concrete Composites*, vol. 32, no. 2, pp. 110-5.

Kovačič, B., Štrukelj, A. & Vatin, N. 2015, 'Processing of signals produced by strain gauges in testing measurements of the bridges', *Procedia Engineering*, vol. 117, pp. 795-801.

Kumar, V., Iqbal, M. & Mittal, A. 2018, 'Study of induced prestress on deformation and energy absorption characteristics of concrete slabs under drop impact loading', *Construction and Building Materials*, vol. 188, pp. 656-75.

Kyi, A.A. & Batchelor, B. 1994, 'An electrical conductivity method for measuring the effects of additives on effective diffusivities in portland cement pastes', *Cement and Concrete Research*, vol. 24, no. 4, pp. 752-64.

Le, J.-L., Du, H. & Dai Pang, S. 2014, 'Use of 2D Graphene Nanoplatelets (GNP) in cement composites for structural health evaluation', *Composites Part B: Engineering*, vol. 67, pp. 555-63.

Lei, L., Wang, Q., Xu, S., Wang, N. & Zheng, X. 2020, 'Fabrication of superhydrophobic concrete used in marine environment with anti-corrosion and stable mechanical properties', *Construction and Building Materials*, vol. 251, p. 118946.

Leung, C.K., Elvin, N., Olson, N., Morse, T.F. & He, Y.-F. 2000, 'A novel distributed optical crack sensor for concrete structures', *Engineering Fracture Mechanics*, vol. 65, no. 2-3, pp. 133-48.

Li, B., Ji, Z., Xie, S., Wang, J., Zhou, J. & Zhu, L. 2019, 'Electromagnetic wave absorption properties of carbon black/cement-based composites filled with porous glass pellets', *Journal of Materials Science: Materials in Electronics*, vol. 30, no. 13, pp. 12416-25.

Li, G., Xiong, G. & Yin, Y. 2009, 'The physical and chemical effects of long-term sulphuric acid exposure on hybrid modified cement mortar', *Cement and Concrete Composites*, vol. 31, no. 5, pp. 325-30.

Li, G.Y., Wang, P.M. & Zhao, X. 2007, 'Pressure-sensitive properties and microstructure of carbon nanotube reinforced cement composites', *Cement and Concrete Composites*, vol. 29, no. 5, pp. 377-82.

Li, H., Xiao, H.-g. & Ou, J.-p. 2004, 'A study on mechanical and pressure-sensitive properties of cement mortar with nanophase materials', *Cement and Concrete Research*, vol. 34, no. 3, pp. 435-8.

Li, H., Xiao, H.-g. & Ou, J.-p. 2006, 'Effect of compressive strain on electrical resistivity of carbon black-filled cement-based composites', *Cement and Concrete Composites*, vol. 28, no. 9, pp. 824-8.

Li, H., Xiao, H. & Ou, J. 2008, 'Electrical property of cement-based composites filled with carbon black under long-term wet and loading condition', *Composites Science and Technology*, vol. 68, no. 9, pp. 2114-9.

Li, W., Dong, W., Shen, L., Castel, A. & Shah, S.P. 2020, 'Conductivity and piezoresistivity of nano-carbon black (NCB) enhanced functional cement-based sensors using polypropylene fibres', *Materials Letters*, vol. 270, p. 127736.

Li, W., Li, X., Chen, S.J., Liu, Y.M., Duan, W.H. & Shah, S.P. 2017, 'Effects of graphene oxide on early-age hydration and electrical resistivity of Portland cement paste', *Construction and Building Materials*, vol. 136, pp. 506-14.

Li, X., Liu, Y.M., Li, W.G., Li, C.Y., Sanjayan, J.G., Duan, W.H. & Li, Z. 2017, 'Effects of graphene oxide agglomerates on workability, hydration, microstructure and compressive strength of cement paste', *Construction and Building Materials*, vol. 145, pp. 402-10.

Liu, B., Xie, Y. & Li, J. 2005, 'Influence of steam curing on the compressive strength of concrete containing supplementary cementing materials', *Cement and Concrete Research*, vol. 35, no. 5, pp. 994-8.

Liu, Q., Gao, R., Tam, V.W., Li, W. & Xiao, J. 2018, 'Strain monitoring for a bending concrete beam by using piezoresistive cement-based sensors', *Construction and Building Materials*, vol. 167, pp. 338-47.

Lu, L. & Ouyang, D. 2017, 'Properties of cement mortar and ultra-high strength concrete incorporating graphene oxide nanosheets', *Nanomaterials*, vol. 7, no. 7, p. 187.

Lu, Y., Zhang, J., Li, Z. & Dong, B. 2013, 'Corrosion monitoring of reinforced concrete beam using embedded cement-based piezoelectric sensor', *Magazine of Concrete Research*, vol. 65, no. 21, pp. 1265-76.

Lu, Z., Li, X., Hanif, A., Chen, B., Parthasarathy, P., Yu, J. & Li, Z. 2017, 'Early-age interaction mechanism between the graphene oxide and cement hydrates', *Construction and Building Materials*, vol. 152, pp. 232-9.

Luheng, W., Tianhuai, D. & Peng, W. 2009, 'Influence of carbon black concentration on piezoresistivity for carbon-black-filled silicone rubber composite', *Carbon*, vol. 47, no. 14, pp. 3151-7.

Luo, J., Chen, X., Crump, J., Zhou, H., Davies, D.G., Zhou, G., Zhang, N. & Jin, C. 2018, 'Interactions of fungi with concrete: Significant importance for bio-based self-healing concrete', *Construction and Building Materials*, vol. 164, pp. 275-85.

Materazzi, A.L., Ubertini, F. & D'Alessandro, A. 2013, 'Carbon nanotube cement-based transducers for dynamic sensing of strain', *Cement and Concrete Composites*, vol. 37, pp. 2-11.

Monteiro, A., Cachim, P. & Costa, P. 2015, 'Electrical properties of cement-based composites containing carbon black particles', *Materials Today: Proceedings*, vol. 2, no. 1, pp. 193-9.

Monteiro, A., Costa, P., Oeser, M. & Cachim, P. 2020, 'Dynamic sensing properties of a multifunctional cement composite with carbon black for traffic monitoring', *Smart Materials and Structures*, vol. 29, no. 2, p. 025023.

Monteiro, A., Loredo, A., Costa, P., Oeser, M. & Cachim, P. 2017, 'A pressure-sensitive carbon black cement composite for traffic monitoring', *Construction and Building Materials*, vol. 154, pp. 1079-86.

Monteiro, A.O., Cachim, P.B. & Costa, P.M. 2017, 'Self-sensing piezoresistive cement composite loaded with carbon black particles', *Cement and Concrete Composites*, vol. 81, pp. 59-65.

Mu, R., Miao, C., Luo, X. & Sun, W. 2002, 'Interaction between loading, freeze–thaw cycles, and chloride salt attack of concrete with and without steel fiber reinforcement', *Cement and Concrete Research*, vol. 32, no. 7, pp. 1061-6.

Mu, T., Liu, L., Lan, X., Liu, Y. & Leng, J. 2018, 'Shape memory polymers for composites', *Composites Science and Technology*, vol. 160, pp. 169-98.

Nalon, G.H., Ribeiro, J.C.L., de Araújo, E.N.D., Pedroti, L.G., de Carvalho, J.M.F., Santos, R.F. & Aparecido-Ferreira, A. 2020, 'Effects of different kinds of carbon black nanoparticles on the piezoresistive and mechanical properties of cement-based composites', *Journal of Building Engineering*, vol. 32, p. 101724.

Nam, I.W., Kim, H.K. & Lee, H.K. 2012, 'Influence of silica fume additions on electromagnetic interference shielding effectiveness of multi-walled carbon nanotube/cement composites', *Construction and Building Materials*, vol. 30, pp. 480-7.

Neild, S., Williams, M. & McFadden, P. 2005, 'Development of a vibrating wire strain gauge for measuring small strains in concrete beams', *Strain*, vol. 41, no. 1, pp. 3-9.

Oberlin, A., Endo, M. & Koyama, T. 1976, 'Filamentous growth of carbon through benzene decomposition', *Journal of Crystal Growth*, vol. 32, no. 3, pp. 335-49.

Ou, J. & Han, B. 2009, 'Piezoresistive cement-based strain sensors and self-sensing concrete components', *Journal of Intelligent Material Systems and Structures*, vol. 20, no. 3, pp. 329-36.

Özgan, E. & Serin, S. 2013, 'Investigation of certain engineering characteristics of asphalt concrete exposed to freeze–thaw cycles', *Cold Regions Science and Technology*, vol. 85, pp. 131-6.

Ozyurt, N., Mason, T.O. & Shah, S.P. 2007, 'Correlation of fiber dispersion, rheology and mechanical performance of FRCs', *Cement and Concrete Composites*, vol. 29, no. 2, pp. 70-9.

Pacheco-Torgal, F. & Jalali, S. 2009, 'Sulphuric acid resistance of plain, polymer modified, and fly ash cement concretes', *Construction and Building Materials*, vol. 23, no. 12, pp. 3485-91.

Papanikolaou, I., Arena, N. & Al-Tabbaa, A. 2019, 'Graphene nanoplatelet reinforced concrete for self-sensing structures–A lifecycle assessment perspective', *Journal of Cleaner Production*, vol. 240, p. 118202.

Papo, A. & Piani, L. 2004, 'Effect of various superplasticizers on the rheological properties of Portland cement pastes', *Cement and Concrete Research*, vol. 34, no. 11, pp. 2097-101.

Park, J.-M., Jang, J.-H., Wang, Z.-J., Kwon, D.-J. & DeVries, K.L. 2010, 'Self-sensing of carbon fiber/carbon nanofiber–epoxy composites with two different nanofiber aspect ratios investigated by electrical resistance and wettability measurements', *Composites Part A: Applied Science and Manufacturing*, vol. 41, no. 11, pp. 1702-11.

Pârvan, M.-G., Voicu, G. & Bădănoiu, A.-I. 2020, 'Study of hydration and hardening processes of self-sensing cement-based materials with carbon black content', *Journal of Thermal Analysis and Calorimetry*, vol. 139, no. 2, pp. 807-15.

Parvaneh, V. & Khiabani, S.H. 2019, 'Mechanical and piezoresistive properties of self-sensing smart concretes reinforced by carbon nanotubes', *Mechanics of Advanced Materials and Structures*, vol. 26, no. 11, pp. 993-1000.

Peng, H., Ge, Y., Cai, C., Zhang, Y. & Liu, Z. 2019, 'Mechanical properties and microstructure of graphene oxide cement-based composites', *Construction and Building Materials*, vol. 194, pp. 102-9.

Pham, N.-P., Toumi, A. & Turatsinze, A. 2018, 'Rubber aggregate-cement matrix bond enhancement: Microstructural analysis, effect on transfer properties and on mechanical behaviours of the composite', *Cement and Concrete Composites*, vol. 94, pp. 1-12.

Polat, R., Demirboğa, R., Karakoc, M.B. & Türkmen, İ. 2010, 'The influence of lightweight aggregate on the physico-mechanical properties of concrete exposed to freeze–thaw cycles', *Cold Regions Science and Technology*, vol. 60, no. 1, pp. 51-6.

Qin, L., Lu, Y. & Li, Z. 2010, 'Embedded cement-based piezoelectric sensors for acoustic emission detection in concrete', *Journal of Materials in Civil Engineering*, vol. 22, no. 12, pp. 1323-7.

Qiu, L., Zhang, G. & Wang, W. 2013, 'The effects of ultrasonic oscillation on the form of carbon nanotubes', *Journal of Petrochemical Universities*, vol. 26, no. 3, pp. 57-61.

Raffoul, S., Garcia, R., Pilakoutas, K., Guadagnini, M. & Medina, N.F. 2016, 'Optimisation of rubberised concrete with high rubber content: An experimental investigation', *Construction and Building Materials*, vol. 124, pp. 391-404.

Rajabipour, F. & Weiss, J. 2007, 'Electrical conductivity of drying cement paste', *Materials and Structures*, vol. 40, no. 10, pp. 1143-60.

Rao, M.C., Bhattacharyya, S. & Barai, S. 2011, 'Behaviour of recycled aggregate concrete under drop weight impact load', *Construction and Building Materials*, vol. 25, no. 1, pp. 69-80.

Reza, F., Batson, G.B., Yamamuro, J.A. & Lee, J.S. 2001, 'Volume electrical resistivity of carbon fiber cement composites', *Materials Journal*, vol. 98, no. 1, pp. 25-35.

Rezania, M., Panahandeh, M., Razavi, S. & Berto, F. 2019, 'Experimental study of the simultaneous effect of nano-silica and nano-carbon black on permeability and mechanical properties of the concrete', *Theoretical and Applied Fracture Mechanics*, vol. 104, p. 102391.

Shamsaei, E., de Souza, F.B., Yao, X., Benhelal, E., Akbari, A. & Duan, W. 2018, 'Graphene-based nanosheets for stronger and more durable concrete: A review', *Construction and Building Materials*, vol. 183, pp. 642-60.

Shang, H.-S., Song, Y.-P. & Qin, L.-K. 2008, 'Experimental study on strength and deformation of plain concrete under triaxial compression after freeze-thaw cycles', *Building and Environment*, vol. 43, no. 7, pp. 1197-204.

She, W., Wang, X., Miao, C., Zhang, Q., Zhang, Y., Yang, J. & Hong, J. 2018, 'Biomimetic superhydrophobic surface of concrete: Topographic and chemical modification assembly by direct spray', *Construction and Building Materials*, vol. 181, pp. 347-57.

Shen, J.T., Buschhorn, S.T., De Hosson, J.T.M., Schulte, K. & Fiedler, B. 2015, 'Pressure and temperature induced electrical resistance change in nano-carbon/epoxy composites', *Composites Science and Technology*, vol. 115, pp. 1-8.

Shi, Z.-Q. & Chung, D. 1999, 'Carbon fiber-reinforced concrete for traffic monitoring and weighing in motion', *Cement and Concrete Research*, vol. 29, no. 3, pp. 435-9.

Siddika, A., Al Mamun, M.A., Alyousef, R., Amran, Y.M., Aslani, F. & Alabduljabbar, H. 2019, 'Properties and utilizations of waste tire rubber in concrete: A review', *Construction and Building Materials*, vol. 224, pp. 711-31.

Singh, A.P., Gupta, B.K., Mishra, M., Chandra, A., Mathur, R. & Dhawan, S. 2013, 'Multiwalled carbon nanotube/cement composites with exceptional electromagnetic interference shielding properties', *Carbon*, vol. 56, pp. 86-96.

Song, G., Gu, H., Mo, Y., Hsu, T. & Dhonde, H. 2007, 'Concrete structural health monitoring using embedded piezoceramic transducers', *Smart Materials and Structures*, vol. 16, no. 4, p. 959.

Song, X.H., Zheng, L.X. & Li, Z.Q. 2006, 'Temperature compensation in deformation testing for smart concrete structures', *Key Engineering Materials*, vol. 326, Trans Tech Publ, pp. 1503-6.

Souradeep, G. & Kua, H.W. 2016, 'Encapsulation technology and techniques in self-healing concrete', *Journal of Materials in Civil Engineering*, vol. 28, no. 12, p. 04016165.

Su, H., Yang, J., Ling, T.-C., Ghataora, G.S. & Dirar, S. 2015, 'Properties of concrete prepared with waste tyre rubber particles of uniform and varying sizes', *Journal of Cleaner Production*, vol. 91, pp. 288-96.

Su, H., Zhang, N. & Li, H. 2018, 'Concrete piezoceramic smart module pairs-based damage diagnosis of hydraulic structure', *Composite Structures*, vol. 183, pp. 582-93.

Sun, M.-q., Liew, R.J., Zhang, M.-H. & Li, W. 2014, 'Development of cement-based strain sensor for health monitoring of ultra high strength concrete', *Construction and building Materials*, vol. 65, pp. 630-7.

Sun, S., Han, B., Jiang, S., Yu, X., Wang, Y., Li, H. & Ou, J. 2017, 'Nano graphite platelets-enabled piezoresistive cementitious composites for structural health monitoring', *Construction and Building Materials*, vol. 136, pp. 314-28.

Sun, W., Mu, R., Luo, X. & Miao, C. 2002, 'Effect of chloride salt, freeze–thaw cycling and externally applied load on the performance of the concrete', *Cement and Concrete Research*, vol. 32, no. 12, pp. 1859-64.

Sun, W., Zhang, Y., Yan, H. & Mu, R. 1999, 'Damage and damage resistance of high strength concrete under the action of load and freeze-thaw cycles', *Cement and Concrete Research*, vol. 29, no. 9, pp. 1519-23.

Suzuki, T., Shiotani, T. & Ohtsu, M. 2017, 'Evaluation of cracking damage in freeze-thawed concrete using acoustic emission and X-ray CT image', *Construction and Building Materials*, vol. 136, pp. 619-26.

Tchoudakov, R., Breuer, O., Narkis, M. & Siegmann, A. 1996, 'Conductive polymer blends with low carbon black loading: polypropylene/polyamide', *Polymer Engineering & Science*, vol. 36, no. 10, pp. 1336-46.

Teomete, E. 2016, 'The effect of temperature and moisture on electrical resistance, strain sensitivity and crack sensitivity of steel fiber reinforced smart cement composite', *Smart Materials and Structures*, vol. 25, no. 7, p. 075024.

Teomete, E. & Kocyigit, O.I. 2013, 'Tensile strain sensitivity of steel fiber reinforced cement matrix composites tested by split tensile test', *Construction and Building Materials*, vol. 47, pp. 962-8.

Ubertini, F., Laflamme, S., Ceylan, H., Materazzi, A.L., Cerni, G., Saleem, H., D'Alessandro, A. & Corradini, A. 2014, 'Novel nanocomposite technologies for dynamic monitoring of structures: a comparison between cement-based embeddable and soft elastomeric surface sensors', *Smart Materials and Structures*, vol. 23, no. 4, p. 045023.

Ubertini, F., Materazzi, A.L., D'Alessandro, A. & Laflamme, S. 2014, 'Natural frequencies identification of a reinforced concrete beam using carbon nanotube cement-based sensors', *Engineering Structures*, vol. 60, pp. 265-75.

Van Tittelboom, K., Wang, J., Araújo, M., Snoeck, D., Gruyaert, E., Debbaut, B., Derluyn, H., Cnudde, V., Tsangouri, E., Van Hemelrijck, D. & De Belie, N. 2016, 'Comparison of

different approaches for self-healing concrete in a large-scale lab test', *Construction and Building Materials*, vol. 107, pp. 125-37.

Vipulanandan, C. & Mohammed, A. 2015, 'Smart cement rheological and piezoresistive behavior for oil well applications', *Journal of Petroleum Science and Engineering*, vol. 135, pp. 50-8.

Wang, J.Y., Soens, H., Verstraete, W. & De Belie, N. 2014, 'Self-healing concrete by use of microencapsulated bacterial spores', *Cement and Concrete Research*, vol. 56, pp. 139-52.

Wang, M. & Chung, D. 2018, 'Understanding the increase of the electric permittivity of cement caused by latex addition', *Composites Part B: Engineering*, vol. 134, pp. 177-85.

Wang, S. & Chung, D. 2006, 'Self-sensing of flexural strain and damage in carbon fiber polymer-matrix composite by electrical resistance measurement', *Carbon*, vol. 44, no. 13, pp. 2739-51.

Wang, W., Dai, H. & Wu, S. 2008, 'Mechanical behavior and electrical property of CFRC-strengthened RC beams under fatigue and monotonic loading', *Materials Science and Engineering: A*, vol. 479, no. 1-2, pp. 191-6.

Wang, Y., Cao, Y., Zhang, P., Ma, Y., Zhao, T., Wang, H. & Zhang, Z. 2019, 'Water absorption and chloride diffusivity of concrete under the coupling effect of uniaxial compressive load and freeze–thaw cycles', *Construction and Building Materials*, vol. 209, pp. 566-76.

Wang, Z., Zeng, Q., Wang, L., Yao, Y. & Li, K. 2013, 'Characterizing blended cement pastes under cyclic freeze–thaw actions by electrical resistivity', *Construction and Building Materials*, vol. 44, pp. 477-86.

Wansom, S., Kidner, N., Woo, L. & Mason, T. 2006, 'AC-impedance response of multi-walled carbon nanotube/cement composites', *Cement and Concrete Composites*, vol. 28, no. 6, pp. 509-19.

Wen, S. & Chung, D. 1999, 'Carbon fiber-reinforced cement as a thermistor', *Cement and Concrete Research*, vol. 29, no. 6, pp. 961-5.

Wen, S. & Chung, D. 2000, 'Uniaxial tension in carbon fiber reinforced cement, sensed by electrical resistivity measurement in longitudinal and transverse directions', *Cement and Concrete Research*, vol. 30, no. 8, pp. 1289-94.

Wen, S. & Chung, D. 2001, 'Carbon fiber-reinforced cement as a strain-sensing coating', *Cement and Concrete Research*, vol. 31, no. 4, pp. 665-7.

Wen, S. & Chung, D. 2003, 'A comparative study of steel-and carbon-fibre cement as piezoresistive strain sensors', *Advances in Cement Research*, vol. 15, no. 3, pp. 119-28.

Wen, S. & Chung, D. 2004, 'Electromagnetic interference shielding reaching 70 dB in steel fiber cement', *Cement and Concrete Research*, vol. 34, no. 2, pp. 329-32.

Wen, S. & Chung, D. 2007, 'Partial replacement of carbon fiber by carbon black in multifunctional cement–matrix composites', *Carbon*, vol. 45, no. 3, pp. 505-13.

Wen, S. & Chung, D. 2008, 'Effect of moisture on piezoresistivity of carbon fiber-reinforced cement paste', *ACI Materials Journal*, vol. 105, no. 3, p. 274.

Whiting, D.A. & Nagi, M.A. 2003, 'Electrical resistivity of concrete-a literature review', *R&D Serial*, vol. 2457, p. 1078.

Wu, B., Huang, X.-j. & Lu, J.-z. 2005, 'Biaxial compression in carbon-fiber-reinforced mortar, sensed by electrical resistance measurement', *Cement and Concrete Research*, vol. 35, no. 7, pp. 1430-4.

Xiao, H., Li, H. & Ou, J. 2010, 'Modeling of piezoresistivity of carbon black filled cement-based composites under multi-axial strain', *Sensors and Actuators A: Physical*, vol. 160, no. 1-2, pp. 87-93.

Xiao, H., Li, H. & Ou, J. 2011, 'Self-monitoring properties of concrete columns with embedded cement-based strain sensors', *Journal of Intelligent Material Systems and Structures*, vol. 22, no. 2, pp. 191-200.

Xu, J. & Yao, W. 2014, 'Multiscale mechanical quantification of self-healing concrete incorporating non-ureolytic bacteria-based healing agent', *Cement and Concrete Research*, vol. 64, pp. 1-10.

Yang, M. & Jennings, H.M. 1995, 'Influences of mixing methods on the microstructure and rheological behavior of cement paste', *Advanced Cement Based Materials*, vol. 2, no. 2, pp. 70-8.

Yin, B., Xu, T., Hou, D., Zhao, E., Hua, X., Han, K., Zhang, Y. & Zhang, J. 2020, 'Superhydrophobic anticorrosive coating for concrete through in-situ bionic induction and gradient mineralization', *Construction and Building Materials*, vol. 257, p. 119510.

Yu, X. & Kwon, E. 2009, 'A carbon nanotube/cement composite with piezoresistive properties', *Smart Materials and Structures*, vol. 18, no. 5, p. 055010.

Yun, S. & Kim, J. 2007, 'Sonication time effect on MWNT/PANI-EB composite for hybrid electro-active paper actuator', *Synthetic Metals*, vol. 157, no. 13, pp. 523-8.

Zhang, L., Ding, S., Han, B., Yu, X. & Ni, Y.-Q. 2019, 'Effect of water content on the piezoresistive property of smart cement-based materials with carbon nanotube/nanocarbon black composite filler', *Composites Part A: Applied Science and Manufacturing*, vol. 119, pp. 8-20.

Zhang, L., Ding, S., Li, L., Dong, S., Wang, D., Yu, X. & Han, B. 2018, 'Effect of characteristics of assembly unit of CNT/NCB composite fillers on properties of smart

cement-based materials', *Composites Part A: Applied Science and Manufacturing*, vol. 109, pp. 303-20.

Zhang, P., Cong, Y., Vogel, M., Liu, Z., Müller, H.S., Zhu, Y. & Zhao, T. 2017, 'Steel reinforcement corrosion in concrete under combined actions: The role of freeze-thaw cycles, chloride ingress, and surface impregnation', *Construction and Building Materials*, vol. 148, pp. 113-21.

Zhang, P., Wittmann, F.H., Vogel, M., Müller, H.S. & Zhao, T. 2017, 'Influence of freeze-thaw cycles on capillary absorption and chloride penetration into concrete', *Cement and Concrete Research*, vol. 100, pp. 60-7.